



City Research Online

City, University of London Institutional Repository

Citation: Mohamed, ZM.E.Q (1988). Hot ductility of steels. (Unpublished Doctoral thesis, City University London)

This is the accepted version of the paper.

This version of the publication may differ from the final published version.

Permanent repository link: <https://openaccess.city.ac.uk/id/eprint/8348/>

Link to published version:

Copyright: City Research Online aims to make research outputs of City, University of London available to a wider audience. Copyright and Moral Rights remain with the author(s) and/or copyright holders. URLs from City Research Online may be freely distributed and linked to.

Reuse: Copies of full items can be used for personal research or study, educational, or not-for-profit purposes without prior permission or charge. Provided that the authors, title and full bibliographic details are credited, a hyperlink and/or URL is given for the original metadata page and the content is not changed in any way.

HOT DUCTILITY OF STEELS

by

Z.M.E.Q. MOHAMED

A dissertation submitted to
The City University
in fulfilment of the requirement
for the degree of
Doctor of Philosophy

JULY 1988

Department of Mechanical Engineering,
The City University,
LONDON.

CONTENTS

	<u>PAGE</u>
LIST OF TABLES	1
LIST OF FIGURES	2
ACKNOWLEDGEMENTS	12
DECLARATION	13
ABSTRACT	14
LIST OF SYMBOLS	15
<u>CHAPTER 1</u> INTRODUCTION	16
<u>CHAPTER 2</u> CONTINUOUS CASTING PROCESS	20
2.1 Mechanics of the Continuous Casting Process	21
2.2 Transverse Cracking	23
2.3 Process Variables and their Remedial Effect on Transverse Cracking	24
<u>CHAPTER 3</u> LITERATURE SURVEY	27
3.1 Introduction	28
3.2 Hot Strength Data	29
3.3 Hot Ductility Curves and Zones of Reduced Ductility	32
3.4 Fracture Mechanism in Relation to Hot Ductility Curves	34
3.4.1 General	34
3.4.2 The right hand side of the trough	34
3.4.3 The middle area of the trough	35
3.4.3.1 Intergranular fracture in the austenite phase	35
3.4.3.2 Intergranular fracture in ($\gamma + \alpha$) phase	38
3.4.4 The left hand side of the trough	40
3.5 Softening Processes	41
3.5.1 General	41
3.5.2 Dynamic recovery	43
3.5.3 Dynamic recrystallisation	44
3.5.4 Influence of dynamic recrystallisation on hot ductility	46
3.6 The Influence of Strain Rate on Hot ductility	49
3.7 The Influence of Grain Size on Hot Ductility	53
3.8 The Influence of Steel Composition on Hot Ductility	56
3.8.1 General	56
3.8.2 Nitride and/or carbides forming elements	56
3.8.3 Oxide and/or sulphides forming elements	62

3.8.4 Elements with segregation tendencies	65
<u>CHAPTER 4</u> EXPERIMENTAL TECHNIQUES	67
4.1 Introduction	68
4.2 Measures of Ductility	69
4.3 Equipment used in Tensile Test	71
4.3.1 Induction heating test	71
4.3.2 Instron test	72
4.4 Microscopy Examination	74
<u>CHAPTER 5</u> EFFECT OF CARBON ON THE HOT DUCTILITY OF MICRO-ALLOYED STEELS	75
5.1 Introduction	76
5.2 Experimental	78
5.3 Results	80
5.3.1 Hot ductility curves	81
5.3.2 Stress - elongation curves	82
5.3.3 Metallography	83
5.4. Discussion	86
5.4.1 Hot ductility behaviour of C-Mn-Al steel on raising the C level	86
5.4.2 Hot ductility behaviour of C-Mn-Al-Nb steel on raising the C level	88
5.5 Conclusions	91
<u>CHAPTER 6</u> EFFECT OF CALCIUM ON THE HOT DUCTILITY OF MICRO-ALLOYED STEELS	92
6.1 Introduction	93
6.2 Experimental	96
6.3 Results	97
6.3.1 Hot ductility curves	97
6.3.2 Fracture examinations	99
6.3.3 TEM examinations	100
6.4 Discussion	101
6.4.1 General effect of Ca treatment	101
6.4.2 Shape of the hot ductility curves	103
6.5 Conclusions	106
<u>CHAPTER 7</u> THE RELATIVE INFLUENCE OF STATIC AND DYNAMIC PRECIPITATION ON THE HOT DUCTILITY OF MICRO-ALLOYED STEELS	107

7.1	Introduction	108
7.2	Experimental	111
7.3	Results	114
7.3.1	Hot ductility curves	114
7.3.2	Stress - elongation curves	115
7.3.3	Influence of holding time at temperatures corresponding to those giving the maximum rate of precipitation	116
7.3.4	Static precipitation of VCN and NbCN	117
7.3.5	Transmission electron microscopy	118
7.3.6	Fracture appearances	119
7.4	Discussion	121
7.4.1	C-Mn-Al (0.068% Al)	121
7.4.2	C-Mn-Al-V steel	122
7.4.3	C-Mn-Al-Nb steel	124
7.5	Conclusions	126
 <u>CHAPTER 8</u> HOT DUCTILITY OF DIRECTLY CAST MICRO-ALLOYED STEELS		128
8.1	Introduction	129
8.2	Experimental	132
8.3	Results	134
8.3.1	Hot ductility curves	134
8.3.2	Metallography	135
8.3.3	Fracture appearances	136
8.3.4	Replicas examinations	138
8.4	Discussion	140
8.5	Conclusions	148
 <u>CHAPTER 9</u> EFFECT OF MANGANESE AND SULPHUR ON THE HOT DUCTILITY OF MICRO-ALLOYED STEELS		150
9.1	Introduction	151
9.2	Experimental	154
9.3	Results	156
9.3.1	Hot ductility curves	156
9.3.2	Peak stresses and critical strain for dynamic recrystallisation	158
9.3.3	Microscopy	159
9.4	Discussion	163
9.4.1	Explanation for the shape of the hot ductility curves	163

9.4.2 Effect of Mn and S on hot ductility	165
9.4.3 Effect of normalising on hot ductility	166
9.5 Conclusions	167
<u>CHAPTER 10</u> THE INFLUENCE OF INCLUSION SHAPE ON THE HOT DUCTILITY	168
10.1 Introduction	169
10.2 Experimental	171
10.3 Results	173
10.3.1 Hot ductility curves	173
10.3.2 Hot strength	174
10.3.3 Stress - elongation curves	175
10.3.4 Grain size measurements	176
10.3.5 Fracture examinations	176
10.4 Discussion	178
10.4.1 Explanation for the shape of the ductility trough	178
10.4.2 Influence of elongated inclusions on hot ductility	179
10.4.3 Influence of dynamic recrystallisation on hot ductility	183
10.4.4 Influence of strain rate on hot ductility	184
10.5 Conclusions	187
<u>CHAPTER 11</u> SUMMARY AND RECOMMENDATIONS	189
11.1 Introduction	190
11.2 Summary	191
11.3 Intergranular fracture	195
11.4 Recommendations	198
APPENDICES	201
1. Carbon extraction replica preparation and examination (Crowther, 1986)	202
2. Publications	204
REFERENCES	206

LIST OF TABLES

- 5.1 Compositions of the steels examined (Wt.%).
- 6.1 Compositions of the steels examined (Wt.%).
- 7.1 Compositions of the steels examined (Wt.%).
- 8.1 Compositions of the steels examined (Wt.%).
- 8.2 Austenite grain sizes for the steels examined in different test conditions.
- 8.3 Precipitate types and sizes for the Nb and Nb/Ti steels in different test conditions.
- 9.1 Compositions of the steels examined (Wt.%).
- 9.2 Critical strain (ϵ_c in %) necessary to nucleate dynamic recrystallisation for the steels examined.
- 10.1 Compositions of the steels examined (Wt.%).
- 10.2 Comparison of activation energy, Q , and stress exponent, n , of present work with previous studies for C-Mn steels.

LIST OF FIGURES

- 2.1 Profile of Gray slab caster
- 2.2 Schematic representation of friction force and tensile force on the skin surface. (after Lankford, 1972).
- 2.3 Effect of slight bulging of slab or offset rolls on stresses in solidifying skin. (after Lankford, 1972).
- 2.4 Surface strain and strain rate resulting from bending (after Lankford, 1972).
- 2.5 Hot ductility curves for Al and Nb containing steels (after Mintz and Arrowsmith, 1979).
- 2.6 Comparison of temperature distribution between mist cooling and spray cooling (after Kawasaki et al., 1979).
- 3.1 Schematic presentation of ductility and strength in the high temperature zone of reduced ductility. (after Suzuki et al., 1980).
- 3.2 Typical schematic diagram of a hot ductility curve showing various regions.
- 3.3 Schematic representation of high temperature ductile with dynamic recrystallisation. (after Ashby et al., 1979).
- 3.4 Mechanism for embrittlement in the two phase zone. (after Suzuki et al., 1982).
- 3.5 Stress-strain curves for a plain carbon and a 2.91 % Silicon steels tested at 1000 °C. (after Saki and Ohashi, 1981).
- 3.6 Schematic representation of the effect of strain rate and temperature on the hot ductility of steels. (after Norstrom and Johansson, 1982).
- 3.7 Influence of strain rate on the hot ductility of a C-Mn-Al-Nb steel. (after Mintz and Arrowsmith, 1979).

- 3.8 The effect of strain rate on hot ductility and grain boundary sliding in a C-Mn-Al-Nb steel. (after Ouchi and Matsumoto, 1982).
- 3.9 Effect of grain size on hot ductility of a plain carbon steel. (after Crowther and Mintz, 1986)
- 3.10 Influence of Al on the hot ductility of C-Mn-Nb-Al steels. (after Mintz and Arrowsmith, 1979).
- 3.11 Influence of Nb on the hot ductility of steels. (after Bernard et al., 1978).
- 3.12 Hot ductility curves for different micro^oalloyed steels, showing the effect of V. (after Mintz and Arrowsmith, 1980).
- 3.13 Effect of S on hot ductility of low carbon steels (after Weinberg, 1979).

- 4.1 Schematic illustration of induction heating equipment for high temperature tensile testing.
- 4.2 Temperature distribution in Induction test piece at different temperatures.
- 4.3 Induction test specimen.
- 4.4 Schematic illustration of Instron high temperature testing equipment.
- 4.5 Instron test piece.

- 5.1 Hot ductility curves for the Al containing steels examined.
- 5.2 Hot ductility curves for the Nb containing steels examined.
- 5.3 Stress - total elongation curves for the Al containing steels examined with different carbon levels.
- 5.4 Stress - total elongation curves for the Nb containing steels examined with different carbon levels.
- 5.5 Fracture at 850 °C (~5 °C below the A_{e3} temperature), showing presence of deformation induced ferrite for the C-Mn-Al steel with 0.11 % carbon content.

- 5.6 Cracks formed along ferrite films in the Nb steel with 0.16% C content, sample tested at 850 °C (~5 °C below the A_{e3} temperature).
- 5.7 0.1% C niobium containing steel tested at 850 °C, showing extensive NbCN precipitation.
- 5.8 0.014% C niobium containing steel tested at 850 °C, showing sparse precipitation of NbCN.
- 5.9 Example of high temperature ductile rupture fracture observed in the 0.15% C aluminium containing steel tested at 950 °C.
- 5.10 Example of intergranular micro-void coalescence fracture observed in the 0.1% C niobium containing steel tested at 790 °C.
- 5.11 Example of intergranular micro-void coalescence observed in the 0.1% C niobium containing steel tested at 840 °C.
- 5.12 Example of mixed intergranular micro-void coalescence and intergranular decohesion fracture, observed in the 0.1% C niobium containing steel tested at 900 °C.
- 6.1 Hot ductility curves for the C-Mn-Al steels with and without calcium additions.
- 6.2 Hot ductility curves for the C-Mn-Al-Nb steels with and without calcium additions.
- 6.3 Stress-Total elongation curves for Al and Nb containing steels, with and without calcium additions.
- 6.4 Mixture of intergranular micro-void coalescence and intergranular decohesion failure observed in the Nb containing steel without Ca treatment (heat G) at 850 °C.
- 6.5 Mixture of intergranular micro-void coalescence and intergranular decohesion failure observed in the Nb containing steel with Ca treatment (heat D) at 850 °C.

- 6.6 Example of intergranular micro-void coalescence (mean fracture mode) failure observed in calcium free C-Mn-Al steel (heat B).
- 6.7 Example of the increasing intergranular decohesion fracture mode with increasing test temperature in the Nb containing steel (heat G).
- 6.8 Intergranular fracture, observed in the Nb containing steel (heat G) tested at 800 °C.
- 6.9 Example of ductile fracture observed in the C-Mn-Al-Ca steel, tested at 800 °C.
- 6.10 NbCN precipitation observed in the Nb containing steel without Ca treatment at 850 °C, with associated X-ray spectrum.
- 6.11 NbCN precipitation observed in the Nb containing steel with Ca treatment (heat D) at 850 °C, with associated X-ray spectrum.
- 6.12 Example of MnS inclusions observed in Nb containing steel without Ca treatment (heat G) at 850 °C, with associated X-ray spectrum
- 6.13 Example of MnS inclusions observed in the Al containing steel without Ca treatment at 870 °C, with associated X-ray spectrum.
- 6.14 Example of (Mn,Ca)S inclusions observed in the Ca treated steels.
- 7.1 Hot ductility curves for the C-Mn-Al-Nb steel.
- 7.2 Hot ductility curves for the C-Mn-Al-V steel.
- 7.3 Hot ductility curves for the C-Mn-Al steel.
- 7.4 Stress-Total elongation curves for the C-Mn-Al steel, with no holding time at test temperature.
- 7.5 Stress-Total elongation curves for the C-Mn-Al steel, with holding time of 15 minutes at test temperature.

- 7.6 Stress-Total elongation curves for the C-Mn-Al-V steel with no holding time at test temperature.
- 7.7 Stress-Total elongation curves for the C-Mn-Al-V steel with holding time of 2 hours at test temperature before deformation.
- 7.8 Stress-Total elongation curves for the C-Mn-Al-Nb steel with no holding time at test temperature.
- 7.9 Stress-Total elongation curves for the C-Mn-Al-Nb steel with holding^{time} of 15 minutes at test temperature.
- 7.10 Stress-Total elongation curves for the C-Mn-Al steel with different holding times at test temperature (850 °C).
- 7.11 Influence of holding time prior to testing on peak stress and hot ductility of the C-Mn-Al steel tested at 850 °C.
- 7.12 Hardness of the C-Mn-Al-V steel following quenching and tempering, after holding for various times at 850 °C.
- 7.13 Hardness of the C-Mn-Al-Nb steel following quenching and tempering, after holding for various times at 950 °C.
- 7.14 Example of fine AlN precipitation in the C-Mn-Al steel tested at 850 °C, after 4 hours holding time.
- 7.15 Coarse AlN precipitation in the C-Mn-Al steel, due to incomplete solution of AlN at 1330 °C, with associated X-ray spectrum.
- 7.16 Mixture of intergranular decohesion and intergranular micro-void coalescence type fracture in the C-Mn-Al-Nb steel tested at 850 °C.
- 7.17 Mixture of intergranular decohesion and intergranular micro-void coalescence type fracture in the C-Mn-Al-V steel tested at 800 °C.

- 7.18 Mixture of intergranular decohesion and intergranular micro-void coalescence type fracture in the C-Mn-Al steel, tested at 850 °C.
- 8.1 Experimental arrangement for measuring hot ductility in the "as cast" condition.
- 8.2 Hot ductility curves for the Nb/Ti steel, occurrence of dynamic recrystallisation indicated by shaded regions.
- 8.3 Hot ductility curves for the Nb steel, occurrence of dynamic recrystallisation indicated by shaded regions.
- 8.4 Hot ductility curves for the Al steel, occurrence of dynamic recrystallisation indicated by shaded regions.
- 8.5 Typical coarse grained structure produced on fast cooling after solidification for the Nb/Ti steel.
- 8.6 Fine grain structure produced on reheating to 1330 °C and quenching in ice brine for the Nb/Ti steel.
- 8.7 Typical wedge type crack found in the Nb containing steel, sample tested at 850 °C in the as cast state.
- 8.8 Evidence of deformation induced ferrite in the Nb/Ti steel, sample quenched from 850 °C after fracture.
- 8.9 Fracture surface of the Nb containing steel in the as-cast condition after testing at 850 °C, showing mixture of intergranular micro-void coalescence and intergranular decohesions.
- 8.10 Interdendrite type of fracture in the Nb containing steel in the as-cast state after testing at 1000 °C, showing lines of coarse angular Mn(Fe)S inclusions.

- 8.11 Interdendritic type of fracture in the Nb containing steel in the "reheated as cast" condition, tested at 900 °C, showing that most of the Mn(Fe)S inclusions have redissolved.
- 8.12 Spherical type sulphides found on the dendritic nodule surfaces of the Nb/Ti steel in the as-cast state after testing at 850 °C.
- 8.13 High temperature ductile rupture found in the Nb/ti steel in the "reheated hot rolled" condition, sample tested at 900 °C.
- 8.14 Typical replicas obtained from the Nb/Ti steel in the as cast state, sample tested at 900 °C, showing coarse grain boundary precipitates and fine matrix precipitation (with associated X ray spectrum for the large particles).
- 8.15 Typical TiN precipitation observed in the Nb/Ti steel in the "reheated hot rolled" condition, with associated X-ray spectrum, for sample tested at 850 °C.
- 8.16 Fine NbCN precipitation observed in the Nb steel in the "as cast" condition at test temperature of 850 °C.
- 8.17 Coarse NbCN eutectic extracted from "as cast" sample tested at 950 °C, with associated X-ray spectrum.
- 8.18 Fine MnS inclusions extracted from "as cas" C-Mn-Al-Nb sample tested at 950 °C, with associated X-ray spectrum.
- 9.19 Variation of minimum R of A values with austenite grain size following testing in the range 700 to 1000 °C at strain rate of $3 \times 10^{-3} \text{ s}^{-1}$.
- 8.20 Hot ductility curves for the as cast steels, A, B, and C.
- 9.1 Effect of Mn content in the steel on the solidification temperature of sulphide inclusions, (after Kinoshita and Kuroki, 1972).

- 9.2 Hot ductility curves for the low S steels, containing Al.
- 9.3 Hot ductility curves for the high S steel, containing Al.
- 9.4 Hot ductility curves for the Nb containing steels
- 9.5 Hot ductility curves for the Al containing steel with low S content in normalised and as received conditions.
- 9.6 Hot ductility curves for the Al containing steel with high S content in normalised and as received conditions.
- 9.7 Variation of peak stress, with test temperature for the steels examined in normalised and as received conditions.
- 9.8 Stress-Total elongation curves for the steels examined in normalised condition.
- 9.9 Stress-Total elongation curves for the steels examined in the as received condition.
- 9.10 Effect of Mn content on the critical strain necessary to nucleate dynamic recrystallisation for the steels examined at 1100 °C in the normalised condition.
- 9.11 Effect of S on the critical strain necessary to nucleate dynamic recrystallisation for the Al containing steels examined in different conditions.
- 9.12 Effect of test temperature on ϵ_c for the steels examined in normalised and as received conditions.
- 9.13 Grain size measurements for the C-Mn-Al steels examined in the normalised condition.
- 9.14 Grain size measurements for the Nb containing steels in the normalised condition.

- 9.15 Variation of austenite grain size with temperature for Al containing steels with high Mn content (1.4%) in normalised and as received conditions.
- 9.16 Fracture of C-Mn-Al steel (heat D), tested at 1000 °C, showing typical intergranular failure.
- 9.17 Example of AlN precipitation observed in the Al containing steels (heats A and B) with low S contents (0.002-0.003% S) at test temperature of 1000 °C, in normalised condition.
- 9.18 Example of AlN precipitation observed in the Al containing steels (heats C and D) with high S contents (0.03-0.032% S) at test temperature of 1000 °C, in normalised condition.
- 9.19 Example of AlN precipitation observed in the Al containing steels with high Mn content (1.4%) at 1000 °C in the as received condition.
- 9.20 Examples of AlN and NbCN precipitation observed in the Al/Nb steels (heats E and F) at test temperature of 1000 °C, in the normalised condition, with associated X-ray spectrum.
- 9.21 Example of MnS inclusions observed in the high S steel (heat D) in the normalised condition, at test temperature of 1000 °C.
- 9.22 Example of MnS inclusions observed in the low S steel (heat A) in the normalised condition, at test temperature of 1000 °C.
- 10.1 Testing orientation, showing the average aspect ratio of MnS inclusions.
- 10.2 Coarse MnS inclusions present in the high S steel.
- 10.3 Hot ductility curves for the high S steel examined at strain rate of $3.3 \times 10^{-4} \text{ s}^{-1}$.
- 10.4 Hot ductility curves for the high S steel examined at strain rate of $1.3 \times 10^{-2} \text{ s}^{-1}$.

- 10.5. Variation of peak stress with test temperature for the three test directions at low and high strain rate.
- 10.6 Plots of $\ln \epsilon_p$ versus $1/T$.
- 10.7 Plot of $\ln \dot{\epsilon}$ against $1/T$ at constant ϵ_p .
- 10.8 Plot of $\ln \dot{\epsilon}$ against $\ln \epsilon_p$ at constant temperature.
- 10.9 Stress-Total elongation curves for the three test directions at strain rate of $3.3 \times 10^{-4} \text{ S}^{-1}$.
- 10.10 Stress-Total elongation curves for the three test directions at strain rate of $1.3 \times 10^{-2} \text{ S}^{-1}$.
- 10.11 Variation in austenite grain size with reheating temperature for different steels.
- 10.12 Typical intergranular failure observed in the high S steel in the short transverse direction at strain rate of $3.3 \times 10^{-4} \text{ S}^{-1}$ at $1100 \text{ }^\circ\text{C}$.
- 10.13 Typical wedge type cracks found in polished section close to fracture. Sample tested at $1000 \text{ }^\circ\text{C}$ at a strain rate of $3.3 \times 10^{-4} \text{ S}^{-1}$ in longitudinal direction.
- 10.14 MnS inclusions cited at the austenite grain boundaries.
- 10.15 Cracks formed along the austenite grain boundaries in the sample tested at $1000 \text{ }^\circ\text{C}$ and strain rate of $3.3 \times 10^{-4} \text{ S}^{-1}$ in transverse direction.
- 10.16 MnS inclusions present on the fracture surface of a short transverse sample tested at $900 \text{ }^\circ\text{C}$ at strain rate of $3.3 \times 10^{-4} \text{ S}^{-1}$.
- 10.17 Sample tested at $1000 \text{ }^\circ\text{C}$ in short transverse direction at strain rate of $3.3 \times 10^{-4} \text{ S}^{-1}$, showing cracks at the outer surface.

ACKNOWLEDGEMENTS

I would like to express my thanks to Dr. B. Mintz for his invaluable supervision, encouragement and the knowledge he imparted on the subject.

Thanks are due to Professor G.T. Done for the provision of laboratory facilities, and to the staff of the Department of Mechanical Engineering for their help, particularly Mr. R. Vipond and Dr. J. Walker.

Thanks are also due to BSC, in particular to Dr. D.N. Crowther, for supplying the steels.

Finally, the financial assistance of Mu'tah University- Jordan is acknowledged.

DECLARATION

I grant powers of discretion to the University Librarian to allow this thesis to be copied in whole or in part without further reference to me. This permission covers only single copies made for study purposes, subject to normal conditions of acknowledgement.

ABSTRACT

The hot tensile test has been used for a variety of steels, to investigate the influence of such factors as inclusions, precipitation, phase transformation and grain size on hot ductility. Tests were performed in the temperature range 700-1000 °C and at a strain rates of (10^{-4} – 10^{-2} S⁻¹), generally to simulate the conditions experienced during the straightening operation in the continuous casting process in which transverse cracks propagate. Two zones of reduced ductility can be identified. The γ - α transformation zone which has been shown to produce a significant ductility trough due to strain concentration in the softer ferrite films surrounding the γ grains, causing voiding around the MnS inclusions which link up to give intergranular failure, and factors which alter the A₃ temperature, such as carbon content, have been shown to produce a change in the temperature at which the ductility trough occurs. The second zone of reduced hot ductility was observed in the austenite region, due to the retardation of dynamic recrystallisation associated with the presence of fine carbides, nitrides and/or inclusions precipitates at the austenite grain boundaries, which allows intergranular cracks to develop. The depth and width of this ductility trough is primarily dependent on the size and amount of precipitates present. The influence of MnS inclusions in reducing hot ductility has been noted above and below the A₃ temperature. Above the A₃, inclusions act in a similar way to fine precipitation preventing dynamic recrystallisation and below the A₃, they offer more sites for micro-voiding to occur. Although grain size refinement improves ductility, it does so as long as similarity in precipitate volume fraction and size exist. Improved hot ductility has been achieved by adding Ca to the steel which reduces the amount of MnS inclusions precipitated during cooling from solution temperature at the austenite grain boundaries.

LIST OF SYMBOLS

a	numerical constant
A	numerical constant
A ₁	numerical constant
A ₀	initial cross section area
A _f	final cross sectional area
b	numerical constant
d _a	grain diameter
d ₀	initial grain size
d _s	subgrain diameter
L	gauge length during continuously cast slab straightening
M	grain boundary mobility.
n	stress exponent
p	driving force for grain boundary migration
Q	activation energy for deformation
R	universal gas constant
R	bending radius for straightening of continuously cast slab
t	slab thickness
T	absolute temperature
v	grain boundary migration velocity
V	continuous casting speed
Z	Zener-Holloman parameter
α	numerical constant
α	ferrite
γ	austenite
δ	solidified skin thickness in continuously cast slab
Δ	tangent point to first bending roll
ε̇	strain rate
ε _c	critical strain for the nucleation of dynamic recrystallisation
ε _{gb}	grain boundary strain
ε _p	strain at peak stress
ε _s	surface strain at continuously cast slab
ε _t	total strain
σ	stress
σ _f	flow stress
σ _p	peak stress

CHAPTER 1

INTRODUCTION

Micro-alloying additions are added to improve the properties of low carbon steels, e.g. tensile strength and toughness. Small additions of elements such as Nb, V and Ti result in improved grain refinement to the extent that fine ferrite grain sizes of 5-10 μm are now common in the finished steel (Honeycombe, 1981).

These improvements have led to the introduction of a new class of High Strength Low Alloy steels (HSLA), now widely used for structural and Pipeline application. As an example, the following figures illustrate the increasing importance of micro-alloyed steels. While world steel production increased by no more than 5% from 1970 to 1982, the consumption of niobium as the most important micro-alloying element doubled during the same period (Meyer et al., 1987). This development is probably the most significant metallurgical achievement of the last 25 years (Woodhead and Keon, 1987).

However, the micro-structure of HSLA steels although giving good room temperature properties do not necessarily give desirable high temperature properties. These HSLA steels, produced by continuous casting route at elevated temperatures, can give rise to a wide variety of defects in the solidified slab. (Brimacombe and Sorimachi, 1977). One serious and expensive defect is known as transverse cracking, described in chapter 2. Stuart (1987) reported that all continuous cast slabs, particularly those containing micro-alloying elements (MAE) are subject to transverse cracking. These cracks are

particularly deleterious, since they form at the slab surface, and hence cannot weld up during subsequent rolling, thus the entire slab must be scrapped (Crowther, 1986).

In the last 15 years, the amount of steel produced by the continuous casting route has increased dramatically, and the adoption of this method is accelerating (Thomas et al., 1986). Thus there is a strong incentive to gain an understanding of the formation of these defects, in order to prevent their occurrence. To achieve this aim, hot tensile tests have been performed using thermal cycles and strain rates designed to simulate the continuous casting process (see chapter 2). These studies have related low ductility failures in hot tensile tests to the occurrence of transverse cracking in continuously cast slabs. Factors identified as being responsible for low reduction of area failures during hot tensile testing, include the γ - α transformation, and the precipitation of carbides, nitrides and/or inclusions at the austenite grain boundaries. It is intended in this study to investigate further these aspects.

This work is part of a larger experimental project, designed and supervised by Dr. B. Mintz at the City University in London. Previous work by Crowther and Mintz (1986a, 1986b, 1986c and 1986d) has examined in detail, the influence of grain size, carbon content and microalloying precipitates on hot ductility of steels. The present work is an extension of these studies and involves the influence of carbon and the relative influence

of static and dynamic precipitation on hot ductility of micro-alloyed steels. In addition, the influence of sulphide inclusions on hot ductility has merited more detailed examination and studies related to them have formed the major part of the Thesis.

CHAPTER 2

CONTINUOUS CASTING PROCESS

2.1 MECHANICS OF THE CONTINUOUS CASTING PROCESS

A typical slab caster is shown in Fig. 2.1. The nature of stresses and strains that can give rise to cracks in the solidifying shell has been discussed by Lankford (1972). It could be said that the continuous casting process is a thermo-mechanical treatment and a brief description will be given herewith based on Lankford's work. In the mould when the velocity of the casting relative to the mould wall is downward, an upward friction force acts on the skin surface (Fig. 2.2), which leads to an axial tensile stress in the skin. Since the friction force is a surface force and eccentric to the resultant axial force, a bending moment occurs and causes additional stress in the skin. Below the mould, ferrostatic pressure can give rise to bulging as shown in Fig. 2.3, the resultant stresses are tensile at the surface and compressive near the solidification front. The transition from vertical to horizontal is accomplished by plastic bending and the straightening of the strand introduces axial strains in the solid shell. During straightening these strains are tensile on the upper surface of the strand and compressive on the lower surface.

Stresses can also be generated from a variety of other sources such as the weight of the strand, misalignment of the casting machine and non uniform cooling in the mould. Following Lankford (1972), Fig. 2.4 illustrates the surface strain and strain rate developed during the straightening process. These strains may be the greatest

to which the slab is subjected during the continuous casting operation.

The surface strain, ϵ_s , due to bending is given approximately by $\epsilon_s = t/2R$, where t is the slab thickness, and R is the bending radius. For typical values of 10 m and a slab thickness of 0.23 m, a surface strain of 1.15 % is expected. The uncertainty in the gauge length necessary to develop the full bending strain could lead to over- or underestimation of the actual strain rate. Lankford (1972) has given 3 values for this gauge length, L (Fig. 2.4):

- the distance from a tangent point to the first bending rolls (Δ),
- a distance equal to the skin thickness (δ), or
- a distance equal to the slab thickness, (t).

The strain rate, $\dot{\epsilon}$, is then given by, $\dot{\epsilon} = \epsilon_s V/L$, where V is the casting speed. For a typical speed of 0.9 m/min. and a suitable values for L (6 to 10 m), the surface strain is in the range $1.7 \times 10^{-3} - 2.9 \times 10^{-3} \text{ S}^{-1}$. Similar results for surface strain and strain rate have been calculated by Bernard et al., (1978).

However, these values are approximate and deal with the deformation of the slab as a whole and locally different values of ϵ_s and $\dot{\epsilon}$ may be obtained.

2.2 TRANSVERSE CRACKING

Transverse cracks on the original slab surface are often difficult to see and they require a control-scarf pass to reveal them. The cracks appear at the base of the oscillation marks, both in the midface region and near the corners, (Brimacombe and Sorimachi, 1977). It is believed that these oscillation marks act as stress concentrators, and hence promote crack formation, which probably starts to form in the mould, and propagate during the straightening operation (Schmidt and Josefsson, 1974).

The depth of transverse cracks varies from 1 mm up to a maximum of 15 mm, although at the corners it may be as much as 50 mm (Farkas et al., 1971 ; Hater et al., 1973). Thus in several cases a scarfing depth in excess of 10 mm may be necessary to eliminate these defects completely.

Schmidt and Josefsson (1974), have shown that the cracks propagate along the austenite grain boundaries, and that coarse grained regions are particularly prone to cracking. A variety of particles have been identified on the crack surfaces, dependent on the steel compositions and process variables, including AlN (Mori, 1974) and MnS, NbCN and various oxides (Cochrane, 1982).

2.3 PROCESS VARIABLES AND THEIR REMEDIAL EFFECT ON TRANSVERSE CRACKING

Attempts have been made to alter the following process variables, in order to minimize the transverse cracking.

A- SLAB SURFACE TEMPERATURE

Micro alloyed steels show a loss of hot ductility in the temperature range 600 - 1000 °C and strain rates in the range 10^{-4} — 10^{-3} S^{-1} as can be seen in Fig. 2.5.

These conditions are close to those experienced during the straightening operation in which transverse cracks propagate. Thus, it would be expected that slab surface temperature above the low ductility region (soft cooling patterns) or below the low ductility region (hard cooling patterns) would produce crack free slabs. Slab surface temperatures have been altered by adjusting the secondary cooling pattern. Offerman et al., (1981) and Mercer and Mcpherson (1979) have reported a reduction in the incidence of transverse cracking using soft cooling patterns. However, the success of this method in reducing transverse cracking was limited, due to the fact that high temperature extent of the ductility trough is more composition dependent than the low temperature extent (Birat et al., 1981). This led Birat et al., (1981) to develop a cooling pattern which reduced surface temperature at the straightener to 700 °C, and this produced a decrease in the frequency of transverse cracking. Similar hard cooling patterns have been used successfully by Nozaki et al., (1978), and by Schmidt and Josefsson (1974). The latter

authors attributed the reduction in cracking to the elimination of the coarse austenite grains with which they had previously associated transverse cracking. Offerman et al., (1981) have warned, that reducing the slab surface temperature to below 700 °C, might at some points below the slab surface, produce temperatures high enough to place it in the low ductility region, leading to the formation of the subsurface transverse cracks.

B - MOULD OSCILLATION FREQUENCY

Kawaski et al., (1987), have found that the high cycle oscillation of the mould is one of the best ways to improve the surface quality and reduce the surface defects caused by oscillation marks. They attributed this improvement in surface quality, to a decrease in the molten steel including inclusions, which overflow the top of the initial solidified shell with increasing mould oscillation frequency. Mercer and Mcpherson (1979), have reported that an increase in mould oscillation frequency at the BSC Ravenscraig led to significant reduction in plate rejection levels, presumably by reducing the stress concentration effect of the oscillation marks.

C- UNIFORM COOLING

It has been shown that cooling uniformity is difficult to achieve in the secondary cooling zone, using hard or soft cooling patterns (Offerman et al., 1981). The impingement of cooling sprays can lead to oscillation in the slab temperature near the slab surface, as can be seen in Fig. 2.6.

This uneven cooling, leads to thermal shock on the slab surface. The thermal stresses set up by this effect are in themselves enough to form cracks, (Tomono, 1977). Thus the introduction of a more uniform cooling pattern, which eliminates these temperature oscillations has been shown to reduce transverse cracking (Nozaki et al., 1978 ; Coleman and Wilcox, 1985 and Kawasaki et al., 1987). Kawasaki et al., (1987). have used Mist Spray Cooling Technique (water+ air) to achieve even cooling (Fig. 2.6) . The reduction of transverse cracking by this method has been attributed to the smaller thermal shock obtained in this method, than of water spray alone.

The influence of cyclic temperature oscillations on the hot ductility of C-Mn-Nb-Al steels has also been examined by Mintz et al., (1987). The amplitude and period of temperature oscillation was found to be critical in determining hot ductility. Small cyclic oscillations reduced the amount of NbCN precipitation and improved ductility.

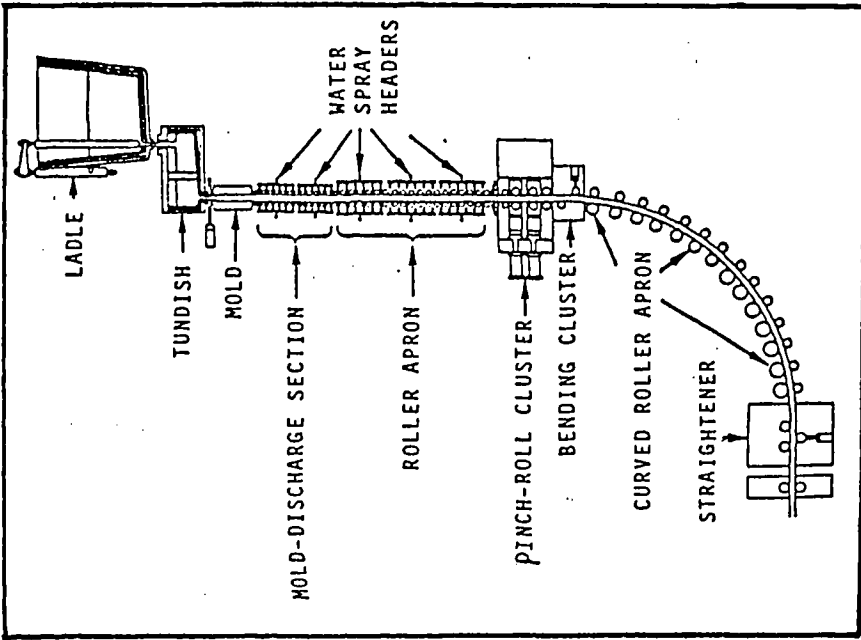


Fig. 2.1 Profile of Gray slab caster

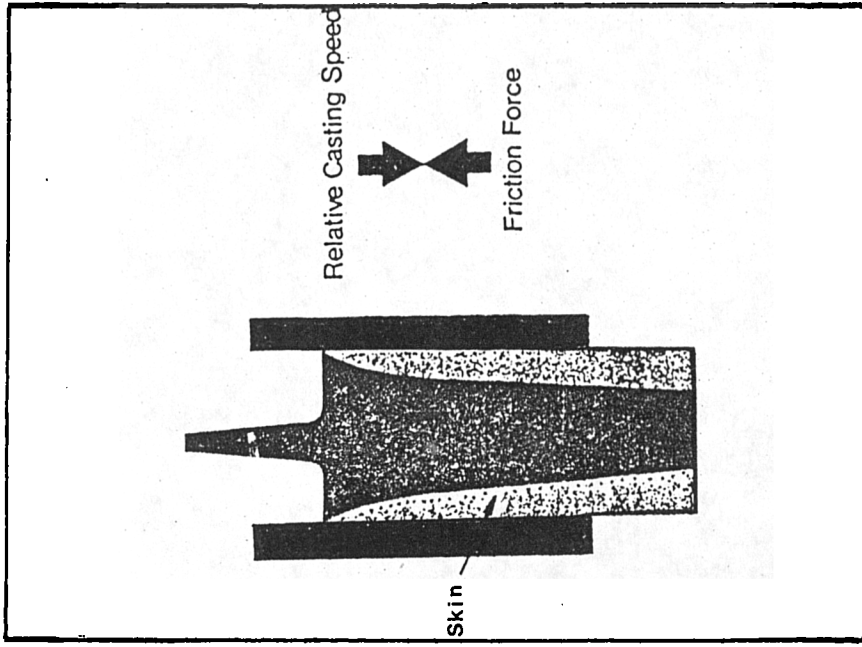


Fig. 2.2 Schematically representation of friction force and tensile force on the skin surface. (after Lankford, 1972)

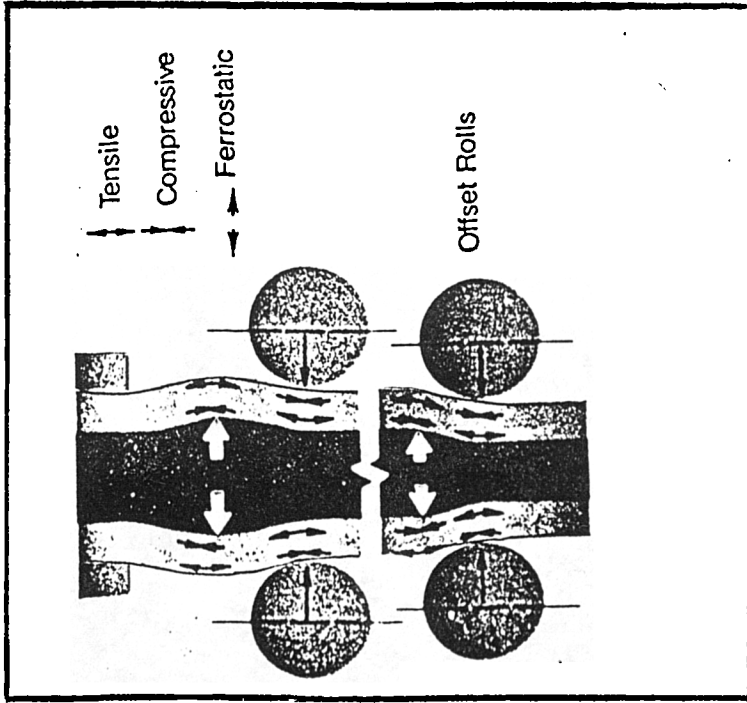


Fig. 2.3 Effect of slight bulging of slab or offset rolls on stresses in solidifying skin. (after Lankford, 1972).

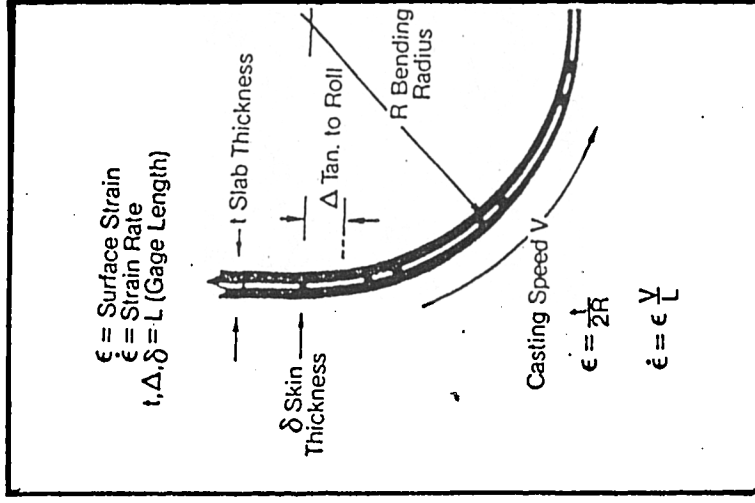


Fig. 2.4 Surface strain and strain rate resulting from bending. (after Lankford, 1972)

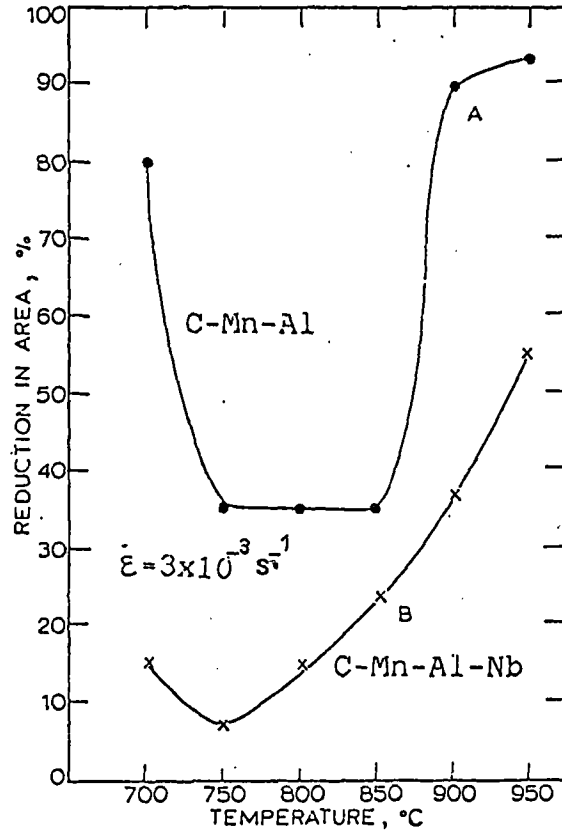


Fig. 2.5 Hot ductility curves for Al and Nb containing steels (After Mintz and Arrowsmith, 1979)

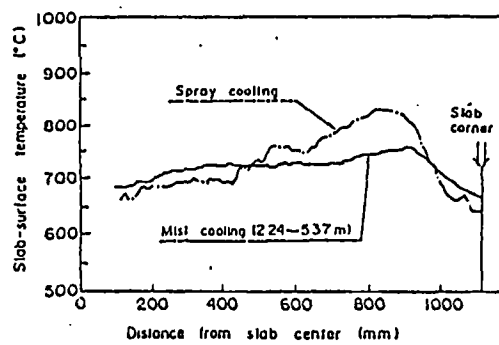


Fig. 2.6 Comparison of temperature distribution between mist cooling and spray cooling. (After Kawasaki et al., 1987).

CHAPTER 3

LITERATURE SURVEY

3.1 INTRODUCTION

Hot ductility of steels has been the subject of numerous investigations, and considerable progress has been achieved in understanding this phenomenon. However, prior to 1975 most of the previous work had been concentrated on either high strain rate deformation aimed to simulate rolling or forging operations or has involved creep tests resulting in very low strain rates.

The continuously cast slab straightening operation is carried out at strain rates in the range $10^{-4} - 10^3 \text{ S}^{-1}$ as described in chapter 2 and there is less information available on strength, structure and ductility at high temperatures for these immediate strain rates. It is intended in this chapter to briefly review the literature describing high temperature mechanical properties, in particular ductility. Special attention will be paid to examinations using intermediate strain rates and steels with micro-alloying additions of Nb, V, Al and Ti, as well as steels with varying amount of S, (modified and unmodified inclusions).

3.2 HOT STRENGTH DATA

The mechanical properties derived from the tensile test are strongly dependent on test temperature and strain rate used in the test. In general, strength decreases and ductility increases as the test temperature is increased at the same strain rate. The effect of strain rate on the mechanical properties is more complex (see section 3.6) and is temperature and composition dependent. Many structural changes, which may alter the general behaviour of the metal, such as recovery, recrystallisation or precipitation could occur in certain temperature ranges due to the combined effect of heat and deformation.

Sellars and Tegart (1966), have shown that hot working data can be correlated using the relation-ship, first proposed by Garafalo (1963), from creep studies.:

$$\dot{\epsilon} = A(\sinh \alpha \sigma)^n \exp(-Q/RT) \quad (3.1)$$

where $\dot{\epsilon}$ is the strain rate in S^{-1} , T is the absolute temperature in K, σ is the stress (either peak or steady state) in N/mm^2 , R is the universal gas constant in $KJ/Kg \text{ mol K}$, A , α and n are temperature independent constants, and Q is an activation energy in KJ/mol .

For small values of α and lower stresses ($\alpha \sigma < 0.8$),:

$$\sinh \alpha \sigma = \alpha \sigma$$

This can be proved if we recall the definition of the hyperbolic sine function:

$$\sinh \alpha \sigma = (e^{\alpha \sigma} - e^{-\alpha \sigma})/2 \quad (3.2)$$

where :

$$e^{\alpha\sigma} = 1 + \frac{\alpha\sigma}{1!} + \frac{\alpha^2 \sigma^2}{2!} + \frac{\alpha^3 \sigma^3}{3!} + \dots \quad (3.3)$$

and

$$e^{-\alpha\sigma} = 1 - \frac{\alpha\sigma}{1!} + \frac{\alpha^2 \sigma^2}{2!} - \frac{\alpha^3 \sigma^3}{3!} + \dots - \dots \quad (3.4)$$

Substitution of equations 2.3 and 2.4 in equation 2.2 gives:

$$\sinh \alpha\sigma = \alpha\sigma \dots \dots \dots \quad (3.5)$$

Substitution of equation 2.5 in equation 2.1 gives:

$$\dot{\epsilon} = A_1 \sigma^n e^{-Q/RT} \dots \dots \dots \quad (3.6)$$

This relationship has been successfully applied for a number of alloys in the austenitic state, including plain carbon steels (Tegart, 1967 ; Crowther and Mintz, 1986a) and micro alloyed steels (Crowther et al., 1987 ; Sanker et al., 1979). The value of Q may remain constant over a wide range of strain rates, but in some cases different values are obtained for creep and hot working conditions (Jonas et al., 1968). In the former case, Q is equal to the activation energy for self diffusion, and is indicative that the rate controlling softening process is dynamic recovery over a wide range of strain rates. In the later case, the higher activation energy for hot working is taken to be due to the operation of dynamic recrystallisation (Tegart, 1967). Steels in the austenitic state, during hot working and intermediate strain rates belong to the second group, in which dynamic recrystallisation is the operative softening process (Jonas et al., 1968 and Crowther et al., 1987).

If equation 3.6 is obeyed, a plot of $\ln\sigma$ versus $1/T$ will give a straight line. An activation energy for defor-

mation, Q , is obtainable from the gradient of the plot of $\ln \dot{\epsilon}$ against $1/T$ at constant stress, since taking the natural logarithm of both sides in equation 3.6 gives:

$$\ln \dot{\epsilon} = (\ln A_1 + n \ln \sigma) - (Q/R)T \quad (3.7)$$

which is the linear form of straight line with the gradient Q/R . The stress exponent, n , is determined from the gradient of the plot of $\ln \dot{\epsilon}$ against $\ln \sigma$ at constant temperature and the straight line equation will be:

$$\ln \dot{\epsilon} = (\ln A_1 - Q/RT) + n \ln \sigma \quad (3.8)$$

3.3 HOT DUCTILITY CURVES AND ZONES OF REDUCED DUCTILITY

In general, the hot ductility of steels is very good. However, there are two distinct temperature ranges in which its ductility drops markedly. The first drop occurs within about 50 °C of the solidus temperature (Hot tearing) and the ductility in this range is virtually zero as can be seen in Fig. 3.1. The ductility is reduced by the incipient grain boundary melting (Weinberg, 1979) and/or micro-segregation of S and P residuals at solidifying dendrite interfaces which lowers the solidus temperature locally in the interdendritic regions (Thomas et al., 1986)

The second range of reduced ductility, could be observed from test temperatures as high as 1200 °C to as low as 700 °C (intermediate-temperature zone). This range is of a particular relevance to the temperature range in the continuous casting process, where transverse cracks occur in the strain rate range of 10^{-4} — 10^{-3} s⁻¹. In this wide temperature interval, reduction of area can have almost any value, from a minimum of about 10 % to almost 100 %, which indicates that there is always some local deformation (Wilber et al., 1975). This small local deformation distinguishes low ductility cracking in this region from that in the high temperature region where hot tearing occurs.

This ductility trough range can be divided further into two overlapping temperature zones in which different embrittling mechanism operate as will be discussed in the

next section. The first zone is while the steel is entirely in the austenite phase (from A_{e_3} temperature to as high as 1200°C) and the other zone is closely associated with γ - α transformation. It lies in a lower temperature range in the two phase austenite/ferrite region.

3.4 FRACTURE MECHANISMS IN RELATION TO HOT DUCTILITY CURVE

3.4.1 GENERAL

Traditionally, fractures at elevated temperatures have been classified as intergranular or transgranular fracture. The former one is the operative fracture mode in the continuous casting process, leading to the transverse cracks. Intergranular crack nucleation and growth has been covered extensively by Evans (1984), and only a brief discussion will be introduced in this review.

The hot ductility curve, Fig. 3.2, can be divided into three regions independent of steel structure (γ or $\gamma + \alpha$),:

- (a) the right hand side and (b) the left hand side of the ductility trough, with high reduction of area values ($\geq 70\%$), in which transangular fracture mode operates.
- (c) the third region is the middle area of the trough (R of A values $\leq 60\%$), in which intergranular fracture mode operates.

3.4.2 THE RIGHT HAND SIDE OF THE TROUGH

In this zone, the high temperature ductile rupture (HTDR) usually occurs and is associated with dynamic recrystallisation. Large voids appear on the fracture surface and apparently they are not associated with second phase particles (Crowther and Mintz, 1986a). Wray (1981) has observed this mode of failure in austenitic iron. Mintz (1988), believed that dynamic recrystallis-

ation and movement of grain boundaries prevent these voids linking up giving high R of A values. Fig. 3.3 shows this failure mode schematically after Ashby et al., (1979).

3.4.3 THE MIDDLE AREA OF THE TROUGH

3.4.3.1 INTERGRANULAR FRACTURE IN THE AUSTENITE PHASE

Researchers do agree to a large extent that intergranular fracture observed in the single austenite phase can be explained by the action of second phase particles at the γ grain boundaries. However, different mechanisms have been suggested as how these particles operate to reduce ductility. It appears that more than one mechanism contributes to the final fracture, operating both simultaneously and independently. Under any particular set of experimental conditions, any one of these mechanisms could predominate.

ACTIONS OF SECOND PHASE PARTICLES:

The mechanisms are listed as follows:-

a- Second phase particles providing initiation sites for void nucleation at the austenite grain boundaries:

Under stress, small precipitates assist in initiating micro-voids at the austenite grain boundaries and with increasing strain, the cavity density increases (Dyson and Mclean, 1972). Growth of initiated cracks occur by spreading along the grain boundary (Reynolds and Gladman, 1980). With increasing cavity density and growth, a limit is reached and intergranular fracture with low

ductility occurs. This fracture type has been observed by Crowther and Mintz (1986a) and pointed out as intergranular micro-void coalescence (IMC), in which microvoids often associated with second phase particles cover the facets of the austenite grains.

b- Second phase particles hindering or preventing grain boundary mobility:

This mechanism encourages cavity coalescence leading to intergranular fracture (Vodopivec, 1978 and Funnell, 1980). Mintz and Arrowsmith (1979), suggest that a critical particle size exists, above which grain boundary migration can occur. This size would be a function of particle volume fraction, initial grain size and the stored energy of deformation. Provided there is a sufficiently large number of precipitates smaller than this critical size, grain boundary pinning occurs with resultant loss of ductility.

c- Second phase particles encouraging grain boundary sliding:

According to Suzuki et al., (1980) and Funnell and Davies (1978), the voids nucleate, grow and coalesce along the austenite grain boundary by the relative movement of neighboring grains along the boundary, i.e. grain boundary sliding.

From creep studies (Garafalo, 1968) and hot working tests (Tegart, 1967), two types of intergranular cracking occur, and both require grain boundary sliding to nucleate the cavity. These two types are Wedge shaped cracks (W type)

and Round cavities (R type). The former one initiates mostly at grain boundary triple points and are associated with creep conditions involving moderate creep temperatures and high stress levels. The latter one is believed to initiate at the grain boundary ledges and at fine second phase particles at the grain boundary and occurs at higher creep temperatures and lower stresses. As the temperature is raised, the number of cavities per unit length of grain boundary increases in the same way that grain boundary sliding increases with temperature.

This type of fracture due to the grain boundary sliding has been observed by Crowther and Mintz (1986a) and called intergranular decohesion (ID), characterised by flat austenite grain facets, which show particles which are not associated with micro-voids

d- Second phase particles strengthening the matrix:

It has been suggested that the extensive matrix precipitation and the introduction of precipitate free zones, sometimes observed in micro-alloyed steels, concentrates strain at the austenite grain boundaries, hence promoting intergranular fracture and low ductility. (Bernard et al., 1978 ; Wilcox and Honeycombe, 1984 ; Maehara and Ohmori, 1984).

3.4.3.2 INTERGRANULAR FRACTURE IN (γ + α) PHASE

Hot tensile test have been performed on plain carbon and micro-alloyed steels to determine whether the ductility loss associated with the two phase region is responsible for transverse cracking in continuously, cast slabs. Some of these tests have produced conflicting results. Bernard et al., (1978), have observed that the austenite/ferrite transformation leads to an improvement in hot ductility for a range of Al and Nb containing steels. Wilcox and Honeycombe (1984) reported little influence of transformation on the hot ductility of C-Mn, C-Mn-Al, and C-Mn-Nb-Al steels. In contrast, other authors have reported that ductility troughs were associated with the two phase region for C-Mn and C-Mn-Al steels. (Crowther and Mintz, 1986a ; Mintz and Arrowsmith, 1979; Yamanaka et al, 1980; Wray 1981; Suzuki et al., 1982). In these troughs, fracture has been observed to occur within the pro-eutectoid ferrite at second phase particles. Some other investigations have shown that for Al and Nb containing steels, phase transformation is of secondary importance in controlling hot ductility, as the loss of ductility associated with AlN and NbCN precipitation is dominant. (Ouchi and Matsumoto, 1982 and Ohmori and Maehara, 1984).

However, relating the loss in ductility to the A_{r3} temperature is often complicated (Thomas et al., 1986), because the γ - α phase transformation is influenced by alloying elements, cooling rate, and strain rate. On the other hand, deformation itself has been shown to raise the

Ar₃ temperature. Bernard et al., (1978), have shown that transformation temperatures determined metallographically from quenched, fractured C-Mn-Nb-Al tensile sample were approximately 50 K higher than those determined by dilatometry, for the same cooling rates. Roberts et al., (1980) and Kozasu et al., (1977), carrying out experiments simulating hot working, have both found after heavy hot deformation that the Ar₃ temperatures can be raised by 100 K.

The mechanisms that have been proposed to control the embrittlement in this region are the continuation of the action of precipitates as described in the previous section in the single phase austenite (Ericson, 1977 and Suzuki et al., 1981) and/or the grain boundary weakness due to strain concentration in the thin ferrite films forming along the austenite grain boundaries causing cavitation around inclusions which link up to give intergranular failure, (Crowther and Mintz, 1986a), as can be seen in Fig.3.4.

This occurs because in the two phase region, ferrite is more ductile than austenite (Robbins et al., 1967 and Fuchs, 1975). This could be partly due to the higher atomic diffusivity of iron in ferrite and partly to the larger number of slip systems in bcc compared with fcc atomic structure as Robbins et al., (1967) proposed. In addition, the austenite matrix can be hardened further by intergranular precipitates such as NbCN (Mintz and Arrowsmith, 1979 and Wilber et al., 1975), thus enhancing the strain concentration in the softer ferrite phase.

3.4.4 THE LEFT HAND SIDE OF THE TROUGH

In this region, low temperature ductile rupture occurs, (LTDR). Voids nucleated at the second phase particles within the grains, grow during deformation and coalesce to produce fracture (Crowther, 1986). During these fracture processes, local recovery is taking place and this delays the onset of void nucleation and void coalescence (Smallman, 1985) leading to good hot ductility.

3.5 SOFTENING PROCESSES

3.5.1 GENERAL

Deformation of micro alloyed steels at elevated temperatures is a complex material process in which mechanical working interacts with various metallurgical processes such as dynamic softening including recovery and recrystallisation. During hot working, all metals undergo a limited amount of dynamic recovery (Sellars and Tegart, 1972). With increasing strain the process continues in ferritic alloys until a final substructure has been established. In materials of low stacking fault energy such as austenitic alloys, the process goes to an end and the metal can undergo dynamic recrystallisation if sufficiently large strains are reached. The distinct effects of the two different softening mechanisms are shown in Fig. 3.5., for a plain carbon steel, with two levels of silicon. Steel A had been given an addition of 2.91 % Si to stabilize the α phase so that the bcc lattice was retained at 1000°C. i.e. a high stacking fault energy state. Steel B, contained only 0.028% Si, so that it was fcc at the same temperature, i.e. a low stacking fault energy state. It is evident that both the yield stress and steady state flow stress are relatively low in the high stacking fault energy steel A. At the same time steel B, with the very low Si level, gave yield and flow stresses about three times higher, suggesting that the dislocation densities are greater in the low stacking fault energy steel.

The inter-relationship of stacking fault energy, to dis-

location density has been generally accepted. Swann and Nutting (1961), Hirsh (1958) and Heidenreich and Shockly (1948), have all concluded that metals deformed under similar test conditions, show increasing dislocation density as the stacking fault energy is reduced. Since the stored energy of deformation is a function of the elastic strain energy contributed by dislocations (Cotterill and Mould, 1976), the stored energy will be proportional to dislocation density. These high levels of stored energy in low stacking fault energy materials are considered essential to obtain the differences in stored energy levels required to nucleate dynamic recrystallisation as reported by Tegart (1967).

In ferritic alloys with high stacking fault energy, dynamic recovery is the sole softening mechanism, where, climb and cross slip are relatively easy. As a result, the misorientation of the sub-boundaries is maintained sufficiently low so that they are unable to migrate as grain boundaries of recrystallisation nuclei (Dieter, 1984). If climb and cross slip are not easy processes another mechanism is established (dynamic recrystallisation) at larger strains in the low stacking fault energy materials, such as austenitic alloys. In these materials, the smaller subgrains and densely tangled dislocations in the cell walls encourage the creation of new grains. When the misorientation between subgrains reaches approximately 10° , the subgrains act as recrystallisation nuclei and dynamic recrystallisation then occurs as the softening process, as reported by Dieter (1984).

3.5.2 DYNAMIC RECOVERY

The micro-structural evidence for dynamic recovery has been reviewed by Jonas et al., (1968). This review indicates that the grains of the original micro-structure become elongated in the direction of hot working and appear fibrous. This distortion of grain boundaries is accompanied by subgrain formation until the final micro-structure is reached with narrow and well defined subgrains. Subgrain size and mis-orientation, and dislocation density between the subboundaries remain constant. A situation is reached in which dislocation generation and annihilation rate are equal, and the strain hardening rate is reduced to zero, leading to the establishment of steady state flow, as shown in Fig.3.5.

For iron, it has been shown that the subgrains assume their final size at strains of 0.2-0.3 for strain rates of 0.05 to 1.5 S^{-1} (Glover and Sellars, 1973). The mean subgrain size is increased by increasing temperature and decreasing strain rate, and is related to the Zener-Holloman parameter Z , by:

$$d_s^{-1} = a + b \log Z \quad (3.9)$$

where, d_s is the mean subgrain diameter, a and b are constants and $Z = \dot{\epsilon} \exp(Q/RT)$, (McQueen et al., 1967).

It should be noted that, solid solution alloying additions to pure metals reduce the stacking fault energy, and hence makes dynamic recovery more difficult, and as a consequence, the flow stress is increased.

It would be expected that the remedial effect of dynamic recovery on intergranular fracture of micro-alloyed steels

in the austenite phase is very limited, since such a process does not readily occur. In materials in which dynamic recovery occurs readily such as ferritic alloys, the initiation of "W" type cracks could be diminished, since they have low flow stresses and flow readily at triple points to relieve stress concentrations. In addition, metals which are susceptible to dynamic recovery may form "scalloped" grain boundaries, which diminishes grain boundary sliding and hence reduces intergranular crack nucleation (McQueen and Jonas, 1975). In such metals, ductility increases with increasing temperature, because the stress relieving processes are more sensitive to temperature than those promoting crack nucleation (Gittins, 1977).

3.5.3 DYNAMIC RECRYSTALLISATION

One of the most important experimental factors involved in the analysis of dynamic recrystallisation is the need for accurate flow curves. In the initial stages of hot deformation, the flow stress raises to a maximum and then falls, either to a steady state stress (at low temperatures and high strain rates, i.e. high Z) or to a periodic value oscillating about a mean (at high temperatures and low strain rates, i.e. low Z), as Tegart and Gittins (1977) reported. According to Rossard (1973), nucleation of dynamic recrystallisation occurs at a critical strain level, ϵ_c , which is less than the strain at the peak stress, ϵ_p , as measured from the flow curve and is given by :

$$\epsilon_c = 0.83 \epsilon_p \quad (3.10)$$

Although, for all practical purposes the strain to the peak stress can be regarded as the critical strain for recrystallisation (Tegart and Gittins, 1977).

ϵ_c increases as the initial grain size, d_0 , increases (Roberts et al., 1979 ; Sellars, 1980 ; Ruibal et al., 1984) and as Z increases (McQueen and Jonas, 1975 ; Sellars, 1980).

At low strain rates nucleation of dynamic recrystallisation has been observed at the existing grain boundaries (Luton and Sellars, 1969 ; Roberts et al., 1979). At higher strain rates recrystallisation nuclei throughout each grain have been noted, (McQueen and Bergesson, 1972).

Metallographic studies have established that the mechanism of nucleation is the bulging of an existing grain boundary which has been pinned by sub-boundaries to produce a scalloped boundary due to the strain energy differences across the boundary (McQueen and Jonas, 1975 ; Luton and Sellars, 1969).

The periodic oscillations observed in the region beyond the peak stress, have been explained by Sellars and Tegart (1966), as follows:

As deformation continues, the stored energy within the recrystallised grains increases until the critical level for recrystallisation is reached. At this stage, the flow stress falls as recrystallisation proceeds again, and the repetition of this process leads to the cyclic flow curves observed for low strain rate deformation.

3.5.4 INFLUENCE OF DYNAMIC RECRYSTALLISATION ON HOT DUCTILITY

Solid solution alloying reduces the rate of dynamic recovery, and hence might be expected to promote dynamic recrystallisation. However, the rate of grain boundary migration is also reduced by alloying additions and this reduces the rate of dynamic recrystallisation. For some alloys this reduction in the rate of dynamic recrystallisation can lead to the formation of the ductility trough. The technical importance of this phenomenon for the production of controlled rolled micro-alloyed steels has meant that the subject has been investigated extensively. Many investigations (LeBon et al., 1975 ; Sekine and Maruyama, 1976 ; Weiss and Jonas, 1979 ; Ouchi and Okita, 1982) have all shown that increasing Nb additions increases ϵ_p . Weiss and Jonas have shown that this effect is due to solute drag on grain boundaries at high strain rates, and the dynamic precipitation of fine NbCN at slower strain rates, which reduces grain boundary migration rates. The nucleation of dynamic recrystallisation can be delayed until the dynamic precipitation of NbCN is complete. Similar studies on the influence of V on dynamic recrystallisation by Akben et al., (1981) have shown that V in solution retards dynamic recrystallisation, though not to as great extent as Nb. Dynamic precipitation of VCN also increases ϵ_p .

An increase in hot ductility with the onset of dynamic recrystallisation has been reported for a wide range of austenitic alloys including:

Fe-25% Ni (White and Rossard, 1968), in a range of Fe-Ni alloys, (Evans and Jones, 1976), in Cupro-Nickels (Evans and Jones, 1978), and in austenitic stainless steels (Bywater and Gladman, 1976 ; Ouchi and Okita, 1982). In all these studies, high ductility failures were associated with dynamic recrystallisation. However, dynamic recrystallisation is a necessary requisite for good hot ductility but does not guarantee it, as has been shown by Wray (1975) and Crowther et al., (1987). Although the steels examined exhibited dynamic recrystallisation, they nevertheless failed in an intergranular manner with low ductility.

Studies by Bernard et al., (1978) on the hot deformation of Nb- microalloyed steels also show a ductility trough within the temperature range in which dynamic recrystallisation does not occur, due to the retardation of recrystallisation by the Nb additions, and they use this argument to explain the occurrence of the ductility trough. However, other workers (Ouchi and Matsumoto, 1982), have shown that the complex hot ductility behaviour of Nb containing steels cannot be explained by dynamic recrystallisation arguments alone. They studied the influence of strain rate on the hot ductility of micro-alloyed steels and their results showed that the temperature range of minimum hot ductility did not change with strain rate. They pointed out that since the critical strain for nucleation of dynamic recrystallisation decreased with decreasing strain rate, tests performed at lower strain rates might be expected to have a narrower ductility trough, due to an earlier onset of dynamic recrystall-

isation. In contrast, Wilcox and Honeycombe (1984) have shown that the hot ductility of a C-Mn-Nb steel can increase rapidly with increasing temperature before the onset of dynamic recrystallisation. They concluded, that the precipitation of NbCN, rather than dynamic recrystallisation, was the most important factor controlling hot ductility. However, in a C-Mn-Al and C-Mn-Al-Nb steels, Wilcox and Honeycombe showed that ductility improved when a strain sufficient to nucleate dynamic recrystallisation could be applied before fracture.

3.6 THE INFLUENCE OF STRAIN RATE ON HOT DUCTILITY

The rate at which strain is applied to a specimen can have an important role on hot ductility, (Sellars and Tegart, 1972 ; Sankar et al., 1979). A philosophical model for strain rate effects on hot ductility of steels has been proposed by Norstrom and Johansson (1982) as shown in Fig.3.6. At lower strain rate, recovery is active, which reduces the driving force for dynamic recrystallisation and thereby delays the ductility – improving recrystallisation processes. At higher strain rates, the lack of time again prevents recrystallisation, possibly leading to early transgranular ductile fracture. Thus, the best ductility should occur at intermediate strain rates, especially if the temperature is high enough to allow recrystallisation. The absolute magnitude of the optimum strain rate will depend on the creep, recovery and recrystallisation characteristics which depend on steel composition. However, there is a lack of experimental data to prove the Norstrom and Johansson model.

Of particular relevance to the continuous casting process are those studies conducted above 700 °C in the strain rate range $10^{-4} - 10^{-3} \text{ S}^{-1}$, as these are believed to be the conditions experienced during the continuously cast slab straightening process (see chapter 2). For irons and steels tested under these conditions, the influence of strain rate on hot ductility is temperature and composition dependant, and three temperature regimes can be recognized :

A- FROM THE SOLIDUS TEMPERATURE TO 1200 °C

Suzuki et al., (1982), investigated the influence of strain rate (10^{-3} — 20 S^{-1}) on hot ductility for a high purity electrolytic iron and for a 0.4% C steel. They found that ductility near the melting point does not depend on strain rate. Similar results have been obtained by Norstrom and Johansson (1982), after examining two low-alloy carbon steels and two austenitic stainless steel in the strain rate range 2.5×10^{-4} — $5 \times 10^{-2} \text{ S}^{-1}$.

This behaviour has been related to the presence of a liquid film along the grain boundaries or dendrite interfaces. Other workers (Weinberg, 1979 ; Rogberg, 1983) have reported that the embrittlement near the melting point is due to incipient melting at grain boundary and/or dendrite interface, and thus strain rate would be expected to have no influence on the fracture process in this temperature range.

B- FROM 1200 TO 1000 °C

In this temperature range, conflicting results have been reported for the influence of strain rate on hot ductility. While Lankford (1972) has reported no influence of strain rate on hot ductility for a range of plain carbon steels, Suzuki et al., (1982) have reported an increase in ductility with decreasing strain rate between 5×10^{-3} and 20 S^{-1} for a plain carbon steel. Yasumoto et al., (1985) have also reported an increase in hot ductility as the strain rate is reduced from 2.3 S^{-1} to 0.01 S^{-1} for a range of C-Mn-Al steels. Suzuki et al., and Yasumoto et al., have

explained their results as being due to coarsening of (Fe,Mn)S and (Fe,Mn)O intergranular precipitates occurring during the long test times at slow strain rates, which reduces the embrittling effect of these precipitates.

C- FROM 1000 TO 700 °C

In this temperature range, it is fairly well agreed that decreasing the strain rate, reduces the hot ductility, Fig. 3.7.

This behaviour, has been found by Wray (1975) on pure irons, and by Carlsson (1964), Bernard et al., (1978), Mintz and Arrowsmith (1979), Ouchi and Masumoto (1982) Wilcox (1982), Crowther et al., (1987) and Maehara and Ohmori (1984) on plain carbon and micro-alloyed steels.

In addition, some investigators (Mintz and Arrowsmith, 1979 ; Maehara and Ohmori, 1984) have reported a broadening of the ductility trough with decreasing strain rate. Ouchi and Matsumoto (1982) have explained this result by the fact that an increase in the strain rate leads to a decrease in grain boundary sliding as shown in Fig. 3.8. by taking the $\epsilon_{gb} / \epsilon_t$ as the measure of grain boundary sliding, where ϵ_{gb} is the grain boundary strain, and ϵ_t the total strain.

In addition, an increasing strain rate will produce an increase in the grain boundary migration velocity, v , through the equation of Lucke and Stuve (1963):

$$v = M(C, T) P(C, \dot{\epsilon}, T) \quad 3.11$$

where M is the grain boundary mobility and includes terms

describing the influence of composition C, and temperature, T, and P is the driving force for grain boundary migration. As pointed out by Evans and Jones (1976) and Mintz and Arrowsmith (1979), a rapidly migrating grain boundary isolates cracks, inhibiting their propagation thus improving ductility.

3.7 THE INFLUENCE OF GRAIN SIZE ON HOT DUCTILITY

The majority of investigations on the influence of grain size on hot ductility have shown that ductility decreases with increasing grain size, Fig. 3.9, for a wide range of metals and alloys including copper (Fleck et al., 1970), alpha brass (Taplin and Whittaker, 1963), austenitic steels (Bywater and Gladman, 1976), and plain carbon steel (Crowther and Mintz, 1986b). For micro-alloyed steels, which are susceptible to transverse cracking during the straightening of hot continuously cast strands, cracks were associated with coarse austenite grains, and Schmidt and Josefsoon (1974) have reported that such cracking is reduced, when the formation of coarse austenite grains is prevented, by the use of suitable secondary cooling patterns.

Indeed, many hot tensile studies, have determined coarse grain size to be associated with lower ductility (Suzuki et al., 1981 ; Bernard et al., 1978 ; Offerman et al., 1981 ; Mintz and Arrowsmith, 1980), whilst several other studies found fine grains to be worse (Weinberg, 1979); Funnell and Davies, 1978 ; Funnell, 1980), and some even conclude that grain size is not important in influencing hot ductility (Ouchi and Matsumoto, 1982 ; Carlsson, 1964). The major problem in such studies has been in distinguishing between the effects of grain size, precipitation and thermal history of the steel on hot ductility, because they are intrinsically related to each other and any one of them could be highly influential to hot ductility.

These difficulties lead Crowther and Mintz (1986c), to design an exercise for three micro-alloyed steels which would isolate the influence of grain size on hot ductility from that of precipitation. By heating above the solution treatment temperatures, a wide range of austenite grain size prior to testing was obtained. Precipitation for each steel remained constant but grain size varied. They concluded, that although grain size was important, precipitation had the dominant influence on hot ductility.

The reason for coarse grain structures having poor hot ductility has been explained by Evans (1969) as being due to the increased sliding rate producing an increased grain boundary cavity growth rate. However, it is now believed that creep ductility, when intergranular fracture occurs, is controlled by the final stages of fracture, rather than the nucleation and early stages of growth of grain boundary cavities (Fleck et al., 1970 ; Kutumba et al., 1975). In the later stages of crack growth, a propagating grain boundary crack must grow through triple points, and it seems likely that the ease of propagation of a crack through a triple point, and the number of triple points encountered, will be an important factor in determining creep ductility. Thus a coarse grained material, with few triple points than a fine grained material will be more susceptible to intergranular cracking. It has also been pointed out that the crack aspect ratio will influence the ease of crack propagation through triple points (Fleck et al., 1970). In coarse grained material, crack aspect ratio and hence stress concentration at the crack tip, will be

high, allowing such cracks to readily grow through triple points. The reverse is true for fine grained materials.

3.8 INFUENCE OF STEEL COMPOSITION ON HOT DUCTILITY

3.8.1 GENERAL

The composition of the steel plays an important role in determining hot ductility and has received the greatest attention by researchers. The hot ductility studies of Suzuki et al., (1981), Suzuki et al., (1982) and Robbins et al., (1967) on high purity iron, revealed no intergranular fracture in the austenite phase, whilst plain carbon and micro-alloyed steels (Crowther and Mintz, 1986a ; 1986b), show embrittlement in this phase. These observations suggest that intergranular fracture is not possible without some precipitates or second phase particles (Thomas et al., 1986); and reveal the importance of even minor amount of residual elements in the steels.

For micro-alloyed steels tested in the temperature range 700-1000 °C at strain rates in the range 10^{-4} - 10^{-3} S⁻¹, three groups of elements may be defined:-

Nitride and/or Carbide forming elements (precipitation);
Oxide and/or Sulphide forming elements (inclusions) and
elements with a tendency to segregate to the boundaries.

3.8.2 NITRIDE AND/OR CARBIDES FORMING ELEMENTS

A- NIOBIUM AND ALUMINIUM

Nb and Al are known to be the most influential elements in reducing hot ductility and the mechanism is quite similar. Both elements and other refining elements such as V are dissolved in the austenite at higher temperatures and precipitate during cooling preferentially at the austenite grain boundaries (Wilcox and Honeycombe, 1980); These fine

particles are effective in preventing grain boundary mobility at high temperature, leading to intergranular failure. Usually, Nb precipitates as $\text{NbC}_{0.8} \text{N}_{0.25}$ in high N steels (Ouchi and Matusumoto, 1980 ; Watanabe, et al., 1977), or $\text{NbC}_{0.75}$ in low N steels (Gielen, 1981), whereas Al precipitates as AlN under appropriate set of conditions at elevated temperatures. Increasing any one of them causes a further drop in ductility values (Mintz and Arrowsmith, 1979) as can be seen in Figs. 3.10-3.11.

Nb is even more influential than Al in extending the trough to higher temperatures (Suzuki et al., 1982 ; Mintz and Arrowsmith, 1979). Mintz and Arrowsmith, reported that increasing the Al in a Nb containing steel aggravates the effect of the NbCN precipitates, causing them to become finer, more closely spaced and concentrated at the grain boundaries. No AlN was found to be present in their steels.

As well as influencing hot ductility by the pinning effect of these particles, it has been suggested that the extensive matrix precipitation of NbCN sometimes observed in Nb containing steels, concentrates stress at the austenite grain boundaries, and hence promotes intergranular fracture and low ductility. (Crowther and Mintz, 1986c ; Bernard et al., 1978 ; Wilcox and Honeycombe, 1984 ; Maehara and Ohmori, 1984) .

The experimental conditions such as strain rate or holding times at test temperatures does affect the precipitation kinetic of these elements. For example, deformation accelerates the precipitation of NbCN in austenite.

The dynamically precipitated NbCN particles are finer than the equivalent static precipitation at the same test temperature (Weiss and Jonas, 1980). This led Mintz and Arrowsmith (1979), to suggest that dynamic precipitation of NbCN would have a greater detrimental effect on hot ductility than static precipitation. On the other hand, precipitation of AlN occurs slowly after solution treatment, but the rate increases by the application of strain (Vodopivec 1973), and it has been shown by Vodopivec (1978) and Wilcox (1982) that static AlN precipitation as opposed to dynamic is more detrimental to hot ductility. The slow rate of AlN precipitation, means that under appropriate cooling conditions, Al has little influence on hot ductility. Mintz and Arrowsmith (1980), showed that Al additions to a plain carbon steel made no difference to hot ductility, when the steels were cooled from solution to test temperature at 60 °C/min. This cooling rate was sufficiently high to suppress AlN precipitation.

B- VANADIUM

V is another common micro-alloying element in the steel, and it appears from the literature that this element has a less detrimental effect on the hot ductility of steels than Nb and Al, (Crowther et al., 1987 ; Mintz and Arrowsmith, 1980), as can be seen in Fig. 3.12. Crowther et al., (1987)

Crowther et al., (1987), attributed this behaviour to the presence of V(C,N) mostly in the matrix and only on occasions at the austenite grain boundaries. Offerman et al., (1981) and Mintz and Arrowsmith (1980), believe that V

acts in a similar manner to Nb but has a reduced effect because of the higher solubility of VN in austenite.

However, some workers claim that V may improve hot ductility (Irvine and Pickering, 1957) particularly at lower temperatures since it hinders AlN precipitation (Blum et al., 1966). Coleman and Wilcox (1985), showed the slight detrimental effect of V can be reduced by the addition of Al. They explained these results by the decrease in intergranular VN precipitation, due to the preferential formation of AlN. This produces a reduction in matrix hardening by VN, and hence a more uniform strain distribution between matrix and grain boundary.

C- TITANIUM

Ti is the unique nitride former, which is beneficial to hot ductility. This beneficial effect has been attributed to the reduction of N available to form NbCN (Ouchi and Matsumoto, 1982) or AlN (Coleman and Wilcox, 1985).

Ti combines preferentially with N at higher temperatures and precipitates randomly as a TiN stable compound due to its lower solubility, leaving less N for the subsequent precipitation of detrimental nitrides.

Mintz et al., (1980) investigated the influence of Ti on hot ductility of micro-alloyed steels using hot tensile tests and a cooling rate from the solution temperature of 60 °C/min., to approximate that experienced during continuous casting. They noted an improvement in the hot ductility of a C-Mn-Al steels with Ti additions. However, these

results could not be explained by the preferential formation of TiN as opposed to AlN, since the rapid cooling rate employed suppressed the precipitation of AlN. They attributed the observed improvement of ductility to the fine austenite grain size produced by the stable TiN precipitates.

D- NITROGEN

It is reasonable to suggest that N is detrimental to hot ductility, since nitride precipitates (Al or Nb) are largely responsible for lowering ductility. This has been proved experimentally in many investigations (Mintz and Arrowsmith, 1980 ; Ouchi and Matusumoto, 1982 ; Offerman et al., 1981). However, its effect is not as dramatic as Al or Nb (Thomas et al., 1986).

E- CARBON

Mixed views have been reported on the effect of C on hot ductility of micro-alloyed steels. While Ouchi and Matsumoto (1982) and Maehara et al., (1985), suggest that increasing the C in the range 0.05 to 0.3% has no effect on hot ductility of Nb containing steels, Hannerz (1985) and Suzuki et al., (1984a) found an improvement in hot ductility on raising the C content in a similar C range for C-Mn-Al steels. However, it appears that the role of C on hot ductility of micro-alloyed steels is unclear and more work must be done to establish this role.

For plain carbon steels, Crowther and Mintz (1986a) have investigated the hot ductility behaviour in the temp-

erature range 700 - 1000 °C. They found that raising the C content from 0.04 to 0.28% caused the trough to move to lower temperatures in agreement with the observed changes in transformation temperature. Failure was by strain concentration in the softer ferrite phase enveloping the austenite grains, causing void formation at MnS inclusions with gradual crack linkage leading to intergranular failure. However, raising the C level above 0.28% caused a change in fracture mode. Instead of moving the ductility trough to lower temperatures in accordance with a lower transformation temperature, the temperature of the start of the trough was raised by over 100 K. Failure was now by grain boundary sliding in the austenite.

3.8.3 OXIDE AND/OR SULPHIDE FORMING ELEMENTS

A- MANGANESE AND SULPHUR

Kiessling (1968) has suggested that hot shortness exhibited by some steels in the temperature range 900 - 1150 °C, is due to the presence of the low melting point compound FeS, which forms liquid films at the austenite grain boundaries, and a theoretical Mn/S ratio of 1.7 is required to prevent its formation. In practice much higher ratios are commonly used. Suzuki et al., (1982) and Lankford (1972) reported that a ratio greater than 20 is required to remove the detrimental effect of FeS on the hot ductility.

However, Wright and Quarrell (1962) and Ouchi and Matusumoto (1980) have reported that a high Mn level (>1.6) reduces the hot ductility, possibly due to the matrix hardening. Also, S itself is detrimental to hot workability even when the Mn/S ratio is sufficiently high to prevent FeS formation (Bellot and Gantois, 1978). High S steels have a larger volume fraction of MnS inclusions which can reduce the hot workability. They are particularly damaging at high temperatures (1000 - 1200 °C) and at high strain rates ($> 10^{-3} \text{ S}^{-1}$). Increasing S content both deepens (Lankford, 1972) and widens (Suzuki et al., 1982 ; Weinberg, 1979) the hot ductility trough as can be seen in Fig.3.13. Suzuki et al., (1982) have identified sulphides and oxides on intergranular fracture surfaces, whilst Yasumoto et al., (1985) have shown using carbon extraction replicas, that intergranular failures were associated with extensive grain boundary and matrix precipitation of (Mn,Fe)S.

It is unlikely that this form of high temperature embrittlement influences the transverse cracking of micro-alloyed continuously cast slabs, as these grades of steels typically have Mn/S ratios greater than 70, a composition which is not susceptible to this form of cracking (Weinberg, 1979).

Mintz (1979), simulated the continuous casting of a Nb containing steels using a Gleeble machine, and has shown that S levels in the range 0.001 to 0.022 Wt. % gave identical reduction of area values in the temperature range 750 - 1000 °C. He suggested that, it is the amount of S taken back into solution and reprecipitated at the austenite grain boundaries prior to deformation which controls the hot ductility, and on reheated samples this would be the same, in accord with Turkdogan et al., (1955) solubility data.

Turkdogan et al., (1955), have shown that the maximum solubility of S at 1330 °C, (the solution temperature used in the test), for an inclusion surrounded by 1.4% Mn is very low, ~ 0.001%. Thus it is possible that the amount of the MnS precipitated at the boundaries will be very low and independent of S level, provided the total S level is \geq 0.001%.

Coleman and Wilcox (1985) have reported that MnS particles act as cavity nucleation sites during transverse cracking and the removal of MnS particles from grain boundaries by rare earth treatment reduces transverse cracking.

B- OXYGEN

The effect of O on hot ductility of steels is mainly through its influence on the amount and composition of oxide inclusions (Gittins, 1977). Thus, it would be expected that increasing the O content reduces hot ductility by increasing the volume fraction of oxide inclusions. However, O has been seen to have only a slight deleterious effect (Tanaka et al., 1981), presumably due to its contribution to (Fe,Mn,Al) inclusions and reduction in internal cleanliness.

C- MISCH METALS

In general less information is available on the effect of these elements (Ca, Ce, La) on the hot ductility of steels, but they could be beneficial to hot ductility. Coleman and Wilcox (1985) have reported that Ca or Ce additions can produce crack free continuously cast slab, due to the removal of sulphides from the austenite grain boundaries as the rare earth sulphides solidify in the melt. Sopher (1958) reported that additions of misch metal to a plain carbon steel improved its ductility near the melting point. This was attributed to the reduced S levels associated with increasing misch metal additions, and also to the formation of rare earth sulphides, with high melting points.

A pronounced improvement in hot ductility due to the Ca treatment is evident when measuring the ductility of plates in the longitudinal and transverse direction of rolling. Crowther and Mintz (1986d) have shown that Ca treatment of

a C-Mn-Al steel removed the effect of testing direction on the hot ductility of steel and gave rise to a very shallow trough. Recently, Crowther et al., (1987), have shown, that an Al containing steel treated with Ca gave better hot ductility than a calcium free steel. However, this improvement has so far only been noted on samples heated from room temperature to test temperature. Of more importance is the case for samples cooled down after solution treating as this is the continuously cast situation.

3.8.4 ELEMENTS WITH SEGREGATION TENDENCIES

The most noted element for segregation is P, as it segregates strongly between growing dendrites during solidification, and it has been shown that high P levels can lead to internal cracks in continuously cast slabs (Fujii et al., 1975 ; Brimacombe and Sorimachi, 1977). Fractography of internal cracks formed near the solidus temperature has revealed smooth fracture surfaces, which is often indicative of the presence of a liquid film at the time of crack formation. In accordance with this picture, it has been shown that P reduces strength and ductility near the solidus temperature (Sopher, 1958). Thus increasing P levels can lead to increased cracking in steels at temperatures from 1340 °C to the solidus temperature. The influence of P on the formation of transverse cracks, which propagate at much lower temperatures, is less certain. Mintz and Arrowsmith (1979) have reported a slight beneficial effect of increasing P levels on the hot ductility of C-Mn-Nb-Al steels. They have suggested that this is due

to P atoms preventing the nucleation of NbCN at grain boundaries, by occupying NbCN nucleation sites.

However, Ouchi and Matsumoto; (1982) have reported that P levels between 0.004 and 0.026% have no influence on hot ductility of C-Mn-Nb-Al steels.

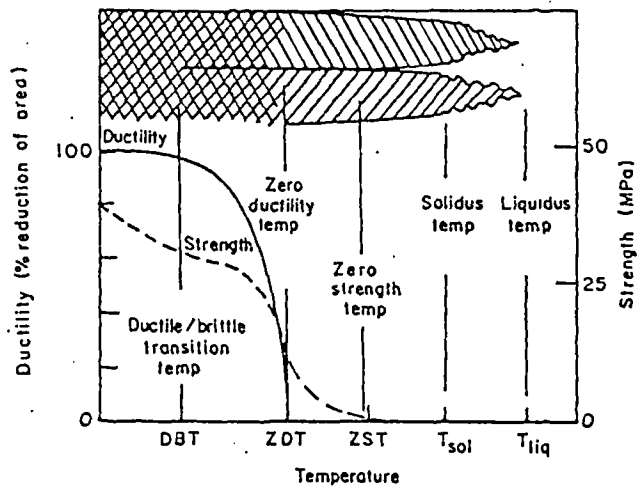


Fig 3.1 Schematic presentation of ductility and strength in the high temperature zone of reduced ductility (after Suzuki et al., 1980)

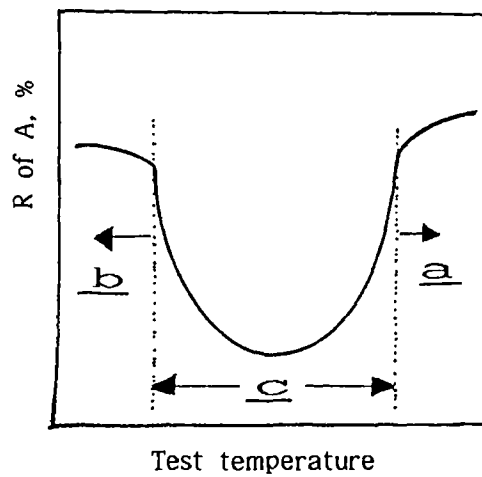


Fig. 3.2 Typical schematic diagram of a hot ductility curve showing various regions.

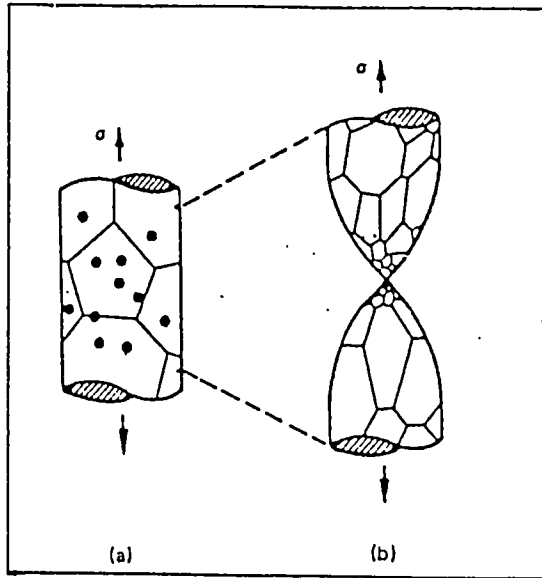


Fig. 3.3 Schematic representation of rupture with dynamic recrystallisation. (After Ashby et al., 1979)

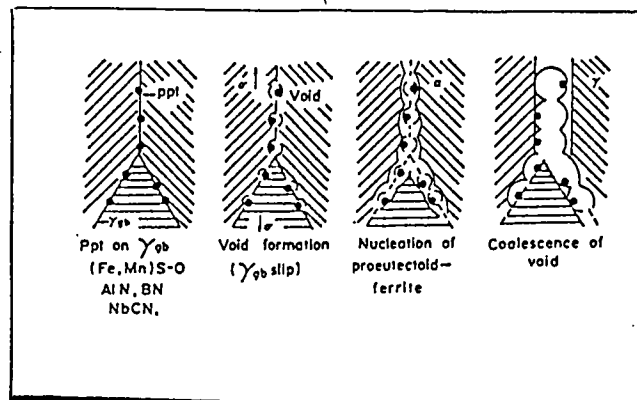


Fig. 3.4 Mechanism for embrittlement in the two phase zone (After Suzuki et al., 1982)

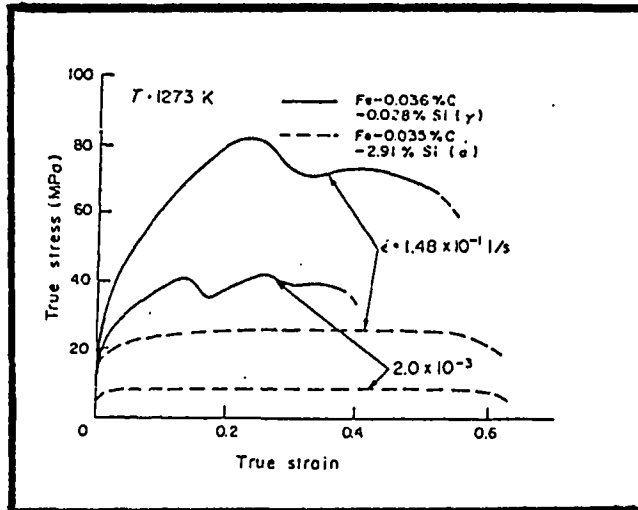


Fig. 3.5 Stress - strain curves for a plain carbon and a 2.91% Silicon steels tested at 1000 °C (After Sakai and Ohashi., 1981)

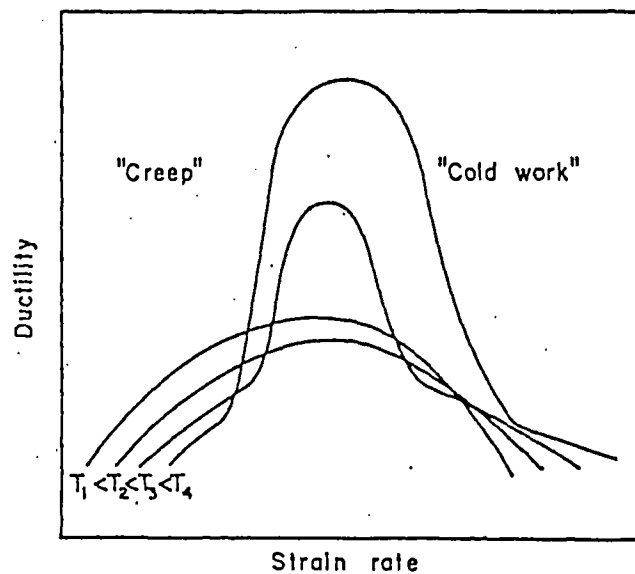


Fig. 3.6 Schematic representation of the effect of strain rate and temperature on the hot ductility of steel (After Norstrom and Johansson, 1982).

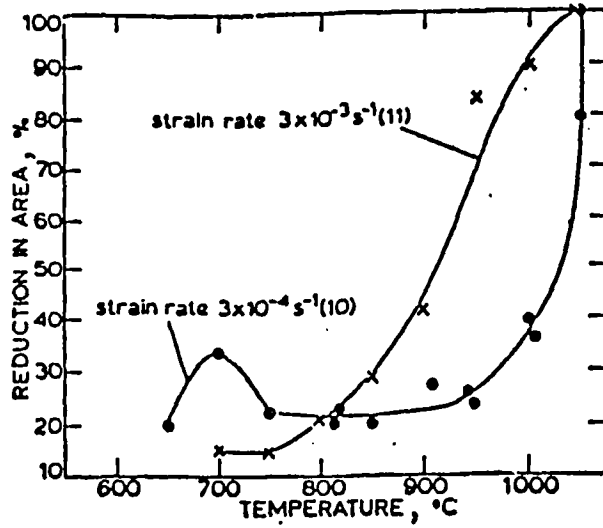


Fig. 3.7 Influence of Strain rate on the hot ductility of a C-Mn-Al-Nb steel. (After Mintz and Arrowsmith, 1979).

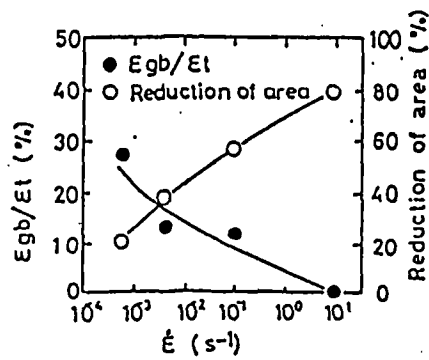


Fig. 3.8 The effect of strain rate on hot ductility and grain boundary sliding in a C-Mn-Nb-Al steel. (After Ouchi and Matsumoto, 1982)

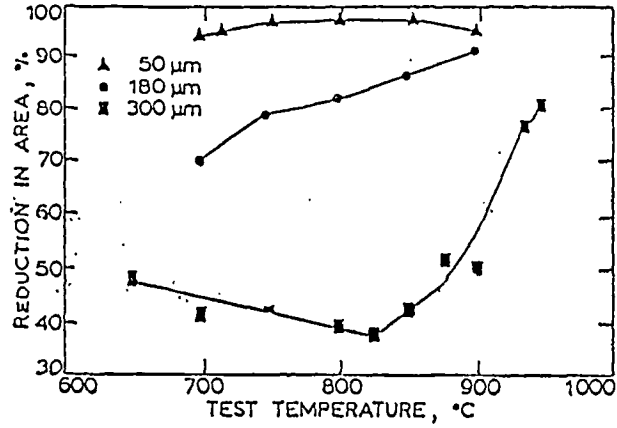


Fig. 3.9 Effect of grain size on hot ductility of a plain carbon steel.
(After Crowther and Mintz, 1986b).

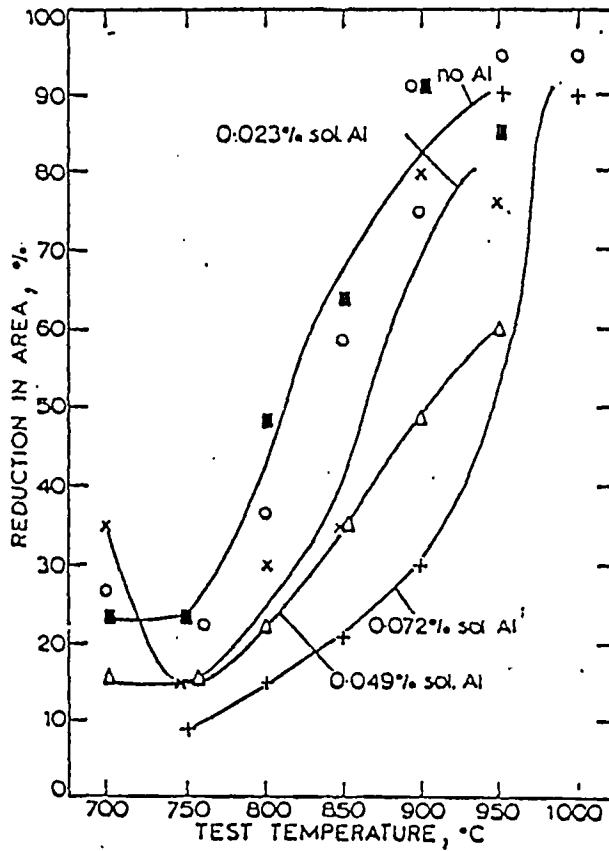


Fig. 3.10 Influence of Al on hot ductility of C-Mn-Nb-Al steels.
(After Mintz and Arrowsmith, 1979).

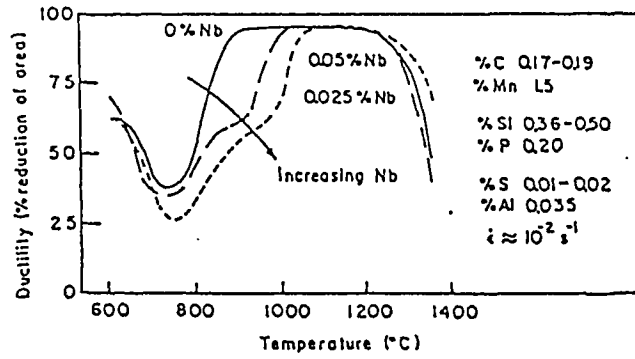


Fig. 3.11 Influence of Nb on hot ductility of C-Mn-Nb-Al steels.

(After Bernard et al., 1978).

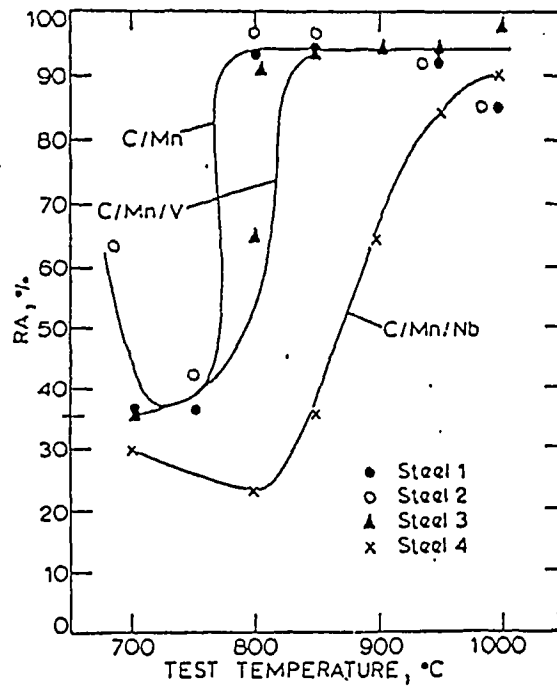


Fig. 3.12 Hot ductility curves for different micro-alloyed steels, showing the effect of V (After Mintz and Arrowsmith, 1980).

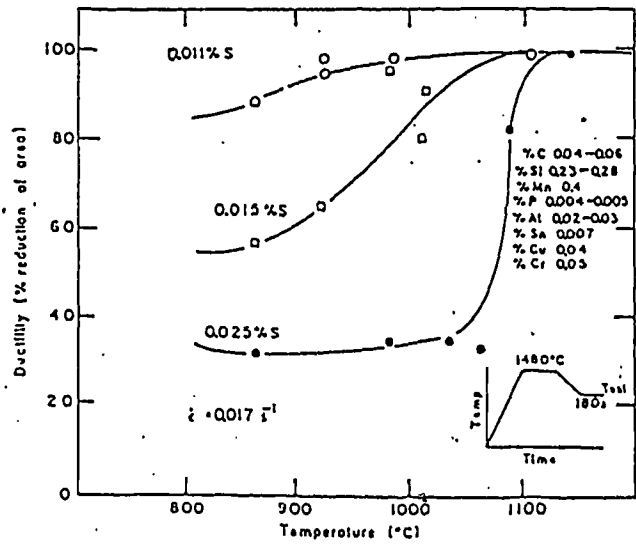


Fig. 3.13 Effect of S on hot ductility of low carbon steel (After Weinberg, 1979).

CHAPTER 4

EXPERIMENTAL TECHNIQUES

4.1 INTRODUCTION

Different methods have been applied to determine the hot workability of steels, but the only ones capable of providing quantitative information of fracture behaviour are the torsion test, impact test and tensile test. In the present work only the tensile test is used, since the first two have higher strain rates and larger strains which are suitable to simulate the hot rolling processes. Results obtained from the tensile test, on the hot ductility of steels, have been found to correlate remarkably well with a variety of cracking problems in the continuous casting process, (Thomas et al., 1986), since such cracks form at strains of between 1 and 2%, which is usually below the value required for sample necking, (Lankford, 1972).

The simulation of the continuous casting process with a hot tensile test, has been questioned owing to the difficulty of reproducing an "as cast" structure by reheating solid material from ambient temperature. Casting in situ and tensile testing (after cooling to test temperatures) presents problems and as a result only few investigations (see chapter 8) have been carried out on as cast materials. However, the hot ductility behaviour of some micro-alloyed steels in the as cast state will be examined in chapter 8, and possibly this represents a better simulation of the true casting conditions.

Another principal disadvantage of the simple tensile test is the difficulty in maintaining a constant true strain rate as straining proceeds. However, hot ductility

is relatively insensitive to change in strain rate, often requiring a change in strain rate of a factor of 10 to produce noticeable changes in ductility, (Suzuki et al., 1982). It is estimated that the changes in strain rate as straining proceeds, are less than this and tests using a constant cross head speed have proved to be adequate for the study of hot ductility, (Crowther, 1986).

4.2 MEASURES OF DUCTILITY

The concept of hot ductility is related to the allowable deformation that metals and alloys can withstand without risk of cracking during hot working. It is an important parameter in steel technology, since it helps to determine the success or efficiency of some of the most important steel processing operations. It plays an important role in casting, in hot working by forging or rolling and in fabrication by welding of the final product, (Wilber et al., 1975). The conventional measures of ductility that can be obtained from the tensile test are:

- a- amount of uniform elongation
- b- the total elongation at fracture
- c- the reduction in area at the point of fracture.

The first measure can be a useful one if little or no necking has occurred, as sometimes happens with brittle intergranular fractures. In the present study it is not a suitable parameter for comparing the wide range of ductility levels expected to occur, when the test temperature is varied over a wide range of temperature.

The second measure, total elongation, makes the comparison

of ductility more difficult, since an appreciable fraction of the plastic deformation will be concentrated in the necked region of the specimen in addition to the uniform elongation. The values of these two components are a complex function of test temperature, strain rate, composition and micro-structure (Crowther, 1986). Beside that, the value of the total elongation, will depend on gauge length L_0 over which the measurement was taken. The smaller the gauge length the greater will be the contribution to the overall elongation from the necked region and the higher will be the value.

The reduction of area does not suffer from this difficulty and provides quantitative information on fracture strain at the point of fracture, irrespective of sample fracture geometries. This value (R of A) is related to the initial cross sectional area, A_0 , and final cross sectional area, A_f , by:

$$R \text{ of } A = (A_0 - A_f) / A_0 \text{ (\%)}$$

Thus, reduction in area is suitable for the comparison of ductility over a wide range of temperatures and is the parameter used in this study.

To obtain the R of A values from fractured tensile samples, the fractured ends were examined under a low power (x20) microscope, and 10 measurements of the diameter at fracture to the nearest 0.05 mm taken. Reduction in Area values were then calculated, assuming that the cross section of the fractured samples remained circular.

4.3 EQUIPMENTS USED IN TENSILE TEST

4.3.1 INDUCTION HEATING TEST

The experimental rig used to heat and test the specimens, consisted of an Induction Furnace and a Hounsfield Tensometer. The equipment is shown schematically in Fig. 4.1. The heating section was a large induction generator connected to copper coils, which were wrapped around a silica glass tube. The tube was supported by the grips of the tensometer in which the specimen was placed. The tube consisted of two glass pipes at right angles to each other. The main pipe, as has been stated previously, contained the Argon gas envelope, necessary to prevent oxidation. The second pipe was connected to an Argon gas bottle and allowed the constant replenishment of the gas envelope as well as creating a back-pressure in the tube to prevent the external atmosphere from entering. An Argon flow-rate of 4 Litre/min. was utilised during heating and testing, but this was increased to 20 Litre/min. after fracture to ensure that the rate of cooling was high enough to prevent any significant precipitation taking place between the test and room temperatures.

The temperature was measured, using a platinum/platinum - 13% rhodium thermocouple connected to a desk top potentiometer. Standard tables were used to convert the Potentiometer reading from milli volts to degree celsius. The thermocouple was placed inside the specimen through the axial 2 mm hole in the specimen, via the tensometer grip, the tip of the thermocouple coming to rest in the centre of the specimen. A ceramic covering was placed over the

thermocouple to protect it during the test.

Tests have been performed at different strain rates and cooling rates from solution temperature to test temperatures. The strain rate depended on the crosshead speed and the gauge length being strained in the copper coils during the test and the exact values will be given in the next chapters. The induction coil provided a zone of uniform temperature, (30 mm) long, as can be seen in Fig. 4.2.

In each case, any sample which failed outside the zone of uniform temperature was discarded. Repetition of 5 tests gave a standard deviation of 6% about the mean reduction in area values of 45%. The sample used in the test is shown in Fig. 4.3, having a diameter of 7.93 mm and 70 mm length.

4.3.2 INSTRON TESTS

The second piece of tensile test equipment used was an Instron model 1026 equipped with a split platinum wound furnace, illustrated in Fig. 4.4. The tensile samples, having a diameter of 5.04 mm and gauge length of 25.4 mm are shown in Fig. 4.5. Temperature control was used by means of Pt v Pt 13% Rh thermocouple connected to a purpose build Isoheat temperature controller unit, capable of maintaining fixed heating and cooling rates.

However, preliminary work in which 3 samples all fractured near the top end of the gauge length, indicated that

there was substantial temperature gradient along the length of the gauge length. The gradient was checked by spot welding three lengths of Chromel-Alumel thermocouples, to the top, middle and bottom of the specimen gauge length. It was found that the top thermocouple gave the highest reading with the bottom registering the lowest. This was found to be caused by the gaps at the top and bottom of the furnace which led to convection currents of the hot air circulating in the furnace. This was overcome by plugging the top and bottom of the furnace with an insulating material (Kaowool) and incorporating an Insulator (Superlux) to the top and bottom of the grips. The temperature gradient was eliminated by this means, the maximum difference in reading between any position along the length of uniform hot zone being $\pm 2^{\circ}\text{C}$. In addition, the thermocouple welded on the specimens surface in the middle position, had shown that the temperature controller unit reading was 10°C higher than the actual sample surface temperature. Test temperatures were taken to be the sample surface temperature, i.e. 10°C less than the temperature controller reading.

Tests were conducted in a flowing Argon atmosphere, and the samples were also nickel plated, as described by Crowther (1986) to prevent decarburization.

Tensile tests were performed using constant crosshead speeds in the range 0.5 - 50 mm/min.. An indication of the scatter on the results was obtained by repeating 5 tensile tests. The standard deviation about the mean reduction in area of 60% was $\pm 5\%$.

4.4 MICROSCOPY EXAMINATION

Three microscopes have been used in the present work:

a- OPTICAL MICROSCOPE:

The microscope used was a Vickers optical microscope attached to a 35 mm Camera. Specimens were prepared from fractured tensile test pieces and were taken from 1 mm behind fracture surfaces. They were then mounted in clear perspex, to allow an identification tag to be incorporated into the mount, using the Metaserv automatic mounting press. The mounted specimens were then polished using wheels of varying coarseness down to 0.25 μm . Etching was accomplished using 2% Nital, washing with Water and drying using Alcohol and a Metaserv specimen dryer.

b- SCANNING ELECTRON MICROSCOPE:

The microscope used was a JEOL T-100, operating at 25 KV. Specimens were prepared from fractured tensile test samples. The fracture surface was removed from the remainder of the tensile test specimen and attached to a brass disc by means of Colloidal Silver. When dry, the samples were ready to be examined.

c- TRANSMISSION ELECTRON MICROSCOPE:

The microscope used was a JEOL 100B TEM operating at 60 KV. The microscope was equipped with an EDAX X-ray, (Energy Dispersive Analysis System). Some fractured samples were prepared to examine under this microscope by means of Carbon Replicas, extracted from ~ 1 mm behind the fracture surfaces. Carbon extraction replica preparation and examination techniques were the same as used by Crowther (1986) and are described in Appendix 1.

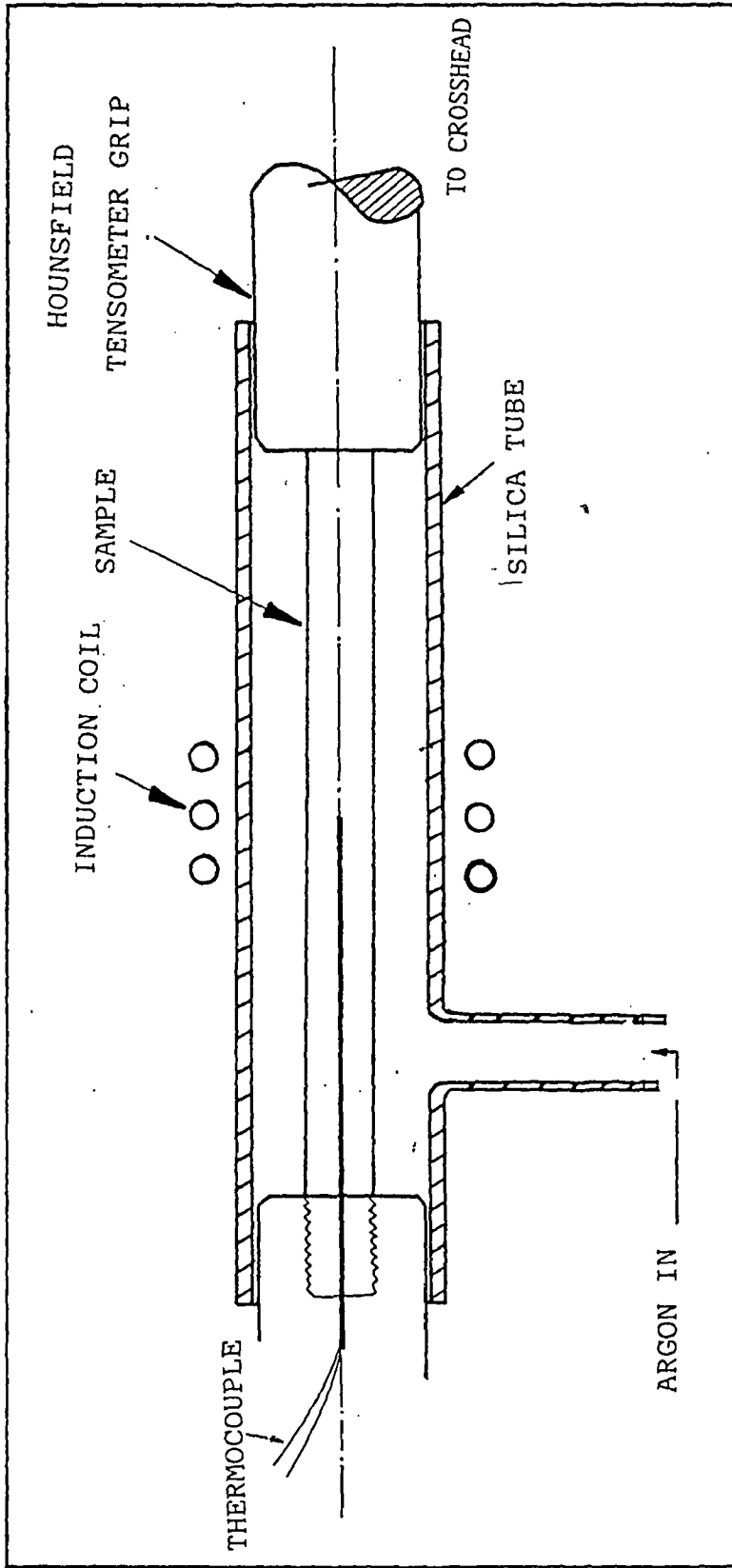


Fig. 4.1 Schematic illustration of induction heating equipment for high temperature tensile testing.

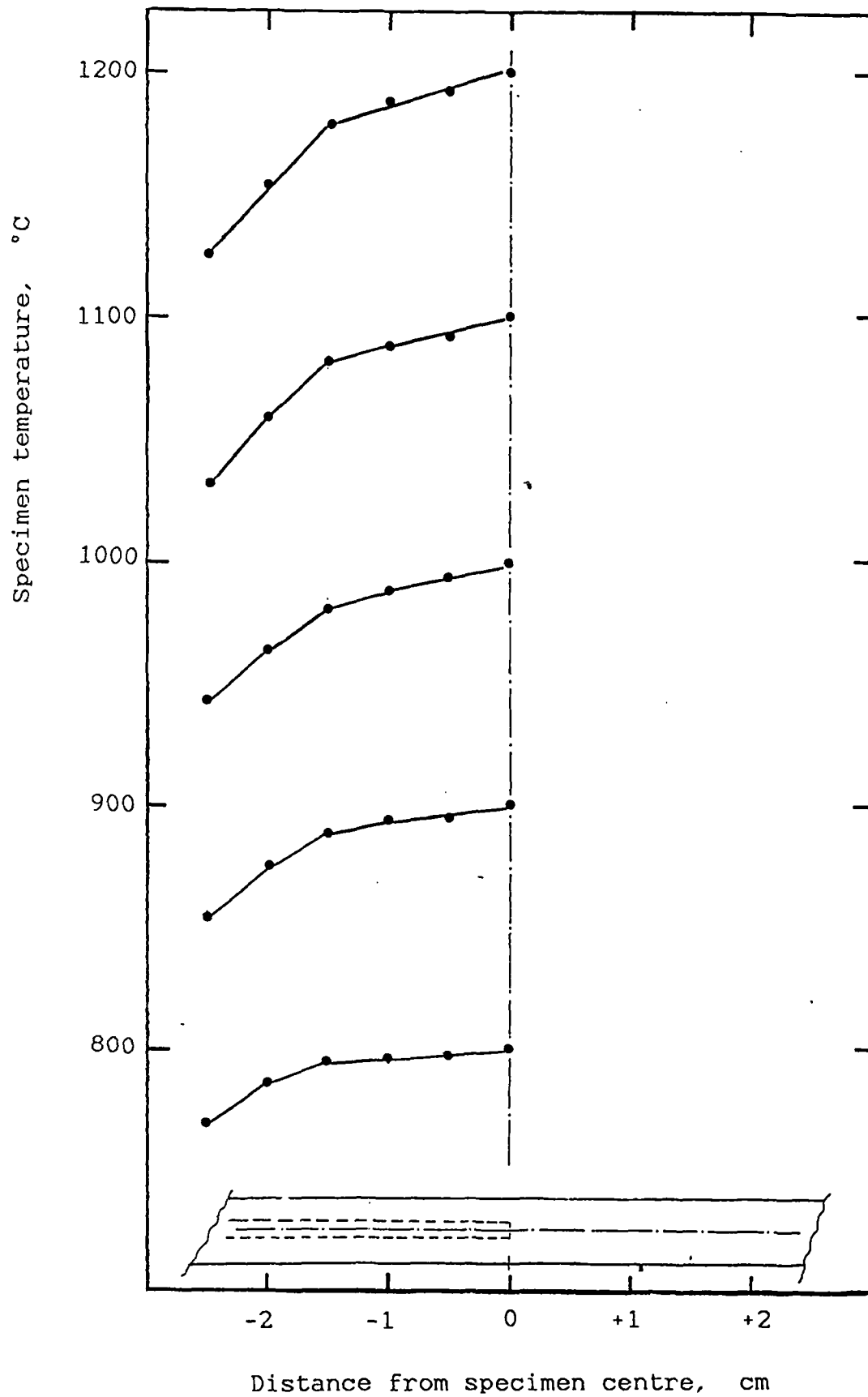


Fig. 4.2 Temperature distribution in Induction test piece at different temperatures.

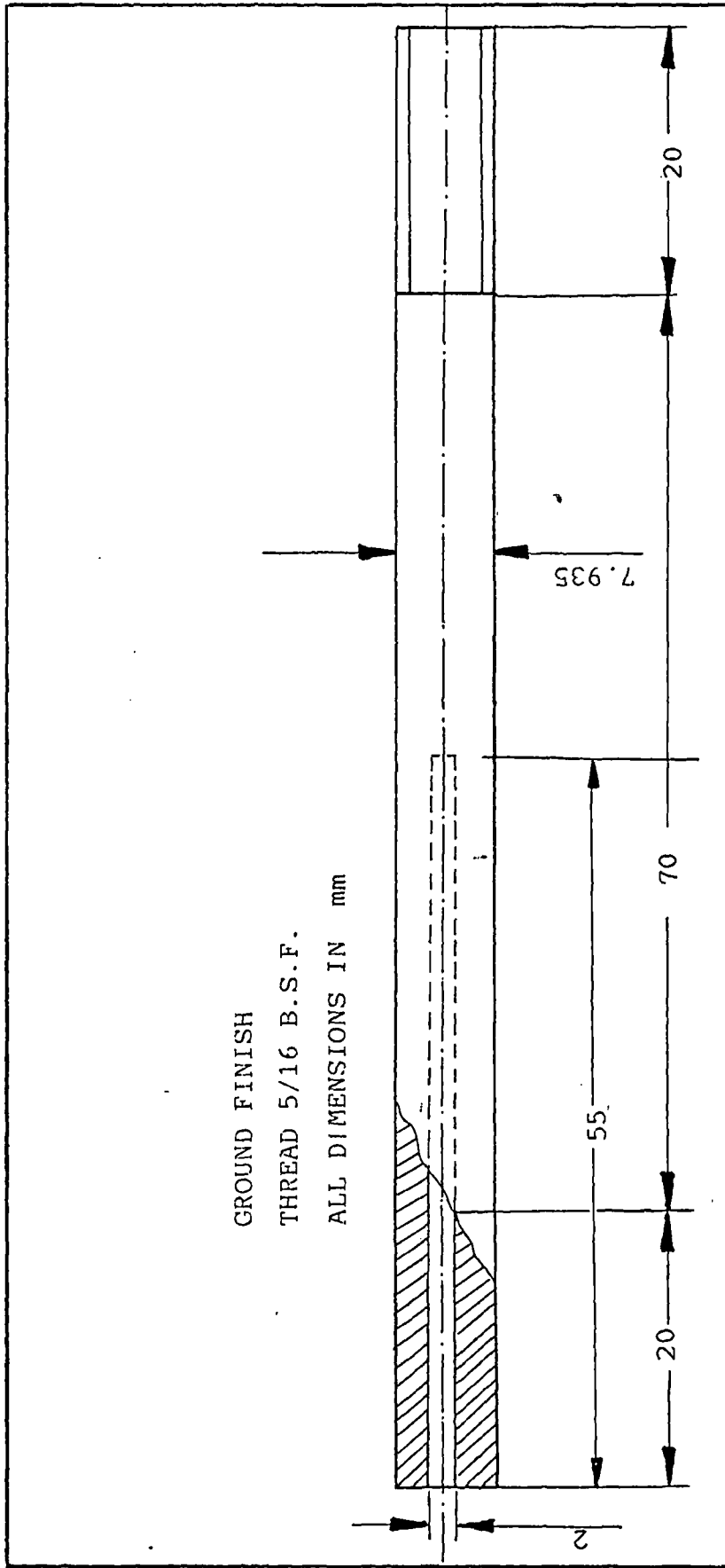


Fig. 4.3 Induction test specimen.

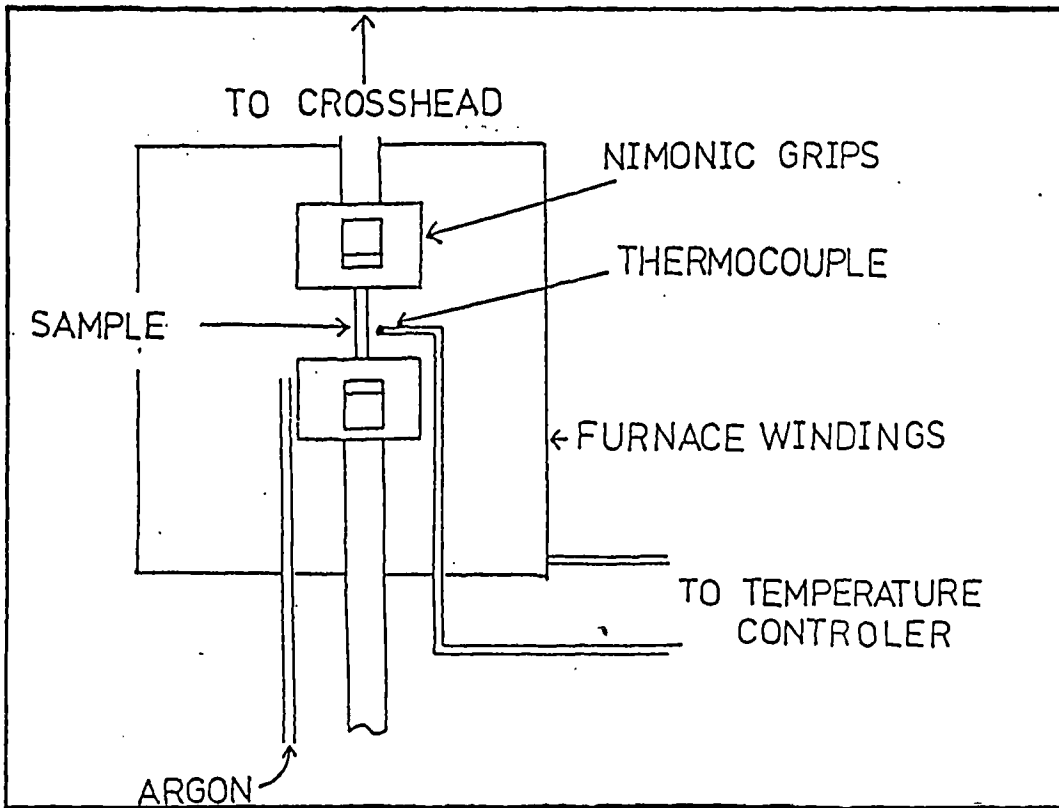


Fig. 4.4 Schematic illustration of Instron high temperature testing equipment

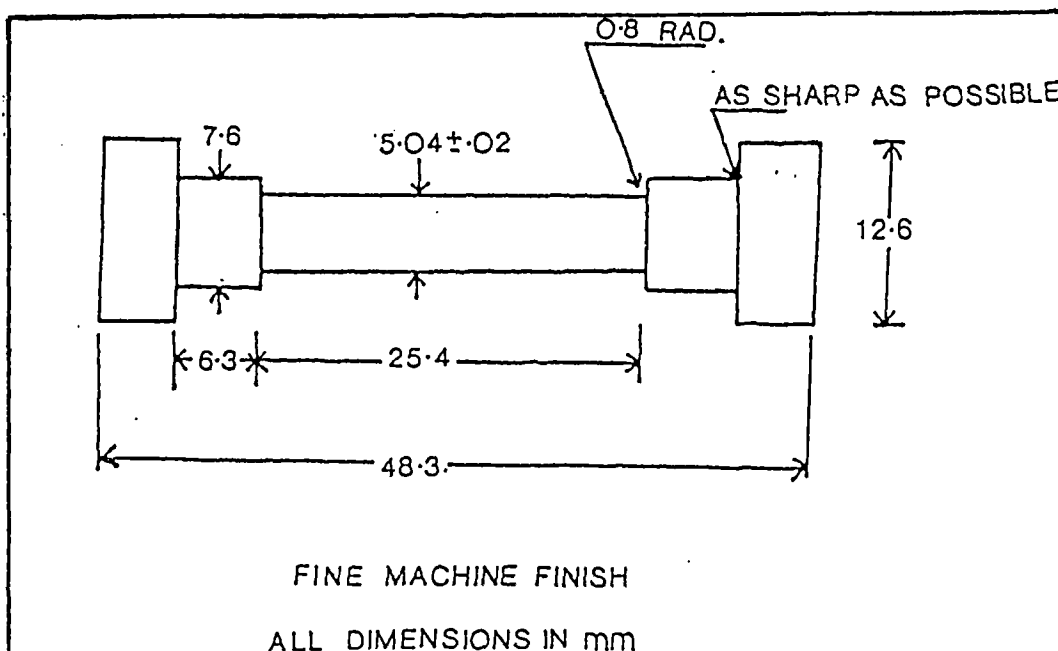


Fig. 4.5 Instron test piece

CHAPTER 5

EFFECT OF CARBON ON THE HOT
DUCTILITY OF MICRO-ALLOYED
STEELS

5.1 INTRODUCTION

Crowther and Mintz (1986^a) have investigated the hot ductility of C-Mn steels with carbon contents from 0.04 to 0.65% in the temperature range 700 to 1000 °C after first heating to 1330 °C to produce a coarse austenite grain size. A ductility trough was found for all the steels examined. Raising the C content from 0.04 to 0.28% caused the trough to move to lower temperatures in agreement with the observed changes in transformation temperature. Failure was by strain concentration in the softer ferrite phase enveloping the austenite grains, causing void formation at MnS inclusions with gradual crack linkage.

However, raising the C level above 0.28% caused a change in fracture mode. Instead of moving the ductility trough to lower temperatures in accord with a lower transformation temperature, the temperature at the start of the trough was raised by over 100 K. Failure was now by grain boundary sliding in the austenite. Generally plain C-Mn steels have higher minimum ductility values compared with the micro-alloyed steels, and are not subject to transverse cracking during continuous casting. As the poor ductility of micro-alloyed steels in the temperature range 700-1000 °C is believed to cause these transverse cracks, the influence of C on hot ductility of these steels is of great interest. In the case of micro-alloyed steels, fracture in the ductility trough is always intergranular and has been generally assoc-

iated with the presence of NbCN and/or on occasions AlN precipitation at the austenite grain boundaries, preventing them from movement and allowing cavitation processes to occur, leading to the intergranular failure.

Previous work on the influence of C on hot ductility of micro-alloyed steels, has tended to suggest that increasing the C level has either no effect or improves the hot ductility. Ouchi and Matsumoto (1982) and Maehara et al., (1985) found that increasing the C in the range 0.05 to 0.3% had no influence on the hot ductility of Nb containing steels. In contrast, Hannerz (1985) and Suzuki et al., (1984a) found an improvement in hot ductility on raising the C content in a similar C content range for C-Mn-Al steels.

Clearly there is a need to establish more precisely the role of C in influencing the hot ductility of micro-alloyed steels and this has formed the basis for the present chapter.

5.2 EXPERIMENTAL

C-Mn-Al and C-Mn-Al-Nb steels were chosen for examination. The range of C examined in the C-Mn-Al steels was 0.056 to 0.15% C and for the C-Mn-Al-Nb steel .014 to .16% C. The full compositions of the Nb and Al containing steels are given in Table 5.1. The steels were supplied as hot rolled 12 mm plate. Tensile samples having a length of 70 mm and diameter 7.93 mm were machined from the plates with their axis parallel to the rolling direction. Hot ductility tensile tests were carried out on a Hounsfield Tensometer and heating was supplied by an induction heater, as described in chapter 4. The samples were protected from oxidation by an Argon atmosphere.

Samples were heated in 15 minutes to 1330 °C, held 5 mins., prior to cooling to test temperatures in the range 700 - 1000 °C at an average rate of 60 °C/min., to simulate the continuous casting processes. Samples were held for 5 mins., at test temperatures before straining to failure at $3 \times 10^{-3} \text{ S}^{-1}$.

Fracture surfaces were examined using a JEOL T100 SEM operating at 25 KV. Carbon extraction replicas were prepared as described in Appendix 1 from transverse sections approximately 1 mm behind the fracture surface, and examined using a JEOL 100 KV, TEM, operating at 60 KV. The austenite grain size prior to testing was established by heating samples to 1330 °C for 5 mins., using a muffle furnace. The samples were then cooled at a rate to give outlinement by ferrite. Austenite grain sizes were then determined using the linear intercept method

Transverse sections, including the place of fracture, were taken from the broken samples and also prepared for metallographic examination. Although cooling rates after fracture were fast, they were not always fast enough to prevent further transformation occurring during cooling to room temperature. However, ferrite formed after fracture could readily be distinguished from that present before, as the former shows side plate formation (Crowther and Mintz, 1986a).

5.3 RESULTS

5.3.1 HOT DUCTILITY CURVES

The curves of Reduction in Area against test temperature for Al and Nb containing steels with different C levels are shown in Figs. 5.1 and 5.2, respectively. All the steels show a marked ductility trough with different depths, widths and positions dependent on the steel composition.

For Al containing steels, with different C levels, ductilities start to fall at 900 °C and reach a minimum of 47 to 50% R of A in the temperature range 750 - 800 °C, dependent on the C content of the steel, Fig. 5.1. The major effect of increasing the carbon content was to shift the hot ductility curve to lower temperature. Raising the C level from 0.056 to 0.15% caused the ductility trough to shift to lower temperatures by approximately 70 °C. For all steels examined, ductility starts to recover, when the test temperature is further lowered to 700 °C.

These shifts in the hot ductility curves to lower temperatures with increasing C contents are consistent with the transformation mainly controlling the hot ductility. The Ae_3 temperatures calculated using Andrews' formula (1965) are indicated in Figs. 5.1-5.2.

The change in the Ae_3 temperature on raising the C level from 0.056% to 0.15% is 45 °C compared to the observed ductility trough shift of 70 °C. The close agreement of the calculated Ae_3 temperatures to the temperature at which ductility starts to fall is due to deformation

raising the transformation temperatures bringing them closer to the equilibrium (Ae_3), previous work by Bernard et al., (1978) has shown that transformation temperatures determined metallographically from quenched, fractured C-Mn-Al-Nb tensile samples were approximately 50 °C higher than those determined by dilatometry for the same cooling rates. However, Roberts et al., (1980) and Kozasu et al., (1977), carrying out experiments simulating hot rolling, have both found after heavy deformation that the Ar_3 temperatures can be raised by 100 °C.

For the Nb containing steels with C contents of 0.1 and 0.16%, ductility starts to fall at 1100 °C and reaches a minimum at 800 °C, whereas for the C content of 0.014%, ductility starts to fall at 950 °C and again reaches a minimum at 800 °C, Fig. 5.2. For all Nb containing steels, ductility starts to recover when the test temperature is further lowered to 750 °C. Raising the C level increased both the depth of the trough and its width. However, the position of the minimum ductility temperature did not change with increase in carbon content, this being constant at 800 °C. For the temperature range in excess of 800 °C differences in hot ductility between the 0.1% and 0.16% steel were small, the higher C steel having ~ 5% lower R of A. However, quite marked changes in hot ductility were apparent when the C level was reduced to 0.014%, a further improvement in hot ductility of ~ 25% in R of A being observed.

5.3.2 STRESS -ELONGATIONS CURVES

The stress - total elongation curves for the steels examined are shown in Figs. 5.3 and 5.4. For Al containing steels, Fig. 5.3, fluctuations in the flow curves at test temperatures $\geq 900^{\circ}\text{C}$ were observed for all the C levels examined. These fluctuations arrowed in the figure are similar to those associated with dynamic recrystallisation, (Wilcox and Honeycombe, 1984).

Dynamic recrystallisation was also observed in the Nb containing steels at test temperatures $\geq 950^{\circ}\text{C}$ for the lowest C steel (0.014%) and at temperatures in excess of 1000°C for the higher C steels (0.11 and 0.16%). The delay in the onset of dynamic recrystallisation on raising the C level can be clearly seen in Fig. 5.4, where dynamic recrystallisation for the highest C steel is only observed at a test temperature as high as 1100°C .

It should be noted that in the two groups of micro-alloyed steels examined, the peak stress increases slightly with increasing C content, in agreement with the work of Crowther and Mintz (1986a) and Suzuki et al., (1984a).

5.3.3 METALLOGRAPHY

Austenite grain size measurements for Al and Nb containing steels with different C levels prior to testing show that grain size is independent of C content in both groups of steels, and is approximately 280 μm in Al containing steels and 490 μm in Nb containing steels.

Evidence for deformation induced ferrite was found, both in Al and Nb containing steels, as can be seen in Figs. 5.5 and 5.6.

In the Al containing steels, ductility starts to fall at the onset of transformation when thin films of ferrite surround the austenite grains allowing strain concentration to occur. For the Nb containing steels, ductility started to fall at 1000 °C and no ferrite outlinement was observed, since this temperature was much higher than the A_{e3} temperature. In this case it was likely that precipitation mainly controlled the hot ductility behaviour of these steels.

However, examination of carbon extraction replicas revealed no AlN precipitates in any of the steels examined in samples fractured at temperatures corresponding to the minimum ductility. Nevertheless, extensive NbCN precipitation both at the grain boundaries and within the matrix was found in the 0.1 and 0.16% C steels (Fig. 5.7) at test temperature of 850 °C (~ the minimum ductility temperature). This NbCN precipitation was sparse in the 0.014% C steel at the same test temperature, Fig. 5.8.

SEM fractography revealed three distinct fracture modes:-

a- High temperature ductile rupture (HTDR) observed in all steels for R of A values $\geq 90\%$, Fig. 5.9.

Wray (1975) has observed this mode of failure in austenitic iron. In the present work, large voids are apparent on the fracture surface and apparently not associated with second phase particles. Crowther and Mintz (1986) showed the same observations in plain carbon steels and micro-alloyed steels (1986c) for R of A values greater than 80%. They believed that the large voids apparent on the fracture surface were originally intergranular cracks, formed at an early stage of deformation. As deformation proceeds, the original grain boundary crack is distorted into an elongated void, until final failure occurs by necking between these voids.

b- Intergranular micro-void coalescence (IMC). This failure mode was observed in all the steels examined, particularly for the Al containing steels, at the lower R of A values, Fig. 5.10 and 5.11. Micro-voids, often associated with second phase particles, cover the facets of the austenite grains.

c- Intergranular decohesion (ID) was observed at the lower ductility values, particularly for the Nb containing steels, Fig. 5.12. This mode of failure is distinguished from the IMC by flat austenite grain facets, which, although showing MnS inclusions, lack micro-voiding. These ID failures were similar to those observed by Crowther and Mintz (1986c), Ouchi and Matsumoto

(1982) and Maehara and Ohmori (1984), and are believed to be due to grain boundary sliding.

It should be noted that, mostly fractures were a mixture of IMC and ID with the tendency for the proportion of ID to increase with increasing test temperature inside the trough (compare Figs. 5.10-5.12).

5.4 DISCUSSION

5.4.1 HOT DUCTILITY BEHAVIOUR OF C-Mn-Al STEEL ON RAISING THE C LEVEL

The precipitation of AlN after solution treatment has been shown to be very sluggish (Gladman and Pickering, 1967). Very high concentration of Al and N are required before AlN is able to precipitate out (see chapter 7). It has been shown by Crowther and Mintz (1985), that for the 0.15% C steel having 0.017% soluble Al and 0.006% N, no precipitation of AlN occurred after holding, for six hours at 850 °C, the temperature corresponding to that for the maximum rate of precipitation. Dynamic precipitation at these concentrations has also not been observed (see Chapter 7). Michel and Jonas (1981) have shown that in order to obtain dynamic precipitation of AlN at a temperature of 875 °C, the solubility product $[Al] \cdot [N] \geq 6.8 \times 10^{-4}$. It is therefore not surprising that no precipitation of AlN has been observed in samples tested in the temperature range 750 to 850 °C, the temperature range of low ductility and intergranular fracture.

It is therefore reasonable to assume that the behaviour for the C-Mn-Al steel should be identical to that shown by the previously examined plain C-Mn steels (Crowther and Mintz, 1986a). In the latter case the ductility trough was shown to be transformation controlled. The failure mode at the minimum ductility temperature was along thin films of ferrite which formed round the austenite grains generally by deformation induced transformation. The softer ferrite allowed strain concentration to occur causing micro-void

coalescence at MnS inclusions, with the voids eventually linking to give intergranular failure. With coarse grained material as in the present case, (280 μm for the Al containing steels and 490 μm for the Nb containing steels), it has been shown that deformation raises the A_{r3} temperature to the A_{e3} and therefore the initial fall in hot ductility should correspond approximately to the A_{e3} temperature and the shift in the hot ductility curve should be related to the change in the A_{e3} temperature.

The present findings are in reasonable accord with this in that the initial fall in hot ductility corresponds approximately to the A_{e3} temperature and the change in the A_{e3} temperature on raising the C level from 0.056% to 0.15% is 45 °C compared to the observed change of 70 °C. Subsequent recovery of ductility at temperatures just below the A_{r3} has been shown (Crowther and Mintz, 1986a), to take place by thickening of the ferrite films surrounding the austenite grains and/or a reduction in the relative difference in strength between the austenite and ferrite phases. The position of the trough can therefore be defined by the A_{r3} temperature on the low side and the A_{e3} on the high temperature side.

The present results are in agreement with those of Hannerz (1985) who showed that increasing the C content from 0.06 to 0.28% in a C-Mn-Al steel improved hot ductility in the temperature range 750 to 900 °C and Suzuki et al's results (1984a), who found similar improvements on increasing the C level from 0.05% to 0.4% C in a silicon and manganese free steel containing aluminium additions.

Raising the C content has been shown to increase the activation energy for dynamic recrystallisation (Crowther and Mintz, 1986a), and it has been suggested that carbon increases the critical deformation required for dynamic recrystallisation encouraging linkage of cracks by grain boundary sliding. Examination of the load - elongation curves in Fig. 5.3, indicate that this may be so, the strain for dynamic recrystallisation at 1000 °C increasing from 4% for the 0.056% C to 5% for the 0.15% C steel.

5.4.2 HOT DUCTILITY BEHAVIOUR OF C-Mn-Nb-Al STEEL ON RAISING THE C LEVEL

The major difference between the C-Mn-Al steels and the C-Mn-Al-Nb steel was the deepening and widening of the trough particularly at the higher C levels (0.1 and 0.16% C).

Such behaviour (Mintz and Arrowsmith, 1980), has been shown to be due to precipitation of NbCN. The overriding importance of precipitation in controlling the hot ductility in these steels might also be deduced from the observation that the minimum ductility temperature, 800 °C, remains the same with C content. Dynamic precipitation is very marked in Nb containing steels after solution treatment and their very poor hot ductility is ascribed to a combination of extensive matrix and grain boundary precipitation and the tendency to form precipitate-free zones which lead to strain concentration at the grain boundaries. Contrary to AlN precipitation, NbCN precipitation has been shown to be

very fast. Static precipitation of NbCN in an 0.16% C steel similar to the one under examinations has also been shown to start after 1 s at 950 °C and dynamic precipitation is extremely rapid (Crowther and Mintz, 1985). Jonas and Weiss (1979), showed that dynamic precipitation can be complete in about 100 s at 900 °C, the temperature corresponding to the maximum rate of precipitation which is significantly less than the time taken to complete a test (approximately 5 minutes).

It therefore may be a reasonable approximation to assume that most of the precipitation obtained under equilibrium conditions is precipitated out rapidly during the test, at least at temperatures close to that giving the maximum rate of precipitate. In fact the position and shape of the curve can be well explained by using equilibrium solubility data. If Irvine's et al., (1967) solubility formula for NbC is used:

$$\log(\text{Nb}) \cdot (\text{C}) = (-6770/T) + 2.26$$

where T = the absolute temperature K, then the equilibrium volume fraction of NbC present can be calculated. If this is plotted against temperature, Fig.5.2., then it can be seen that there is quite a good agreement between the improvement in hot ductility with increase in temperature and the reduction in the volume fraction of NbC. The better hot ductility behaviour shown by the very low C steel (0.014% C) compared to the higher C steels can readily be explained in terms of much lower volume fraction of precipitation present, Fig.5.7, and the relative insensitivity of raising the C level above 0.1% can also be readily understood as precipitation is not greatly influenced by

further changes in C level.

This relative insensitivity of hot ductility to C level in the range 0.08 to 0.2% has also been noted by Ouchi and Matsumoto (1982) in steels containing 0.03% Nb when tested in the temperature range 600 to 1000 °C after solution treating at 1330 °C. Maehara et al., (1985) have also noted the insensitivity of hot ductility to C level in the range 0.05 to 0.3% C for steels containing 0.05% Nb when tested at 800 and 900 °C after solution treating at 1300 °C. Raising the Nb content from 0.03% to 0.05% would be expected from the solubility data to increase the amount of NbC precipitated and is equivalent to raising the C level. In this higher Nb containing steel a marked improvement in hot ductility on reducing C levels below 0.2% C would only be noted when the C level are extremely low ($< 0.03\%$).

Although a large part of the trough for the two higher C containing steels occurs in the temperature range in which deformation takes place solely in the austenite, the actual minimum ductility occurs below the Ae_3 suggesting that as well as precipitation reducing hot ductility, the strain concentration produced in the thin films of deformation induced ferrite surrounding the austenite grains must also be helping to reduce hot ductility, Fig. 5.6. Subsequent recovery of hot ductility on lowering the temperature further may be due to both a reduction in the amount of NbC precipitated (the kinetics of precipitation are a C curve centred at 900 °C, Jonas and Weiss, 1979), and a thickening of the ferrite film.

5.5 CONCLUSIONS

- 1- Hot ductility troughs of similar depth were obtained for all C-Mn-Al steels examined, but the width and position varied with carbon content.
- 2- Raising the C level in a C-Mn-Al steel moves the hot ductility curves to lower temperatures in accord with the change in A_{e3} and A_{r3} temperatures.
- 3- Aluminium has no influence on hot ductility of the steels examined, because no AlN was formed under the conditions of cooling and strain rate used in the tests.
- 4- The fall in ductility occurs in the Al containing steels due to strain concentration in thin films of deformation induced ferrite, producing voiding round inclusions which gradually link up to give intergranular failure.
- 5- Introducing Nb into the steel widened and deepened the trough.
- 6- Raising the C level in the Nb containing steel has little influence on the position of the trough as ductility is controlled by precipitation of NbC, but the depth and width increased with C level due to the NbC precipitation and quite good agreement was obtained between the degree of NbC precipitation, as calculated from the solubility data and the Reduction of Area values.

Steel	C	Si	Mn	P	S	Nb	Al	N
C-Mn-Al	.056	.42	1.46	.007	.012	—	.034	.007
C-Mn-Al	.11	.32	1.42	.011	.002	—	.038	.0038
C-Mn-Al	.15	.29	1.45	.003	.008	—	.017	.006
C-Mn-Al-Nb	.014	.36	1.48	.015	.006	.028	.033	.007
C-Mn-Al-Nb	.1	.42	1.39	.007	.01	.026	.036	.0075
C-Mn-Al-Nb	.16	.22	1.24	.011	.005	.023	.028	.009

Table 5.1 Composition of the steels examined (Wt. %)

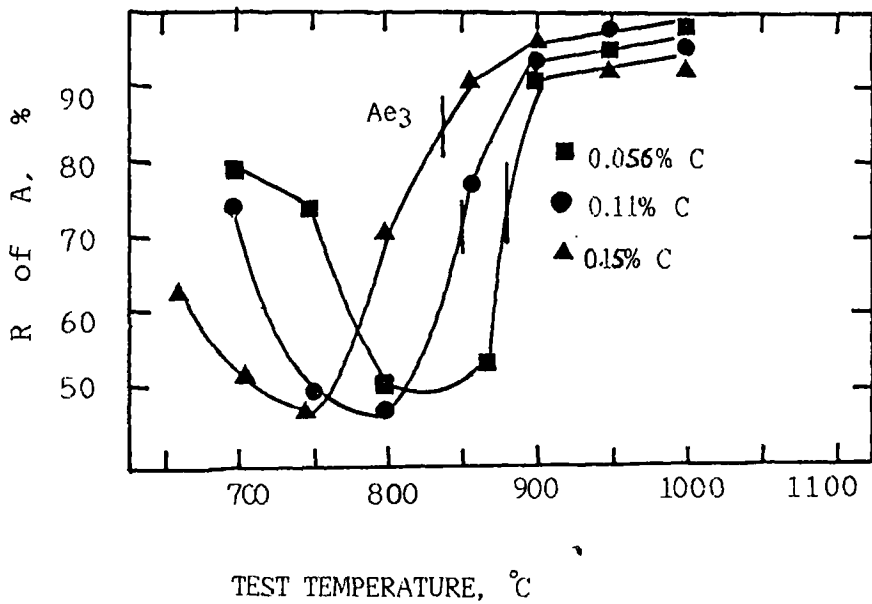


Fig. 5.1 Hot ductility curves for the Al containing steels examined with different carbon levels.

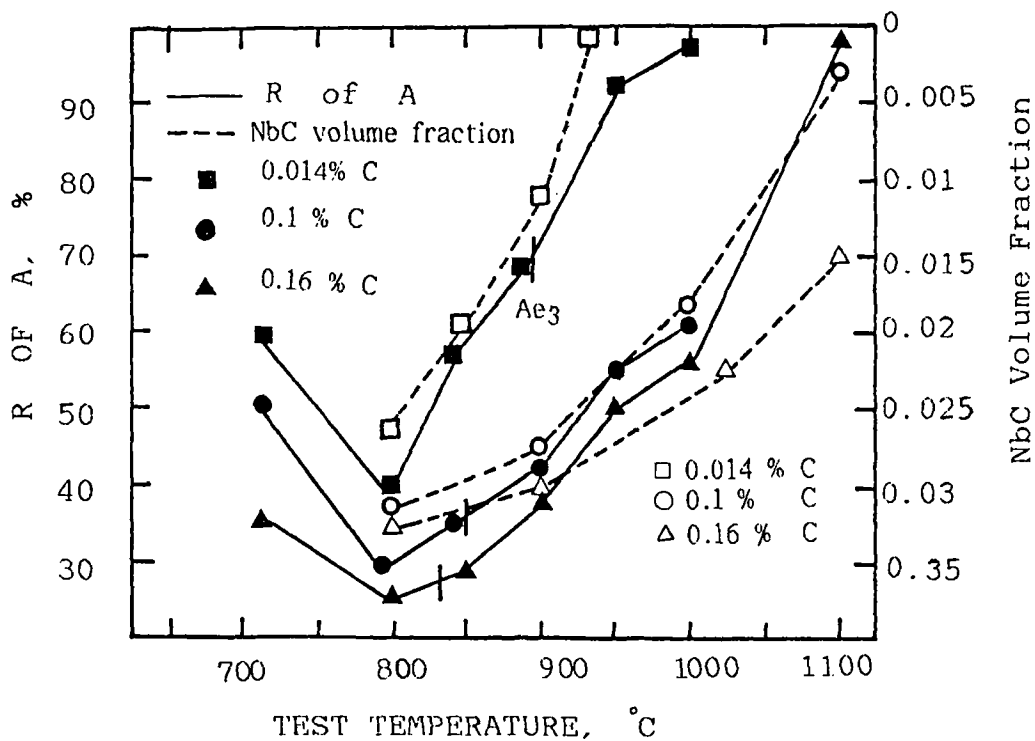


Fig 5.2 Hot ductility curves and NbC volume fraction for the Nb containing steels examined with different carbon levels. (the NbC volume fraction has been calculated after Irvine's formula, 1967).

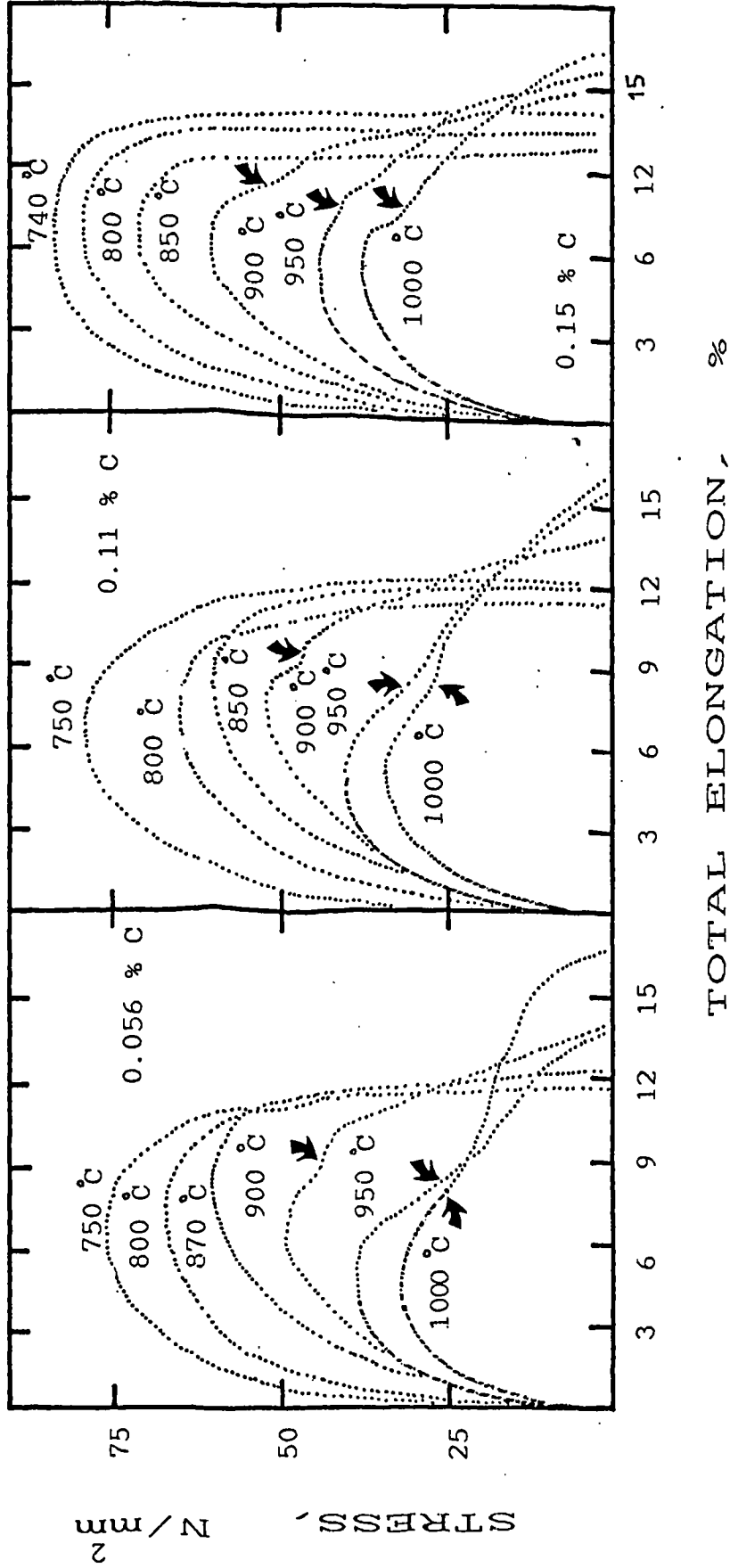


Fig. 5.3 Stress - total elongation curves for the C-Mn-Al steels examined with different carbon levels.

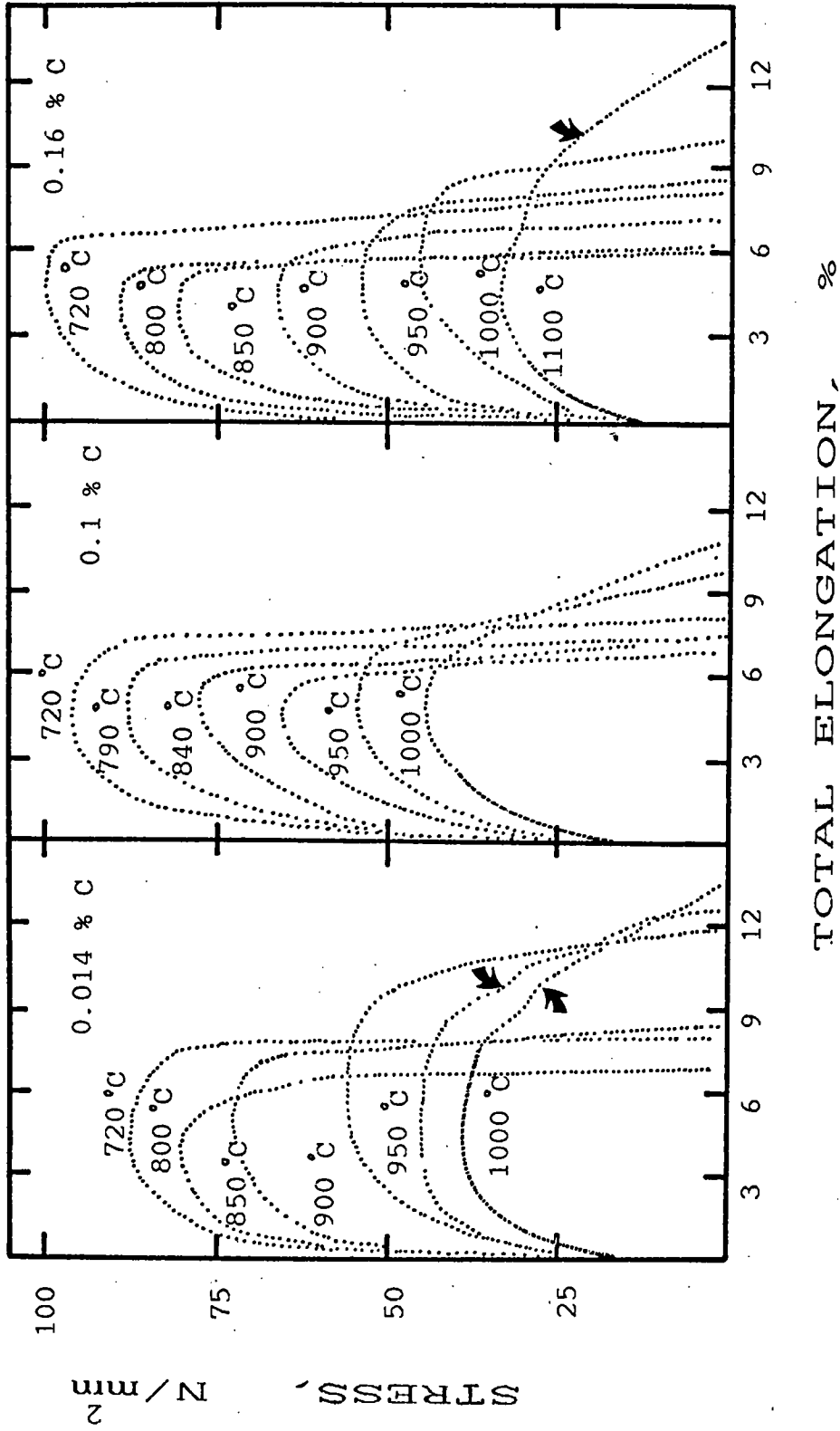
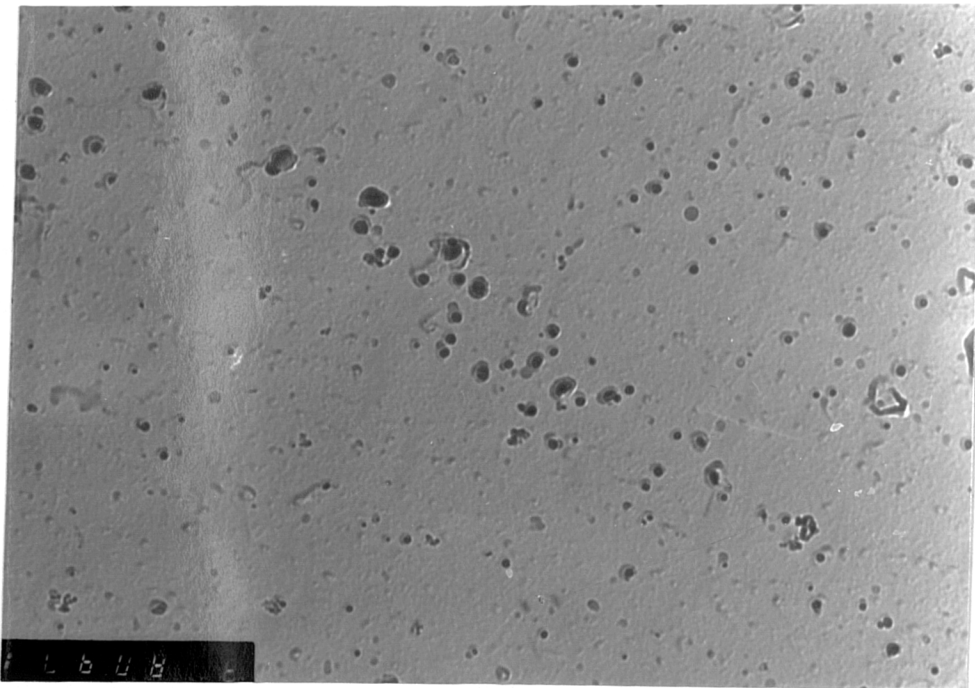
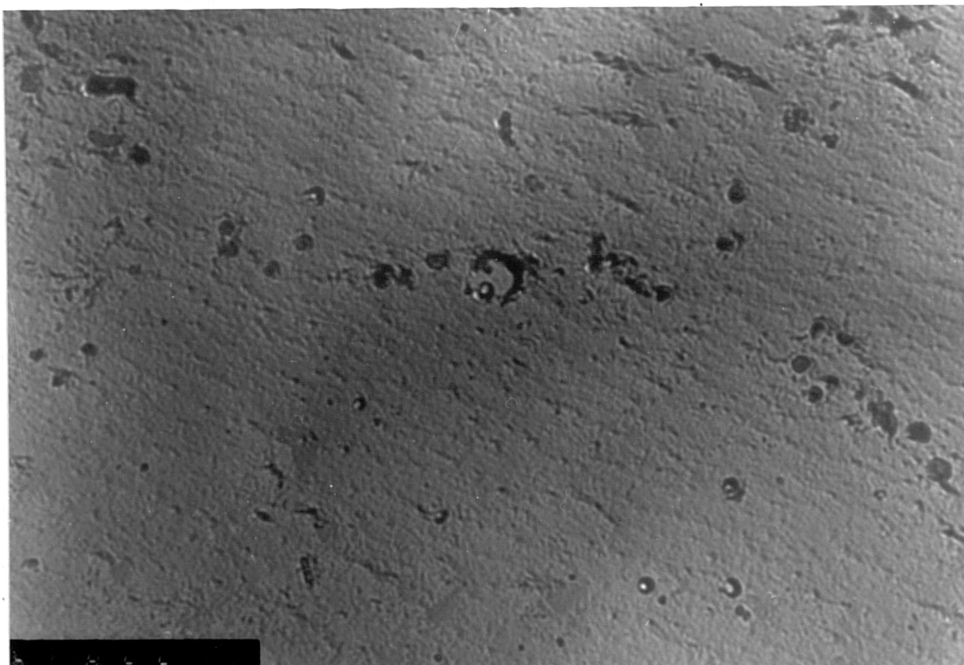


Fig. 5.4 Stress - total elongation curves for the C-Mn-Al-Nb steels examined with different carbon levels.



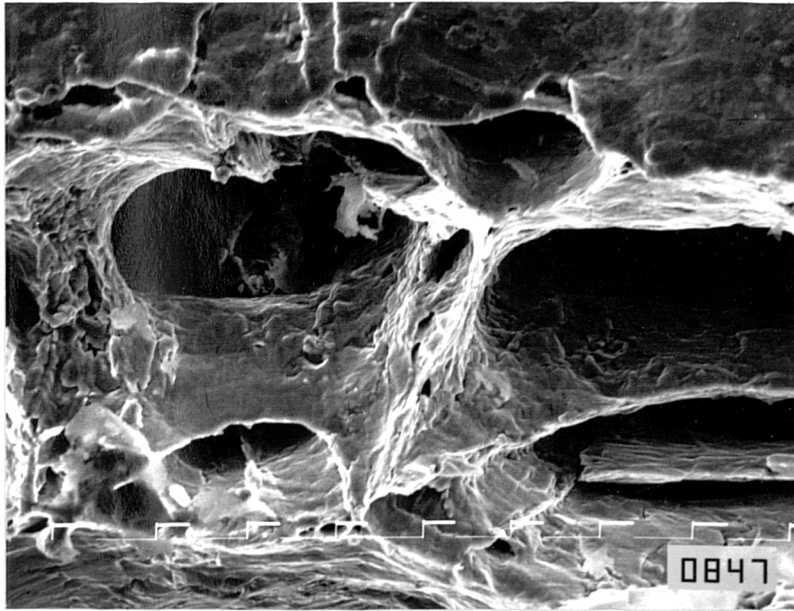
650 nm

Fig. 5.7 0.1% C niobium containing steel tested at 850 °C, showing extensive NbCN precipitation.



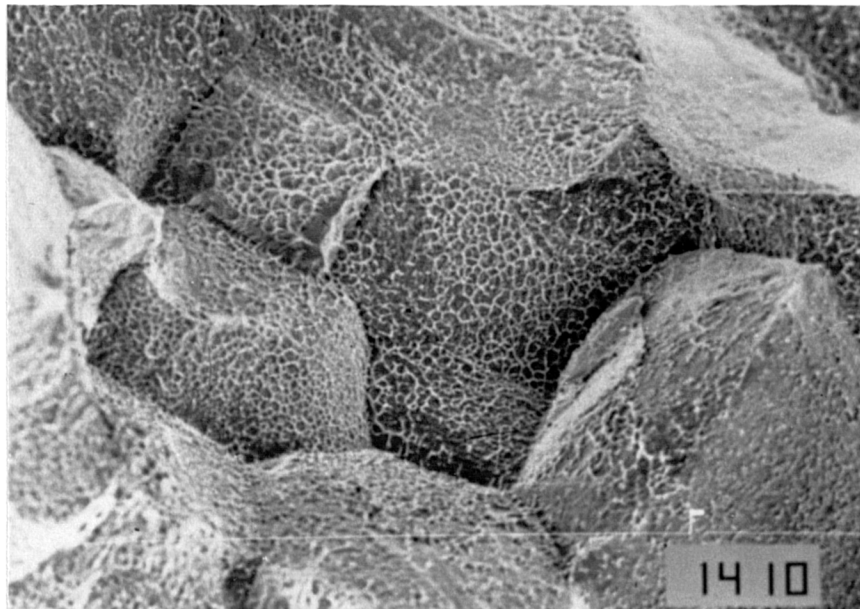
650 nm

Fig. 5.8 0.014% C niobium containing steel tested at 850 °C, showing sparse precipitation of NbCN.



27 μm

Fig. 5.9 Example of high temperature ductile rupture fracture observed in the 0.15% C aluminum containing steel tested at 950 °C.



400 μm

Fig. 5.10 Example of intergranular micro-void coalescence fracture observed in the 0.1% C, niobium containing steel tested at 790 °C.

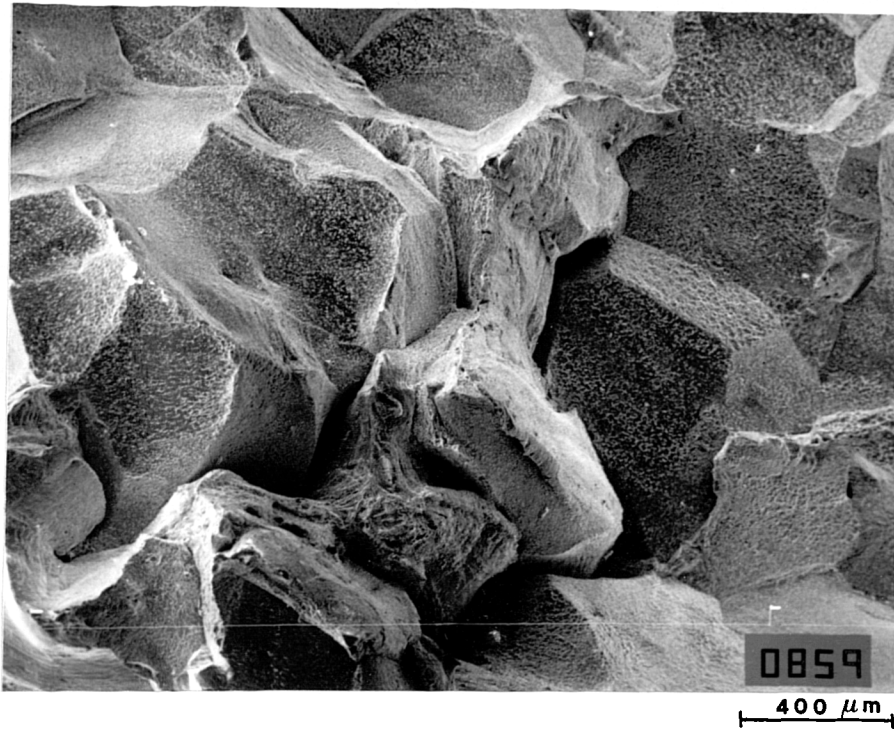


Fig. 5.11 Example of intergranular micro-void coalescence fracture observed in the 0.1 % C niobium containing steel tested at 840 °C.

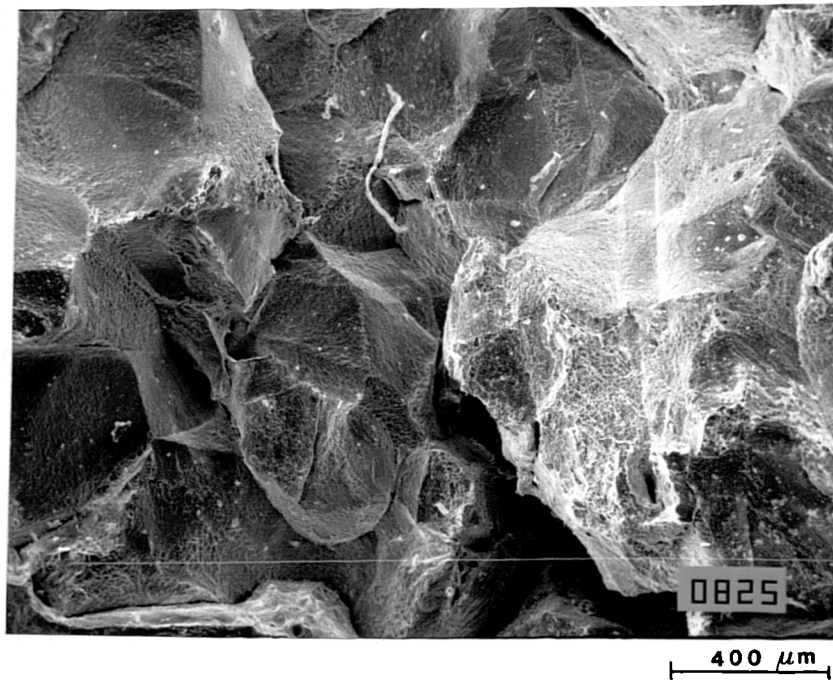


Fig. 5.12 Example of mixed intergranular micro-void coalescence and intergranular decohesion fracture, observed in the 0.1 % C niobium containing steel tested at 900 °C.

CHAPTER 6

EFFECT OF CALCIUM ON THE
HOT DUCTILITY OF MICRO-
ALLOYED STEELS

6.1 INTRODUCTION

It is well known that non metallic inclusions in the steel impair the ductility and hinder its processing. Steel users need steel with a high degree of purity to meet application requirements. This has led the steel corporations to try to produce economical steel with a minimum of impurities. One successful method was the development of a technique, described by Pircher and Klapdar (1977) for Ca treatment, which reduces the number of sulfide and oxide inclusions in the molten steel and at the same time modifies the nature, shape and distribution of these inclusions. Pircher and Klapdar (1977) noted a decrease in the S and O contents of steel treated with Ca, which led to a beneficial effect on ductility and strength at the room temperature.

Hilty and Farrell (1974), reported that adding 88 ppm of Ca to a C-Mn-Al steel containing 0.005% S eliminated the pure MnS inclusions from the steel and only the greenish-yellow CaS phase was observed. In steels containing 0.015% S, free MnS inclusions were observed at all Ca levels (0.018 -0.09%) but the amount decreased with increasing Ca concentration in the steel. However, in using a highly reactive alloying metal, such as Ca, the extent of success in steel cleanliness is mainly determined by the method adopted for their additions (Pircher and Klapdar, 1977) and the optimization of the amount added (Yamaguchi et al., 1979).

Yamaguchi et al., (1979), have examined the hot ductility of a Nickel-base superalloys and they concluded that the greater the S content, the deeper the ductility trough and the more intergranular the fracture appearance.

By adding a small amount of Ca, the hot ductility improved markedly. They attributed the poor hot ductility in the non calcium treated alloys to atomically segregated S weakening the grain boundaries.

A pronounced improvement in hot ductility due to the Ca - treatment is evident when measuring the ductility of plates in the longitudinal and transverse direction of rolling. Crowther and Mintz (1986d), have shown that Ca treatment of a C-Mn-Al steel removed the effect of testing direction on the hot ductility of steel and gave rise to a very shallow trough. Recently, Crowther et al., (1987) , have shown, that Al containing steel treated with Ca give better hot ductility. However, this improvement has so far only been noted on samples heated from room temperature to the test temperatures. Of more importance is the case for samples cooled down after solution treating as this is the continuously cast situation.

In general little attention has been given to the role of sulphides in influencing hot ductility. Crowther and Mintz (1986a) have shown that marked ductility troughs are present in plain C-Mn steel in which there are no micro-alloying additions, when heated to 1330 °C and cooled to test temperature . In this case it has been shown that for steels with $\leq 0.28\%$ C the trough is produced by strain concentration in thin films of the softer deformation induced ferrite which surrounds the grains and this strain concentration produces cavitation round the MnS inclusions, these linking up to give intergranular failure. Coleman and Wilcox (1985), have also suggested that sulphides are important in controlling trans-

verse cracking, as examination of the surfaces of the transverse cracks found in the continuously cast slabs often reveal the presence of MnS inclusions with associated cavitation. They also state that transverse cracking in Nb containing steels is reduced when Ca is added to modify and reduce S levels.

Although, Ca treatment is given to modify inclusions so that instead of elongated inclusions being produced on rolling, spherical inclusions are formed, it will also reduce the amount of S available for precipitation as sulphide. Whereas the room temperature ductility and toughness has been examined for steels with and without Ca treatment, less information is available on the effect of Ca treatment on the hot ductility of micro-alloyed steels. Procuring this information has formed the basis of the present chapter.

6.2 EXPERIMENTAL

The compositions of the seven steels examined are given in Table 6.1. Heats A, B, and C were Al containing steels with different levels of S. From this group heat A had been Ca treated.

Heats D, E, F and G were Nb containing steels, with different levels of S. From this group heats D and E had been Ca treated.

The steels were hot rolled to 12 mm plates. Tensile samples having a length of 70 mm and a diameter of 7.93 mm were machined from the plates with their axis parallel to the rolling direction. Hot tensile tests were carried out on a Hounsfield Tensometer and heating was supplied by an induction heater, as described in chapter 4. The samples were protected from oxidation by an Argon atmosphere.

Samples were heated to 1330 °C in ~ 15 minutes, held for 5 minutes, prior to cooling to test temperature in the range 700 - 1000 °C, at an average rate of 60 °C/min. to simulate the continuous casting process. Samples were held for 5 minutes at test temperatures before straining at $3 \times 10^{-3} \text{ s}^{-1}$.

Fracture surfaces were examined using a JEOL T100 SEM operating at 25 KV. Carbon extraction replicas were prepared from transverse sections approximately 1 mm behind the fracture surfaces, and examined using a JEOL 100 KV TEM operating at 60 KV.

6.3 RESULTS

6.3.1 HOT TENSILE TEST

The curves of percentage reduction in area against test temperature in the range 750-1000 °C for Al and Nb containing steels are shown in Figs. 6.1 and 6.2, respectively. The ductility of Al containing steels, starts to fall at 900 °C and reaches a minimum of ~ 50% in both the Ca free steels. The Ca containing steel gave the best ductility over the temperature range 700-900 °C, with a minimum value of 68% at 850 °C. The shift in the ductility trough in heat C to lower temperatures would from the information in chapter 5 as well as from the previous work by Crowther and Mintz (1986a), most likely be due to the higher carbon content, lowering the transformation temperature in this steel.

As can be seen in Fig. 6.1, increasing the S level from 0.002% in heat C to 0.012% Wt., in heat B, has no effect on the shape or depth of the ductility trough.

The Nb containing steels, also show similar behaviour to the Al containing steels, the addition of Ca being beneficial to hot ductility. Ductility starts to fall at 1000 °C in all cases, reaching a minimum in the temperature range 800-850 °C. An addition of 0.0026% Ca to the Nb containing steel, heat E, improved the hot ductility over the whole temperature range examined, (750-1000 °C). A greater improvement was achieved when the Ca level was increased to 0.004%, heat D, despite the

fact that the steel with 0.004% Ca has more sulphur than the steel with 0.0026% Ca. Again the small increase in S level from .007% (heat F) to .01% (heat G) for the free Ca steels containing Nb (see Table 6.1), did not change the hot ductility.

Dynamic recrystallisation, indicated by shaded region in figs. 6.1-6.2, was observed at test temperatures $\geq 900^\circ\text{C}$ for Al containing steels. In the Nb containing steels, dynamic recrystallisation was first observed in the Ca treated steels at 1000°C , but for steels without Ca treatment, the recrystallisation temperature must be greater than 1000°C .

Comparing the peak stresses for the Al and Nb containing steels, there is no significant difference between steels with and without Ca treatment, Fig. 6.3.

6.3.2 FRACTURE EXAMINATIONS

SEM examination of the fracture surfaces of samples from the Nb containing steels broken at temperatures giving low ductilities ($\leq 60\%$ R of A), showed that the fracture was a mixture of intergranular decohesion (ID) and intergranular micro-void coalescence (IMC), Figs. 6.4-6.5.

In the Al containing steels, intergranular micro-void coalescence was the main fracture mode, Fig. 6.6. Micro-voids, usually are associated with second phase particles, leading to this type of fracture.

It should be noted that the amount of the flat fracture facets observed in samples broken inside the trough, increased with increasing test temperature, especially in the Nb containing steels, indicating that grain boundary sliding in the austenite played an important role in controlling the fracture process, Fig. 6.7.

Metallographic examination using the optical microscope, of transverse sections taken from samples broken at temperatures in the ductility troughs confirmed the nature of the intergranular fracture mode observed under the SEM, Fig. 6.8.

No evidence of intergranular failure was observed in the Al-Ca steel and the fracture was normal intragranular ductile. At higher magnifications, spherical particles could be seen in the dimples formed on the fracture surfaces, Fig. 6.9.

6.3.3 TEM EXAMINATIONS

Examination of carbon extraction replicas taken from transverse section of fractured samples ($\sim 1\text{mm}$ behind the fracture surfaces), revealed no AlN precipitation in any of the steels examined, but the Nb containing steels with and without Ca treatment showed extensive NbCN precipitation at the austenite grain boundaries and within the grains, Figs. 6.10-6.11. It can be concluded from the observations that the Ca treatment does not affect the NbCN precipitation.

On the other hand, many MnS inclusions (0.2 to $0.6\ \mu\text{m}$) have been observed in all the calcium free steels, Figs. 6.12-6.13, (some of them being at the prior austenite grain boundary) and they were much coarser than the NbCN precipitation (the NbCN size were mostly less than $50\ \text{nm}$).

This pattern of inclusion precipitation was not observed in the Ca treated steels. Instead, some isolated (few in number) multiphase inclusions have been observed, Fig. 6.14. Analysis of these inclusions shows that they include Mn, S and a small amount of Ca and sometimes a small amount of Al and Si. They are similar to those observed by Hilty and Farrell (1974), Banks and Gladman (1979) and Pircher and Klapdar (1977).

It should be noted that no pure CaS has been observed, in any of the Ca treated steels, in agreement with many other workers (e.g. Hilty and Farrell, 1974).

6.4 DISCUSSION

6.4.1 GENERAL EFFECT OF Ca TREATMENT

The hot ductility curves for the C-Mn-Al and C-Mn-Al-Nb steels are given in Figs. 6.1 and 6.2 respectively. It can be seen that adding Ca in all cases improves the hot ductility. Although calcium steels generally have both modified sulphides and lower total S levels, the better hot ductility is not a consequence of the generally lower S levels. For example, steels A and C have similar total low S levels but the calcium containing steel, steel A, has the better hot ductility.

The displacement by 50 °C to lower temperatures of the curve for steel C compared to that for steel B is due to steel C having a higher carbon content, Fig. 6.1. Taking this into account, steels B and C have very similar hot ductilities but very different total S levels. Also for the C-Mn-Al-Nb steels, steel D and F have very similar low S levels but again the calcium containing steel has the better hot ductility. Modification is not likely to be an important factor for the improved hot ductility of calcium containing steels as in the calcium free steels the MnS present at the austenite grain boundaries after heating to 1330 °C and cooling to the test temperature are also generally spherical, Figs. 6.12-6.13.

In the present instance it is the amount of sulphur which goes back into solution at 1330 °C and

subsequently reprecipitates out at the new austenite boundaries formed on reheating which controls the hot ductility. In the case of the calcium free steel, the solubility data of Turdogan et al., (1955), indicates that for a steel with 1.4% Mn, only 0.001% sulphur redissolves at 1330 °C. Hence hot ductility curves obtained after heating to 1330 °C and cooling to test temperatures in the range 1000° to 700 °C have been shown to be the same for for C-Mn-Al-Nb steels (S= 0.007 to 0.01%) and for C-Mn-Al steels (S= 0.002 to 0.012%). This is in accord with the work of Mintz (1979), who showed that increasing S from 0.001 to 0.022% in a Nb containing steels does not affect the hot ductility behaviour of the steels examined.

The improvement in hot ductility is therefore in the present instance most likely to be related to the smaller amount of S available for precipitation on cooling from 1330 °C when calcium sulphide rather than manganese sulphide is present. Although no data is available, the solubility of calcium sulphide at 1330 °C is likely to be extremely low. Commercially it is recommended that the Ca/S ratio should be 2:1 to obtain pure calcium sulphide, (Mintz, 1988). In these laboratory casts the Ca/S ratio is 1:1, so that some of the sulphides will be MnS or contain Ca in them so that a greater amount of S than given by the CaS solubility product might be expected. Nevertheless the amount of S able to redissolve at 1330 °C will be very much less than when calcium is not present. Replica examinations

indicate that whereas lines of MnS particles, Fig. 6.12-6.13, can often be found, probably at the prior austenite grain boundaries in steels without Ca treatment, only few isolated sulphides are found in the Ca treated steels, Fig. 6.14.

6.4.2 SHAPE OF THE HOT DUCTILITY CURVES

In the case of the C-Mn-Al steels, A, B, and C, no AlN precipitation was found in these steels in accord with previous observations (see chapter 5).

Precipitation of AlN after solution treatment at 1330 °C has been shown to be very sluggish, requiring many hours of holding at 900 °C, before precipitation starts (see chapter 7). In the absence of AlN precipitation the hot ductility behaviour would be expected to be identical to that shown by a plain C-Mn steel. Previous work on C-Mn steels (Crowther and Mintz, 1986a), has shown that tensile fracture at the minimum ductility temperature is along thin films of ferrite which form around the coarse austenite grains by deformation induced transformation. The softer ferrite allows strain concentrations to cause ductile voiding at the MnS inclusions and the voids eventually link up to give intergranular failure.

Although the Ar_3 temperatures have not been obtained, it has been shown (Crowther and Mintz, 1986a), that for coarse grained steels deformation raises the Ar_3 temperature to the Ae_3 temperature. Thus it might be expected that the greater the volume fraction of inclusions present in the

thin ferrite films the easier it will be to produce intergranular failure.

Fracture observation on samples broken at temperatures giving minimum ductility do show typically intergranular micro-void coalescence failures, Fig. 6.6, and fracture is observed to take place along thin films of deformation induced ferrite, (see chapter 5). Whereas it was possible to readily find spherical MnS at prior austenite grain boundaries, Fig. 6.13, few sulphides were observed in the calcium treated steels.

In the Nb containing steels examined, again no AlN precipitation was observed but extensive NbCN precipitation was found at the austenite grain boundaries and sometimes in the matrix, for steels with and without Ca treatment. Thus the improvement in hot ductility shown by the Ca treated steels is due to the fewer inclusions at the boundaries. This improvement was more marked at test temperatures above the A_{e3} temperature, Fig. 6.2.

Detailed examination of the fracture surfaces under the SEM for the Nb containing steels show that around 50% of the fracture surfaces were by grain boundary sliding in the austenite. Flat fracture facets are observed, Fig. 6.7 and no cavitation is associated with the inclusions. Inclusions may then be acting in a similar way to the fine micro-alloyed precipitates pinning the austenite grain boundaries and also acting as weak interfaces encouraging grain boundary sliding. Although, NbCN precipitation was similar for Ca free

and containing steels, the hot ductility of calcium free steels remained well below that of the Ca containing steels even for temperatures as high as 1000 °C, Fig. 6.2. This temperature corresponds to full restoration of ductility (~ 90% R of A) and operation of dynamic recrystallisation in the Ca treated steels. It is possible that the large number of inclusions at the austenite grain boundaries are responsible for this delay in the onset of dynamic recrystallisation for steels without Ca treatment and probably accounts for the worse hot ductility exhibited by the Ca free steels at temperatures above the A_e temperature. This is in accord with the work in chapter 10, which shows that MnS inclusions restrain grain boundary movement making dynamic recrystallisation more difficult.

6.5 CONCLUSIONS

1. Calcium treatment improves the hot ductility of micro-alloyed steels after solution treating at 1330 °C and cooling to test temperatures. This improvement is due to the much lower solubility of CaS compared to MnS at 1330 °C, reducing the amount of S available for subsequent precipitation as fine sulphides at the austenite grain boundaries.
2. In the case of Al containing steels no micro-alloying precipitation was observed. The ductility troughs were mainly due to strain concentration in the softer ferrite films which surround the γ grains. Voids are formed at inclusions situated at the boundaries and these gradually link up to give failure. Decreasing the number of these inclusions by adding Ca might be expected to result in better hot ductility. In addition the volume fraction of sulphides were observed to influence the temperature for the onset of dynamic recrystallisation, this being higher for the Ca free steels.
3. Similar behaviour was noted for Nb containing steels, but in this case in addition to the inclusions influencing hot ductility, NbCN precipitation occurred at the γ boundaries both in Ca free and Ca treated steels. This has the effect of extending the trough to higher temperatures due to delaying the onset of dynamic recrystallisation. Again inclusions reduced hot ductility above the Ae_3 by delaying the onset of dynamic recrystallisation encouraging grain boundary sliding.

Code	Steel	C	Si	Mn	P	S	Nb	Al	N	Ca
A	C-Mn-Al-Ca	.065	.46	1.42	.007	.004	-	.042	.0066	.004
B	C-Mn-Al	.056	.42	1.46	.007	.012	-	.034	.0075	-
C	C-Mn-Al	.11	.32	1.42	.011	.002	-	.038	.0038	-
D	C-Mn-Al-Nb-Ca	.086	.53	1.41	.007	.005	.025	.041	.0048	.004
E	C-Mn-Al-Nb-Ca	.1	.41	1.35	.015	.003	.023	.035	.006	.0026
F	C-Mn-Al-Nb	.098	.3	1.41	.009	.007	.031	.04	.0042	-
G	C-Mn-Al-Nb	.1	.42	1.39	.007	.01	.026	.036	.0075	-

Table 6.1 Composition of the steels examined (W. %)

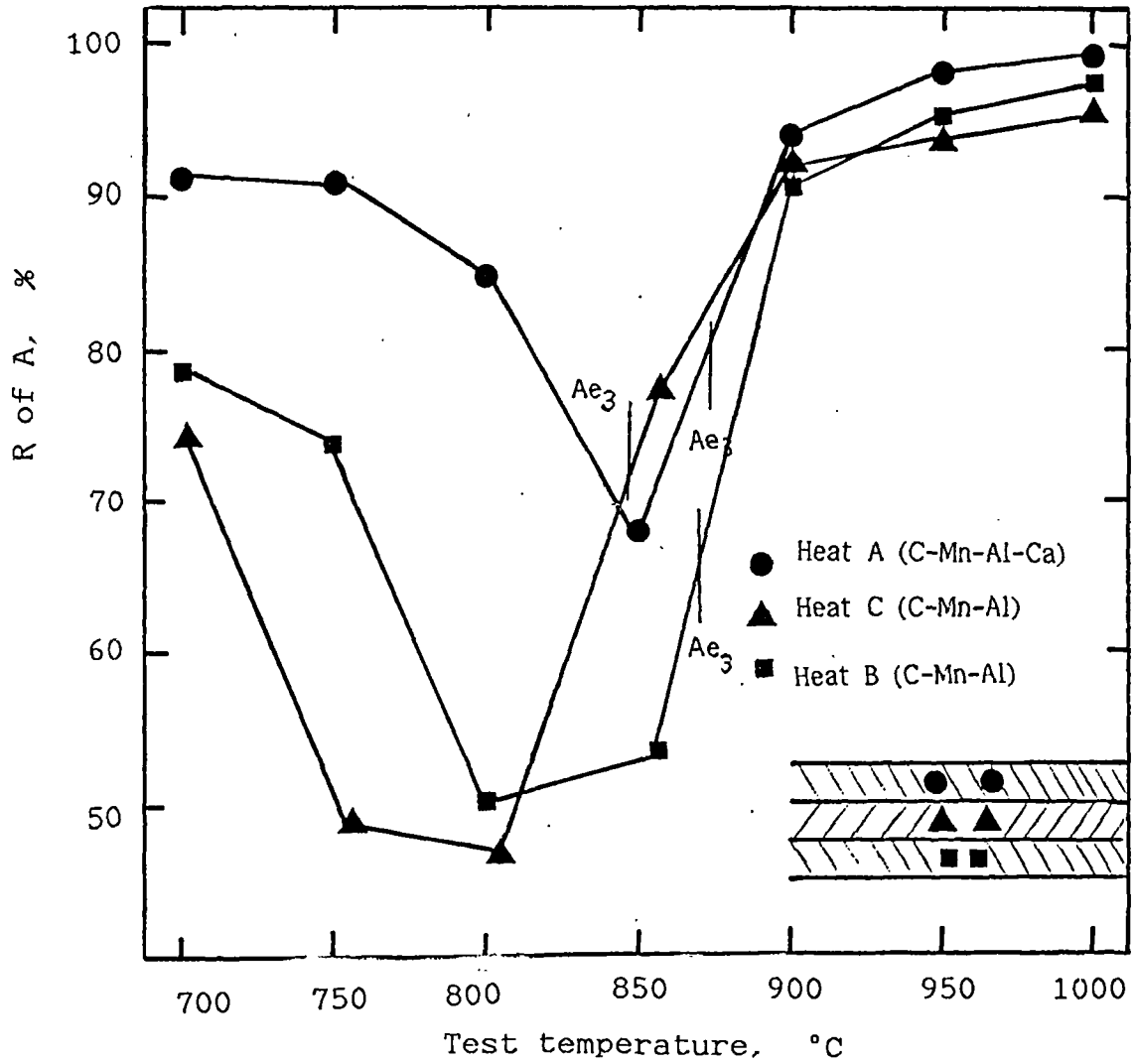


Fig. 6.1 Hot ductility curves for the C-Mn-Al steels with and without calcium additions.

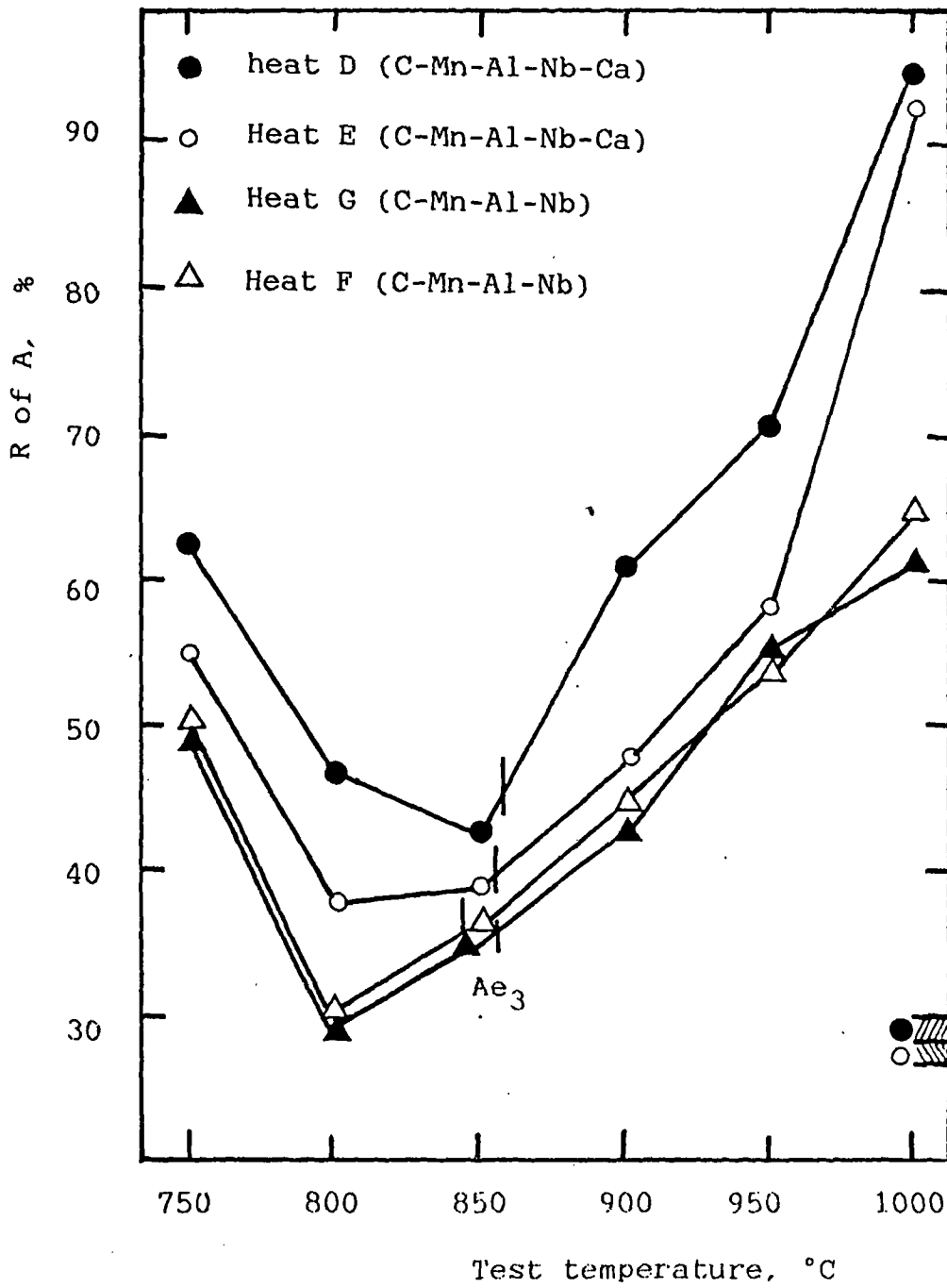


Fig. 6.2 Hot ductility curves for the C-Mn-Al-Nb steels with and without calcium additions.

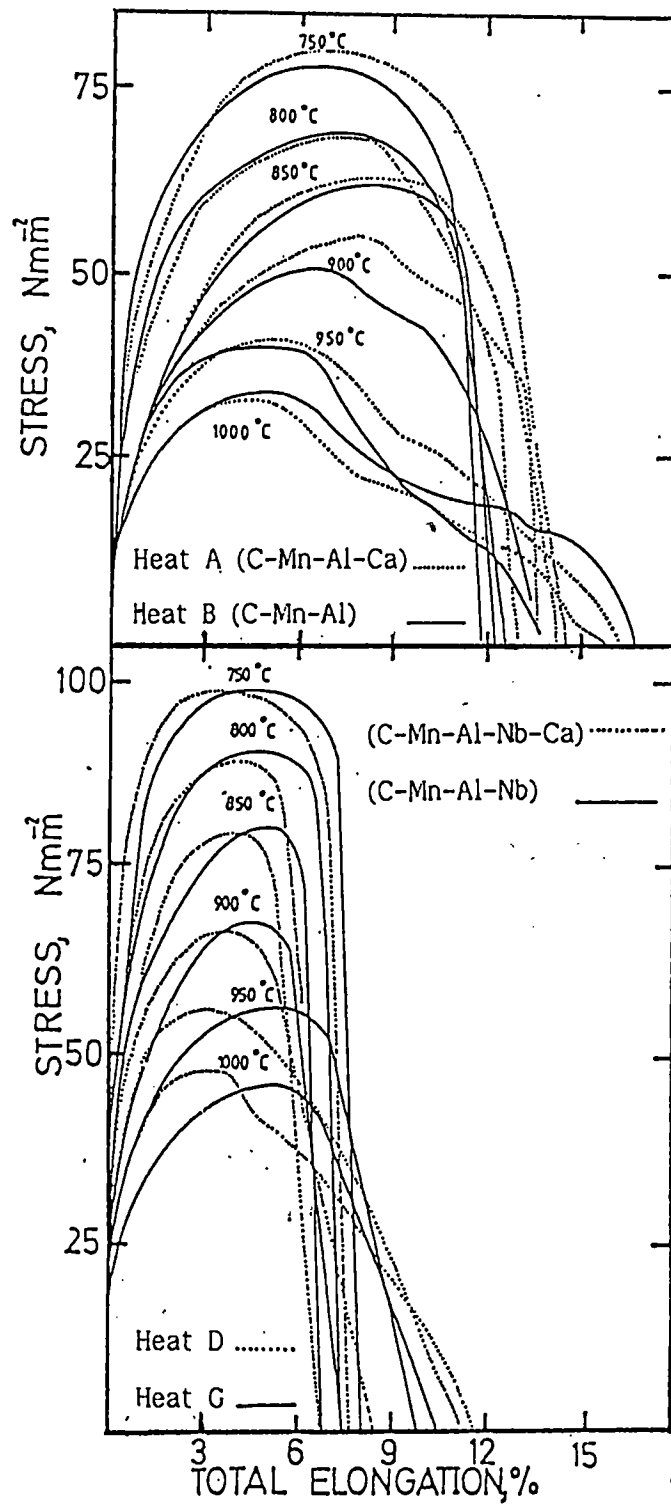


Fig. 6.3 Stress-Total elongation curves for Al and Nb containing steels, with and without calcium additions.

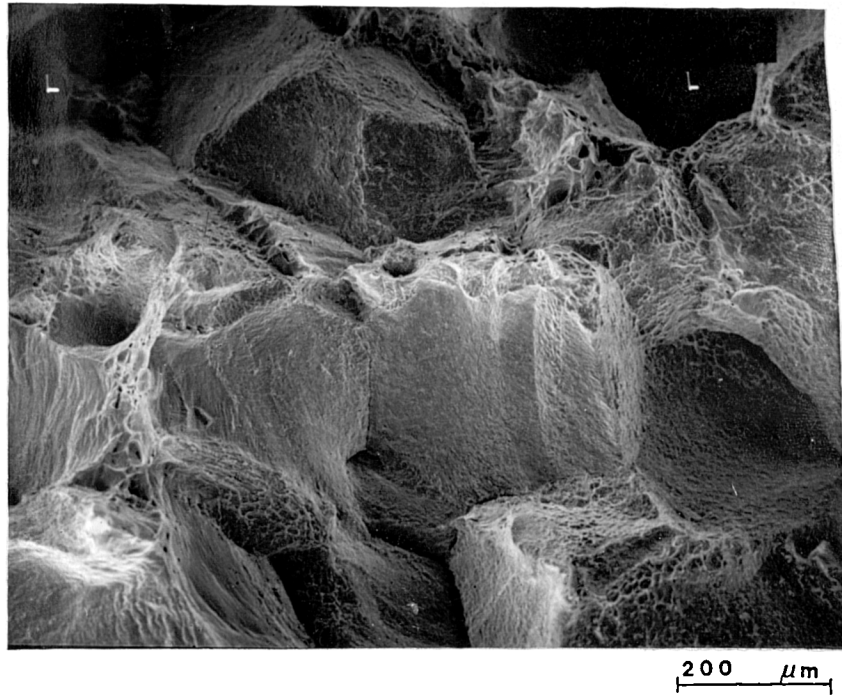


Fig. 6.4 Mixture of intergranular micro-void coalescence and intergranular decohesion failure observed in the Nb containing steel without Ca treatment (heat G) at 850 °C.

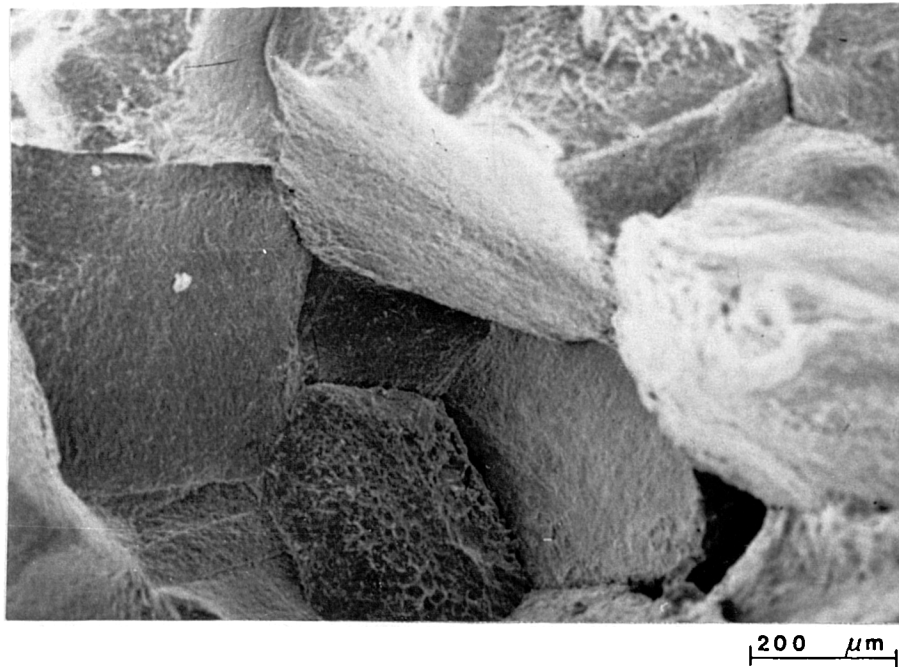
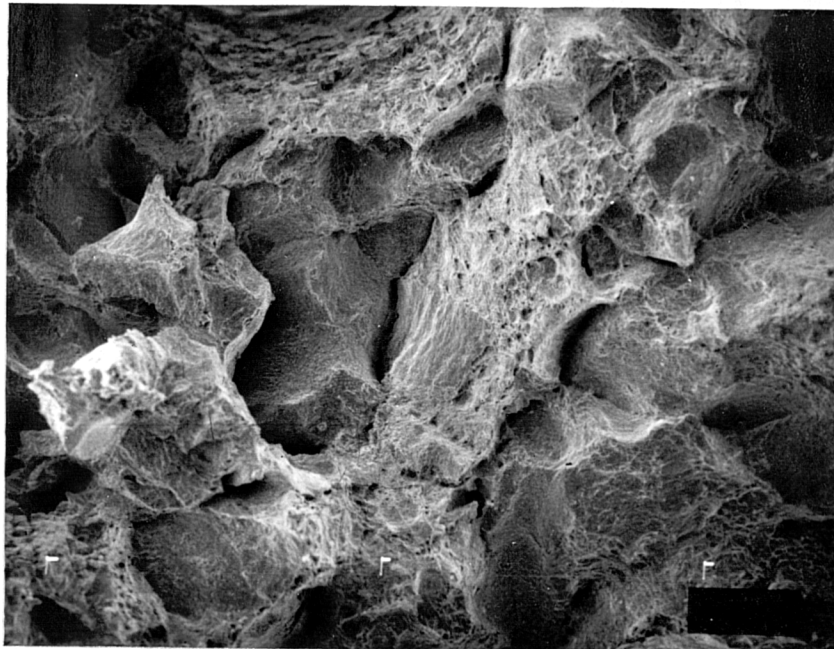
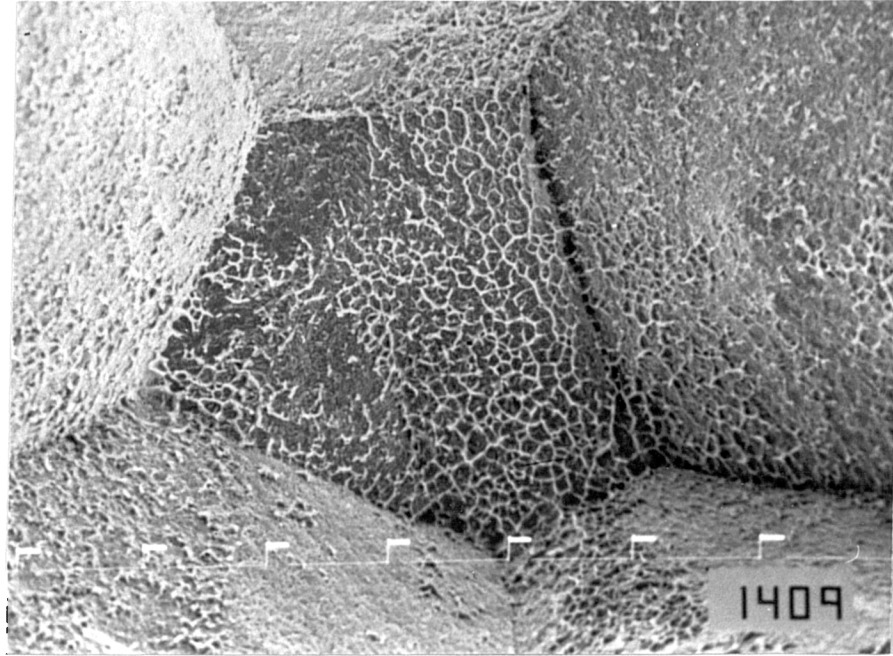


Fig. 6.5 Mixture of intergranular micro-void coalescence and intergranular decohesion failure observed in the Nb containing steel with Ca treatment (heat D) at 850 °C.

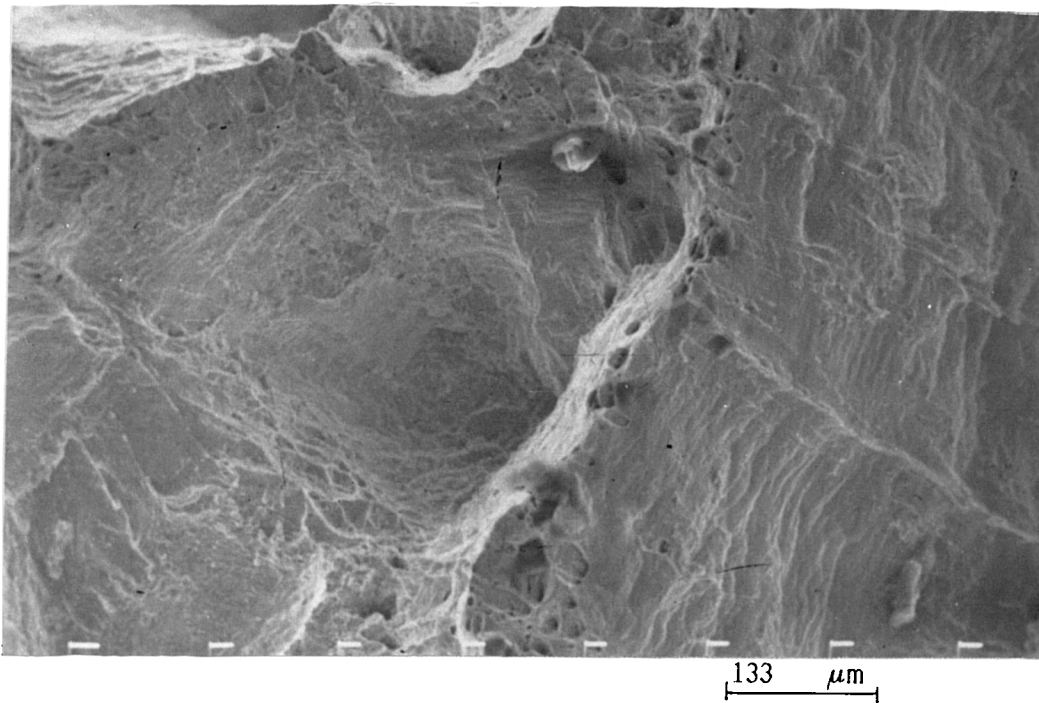


400 μm

Fig 6.6 Example of intergranular micro-void coalescence fracture mode observed in Ca free, C-Mn-Al steel (heat B), tested at 870 °C.



(a). Intergranular micro-void coalescence failure observed at 800 °C.



(b). Intergranular decohesion failure observed at 900 °C.

Fig. 6.7 Example of the intergranular fracture observed in the Nb containing steel (heat G), showing the tendency for the amount of the flat surface to increase with increasing test temperature.

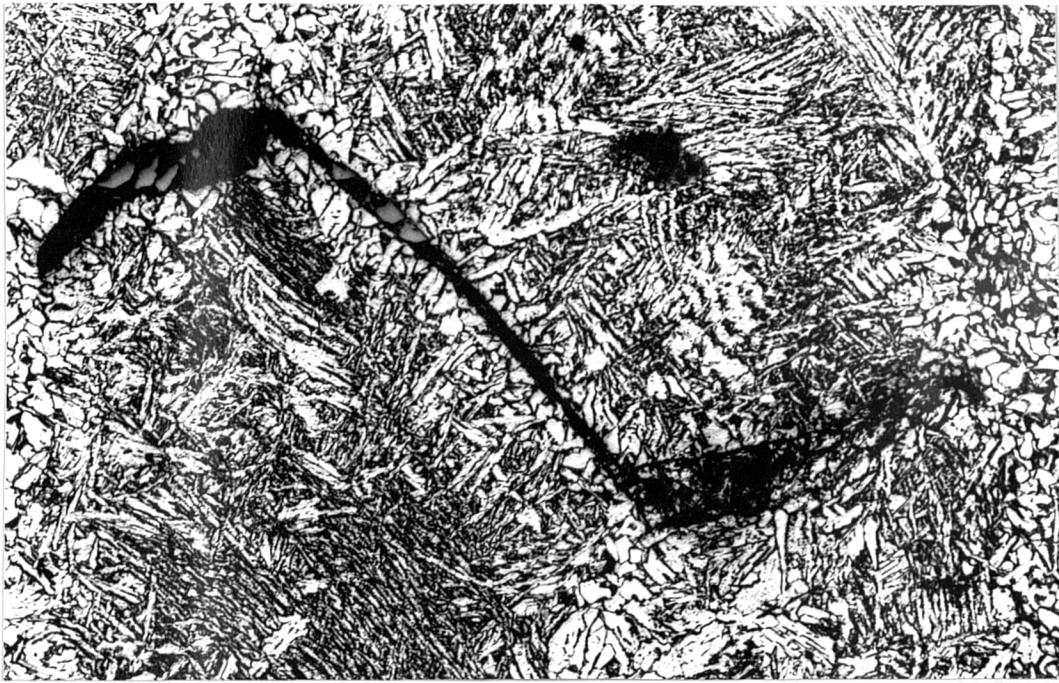


Fig. 6.8 Intergranular fracture observed in the Nb containing steel (heat G), tested at 800 °C.

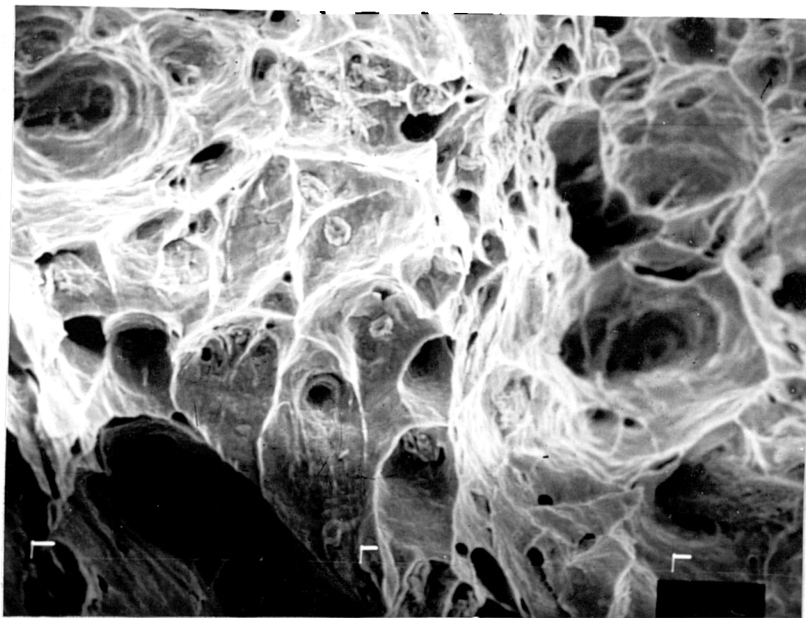
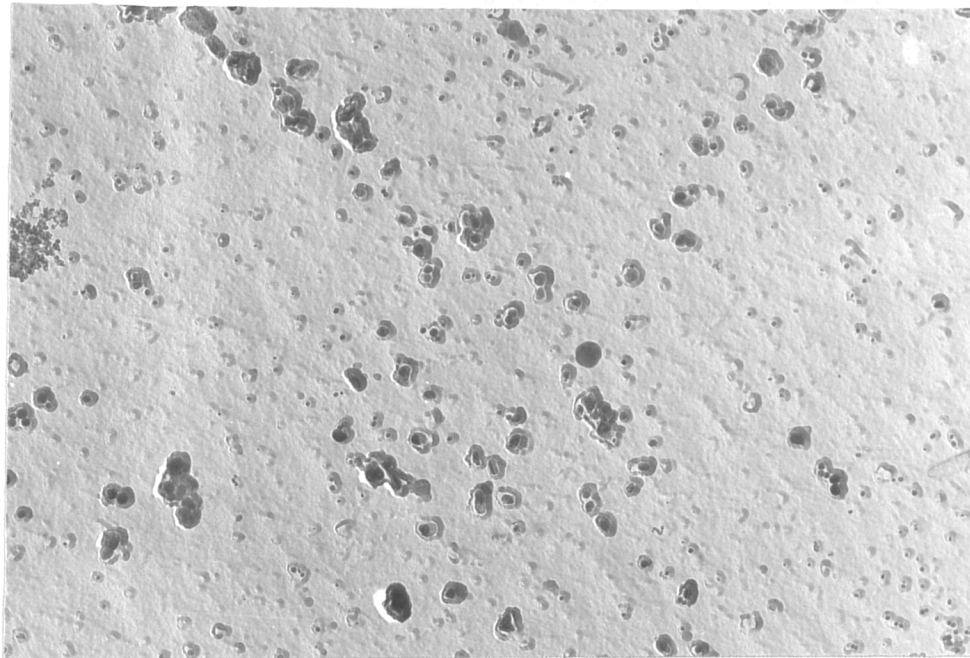


Fig. 6.9 Ductile fracture observed in the C-Mn-Al-Ca steel, tested at 800 °C.



650 nm

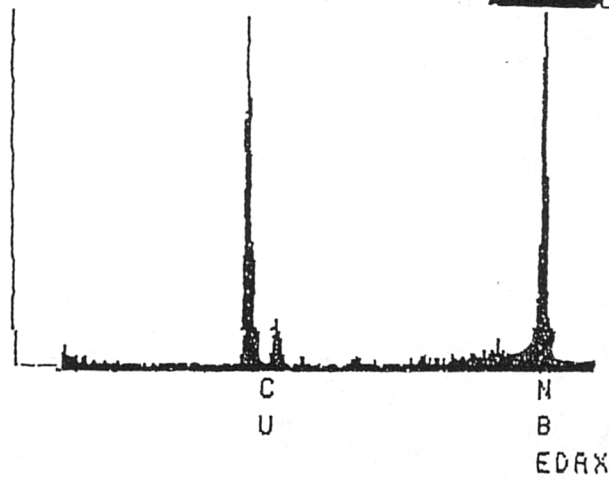
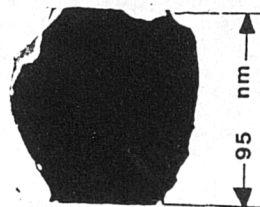
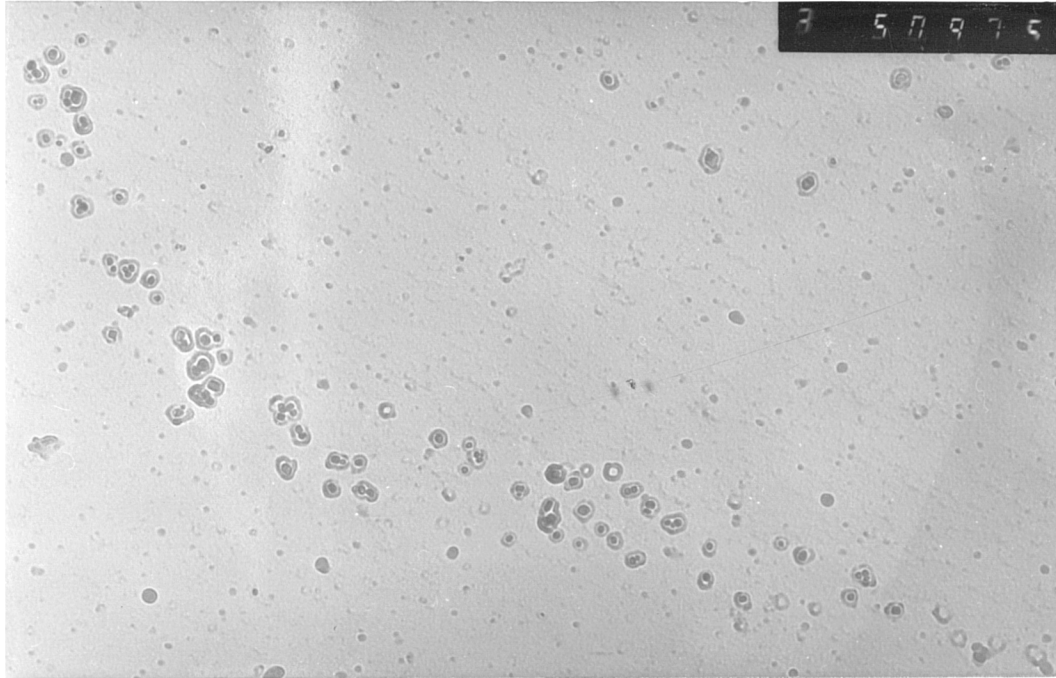


Fig. 6.10 Example of NbCN precipitation observed in the C-Mn-Al-Nb steel (heat F) at test temperature of 850 °C, with associated X-ray spectrum.



650 nm

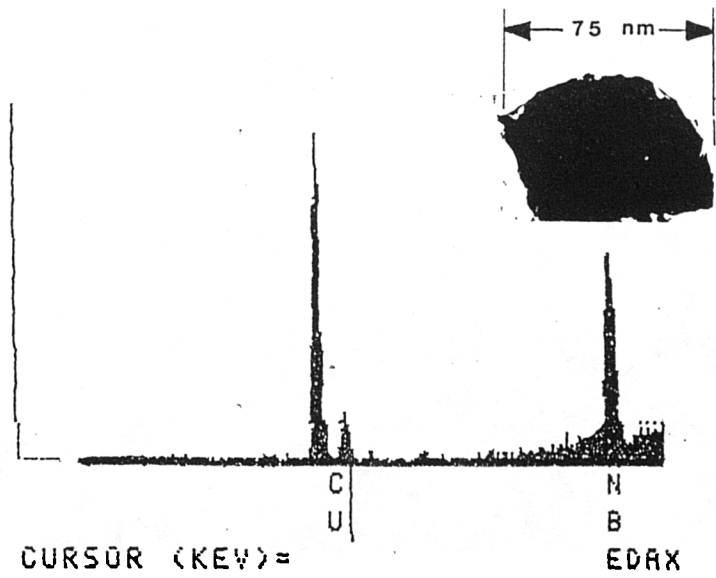
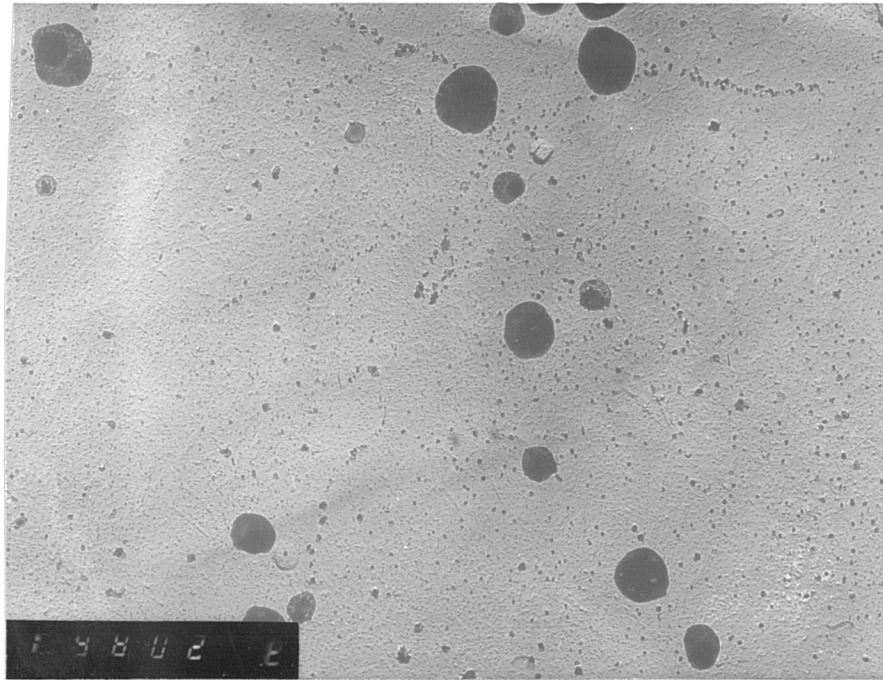


Fig 6.11 Example of NbCN precipitation observed in the C-Mn-Al-Nb-Ca steel (heat D) tested at 850 °C. with associated X-ray spectrum.



1.5 μm

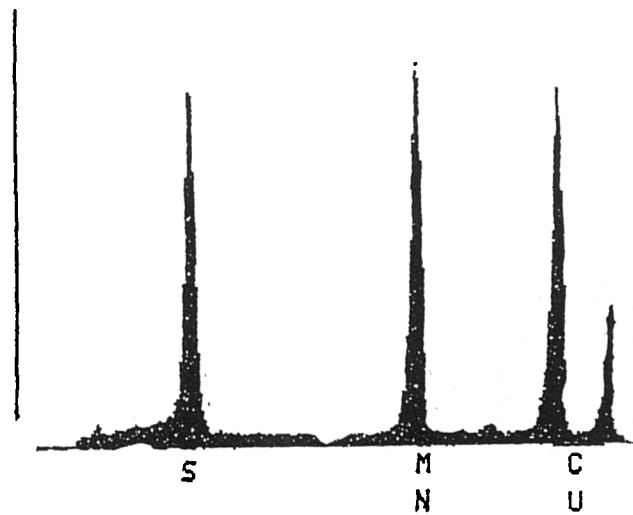
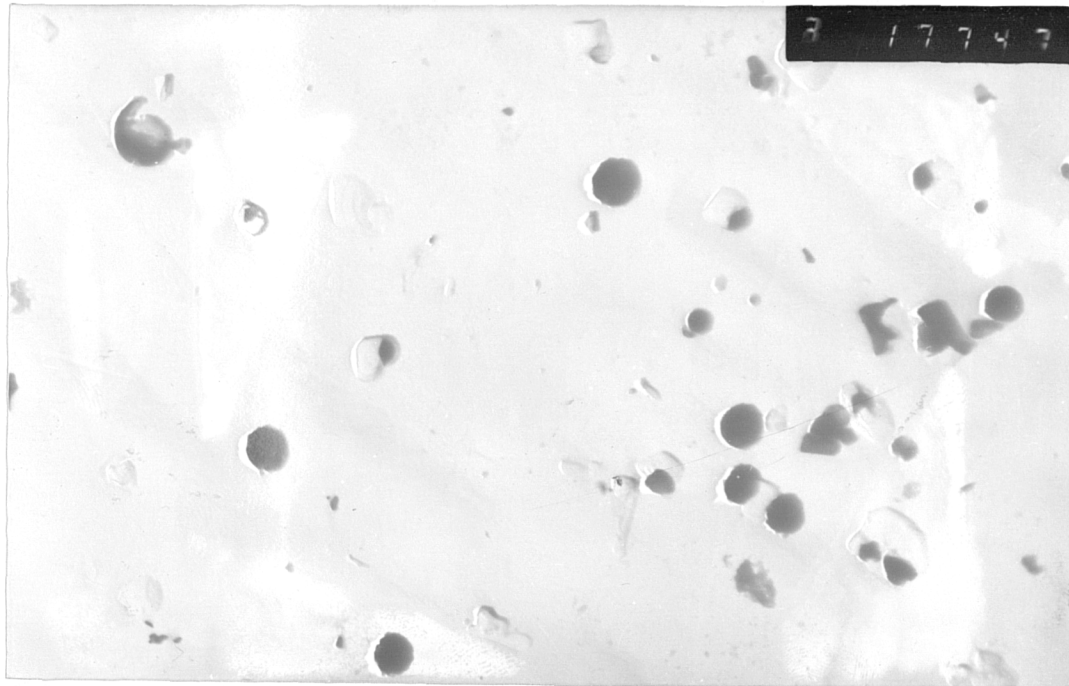


Fig. 6.12 MnS inclusions observed in the C-Mn-Al-Nb steel (heat G) at test temperature of 850 °C, with associated X-ray spectrum.



1.54 μm

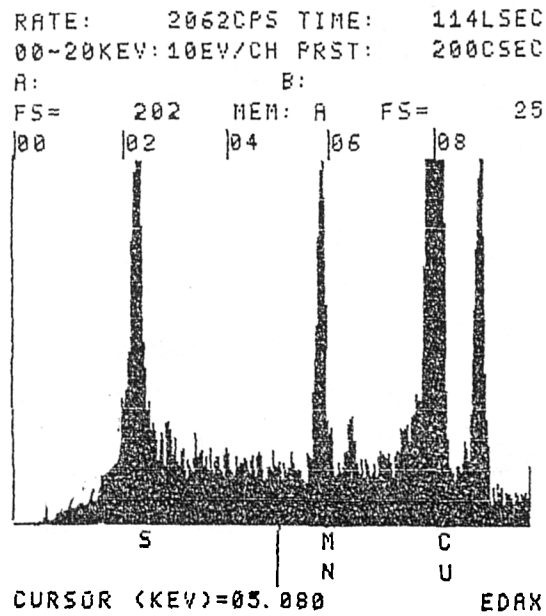
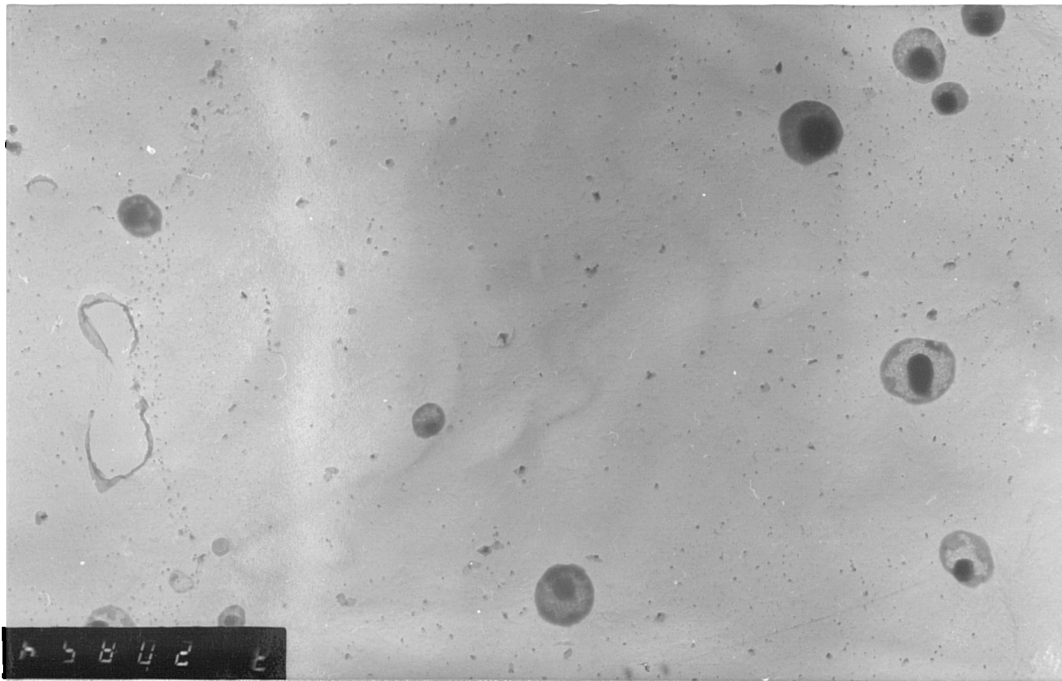
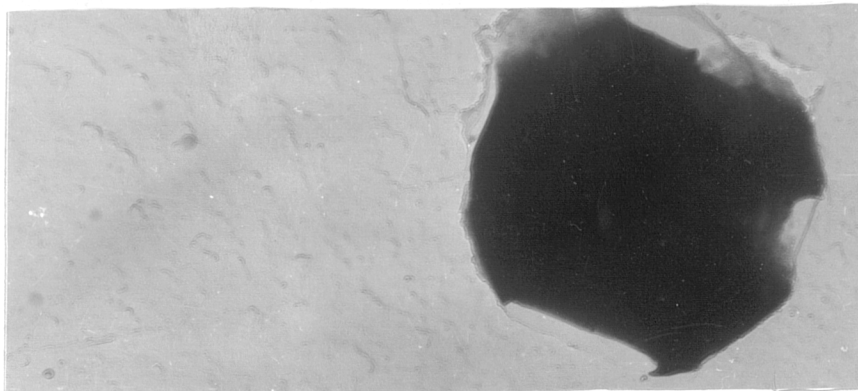


Fig. 6.13 MnS inclusions observed in the C-Mn-Al steel (heat B) at test temperature of 870 °C, with associated X-ray spectrum.



(a).

1.54 μm



(b).

0.52 μm

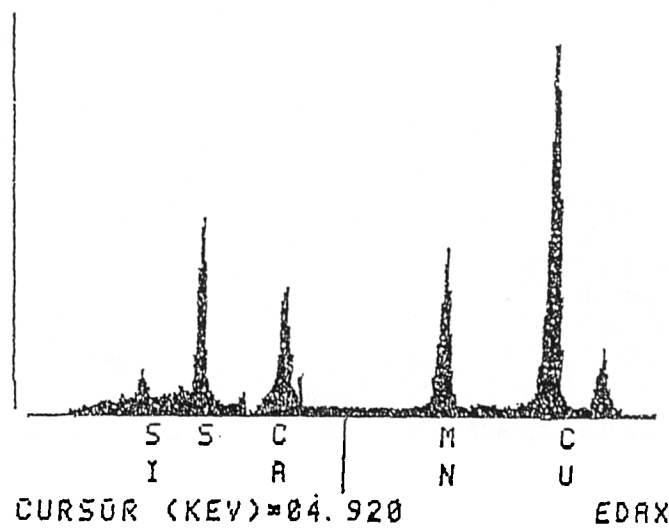


Fig. 6.14 (Mn,Ca)S inclusions observed in the Ca treated steels at 850 °C. with associated X-ray spectrum.
 a. C-Mn-Al-Nb-Ca steel (heat D).
 b. C-Mn-Al-Ca steel (heat A).

CHAPTER 7

THE RELATIVE INFLUENCE OF STATIC AND
DYNAMIC PRECIPITATION ON THE HOT DUCT-
TILITY OF MICRO ALLOYED STEELS

7.1 INTRODUCTION

It is well known, that the precipitation of carbides and/or nitrides play an important role in the fracture behaviour of micro-alloyed steels after certain thermal cycles, and at intermediate strain rates. (Bernard et al, 1978; Mintz and Arrowsmith, 1979; Ouchi and Matsumoto, 1982). This precipitation may be present prior to deformation, or formed during deformation. Precipitation of AlN, NbCN and VCN are accelerated by deformation (Akben et al, 1981; Le Bon et al, 1975; Vodopivec, 1973; Weiss and Jonas, 1979). It is believed that this acceleration of precipitation is due to the introduction of favourable nucleation sites by the deformation process. The exact nature of these nucleation sites can not be determined directly for transformable steels, but it seems likely that these sites are dislocation networks and vacancy clusters. This is supported by the observation of NbCN precipitation on dislocations in austenitic stainless steels following high temperature testing. (Ohmori and Maehara, 1984). The proportion of static and dynamic precipitates present at a particular temperature after deformation is dependent on the cooling rate from the solution temperature, and also on the deformation rate. Slow cooling rates are likely to favour static precipitation. For the particular case of AlN, cooling rates of approximately 1 °C/min. are believed to be required for the precipitation of AlN during continuous cooling, a particularly sluggish reaction. (Gladman and Pickering, 1967). Dynamic precipitation may not occur at very high strain rates,

since deformation usually ceases before the incubation time for dynamic precipitation has been reached. However, static precipitation may subsequently occur in the deformed structure. This static precipitation in a deformed structure occurs at rates intermediate between that of dynamic precipitation, and static precipitation, in undeformed metal. (Weiss and Jonas, 1979). The investigation of Weiss and Jonas (1979) showed that for the dynamic precipitation of NbCN, strain rates of less than 10^{-1} S^{-1} were required the exact values being temperature dependent. A later study by Akben et al (1981) showed that a similar strain rate was required for the dynamic precipitation of VCN. Another result from a study by Weiss and Jonas (1980) was that dynamically precipitated NbCN was finer than the equivalent static precipitates formed at the same temperature.

Recently, Crowther and Mintz (1985) have shown that both dynamic and static precipitation of NbCN were effective in delaying the onset of dynamic recrystallisation in a C-Mn-Nb-Al steel tested at 950 °C. On the other hand they have found that static precipitation of VCN is more effective than dynamic in retarding recrystallisation in a C-Mn-V-Al steel tested at 850 °C. Unfortunately, they could not draw a conclusion on the relative influence of dynamically and statically precipitated AlN, due to not being able to precipitate AlN in the C-Mn-Al steel examined. This steel held for 6 hours at 850 °C prior to testing failed to precipitate AlN. It is believed that,

this failure to produce precipitation was due to the relatively low Al and N levels present in the steel. Other investigations into the influence of static and dynamic precipitation of AlN have concluded that precipitates present before deformation are more detrimental to hot ductility than those formed during the test. (Vodopivec, 1978; Wilcox, 1982). Wilcox has also concluded that NbCN formed during deformation is more detrimental to hot ductility than that existing prior to deformation.

It can be seen from the foregoing that precipitate volume fraction and size are dependent on whether the precipitate is formed in a dynamic or static situation. Therefore, since both precipitate volume fraction and size play an important role in determining the hot ductility of micro-alloyed steels, it would be expected that dynamic and static precipitates would each have a distinct influence on hot ductility.

It was therefore, decided to extend the previous study by Crowther and Mintz, in which the influence of holding time on hot ductility was examined for Nb, V, and Al containing steels at only one temperature, that for which precipitation was most rapid. It is intended in this study to investigate the influence of holding time on precipitation and hot ductility for a wider temperature range 750-1000 °C for the previously examined Nb and V containing steels and to replace the low Al level steel examined by them for a higher Al containing steel

In addition to this, the relative influence of static and dynamic precipitation of AlN in the high level Al steel will be examined with different holding times at a test temperature of 850 °C.

7.2 EXPERIMENTAL

The compositions of the steels examined are given in Table 7.1. The steels were supplied as 50 kg vacuum melts, which had been control rolled to 12 mm plate, finish rolling 1050 °C. Tensile samples having a length of 70 mm and diameter 7.935 mm were machined from the plate (see Fig. 4.2) with their axes parallel to the rolling direction. The equipment used to heat and test the samples is the induction heating unit described in Chapter 4.

The testing sequence consisted of the following steps:

- a- specimens were austenitized over 40 mm length by heating them to 1330 °C in about 15 to 17 minutes.
- b- specimens were solution treated for 10 minutes at 1330 °C, which was expected to dissolve all precipitates.
- c- samples were then cooled rapidly at an average rate of 100 °C/min. to test temperatures. This cooling rate would suppress pre-test precipitation.

d- samples were either immediately tested or held at the test temperature for a fixed period of time before deformation. The strain rate used was $3 \times 10^{-3} \text{ S.}^{-1}$, being the same strain rate used by Crowther and Mintz. Tests were performed in the temperature range 750-1000 °C. Various holding times were given prior to testing to vary the amount of prior precipitation from zero to a substantial amount.

Holding times at test temperatures for the three steels were:

1 sec. and 15 min. for the C-Mn-Nb-Al steel.

1 sec. and 2 hours for the C-Mn-V-Al steel.

1 sec. and 15 min. for the C-Mn-Al steel.

Tests were also performed at 850 °C on the C-Mn-Al (0.0068 Al% in Wt) steel for holding times prior to testing of 120, 360, 3600, 8100, and 14400 seconds.

850 °C was chosen as the test temperature because it is the temperature corresponding for the maximum rate of precipitation of AlN. (Leslie et al., 1954 ; Akben et al., 1981).

It should be noted that 850 °C is above the Ae_3 temperature calculated using the Andrews' formula (1965) for the C-Mn-Al steel.

Fracture surfaces from broken tensiles were examined using a JEOL T100 Scanning Electron Microscope, operating at 25 KV. Carbon extraction replicas were

prepared from sections approximately 1 mm behind the fracture surface and examined using a Jeol 100 KV Transmission Electron Microscope, operating at 60 KV. The replica technique is described in Appendix 1.

To investigate the static precipitation of NbCN at 950 °C, the method of loss of secondary hardening potential was used. Small samples of the Nb containing steel were solution treated at 1330 °C for 10 minutes and rapidly cooled to 950 °C; and maintained at this temperature for varying lengths of time, after which the samples were quenched in iced brine and tempered at 600 °C for 1 hour. Similar experiments were carried out for the V containing steel at 850 °C, tempering being carried out at 550 °C for ½ hour. Hardness measurements were then taken from these samples using a Vickers DP machine, using a 20 kg load.

The interpretation of this test relies on the assumption that holding time at test temperature before quenching precipitates out in the austenite, VCN in the C-Mn-V-Al steel and NbCN in the C-Mn-Nb-Al steel. leaving less available for precipitating in the ferrite. Prior precipitation in the γ phase is too coarse to cause hardening, but that retained in the solution in the ferrite can subsequently cause hardening on tempering. Hence the lower the hardness value the greater is the amount of the static precipitation formed prior to test.

7.3 RESULTS

7.3.1 HOT DUCTILITY CURVES

The curves of reduction in area against test temperature for short and long holding times are given in Figs. 7.1-7.3 for the C-Mn-Nb-Al, C-Mn-V-Al and C-Mn-Al steels, respectively. All the steels show a marked ductility trough for both holding times. The depth, width, and position of the trough vary with steel composition.

The ductility of the Nb containing steel starts to fall at 1000 °C, and reached a minimum of (30-40%) in the temperature range 800 to 950 °C for both holding times, Fig. 7.1. Ductility is recovered when the temperature is further lowered to 765 °C. Holding this steel for 15 minutes at test temperatures resulted in a better hot ductility (about 10 %) over the temperature range 800 to 1000 °C.

For the V containing steel, Fig. 7.2, reduction in area falls from 99% at 1000 °C and reached a minimum of (35-40%) at 800 °C for both holding time, again ductility was improved as the test temperature was lowered to 765 °C. Increasing the holding time at test temperature from 1 second to 2 hours, impaired the hot ductility (about 8 %) over the temperature range 800 to 950 °C.

Similar behaviour to that shown by the V containing

steel was given by the Al containing steel. Ductility starts to fall at 900 °C for both holding times and reached the minimum of (23-35%) at 800 °C, Fig. 7.3. Extending the holding time to 15 mins., at test temperature deteriorated the hot ductility over the temperature range 765 to 850 °C.

7.3.2 STRESS-ELONGATION CURVES

The stress - total elongation curves for the three steels are shown in Figs.7.4-7.11. At higher deformation temperatures (≥ 900 °C), there were fluctuations in the flow curves for all the tests involving the C-Mn-Al steel, Figs.7.4-7.5. These fluctuations (arrowed in Figures) are similar to those associated with the onset of dynamic recrystallization. (Carlsson,1964; Hannerz et al, 1968). Dynamic recrystallisation was observed for the C-Mn-V-Al steel tested in the temperature range 850-1000 °C for holding times of 1 second and for the temperature range 900-1000 °C after a 2 hour holding time prior to testing, Figs.7.6-7.7. For the C-Mn-Nb-Al steel, fracture occurred before the onset of dynamic recrystallisation for testing temperatures in the range 765-950 °C, Figs. 7.8-7.9. There was some evidence for dynamic recrystallisation occurring at 1000 °C.

For the C-Mn-Al steel tested at 850 °C, with different holding times, varying from 1 to 14400 seconds, no evidence of dynamic recrystallisation has been observed, Fig. 7.10.

7.3.3 INFLUENCE OF HOLDING TIME AT TEMPERATURES CORRESPONDING TO THOSE GIVING THE MAXIMUM RATE OF PRECIPITATION

Fig.7.11, shows the variation of reduction in area and peak stress, σ_p , with holding time prior to testing at 850 °C for the C-Mn-Al steel. Increasing the holding time, decreased the R of A values, falling from 70 % with no holding time to 38 % with a 14400 S holding time prior to testing. The peak stress increases slightly as the holding time increases, rising from 62 Mpa for no holding time to 67 Mpa after a 14400 S, holding time.

Similar R of A behaviour to that shown by the Al containing steel was observed by the Nb containing steel. The improvement of hot ductility from 31 % to 44 % at 950 °C, Fig.7.1, was associated with a lower peak stress value, being 56 Mpa for no holding time and 51 Mpa for a 15 mins., holding time, Figs. 7.8-7.9.

The peak stress for the C-Mn-V-Al steel remained constant for both holding times at 850 °C, despite the 10 % improvement of hot ductility from 22 % with 2 hours holding time to 32 % with no holding time.

The results for the V and Nb containing steels are in a good agreement with previous work by Crowther and Mintz (1985). Previous work by Crowther and Mintz on a lower

Al, C-Mn-Al steel gave reduction of area values of over 95 % for all holding times, and a constant peak stress of 69 Mpa. This illustrates again how difficult it is to precipitate AlN when Al and N levels are too low (0.017% Al, 0.006% N in previous work)

7.3.4 STATIC PRECIPITATION OF VCN AND NbCN

The hardness results used to follow the static precipitation kinetics of VCN in the C-Mn-V-Al steel at 850 °C and NbCN in the C-Mn-Nb-Al steel at 950 °C are shown in Figs. 7.12 - 7.13.

Quenching directly from 1330 °C followed by tempering at 550 °C for ½ hour resulted in a hardness value of 296 Vickers for the C-Mn-V-Al steel. This hardness value corresponds to zero VCN precipitation at 850 °C. When samples are held at 850 °C for more than 100 S, prior to quenching and tempering, hardness values begin to fall, and after holding for 1000 S, at 850 °C the hardness value falls to 210 Vickers. The hardness value remains approximately constant after 10000 S, which indicates that VCN precipitation at 850 °C is virtually complete after this time.

Similar behaviour was observed for the C-Mn-Nb-Al steel. Quenching directly from 1330 °C followed by tempering at 600 °C for one hour resulted in a hardness value of 300 Vickers. This hardness value corresponds to zero NbCN precipitation at 950 °C. Holding the samples at 950 °C for more than 2 mins., prior to

quenching and tempering resulted in a decrease in hardness value. After a 10000 S holding time the hardness value reaches 210 Vickers. Hardness values remain constant after this time, suggesting that NbCN precipitation at 950 °C is complete after this time.

7.3.5 TRANSMISSION ELECTRON MICROSCOPY

Carbon extraction replicas revealed precipitation of AlN in a fine form at the austenite grain boundaries and a coarser form in the matrix in the C-Mn-Al steel after holding for 14400 S prior to testing at 850 °C, Figs. 7.14-7.15.

The coarser precipitation was also present at the same test temperature after a 1 S holding time. These coarse precipitation were found not to change with time. Quenching small samples after simulating the heat treatment prior to tensile testing confirmed that this AlN originated from incomplete solution of AlN at 1330 °C.

Replicas from the Nb and V containing steel were not taken, as Crowther and Mintz (1985), had already carried out extensive examination on these steels. They observed in the Nb containing steel, held for 1 S prior to testing an extensive matrix and grain boundary precipitation of NbCN and in some cases, precipitate free zones adjacent to the grain boundaries. After 7200 S holding time, they observed a coarser

form of NbCN at the grain boundaries in addition to the fine precipitation and after 21000 S holding time, only the coarse grain boundary NbCN precipitate was observed.

In the C-Mn-V-Al steel, they have observed precipitation of VCN in all fractured samples. In the sample held for 1 S prior to test, VCN precipitates were randomly precipitated and in the sample held for 21000 S, precipitation was predominantly at the austenite grain boundaries.

7.3.6 FRACTURE APPEARANCES

An examination was made by the SEM on the fracture surfaces of the three steels examined. Samples broken in the trough, indicated that failure was always intergranular along the γ boundaries, Figs. 7.16-7.18.

Two intergranular failure modes were observed, intergranular decohesion and intergranular micro-void coalescence, the former mode predominating. Similar observations have been noted by Crowther and Mintz (1985) for the V and Nb containing steels.

In the C-Mn-Al steel examined, the intergranular micro-void coalescence mode was dominant for the sample held for 1 S at test temperature of 850 °C, while for the sample held for 135 mins., at the same test temperature, the dominant fracture mode was intergranular decohesion, Fig. 7.18. It should be noted,

that for the sample held for 1 S at 850 °C, quite a large amount of fracture surface was normal ductile rupture, Fig. 7.18a, in accord with its high R of A value (70%).

7.4 DISCUSSION

7.4.1 C-Mn-Al steel (.068 Al% in Wt.)

At the temperature giving the maximum rate of precipitation i.e. 850 °C, increases in holding time reduced hot ductility, Fig. 7.11. This suggests that statically produced AlN is most effective in reducing hot ductility. Similar trends were observed over a wider temperature range for no and long holding times prior to testing, Fig. 7.3.

The hot ductility curves obtained for this steel for short and long holding times show excellent ductility at higher deformation temperatures (≥ 900 °C), associated with the occurrence of dynamic recrystallisation, Figs. 7.4-7.5. The ductility troughs in the temperature range 750-900 °C, indicate, that failure occurs before the onset of dynamic recrystallisation. In accord with this behaviour, the austenite grain structure after fracture, consisted of unrecrystallised grains with a grain size of 414 μm .

The absence of precipitation (other than that present after incomplete solution treatment) in this steel tested after 1 s holding time, at 850 °C, indicates that fracture occurs before the incubation period necessary for dynamic precipitation of AlN has been reached. The time to failure for this test was ~ 300 S, and so the incubation time for the dynamic precipitation

of AlN must exceed this period. Static precipitation at the austenite grain boundaries appeared after considerable holding time prior to testing, which means that AlN precipitation at the grain boundaries is effective in preventing dynamic recrystallisation, leading to the decrease in hot ductility.

These results should be compared to those of Crowther and Mintz (1985), who did not observe any static AlN precipitation in their lower Al level steel even after a holding time of 6 hours at test temperature.

These results suggest that, only at a high level of Al ($\geq 0.068\%$) or high solubility product $[Al] \cdot [N]$, can AlN precipitation occur in a reasonable time prior to testing. This gives rise to impaired hot ductility compared with the excellent hot ductility given by the lower Al steel. It should be noted that no dynamic precipitation of AlN has been observed in this steel, nor in any of the steels examined.

7.4.2 C-Mn-V-Al steel

Increasing the holding time at 850 °C for the C-Mn-V-Al steel, has been shown by Crowther and Mintz (1985) to deteriorate the hot ductility, as with the higher Al steel. Similar behaviour was noted in this work. The samples held for 7200 S always are of worse hot ductility than those tested immediately in the temperature range 750-1000 °C. In this case dynamic precipitation occurred and the results show that static

precipitation of VCN reduces the hot ductility more than the dynamically precipitated VCN.

The hot ductility behaviour of this steel for short and long holding times, can be explained in terms of differences in the precipitation formed prior to test or during the deformation.

The hardness-time curve in Fig. 7.12, indicates that at 850 °C no significant static precipitation of VCN in this steel should occur with a 1 S holding time. However, Crowther and Mintz (1985) have observed in the same steel given a holding time of 1 S, a random precipitation of VCN, suggesting that these precipitates are dynamically formed. Fig. 7.6 shows some evidence of dynamic recrystallisation occurring before fracture in the sample held for 1 S, prior to test at the same test temperature of 850 °C. No evidence for dynamic recrystallisation was found for longer holding times. These results suggest, that the randomly distributed, dynamically precipitated VCN, is only partially effective in preventing dynamic recrystallisation.

Thus it can be concluded that dynamically precipitated VCN is less effective in retarding recrystallisation than statically precipitated VCN, and this leads to static VCN having the greater detrimental effect on hot ductility. Hot ductility curves for no and long holding times, Fig. 7.2, confirmed this conclusion, as holding the samples at 850 °C for 2 hours impaired the hot ductility over the temperature range 750-1000 °C.

7.4.3 C-Mn-Nb-Al steel

In contrast to the V and high Al containing steels, increasing the holding time at the test temperatures for the C-Mn-Nb-Al steel, improved the hot ductility over the temperature range 850-1000 °C, Fig. 7.7, leading to the conclusion that NbCN precipitated during the test is more detrimental to hot ductility than those formed before deformation.

Similar behaviour was noted by Crowther and Mintz (1985) for the same steel tested at 950 °C with different holding times.

The ductility troughs observed in the temperature range 800 - 1000 °C for short and long holding times are typical for a Nb containing steel tested at relatively low strain rates ($3 \times 10^{-3} \text{ s}^{-1}$) after solution treatment. More interesting is the improvement in hot ductility with increasing holding time, suggesting that the NbCN formed during deformation is more detrimental to hot ductility than the NbCN present prior to the test. At the same time the rapid static precipitation rate of NbCN, as demonstrated in this work, Fig.7.13, and by Crowther and Mintz, means that, only the sample tested with a holding time of 1 S, prior deformation, will show a precipitation pattern formed solely during deformation. The remaining samples all contain a proportion of NbCN formed prior to testing.

A possible explanation for the inferior hot ductility obtained with no holding time at test temperatures, in the temperature range 850-1000 °C, are the observations by Crowther and Mintz (1985) of an extensive NbCN precipitation at the austenite grain boundaries and in the matrix, and the tendency to form precipitate free zones as for example in the sample tested at 950 °C with no holding time. This leads to strain concentration at the austenite grain boundaries, and hence reduced hot ductility. It is believed that this matrix precipitation of NbCN was sufficient to produce a slight increase in the peak stress at 950 °C as shown in Figs. 7.8-7.9 and by Crowther and Mintz (1985).

7.5 CONCLUSIONS

1. In a C-Mn-Al steel tested at 850 °C, no dynamic precipitation of AlN occurred, but static precipitation of AlN took place at the γ grain boundaries after a holding time of 14,400 seconds at test temperature leading to reduced hot ductility.
2. Static precipitation of VCN and NbCN in a C-Mn-V-Al and C-Mn-Nb-Al steels as followed by the method of loss of secondary hardening shows that precipitation is rapid and commences in both cases in less than 5 minutes.
3. Full hot ductility curves for the steels examined over the temperature range 750 - 1000 °C for no and long holding times, show that increasing holding time at test temperatures, improved hot ductility for the Nb containing steel, and impaired the hot ductility for V and high Al containing steels.

Thus static precipitation is more effective than dynamic precipitation in the case of V and Al containing steels, whilst the reverse is true for the Nb containing steel. This confirms the finding of Crowther and Mintz. In the case of the Al containing steel as noted in conclusion 1, only static precipitation occurs and this is effective in reducing hot ductility.

4- Full hot ductility curves for no and long holding times converged at high and low testing temperatures, where the rates of precipitation were slow and separated in the temperature range where precipitation rates were high.

steel	C	Mn	Si	S	P	Al	N	V	Nb
C-Mn-Nb-Al	.12	1.44	.29	.009	.003	.015	.01	—	.034
C-Mn-V-Al	.11	1.34	.32	.006	.005	.024	.004	.057	—
C-Mn-Al	.16	1.4	.22	.015	.002	.068	.004	—	—

Table 7.1 Compositions of the steels examined (wt. %)

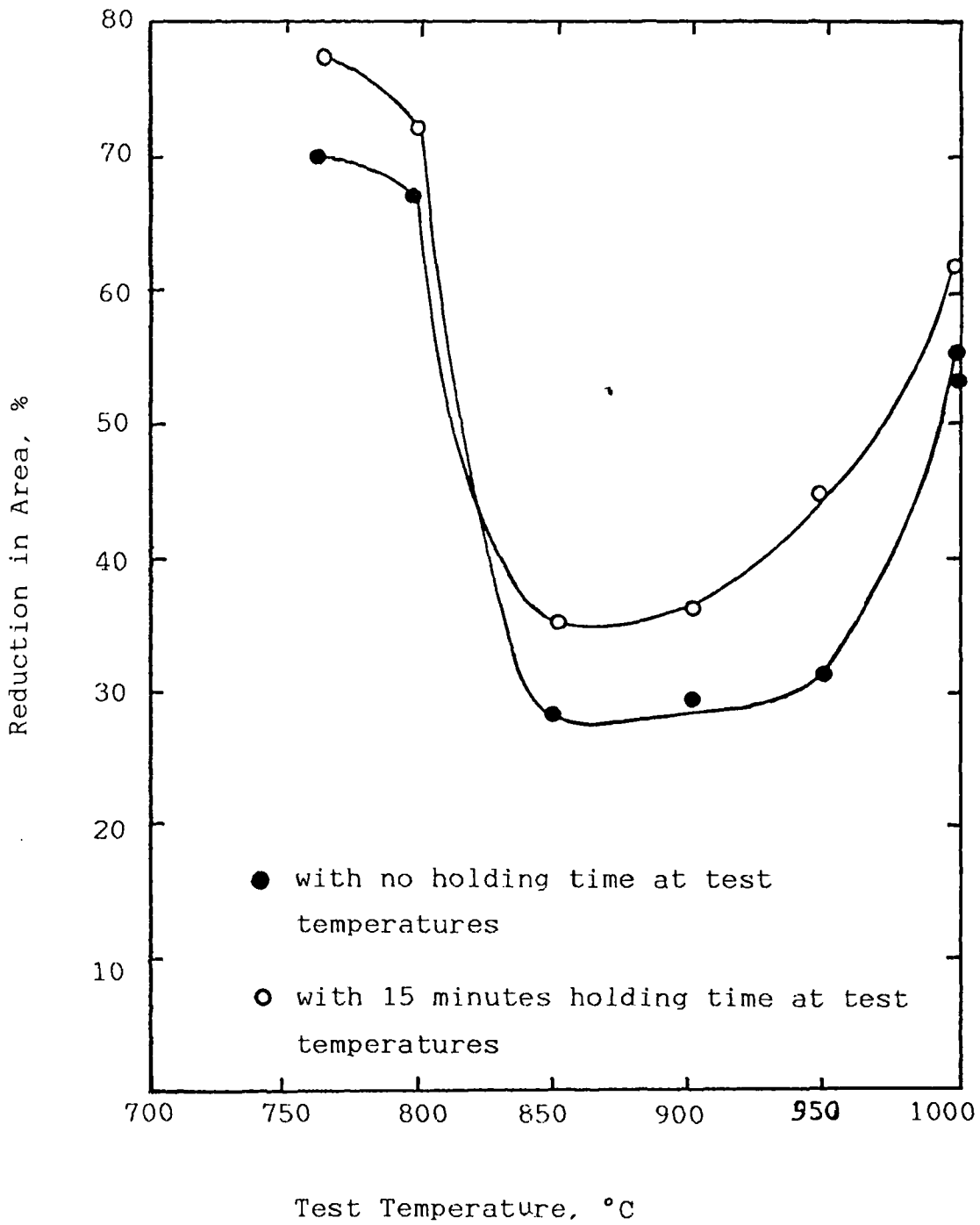


Fig. 7.1 Hot ductility curves for the C-Mn-Al-Nb steel

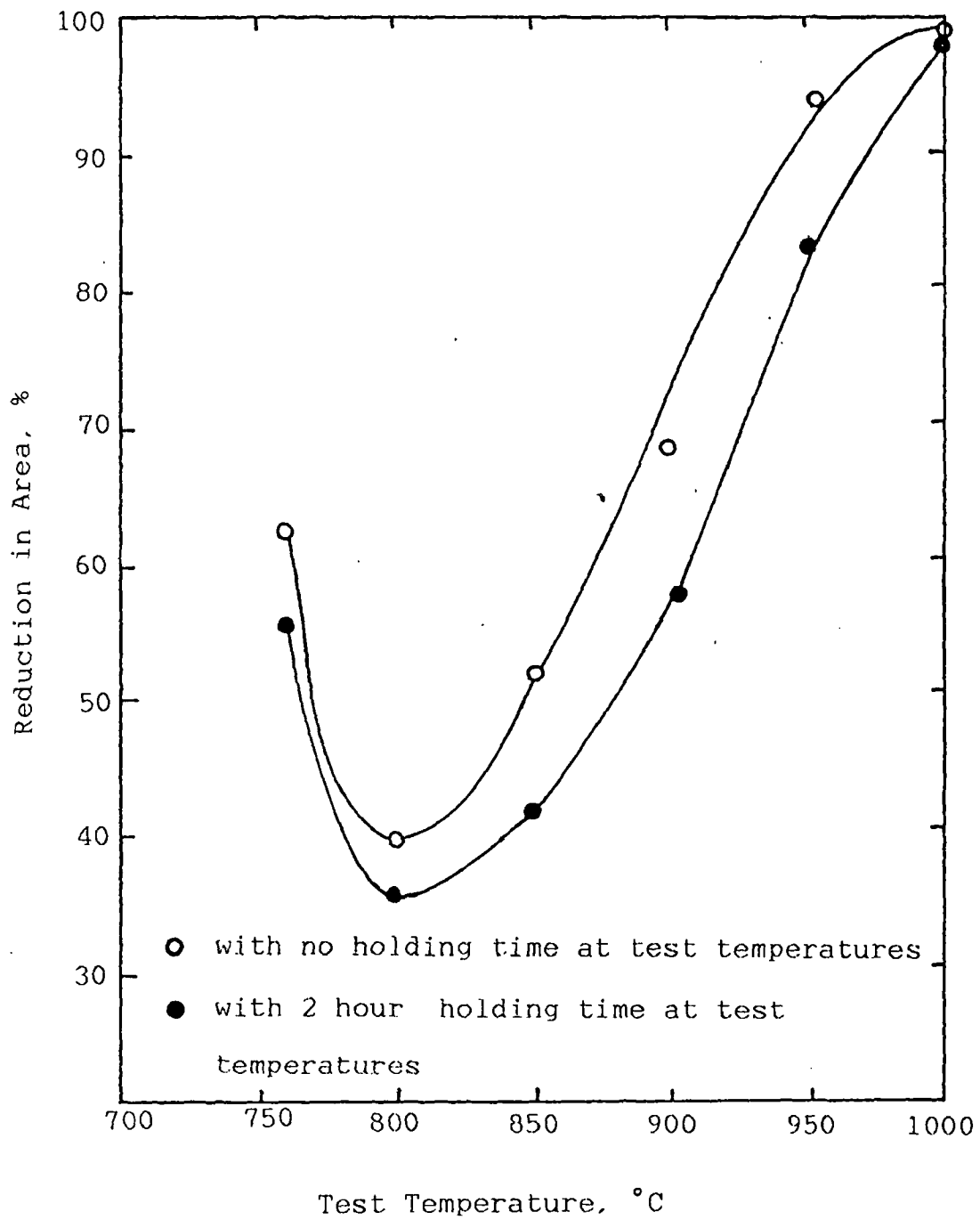


Fig. 7.2 Hot ductility curves for the C-Mn-V-Al steel

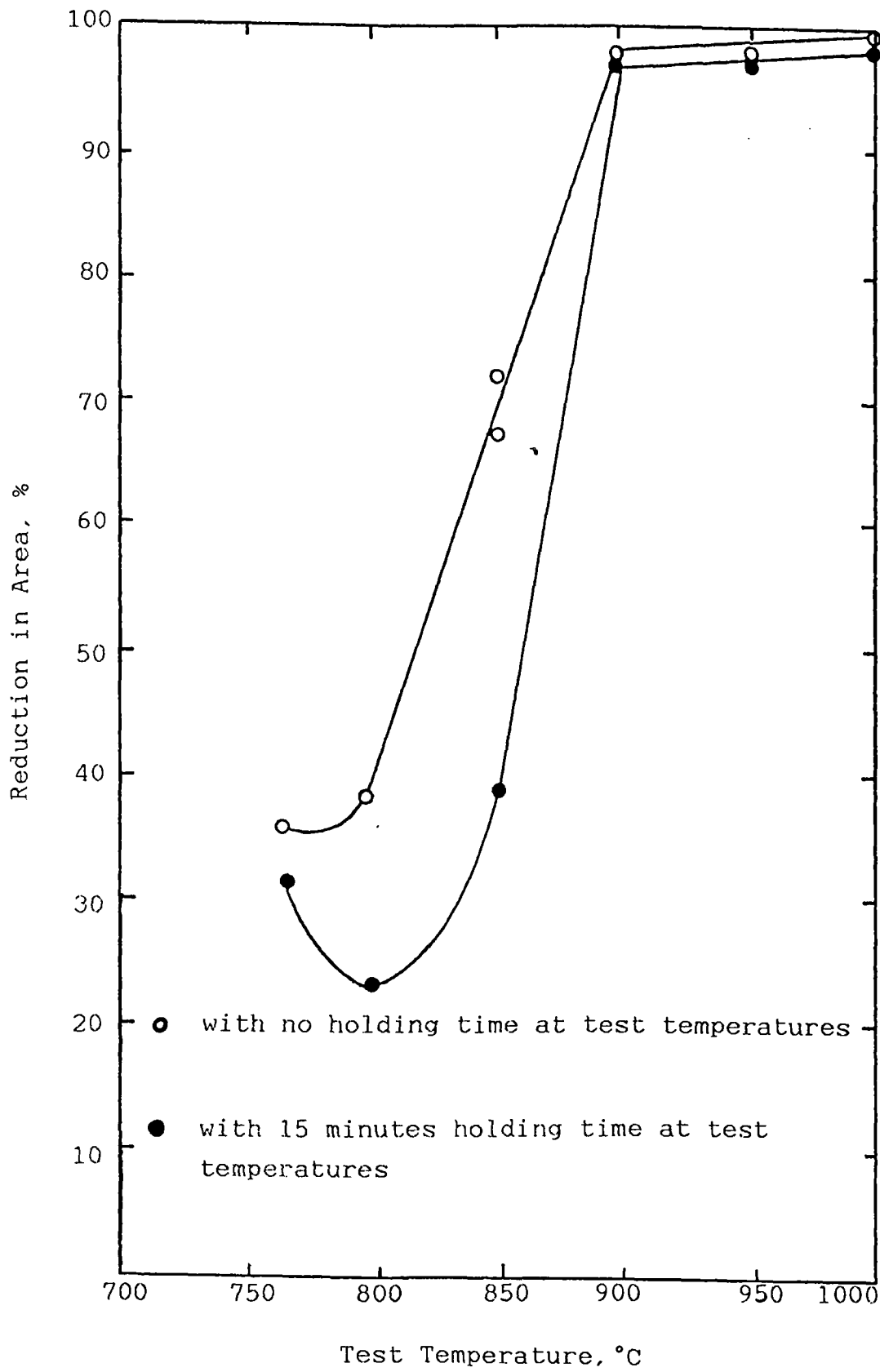


Fig. 7.3 Hot ductility curves for the C-Mn-Al steel

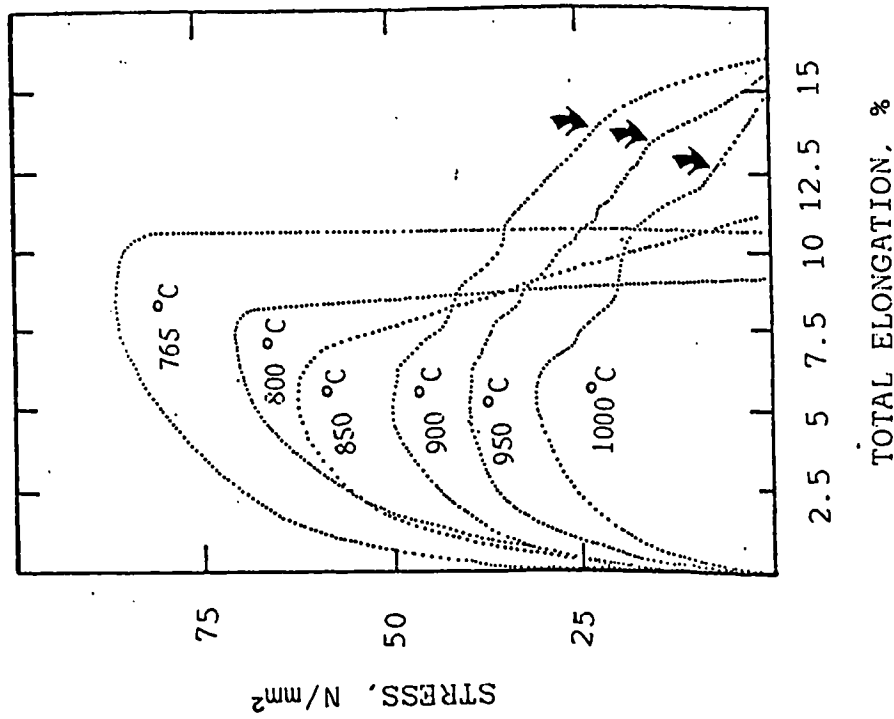


Fig. 7.4 Stress-Total Elongation curves for the C-Mn-Al steel with no holding time at test temperature.

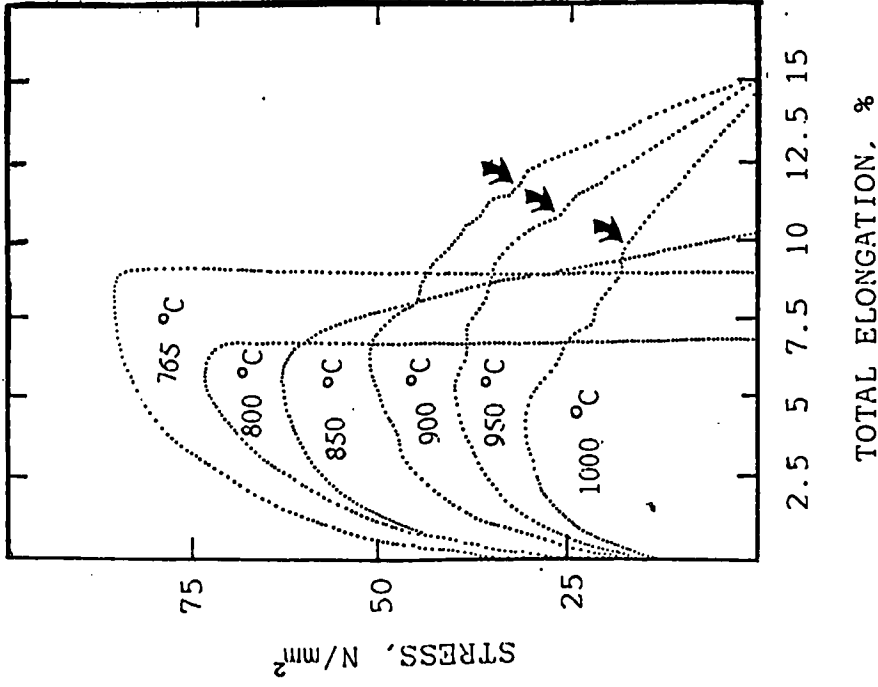


Fig. 7.5 Stress-Total Elongation curves for the C-Mn-Al steel with holding time of 15 minutes at test temperature.

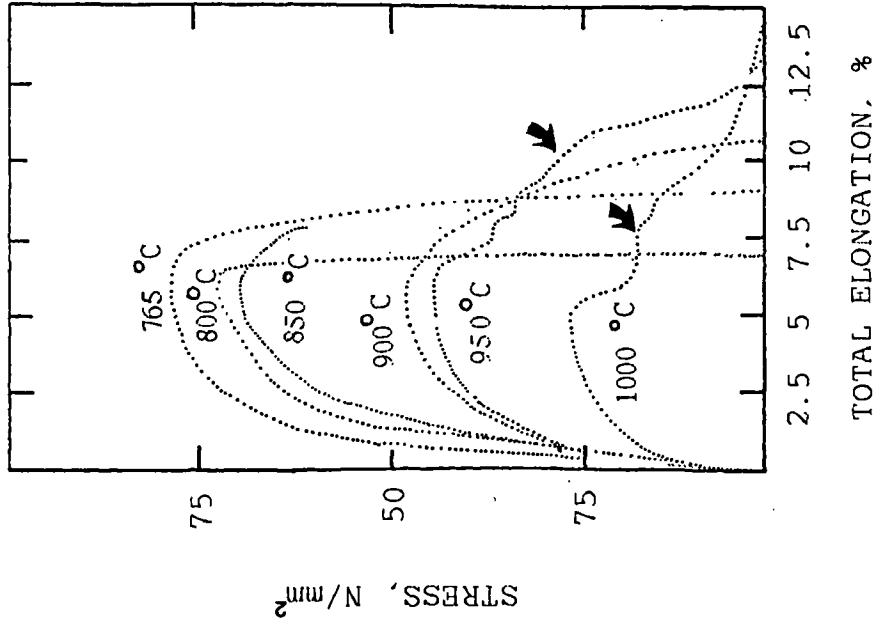


Fig. 7.7 Stress-Total Elongation curves for the C-Mn-V-Al steel with holding time of 2 hours at test temperature before deformation.

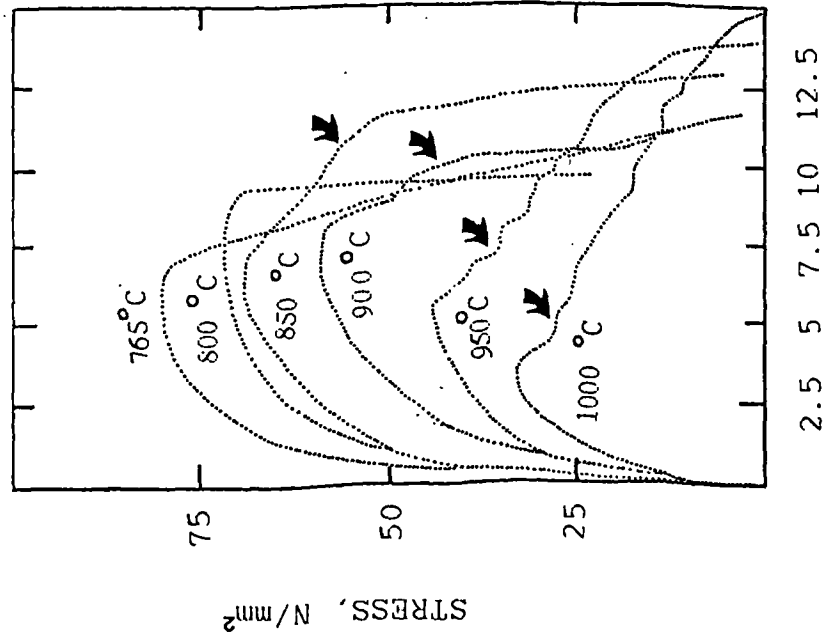
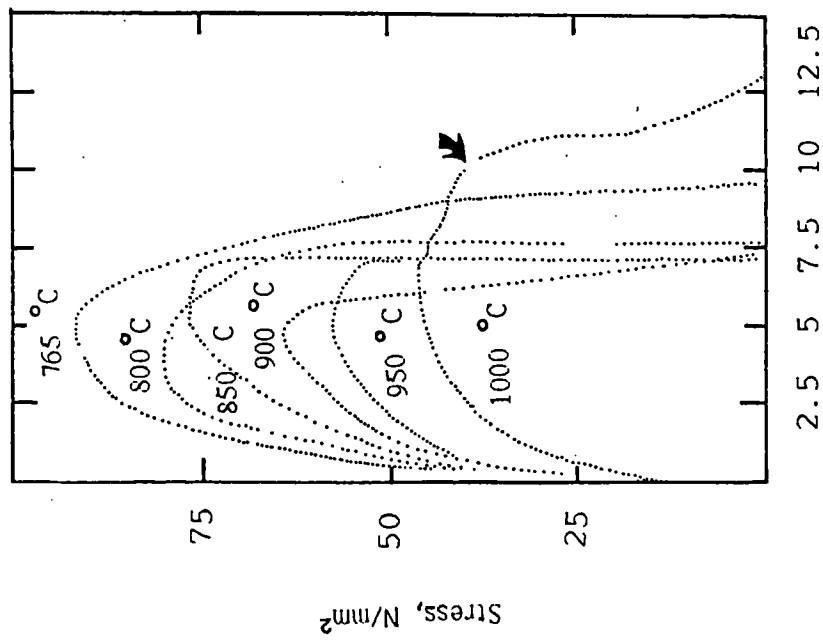
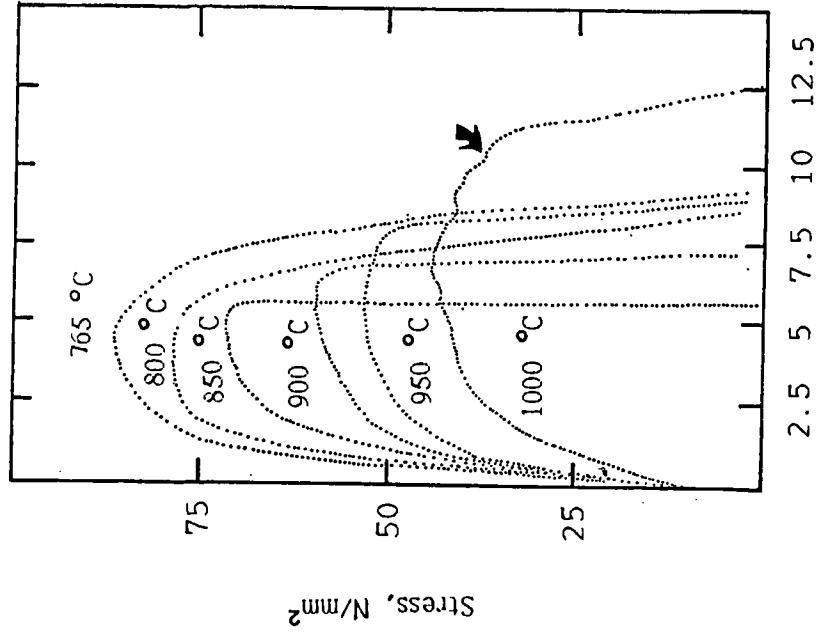


Fig. 7.6 Stress-Total Elongation curves for the C-Mn-V-Al steel with no holding time at test temperature.



TOTAL ELONGATION,

Fig. 7.8 Stress-Total Elongation curves for the C-Mn-Nb-Al steel with no holding time at test temperature



TOTAL ELONGATION, %

Fig. 7.9 Stress-Total Elongation curves for the C-Mn-Nb-Al steel with holding time of 15 minutes at test temperature.

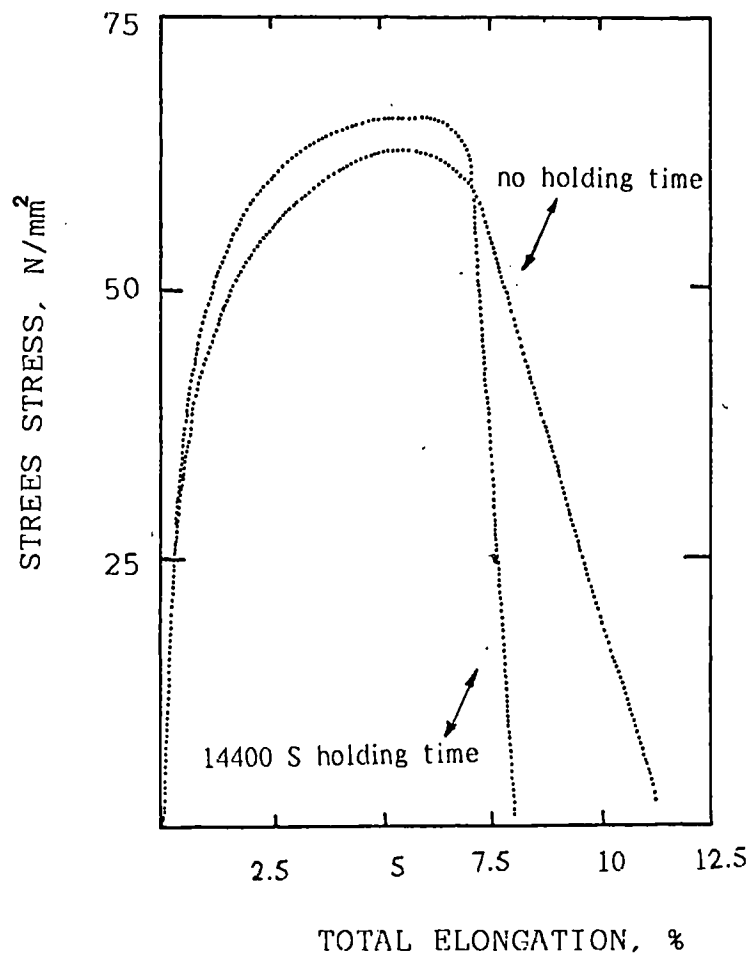


Fig. 7.10 Stress-Total Elongation curves for the C-Mn-Al steel with different holding times at test temperature (850°C).

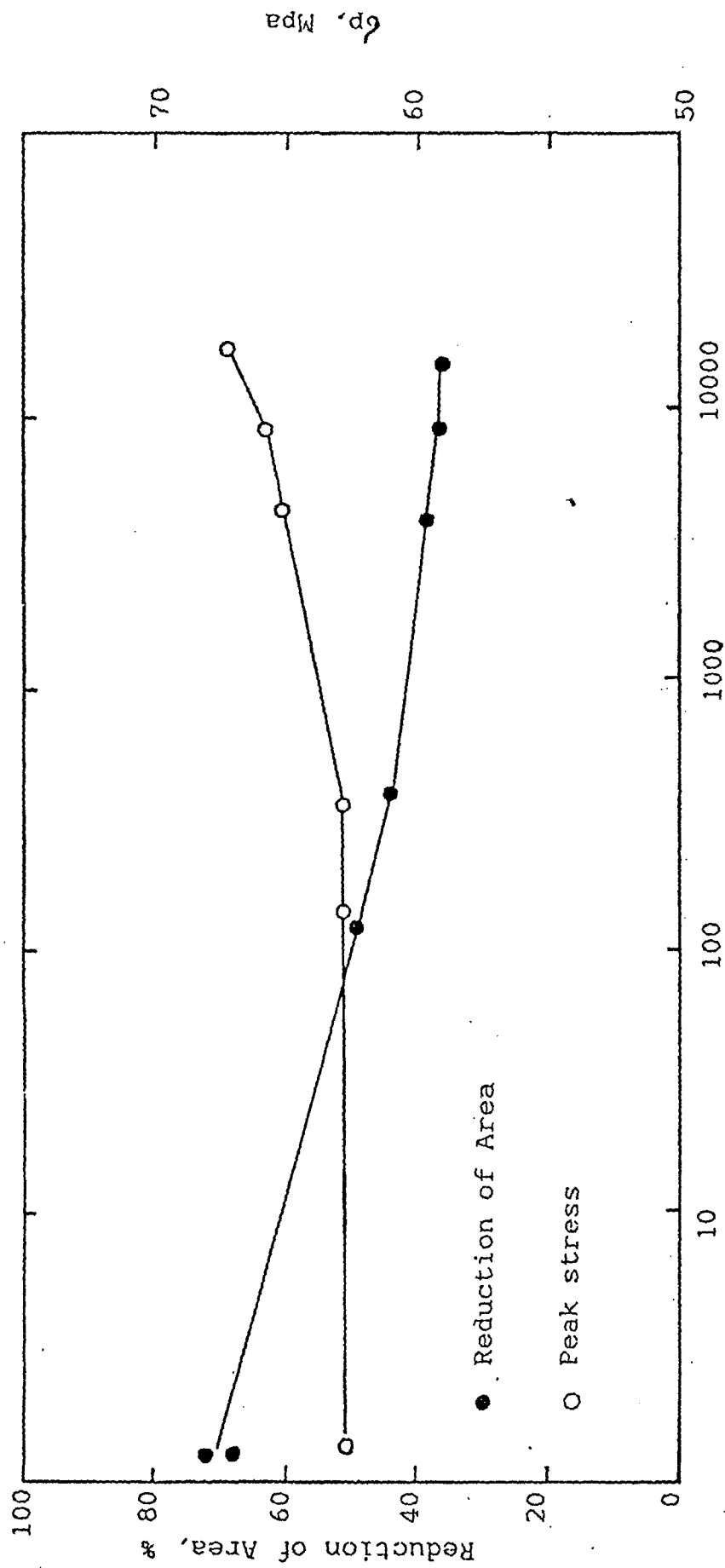


Fig. 7.11 Influence of holding time prior to testing on peak stress and hot ductility of the C-Mn -Al steel tested at 850 °C.

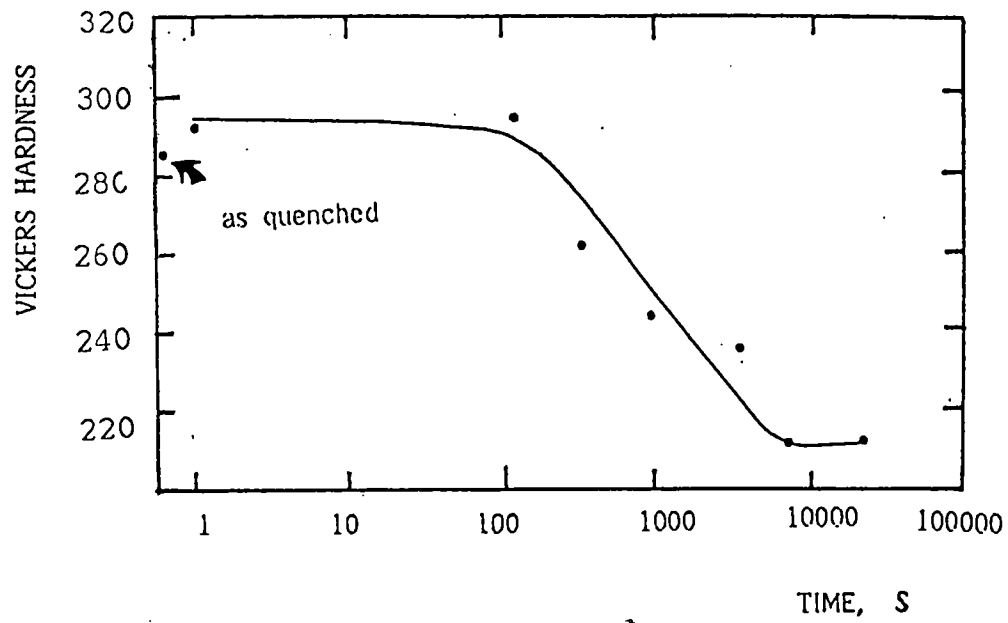


Fig. 7.12 Hardness of the C-Mn-V-Al steel following quenching and tempering, after holding for various times at 850 °C

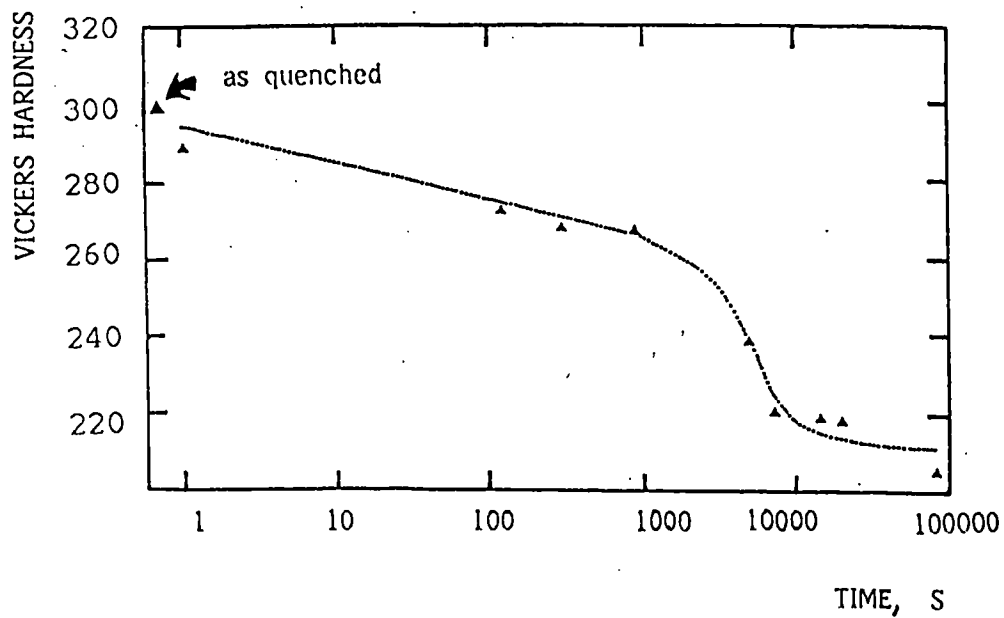
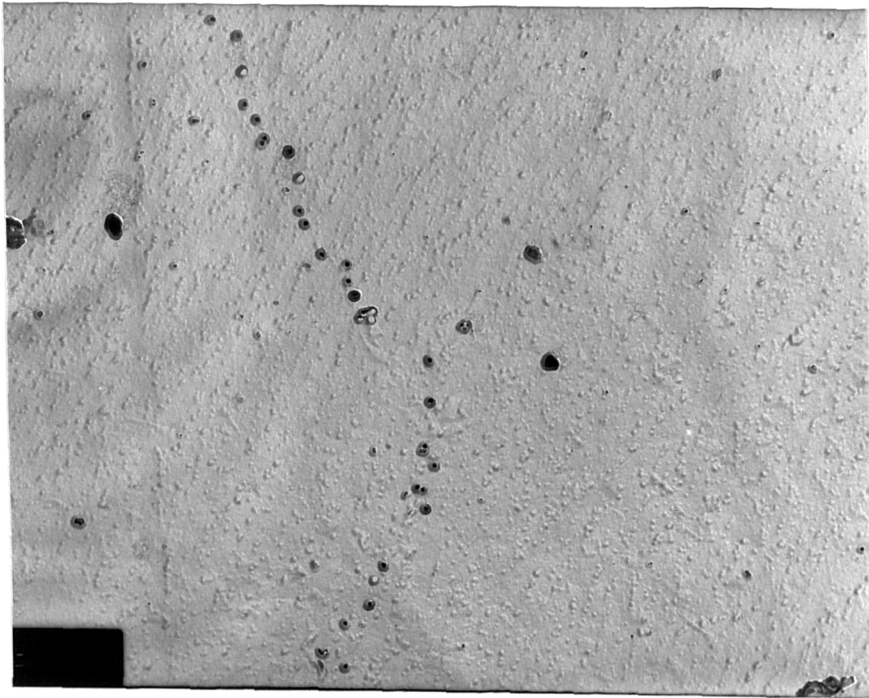
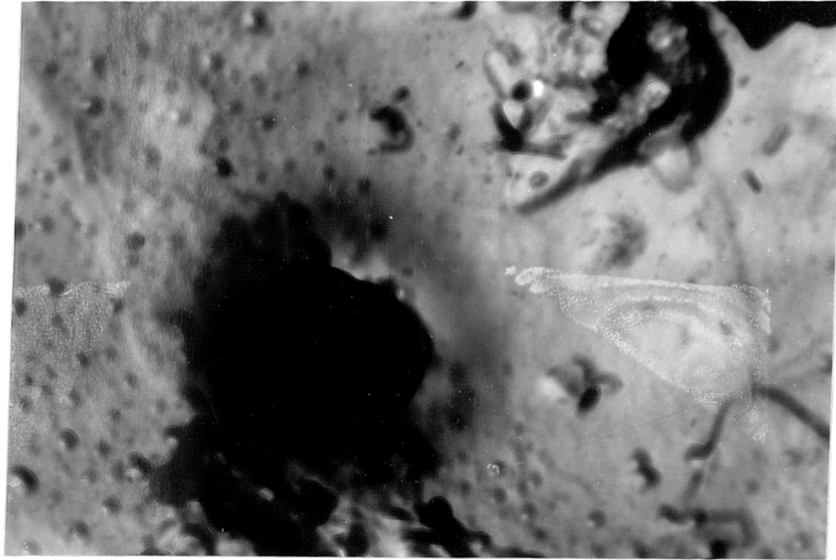


Fig. 7.13 Hardness of the C-Mn-Nb-Al steel following quenching and tempering, after holding for various times at 950 °C.



1.1 μm

Fig. 7.14 Example of fine AlN precipitation in the C-Mn-Al steel tested at 850 °C, after 4 hours holding time.

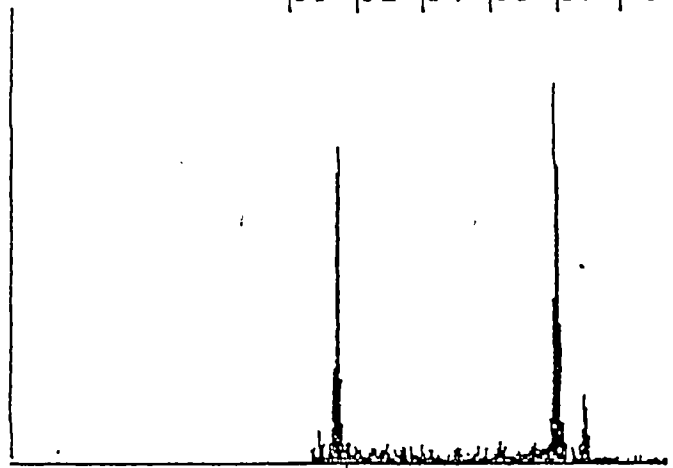


0.95 μm

```

02-JUN-86 13:30:19 PEAK IDENT
RATE:      3390CPS TIME:      9LSEC
00-20KEV: 10EV/CH PRST:     200CSEC
A:          B:
FS=      219  MEM: A   FS=     200
          |00 |02 |04 |06 |08 |10

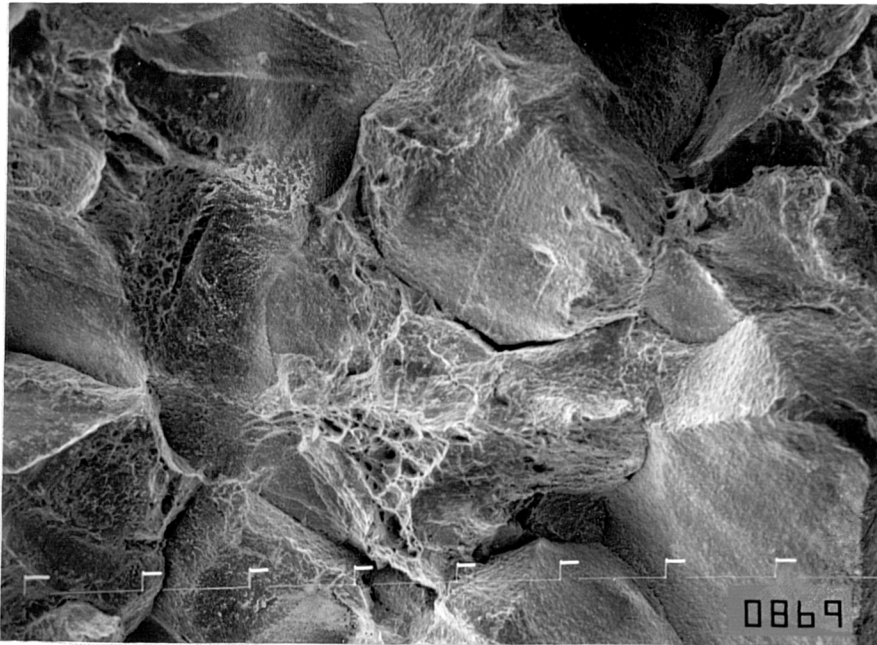
```



CURSÖR (KEV)=01.760

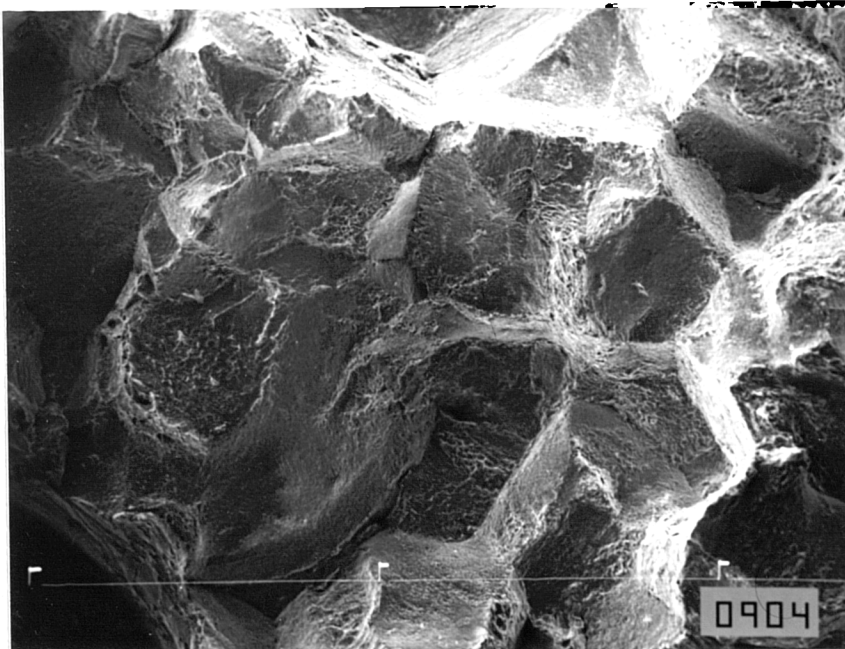
EDAX

Fig. 7.15 Coarse AlN precipitation in the C-Mn-Al steel, due to incomplete solution of AlN at 1330 °C, with associated X-ray spectrum.



166 μm

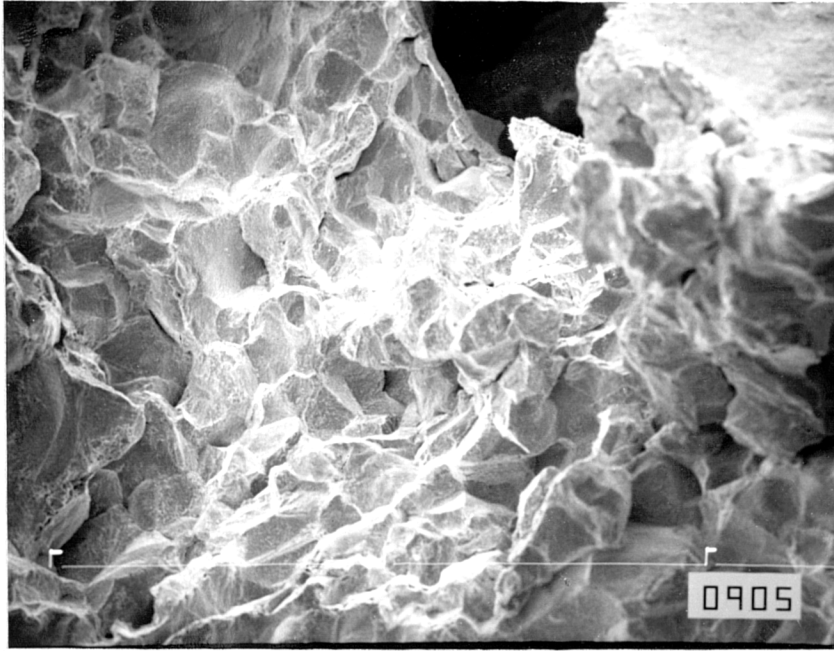
(a). with no holding time at test temperature (28% R of A)



200 μm

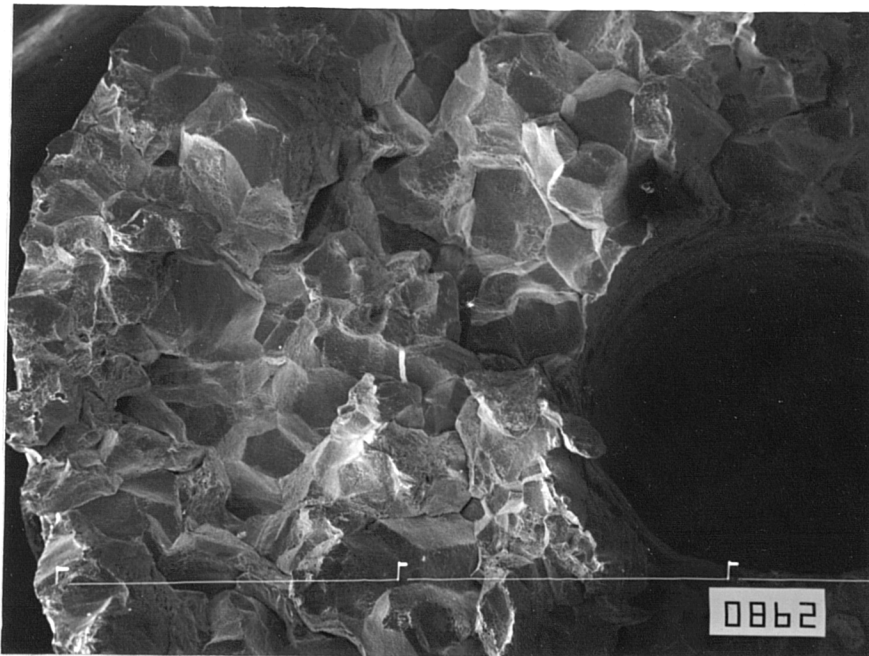
(b). with 15 mins., holding time at test temperature (35% R of A)

Fig. 7.16 Mixture of intergranular decohesion and intergranular micro-void coalescence type fracture in the C-Mn-Al-Nb steel tested at 850 °C.



266 μm

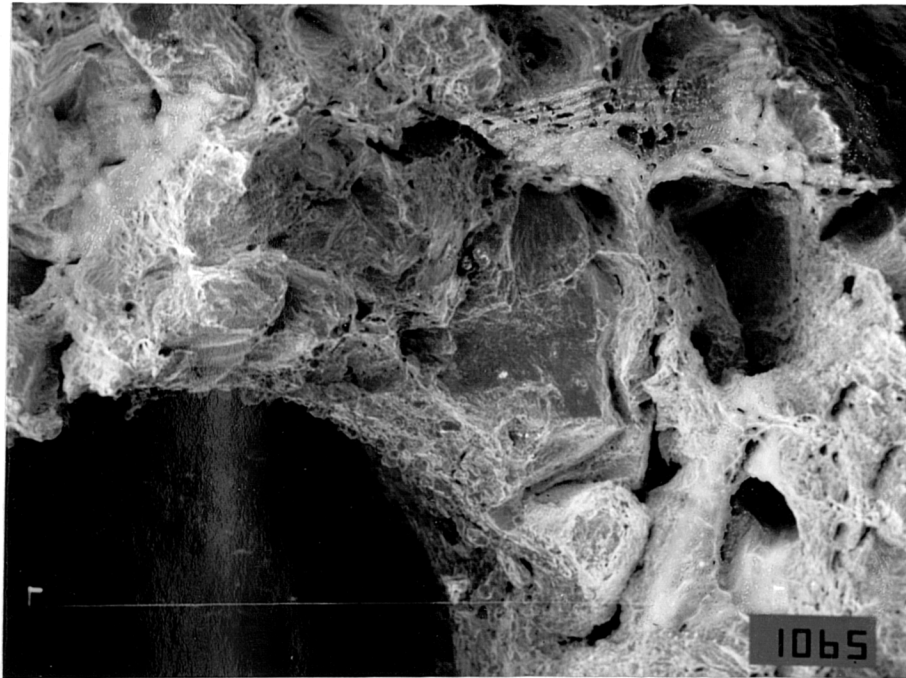
(a). with no holding time at test temperature (20% R of A)



266 μm

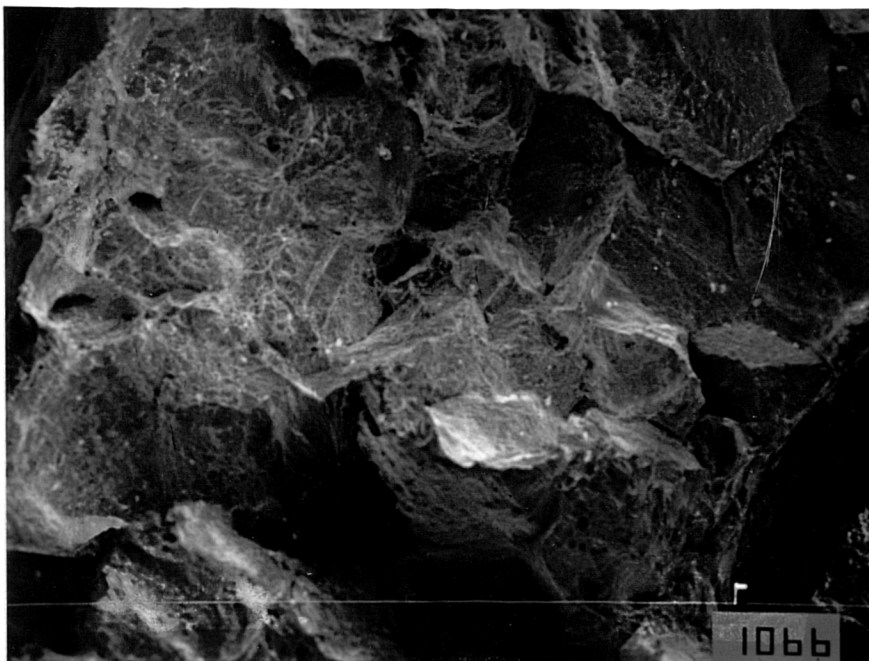
(b). with 2 hours holding time at test temperature (16% R of A)

Fig. 7.17 Mixture of intergranular decohesion and intergranular micro-void coalescence type fracture in the C-Mn-Al-V steel tested at 800 °C.



200 μm

(a). with no holding time at test temperature (70% R of A).



200 μm

(b). with 135 mins., holding time at test temperature (38% R of A)

Fig. 7.18 Mixture of intergranular dehesion and intergranular micro-void void coalescence type fracture in the C-Mn-Al steel tested at 850 °C. (in plate a, a large amount of the fracture surface is ductile rupture in accord with its high R of A value).

CHAPTER 8

HOT DUCTILITY OF DIRECTLY
CAST MICRO-ALLOYED STEELS

8.1 INTRODUCTION

Considerable use has been made in recent years of the simple hot tensile test to obtain an understanding of the transverse cracking problem which may be encountered during the continuous casting of micro-alloyed steels, as has been pointed out in the previous chapters.

The majority of tensile testing has been carried out under conditions in which the steel after processing is reheated above the solution temperature of the micro-alloying precipitates ($\sim 1330^\circ\text{C}$) and then cooled to test temperatures in the range 700 to 1100°C .

Cooling conditions are chosen to be similar to those encountered during continuous casting and the strain rate for tensile testing is chosen to approximate to that undergone at the surface of the strand when it is straightened. These conditions are, however, very different from those experienced during continuous casting. The impingement of the sprays on the strand and the cyclic rise and fall in temperature as the strand moves between the rolls introduces thermal stresses and precipitation patterns which are not produced in the simple tensile test. Another factor which is very different is that cast steels have generally coarser micro-structures and there is pronounced segregation of the impurities particularly sulphur to the interdendritic boundaries which could give different hot mechanical properties to those obtained with reheated samples.

Although hot ductility tests on reheated material have proved to be very useful in helping to solve the problem of transverse cracking, this is probably to a large degree

fortuitous. Because of the difficulty in casting tensile samples in situ and the urgency of finding a solution to the problem of transverse cracking, the simple hot tensile test has become the major technique for assessing susceptibility to transverse cracking. As might be expected, there have been few investigations to determine the hot ductility of directly cast steels, (Lankford, 1972; Harding et al., 1977; Suzuki et al., 1982; Rogberg, 1983). None of these studies have been conducted on Nb or Ti containing steels and only the work of Lankford and Suzuki were aimed at simulating the continuous casting process.

Recently, Mintz et al., (1986) compared the hot ductility of a C-Mn-Al-Nb steel after casting in situ and directly testing in the temperature range 850-1200 °C with its hot ductility after casting and cooling through the transformation followed by solution treating at 1330 °C and cooling to the same test temperature range. Surprisingly the as cast and directly tested material gave the better hot ductility, due to having a coarser precipitate and inclusion distribution.

Although this exercise had given useful information, it was found not to entirely simulate commercial casting conditions in that the segregation in the laboratory samples was more intense allowing concentration of elements into the liquid that is last to solidify round the interdendritic boundaries. This leads to the prod-

uction of (Mn,Fe)S rather than the purer MnS which are found in the continuously cast slab and hot rolled plate. The (Mn,Fe)S can subsequently dissolve more readily on reheating and reprecipitate on cooling in a fine form at the austenite grain boundaries, giving poor hot ductility. In order to try to produce MnS with lower Fe contents, as found in the continuous cast slabs, the cooling rate at solidification has been increased from 60 °C to 100 °C per min.. In addition the work has been extended to examine the as cast hot ductility of a C-Mn-Al and C-Mn-Al-Nb-Ti steels.

8.2 EXPERIMENTAL

The steels were supplied in the hot rolled state and they all had approximately the same base composition with 0.1% C and 1.4% Mn. All the steels contained Al. and the exact compositions are given in Table 8.1. The micro-alloying additions made to the steels were as follows:

steel (A) Nb, Ti and Al

steel (B) Nb and Al

steel (C) contained only Al

Tensile samples having a length of 70 mm and diameter 7.935 mm were machined from the plates with their axis parallel to the rolling direction.

They were placed inside silica tubes with an 0.2 mm diametrical clearance. A 2 mm diameter hole was drilled from one end of each sample to the mid-length of the sample so that a thermocouple could be inserted, Fig. 8.1.

The samples were heated by the induction heating unit described in chapter 4, so that approximately 22 mm of the length at the mid-length position could be melted. The molten region was contained in the tolerance fitted silica sheath which in turn was surrounded by a further silica tube through which argon could be circulated to prevent oxidation occurring. Samples were melted at 1560 °C for 5 mins, resolidified and cooled at (100 °C/min.) to the required test temperature in the range 750 - 1100 °C. They were then held for 5 mins. at test temperature and strained to failure using a strain rate of $5 \times 10^{-3} \text{ S}^{-1}$ (These samples will be referred to in the text as "as cast").

In addition to obtaining the hot ductility directly after casting, samples in the as supplied hot rolled condition have been heated to 1330 °C in ~ 15 mins, held for 5 mins, cooled at 100 °C/min to the test temperature, held for 5 mins, and tested to failure. (Samples referred to in the text as "reheated hot rolled").

In the case of C-Mn-Nb-Al steel, melted samples were also allowed to cool to ~ 100 °C at a cooling rate of 100 °C/min, reheated to 1330 °C, held for 5 mins, cooled at 100 °C/min to test temperatures, held for 5 mins and strained to failure. (Samples referred to in the text as "reheated as cast")

Where possible austenite grain sizes were obtained prior to straining as well as close to fracture of strained samples using the linear intercept measurement on transverse sections.

Carbon extraction replicas were taken close to the fracture surfaces (~ 1 mm) for test temperatures giving the minimum hot ductility, and examined using a Jeol 100 KV TEM, operating at 60 KV.

Fracture surfaces were examined using a Jeol T100 SEM, operating at 25 KV.

8.3 RESULTS

8.3.1 HOT DUCTILITY CURVES

The hot ductility curves of reduction in area (R of A) against test temperature for Nb/Ti, Nb and Al containing steels, (steels A, B and C respectively) for the different test conditions are given in Figs. 8.2-8.4 respectively.

The calculated A_e temperatures using Andrews' (1965) formula have been marked on the curves.

All the steels show a marked ductility trough for all test conditions, except for the Nb/Ti steel which showed a shallow trough when tested in the "reheated hot rolled" condition.

In the case of the Nb/Ti containing steel, steel A, Fig. 8.2, R of A fell from $\sim 90\%$ at 950°C and reached a minimum at 800°C for both "reheated hot rolled" and "as cast" test conditions. Samples tested in the "reheated hot rolled" condition gave much better ductility, R of A values being on average 40% higher for test temperatures of $\leq 900^\circ\text{C}$.

The ductility of the Nb containing steel, steel B, started to fall at 1100°C and reached a minimum at 800°C for the three test conditions examined, Fig. 8.3. For the "reheated hot rolled" and "as cast" conditions ductility fell from $\sim 95\%$ at 1100°C to $\sim 30\%$ to 25% at 800°C . Of the two conditions, the "reheated hot rolled" steel gave slightly better ductility in the temperature range $800 - 900^\circ\text{C}$. The "reheated as cast" material gave the widest and deepest ductility trough in the temperature range 800 to 1050°C , Fig. 8.3.

For the Al containing steel, steel C, Fig. 8.4, the "reheated hot rolled" condition again gave better hot ductility than the "as cast" condition.

Of the three steels examined, the Al containing steel, C, had the highest R of A values in the temperature range 850 to 950 °C in the "as cast" state, and the Nb/Ti steel gave the best hot ductility in the "reheated hot rolled" condition.

8.3.2 METALLOGRAPHY

Grain sizes in the as-cast state were very coarse 800 to 1050 μm , Fig. 8.5. Reheating refined the grain size and this was particularly marked for the Nb/Ti containing steel, Fig. 8.6. Grain size measurements prior to testing and after fracture are given in Table 8.2. Samples quenched after fracture in the temperature range of low ductility showed wedge type cracks, typical of cracks formed by grain boundary sliding, Fig. 8.7. Some evidence for deformation induced ferrite were found in the Nb/Ti steel, quenched from temperatures showing intergranular failure, Fig. 8.8.

8.3.3 FRACTURE APPEARANCES

Nb containing steel

Only the "as cast" and "reheated as cast" conditions were examined as the "reheated hot rolled" condition has been extensively examined in previous chapters and by many other workers, e.g. Mintz and Arrowsmith (1979).

For the Nb containing steel in the "as cast" and "reheated as cast" conditions, the fracture surfaces at low ductilities were a mixture of interdendritic and intergranular failure. Intergranular failure was in turn a mixture of intergranular micro-void coalescence characteristic of inclusion induced failure and intergranular decohesion characteristic of failure due to grain boundary sliding, Fig. 8.9. The former is evidenced by the ductile dimples on the fracture surface and the latter by the flat featureless facets. The interdendritic part of the fracture is probably where micro-shrinkage has occurred, and once "necking" starts to take place the fracture path will seek out such regions. However, examination of these regions has been shown to give very useful information on the segregation patterns occurring on solidification. In the "as cast" condition lines of very coarse angular (Mn,Fe)S inclusions 2 to 6 μm long could be seen which probably mark regions where a number of dendrites meet. Smaller spherical MnS inclusions $\sim 2 \mu\text{m}$ in cross-section were observed on the nodule surfaces, Fig. 8.10. In contrast in the "reheated as cast" condition most of these precipitates had dissolved, Fig. 8.11. These observations are very similar to those previously noted when a slower

cooling rate after solidification was used (Mintz et al., 1986) and suggest that, the faster cooling rate has not resulted in producing a purer MnS less inclined to redissolve on reheating. In accord with this, analyses of the smaller as-cast sulphide inclusions (100 to 200 nm dia) showed them to contain on average 5 to 10% Fe, (see next sub-section).

Nb/Ti containing steel

In the "as cast" condition fracture surfaces were again a mixture of intergranular and interdendritic and similar to those found in the Nb containing steel. Because of the very low S content of the steel fewer sulphides were observed on the nodule surfaces and only spherical sulphides (2 to 3 μm) were present, Fig. 8.12.

Samples from this steel tested in the "reheated hot rolled" condition showed only the higher temperature ductile rupture type of fracture, Fig. 8.13 in accord with the high R of A values obtained throughout the test temperature range. However, there is some indication that at the minimum ductility temperature, some grains have failed intergranularly.

C-Mn-Al steel

Fracture at low ductility in the as-cast state were similar to those observed in the other two steels. Again fine spherical type II (Mn,Fe)S inclusions were present on

the dendritic nodule surfaces. It is possible for the Al and Nb/Ti steels that the very low S levels (0.002 and 0.004% S respectively) make it difficult to nucleate the type III angular sulphides formed in the higher sulphur, Nb containing steel. Fracture in the "reheated hot rolled" condition at low ductilities were the normal intergranular consisting of a mixture of intergranular micro-void coalescence and intergranular decohesion failure.

8.3.4 REPLICAS EXAMINATIONS

In the case of the C-Mn-Al steel no AlN precipitation was detected in either the "as cast" or "reheated hot rolled" conditions. Sulphide distributions did not seem to be markedly different for the two conditions, there being little evidence for segregation to the prior austenite grain boundaries, but S levels were very low making them difficult to find.

Precipitation patterns in the Nb/Ti steel were complex. In the "as cast" condition a coarse type II dendritic precipitate of variable size and shape was present at the austenite grain boundaries, Fig. 8.14. Analysis of these particles showed them to contain a very high level of Nb. Similar precipitates have been observed by Subramanian et al., (1987) and Chen et al., (1987), in continuous cast slabs of Nb/Ti steels and analysed as being NbTi(CN) having greater than 80% Nb. A fine matrix precipitation of niobium rich NbTi(CN) particles was also observed, Fig. 8.14.

In the "reheated hot rolled" condition cubic precipitates of titanium nitride were observed, Fig. 8.15. These had a range of sizes from 20 to 100 nm and were randomly precipitated in the matrix.

Except for the as-cast state, precipitation in the C-Mn-Al-Nb steel was not looked at in detail because of previous extensive examinations.

In the "as cast" state extensive NbCN precipitation was found to be present in a fine form both in the matrix and at the prior austenite grain boundaries, Fig. 8.16. Coarse NbCN eutectics were also observed, Fig. 8.17. Although not examined in the investigation, precipitate and sulphide distribution at the γ grain boundaries have been shown to be finer in the reheated condition with the "reheated as cast" condition showing the finest distributions, (Mintz et al., 1986). Sulphides in the hot rolled condition were found to be pure MnS sulphides for all the three steels, whilst sulphides in the as-cast condition always contained some Fe generally 5 to 10%, (see Fig. 8.18). Full details of the precipitates and sizes are given in Table 8.3.

It should be noted, that the coarse NbCN eutectics in the " as cast " state were not observed in samples tested after reheating to 1330 °C and cooling to test temperatures.

8.4 DISCUSSION

"AS CAST" HOT DUCTILITY

"As cast" material invariably had poor hot ductility and this would seem to be a consequence of their very coarse grain structures (minimum R of A ~30%). The grain size in the as-cast condition varied between 800 and 1050 μm . Previous work has shown that the depth of the trough is very sensitive to the grain size (Crowther and Mintz, 1986 b). At the approximate strain rate used in the present investigation, $5 \times 10^{-3} \text{ S}^{-1}$, even plain C-Mn steels give very low R of A values at coarse grain size, Fig. 8.19. For a plain C-Mn steel, R of A values were as low as 40% at 300 μm the coarsest grain size examined.

However, the Al containing steel, C, although having the coarsest grain size in the as-cast state had the highest R of A values of the three steels examined indicating that the hot ductility in the as-cast state is not governed by grain size alone, Fig. 8.20. Precipitation at γ grain boundaries and within the matrix is also probably reducing hot ductility in the as-cast states for the Nb containing steels A and B. The hot ductility curves for the as-cast steels can be seen to be very similar on the lower temperature side of the trough, the major change occurs on the higher temperature side where the effect of precipitation is to widen the trough and raise the temperature for dynamic recrystallisation, Fig. Fig 8.20. Although precipitation has been shown to widen the ductility trough, to be effective in reducing hot ductility,

precipitation has to be fine (≤ 30 nm) and is most potent when it is situated in a fine form at the austenite grain boundaries preventing dynamic recrystallisation from occurring, Crowther et al., (1987).

Although extensive fine matrix precipitation occurred in the Nb/Ti steel, the grain boundary precipitation was generally too coarse to influence hot ductility. Only a small widening of the trough is therefore apparent, Fig. 8.20.

For the "as cast" Nb containing steel both the matrix and the grain boundary precipitation were fine and closely spaced preventing dynamic recrystallisation from occurring and reducing the hot ductility in the temperature range 800 to 1050 °C.

However, it should be noted that an equally valid explanation to account for the widening of the trough in Fig. 8.20, could be in terms of the hot ductility deteriorating with increasing S level (steel C, A and B having 0.002, 0.004 and 0.01% respectively). The information obtained in chapter 9 suggests that, increasing the volume fraction of sulphides delays the onset of dynamic recrystallisation (Samples have been directly heated to test temperatures without solution treatment) to higher temperature in the same way as precipitation. Further work is required to separate out the individual influence of precipitates and inclusions on hot ductility for steels in the "as cast" conditions.

"REHEATED AS-CAST"

After casting, only the Nb containing steel was reheated to 1330 °C and cooled to test temperatures in the range 750 to 1100 °C. The hot ductility behaviour in this case was worse than in the as-cast. This is in accord with the results from the previous more detailed study, Mintz et al., (1986). In that study it was found that the "as cast" state in addition to having a fine precipitation of NbCN, also contained coarse NbCN eutectics and coarse (Mn,Fe)S inclusions which easily redissolved on solution treating to 1330 °C. On cooling to the test temperature the redissolved NbCN and (Mn,Fe)S reprecipitate in a fine form at the γ grain boundaries reducing hot ductility. In the present instance the (Mn,Fe)S inclusions and NbCN eutectics were again found to redissolve easily on heating to 1330 °C in accord with this argument. Presumably the more extensive precipitation at the boundaries outweighs any benefit to ductility from grain refinement on reheating, and dynamic recrystallisation is delayed to higher temperatures.

"REHEATED HOT ROLLED" CONDITION

The reheated hot rolled condition invariably gave better hot ductility over the "as-cast" and "reheated as-cast" conditions. The most likely explanation for this behaviour is that reheating always produced a finer grain size. Taking each alloy in turn, for the Nb/Ti steel, A, the reheated condition gave particularly good hot ductility

and this reflects its very fine grain size after solution treating at 1330 °C. Crowther and Mintz (1986^b) has shown that for an austenite grain size of 50 μm, a plain C-Mn steel would show R of A values of 70 to 80%, close to the value obtained in the present investigation. Thus the extensive precipitation noted in this steel does not seem to be reducing hot ductility and this is because it is not situated at the γ boundaries and is generally coarse. Particle size varied from 20 to 100 nm. However, this random precipitation is sufficiently fine to refine the grain size on solution treatment.

In the case of the Nb containing steel the slightly better hot ductility shown by the reheated hot rolled state is again probably due to the finer grain size present after solution treatment (refinement from 800 to 500 μm).

Although, not examined in this exercise, previous work by Mintz et al., (1986) has shown that the reheated hot rolled condition would be expected to give less precipitation at the grain boundaries than the "reheated as cast" condition but more than the "as cast" state. This is because the hot rolled steels have pure MnS inclusions which do not dissolve so readily at 1330 °C (only 0.001% redissolves at 1330 °C in a steel with 1.4% Mn, Turkdogan et al., 1955). Fewer fine sulphides are therefore precipitated at the γ grain boundaries on cooling to the test temperature, giving improved hot ductility compared to the "reheated as cast" state, where because of the low Mn level surrounding the MnFeS sulphides all the S probably redissolves and is available for

precipitation in a fine form.

Presumably the worse hot ductility expected from this source is outweighed by the better hot ductility from grain refinement.

In the case of the Al containing steel as no AlN precipitation was observed, the improvement shown by the reheated hot rolled condition over the as-cast, must be due solely to the refinement of grain size that occurs on solution treatment (1050 to 340 μm).

SHAPE OF HOT DUCTILITY CURVES

For the Nb/Ti and Al containing steels, ductility generally remained low until the A_{e3} temperature was exceeded. Crowther and Mintz (1986 *) have shown that for coarse grained steels, low ductility in the temperature range 750 $^{\circ}\text{C}$ to the A_{e3} is due to strain concentration occurring in the thin films of deformation induced ferrite which are formed round the harder austenite grains. An example of these bands are shown in Fig. 8.8 for Nb/Ti steel tested at 850 $^{\circ}\text{C}$ in the "as cast" state and quenched immediately after fracture. Micro-void coalescence occurs at the inclusions situated at the γ boundaries and these link up to give low ductility intergranular failures. Raising the temperature above the A_{e3} , Fig. 8.2, allows dynamic recrystallisation to occur (see shaded regions on curves indicating where dynamic recrystallisation was first observed) and this corresponds to good hot ductility. In the case of the Nb containing steel, because of the pron-

ounced NbCN precipitation and/or possibly increased sulphide precipitation, dynamic recrystallisation is delayed until temperatures well in excess of A_{e3} , and as already discussed the continued poor ductility in this temperature range is believed to be due to the precipitates and/or sulphides pinning the boundaries and matrix dislocations preventing recrystallisation and encouraging grain boundary sliding. The onset of dynamic recrystallisation corresponded in all cases reasonably closely to full recovery of hot ductility.

RELEVANCE OF THE WORK TO CONTINUOUS CASTING

The hot ductility of as-cast material has been shown to be very poor, mainly due to the coarse grain size. This is in agreement with the work of Maehara et al., (1985), who showed that the as-cast grain size of HSLA steels is dependent on the carbon content, being at its coarsest for C levels in the range 0.1 to 0.15%, the range giving the worst hot ductility.

On the basis of the present results it would seem that Titanium is a good addition to make to Nb containing steels to improve their as-cast hot ductility and may lead to a reduced incidence of transverse cracking for straightening temperatures $> 800^{\circ}\text{C}$. This improvement in ductility is probably due to the removal of the fine precipitation of NbCN at the austenite grain boundaries and its replacement by a coarser precipitation of NbTi(CN). A reduced S level may however also be responsible for better hot ductility.

The hot ductility of the directly cast material has been clearly shown to be worse than that given by plate material reheated to 1330 °C and cooled to test temperature. However, differences in hot ductility between the "as-cast" and "reheated hot rolled" condition for the Al and Nb containing steels are small. This probably arises because once the grain size is over 300 μm, further changes in grain size only produce small changes in R of A, Fig. 8. It is also likely that the improvement in hot ductility, due to grain refinement on reheating is to a large degree offset by the finer sulphide and precipitate distributions produced.

Big differences are however apparent between the "as cast" and "reheated hot rolled" conditions for the Nb/Ti steel, but this is not surprising as reheating to 1330 °C does not dissolve the TiN. In the case of Ti containing steels, as cast samples may have to be used to assess the hot ductility during continuous casting. Certainly on the basis of the present results, higher solution temperatures than 1330 °C might be generally recommended for micro-alloyed steels to obtain a better agreement between the "reheated hot rolled" and "as cast" ductility. However, the simulation of the micro-structure and segregation patterns obtained during continuous casting has still not been achieved. Segregation in the as-cast tensile samples is too intense even at the higher cooling rate of 100 °C/min., NbCN eutectics and sulphides high in Fe being produced. Furthermore the cyclic rise and fall in temp-

erature by impingement of the sprays on the strand as it moves between the rolls is known to influence precipitation patterns and hot ductility, Mintz et al., (1987), and this has to be taken account of in any simulation test to asses the likelihood of transverse cracking occurring.

Further work is therefore advocated before any changes are made to the present simple testing procedure used for assessing hot ductility of Al and Nb containing steels during continuous casting, i.e. reheating to 1330 °C and cooling to test temperatures.

8.5 CONCLUSIONS

- 1- Directly cast steel has very poor hot ductility due to the very coarse grain size present.
- 2- Titanium additions to Nb containing steels give slightly worse hot ductility in the "as cast" state than C-Mn-Al steels but better ductility than Nb containing steel. Therefore Ti addition may be useful in preventing transverse cracking in Nb containing steels.
- 3- Fine precipitation at the boundaries as exhibited by as cast C-Mn-Nb-Al steels extends the ductility trough to higher temperatures, delaying the onset of dynamic recrystallisation.
- 4- Reheating hot rolled micro-alloyed steels to 1330 °C and cooling to test temperatures in the range 700 to 1100 °C results in improved hot ductility over directly cast steel. This is mainly due to refinement of the as-cast grain size. In the case of Nb/Ti steels, the relatively coarse TiN precipitation has a very powerful effect in refining grain size at 1330 °C, so that ductility is excellent and only a very shallow trough is observed.
- 5- Reheating to 1330 °C a C-Mn-Al-Nb steel after directly casting, and cooling to test temperatures in the range 700 to 1100 °C results in a lower R of A values compared to the as-cast state. This probably arises because benefits to hot ductility arising from grain refinement are outweighed by an increased precipitation of NbCN sulphides at the γ grain boundaries. The NbCN eutectics

and (Mn,Fe)S present in the as-cast state easily redissolve at 1330 °C and reprecipitate in a fine form at the boundaries on cooling to test temperatures.

6-Reheating hot rolled plates of Nb and Al containing steels to 1330 °C and cooling to test temperatures give rise to only a small improvement in hot ductility. Because the sulphides are pure, it is likely that less S redissolves at 1330 °C and precipitates out at the boundaries on cooling to the test temperature, than in samples reheated after casting. The improvement in hot ductility due to grain refinement is then dominant. The simple hot tensile test seems for these steels to be able to give a reasonable estimate of the likely hot ductility to be encountered during the straightening operation in continuous casting. However, this is not the case for Ti containing steels, as TiN is not taken back into solution at 1330 °C. Assessment of the hot ductility performance of Ti containing steels will probably require hot tensile tests on directly cast material.

Code	steel	C	Si	Mn	P.	S	Ti	Nb	Al	N
A	C-Mn-Nb-Al-Ti	.115	.38	1.48	.019	.004	.02	.023	.023	.008
B	C-Mn-Nb-Al	.1	.42	1.39	.007	.01	—	.026	.036	.007
C	C-Mn-Al	.11	.32	1.42	.011	.002	—	—	.038	.003

Table 8.1 Composition of the steels examined (wt. %)

Steel	Condition	Initial Grain size	Grain Size after testing	
			at various temperatures	900 °C
C-Mn-Nb-Ti-Al	As-cast	950	-	-
	Reheated hot rolled	48	-	23
C-Mn-Nb-Al	As-cast	800	210	400
	Reheated As-cast	-	200	400
	Reheated hot rolled	510	-	350
C-Mn-Al	As-cast	1050	-	-
	Reheated hot rolled	340	-	-

Table 8.2 Austenite grain sizes for the steels examined in different test conditions (in μm)

Steel	Condition	Temp. °C	Grain boundary precipitation		Matrix precipitation Type	Matrix precipitation Size nm
			Type	Inter-pearlite spacing nm		
C-Mn-Nb-Ti-Al	As-cast	900	NbTi(N)	150	NbTiCN	15
	Reheated hot rolled	950	-	-	TiN	20 to 100 Av. 40
C-Mn-Nb-Al	As-cast	900	Nb(CN)	50	Nb(CN)	20
	-	1050	-	-	Nb(CN)	45

Table 8.3 Precipitates present with their size for the

Nb and Nb/Ti steels examined.

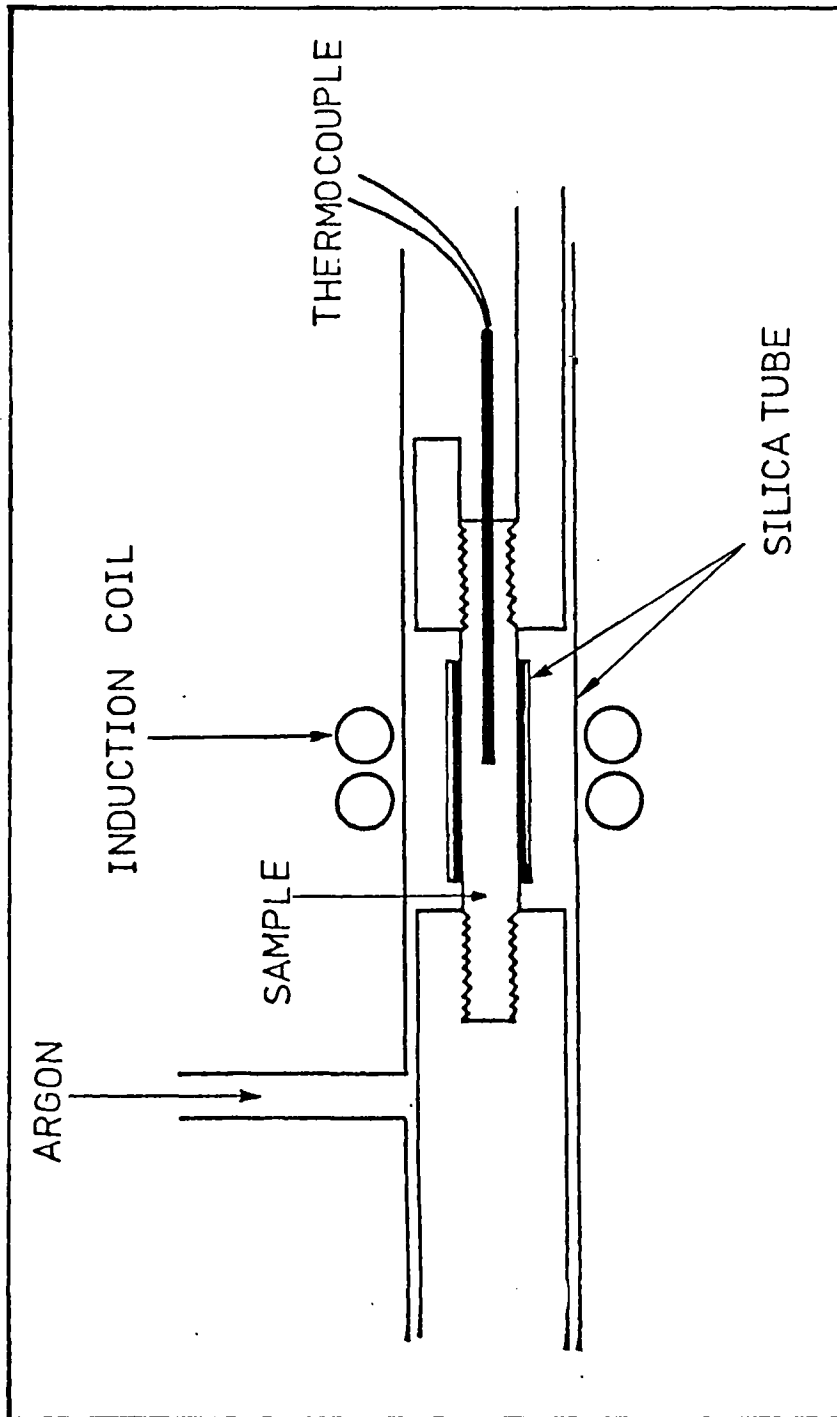


Fig. 8.1 Experimental arrangement for measuring hot ductility in the "as cast" condition.

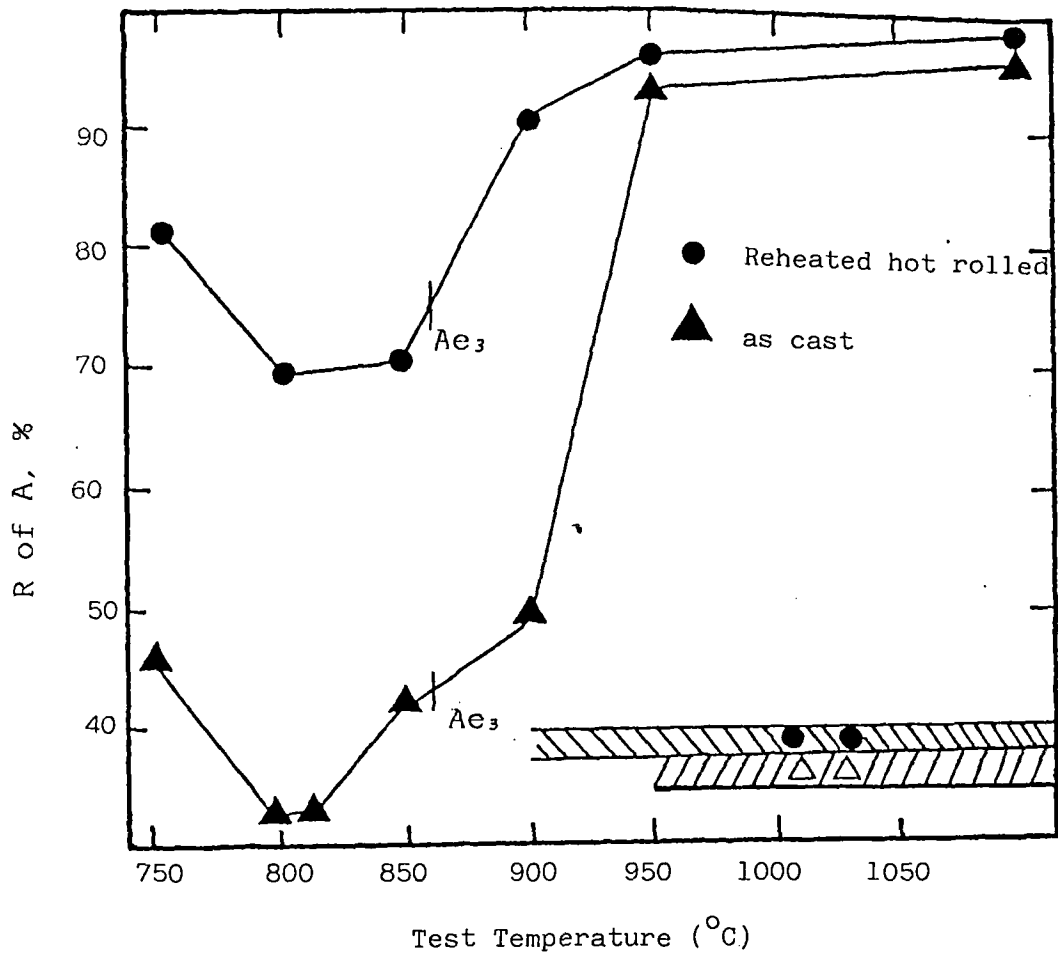


Fig. 8.2 Hot ductility curves for the Nb/Ti steels, occurrence of dynamic recrystallisation indicated by shaded regions.

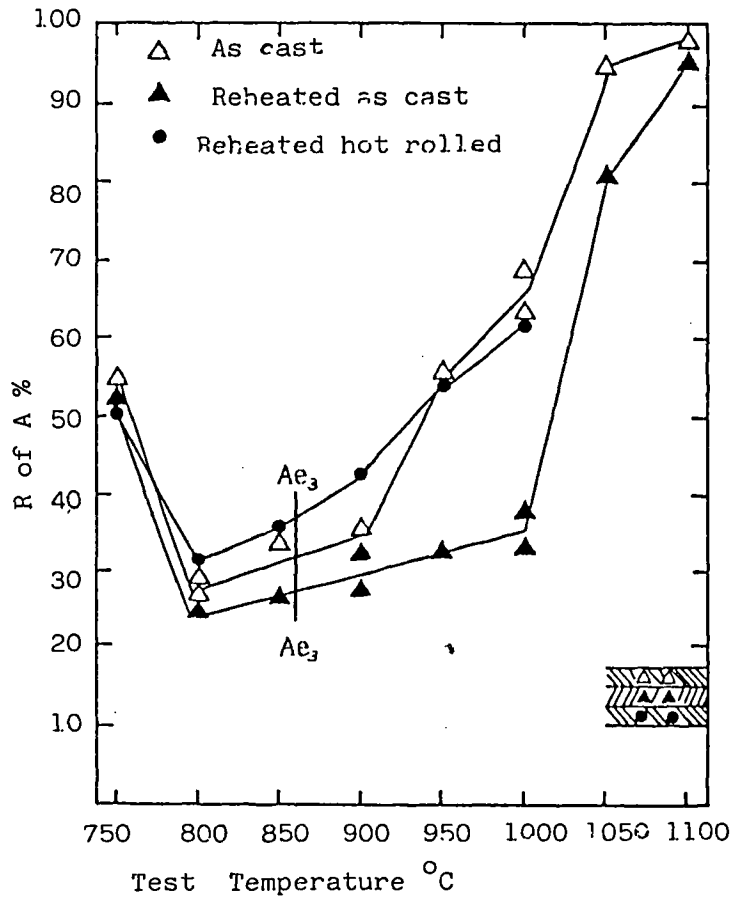


Fig. 8.3 Hot ductility curves for the Nb steel, occurrence of dynamic recrystallisation indicated by shaded regions.

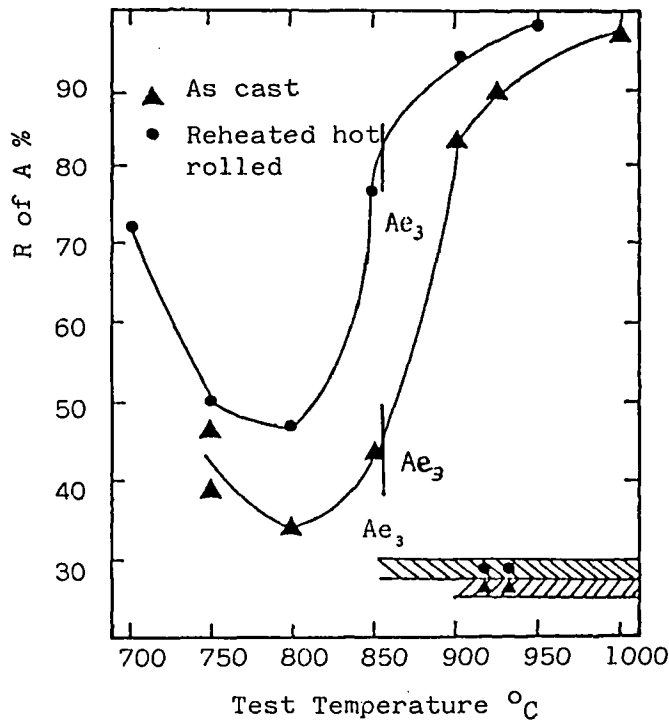
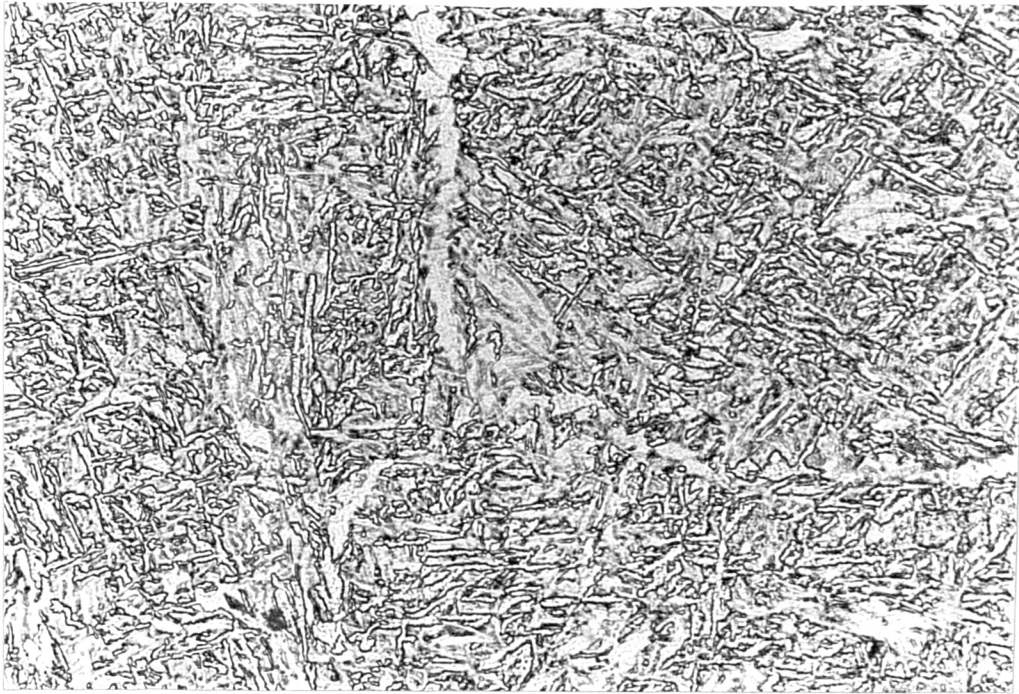
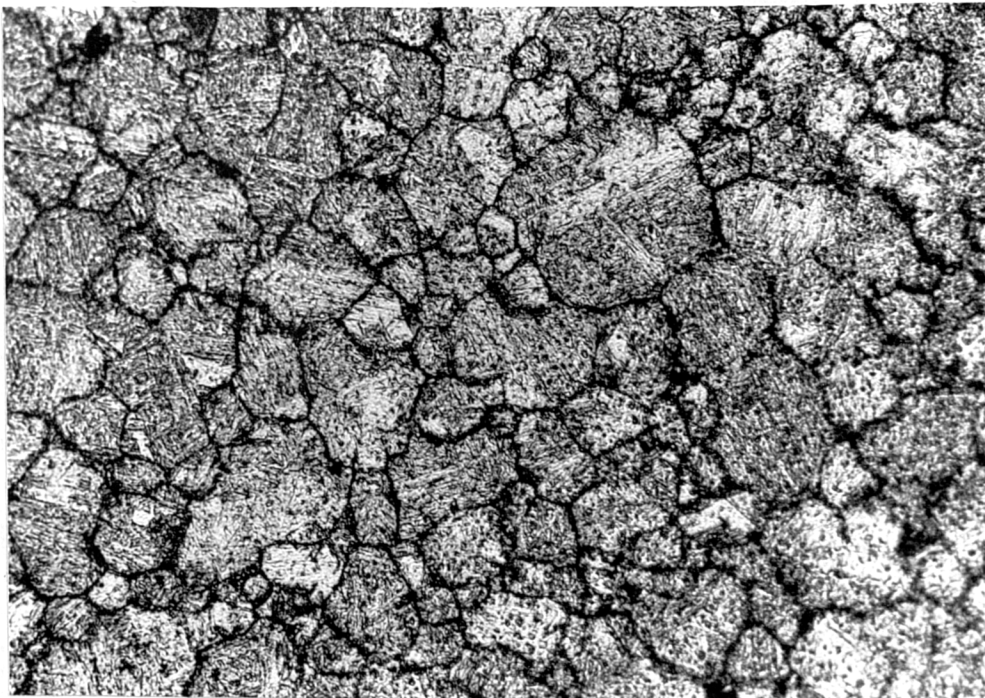


Fig. 8.4 Hot ductility curves for the Al steel, occurrence of dynamic recrystallisation indicated by shaded regions.



100 μm

Fig. 8.5 Typical coarse grained structure produced on fast cooling after solidification for the Nb/Ti steel.



100 μm

Fig. 8.6 Fine grain structure produced on reheating to $1330\text{ }^{\circ}\text{C}$ and quenching in ice brine for the Nb/Ti steel.

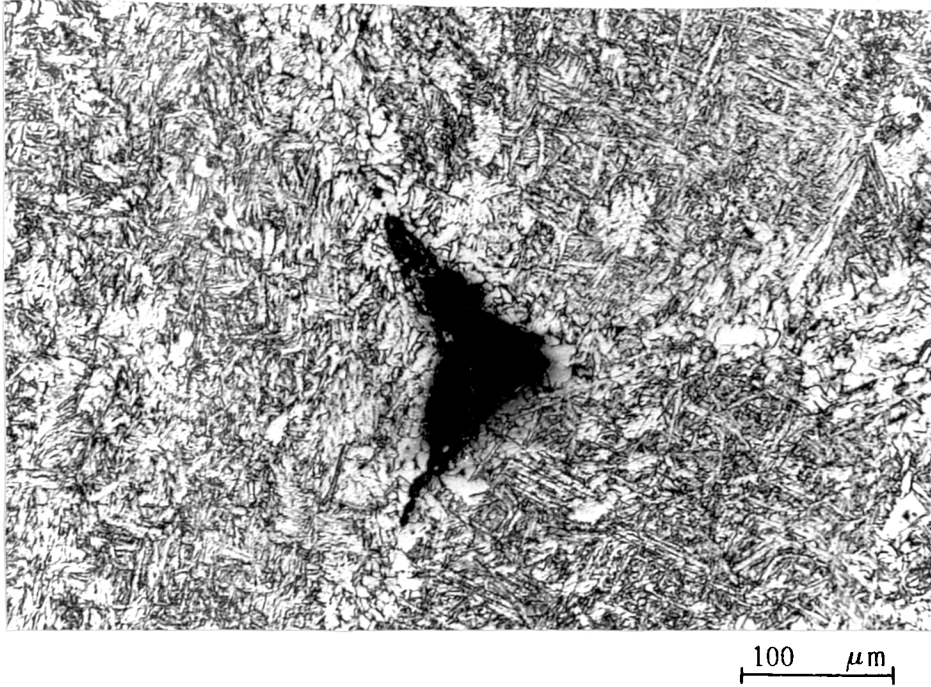


Fig. 8.7 Typical wedge type crack found in the Nb containing steel, sample tested at 850 °C in the as cast state.

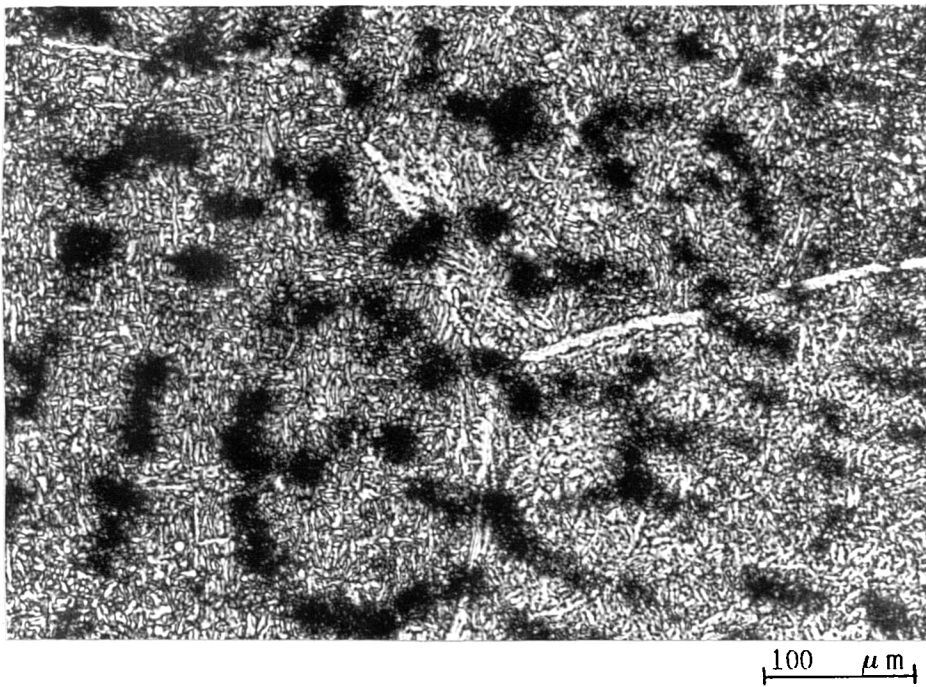


Fig. 8.8 Evidence of deformation induced ferrite in the Nb/Ti steel, sample quenched from 850 °C after fracture.

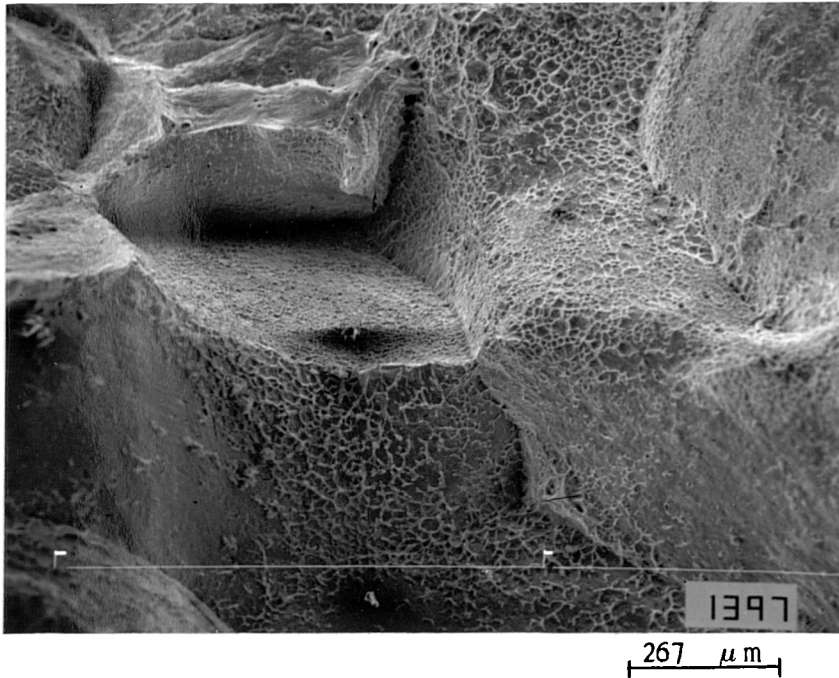


Fig. 8.9 Fracture surface of the Nb containing steel in the as cast condition after testing at 850 °C, showing mixture of intergranular micro-void coalescence and intergranular decohesion.

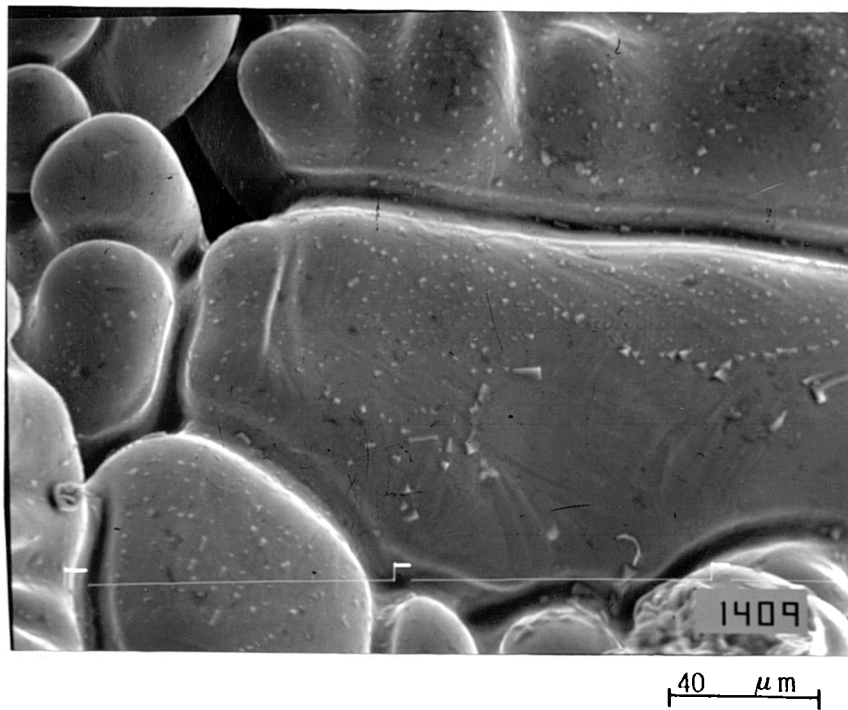
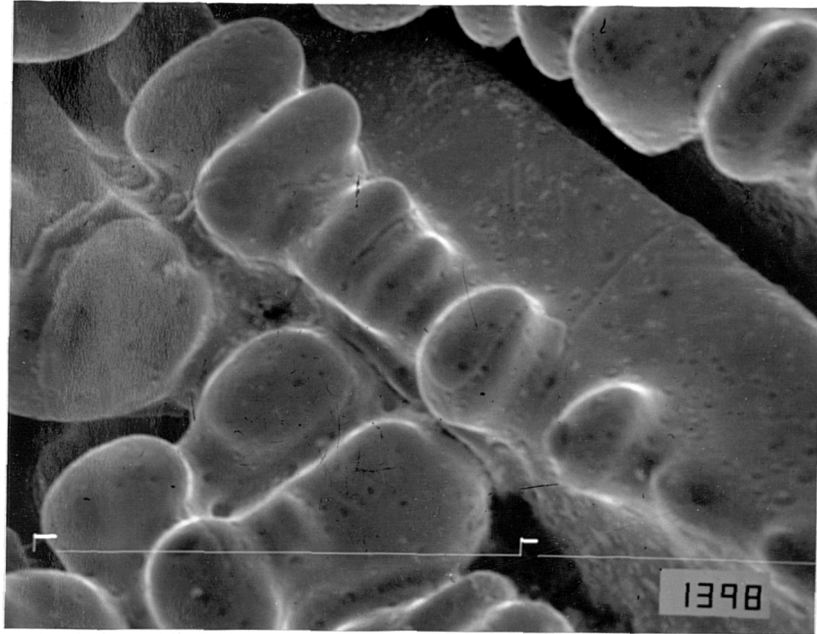
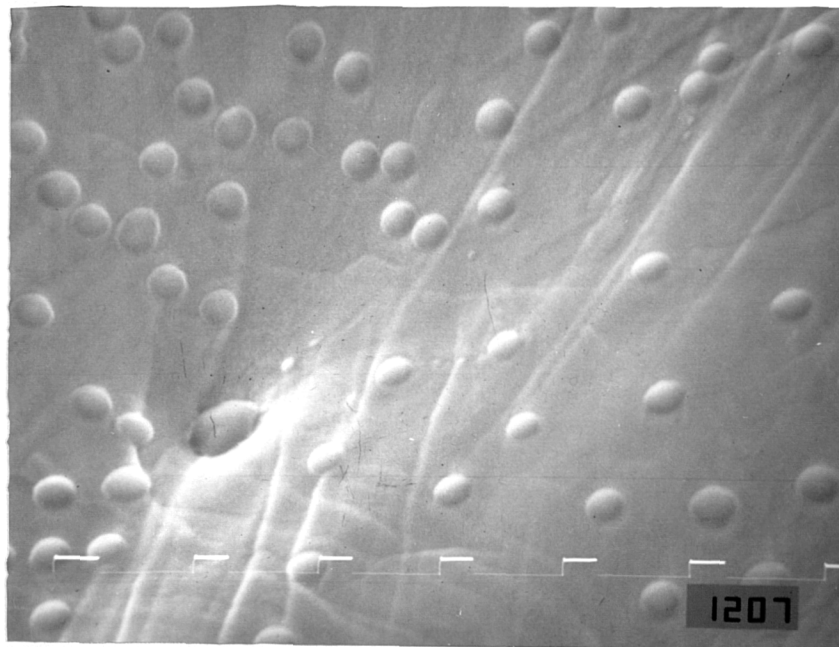


Fig 8.10 Interdendrite type of fracture in the Nb containing steel in the as cast state after testing at 1000 °C, showing lines of coarse angular Mn(Fe)S inclusions.



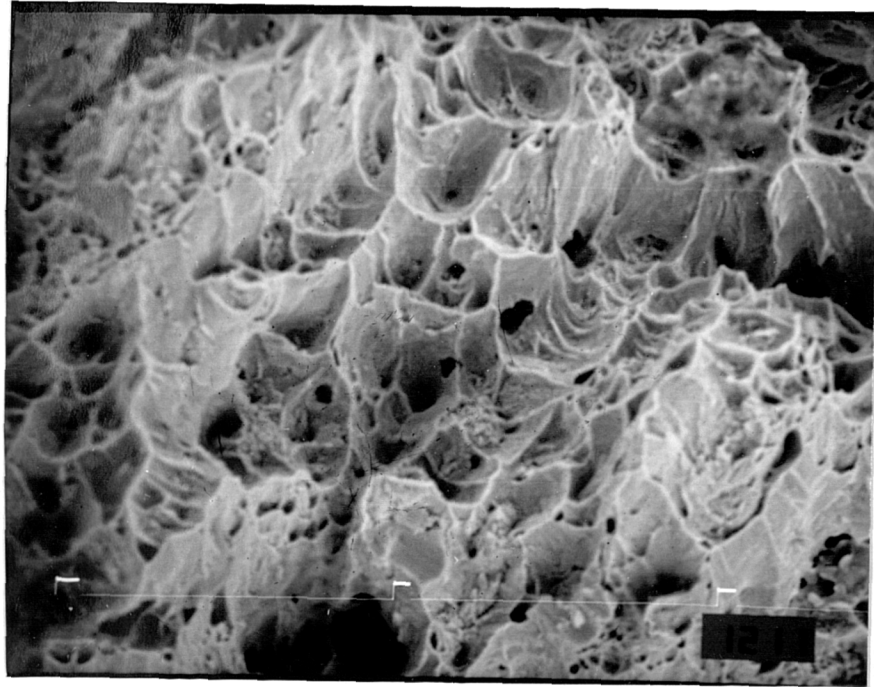
27 μm

Fig. 8.11 Interdendritic type of fracture in the Nb containing steel in the "reheated as cast" condition tested at 900 °C, showing that most of the $Mn(Fe)S$ inclusions have redissolved.



10 μm

Fig. 8.12 Spherical type sulphides found on the dendritic nodule surfaces of the Nb/Ti steel in the as cast state after testing at 850 °C.



40 μm

Fig. 8.13 High Temperature ductile rupture fracture found in the Nb/Ti steel in the "reheated hot rolled" condition, for sample tested at 900 °C.

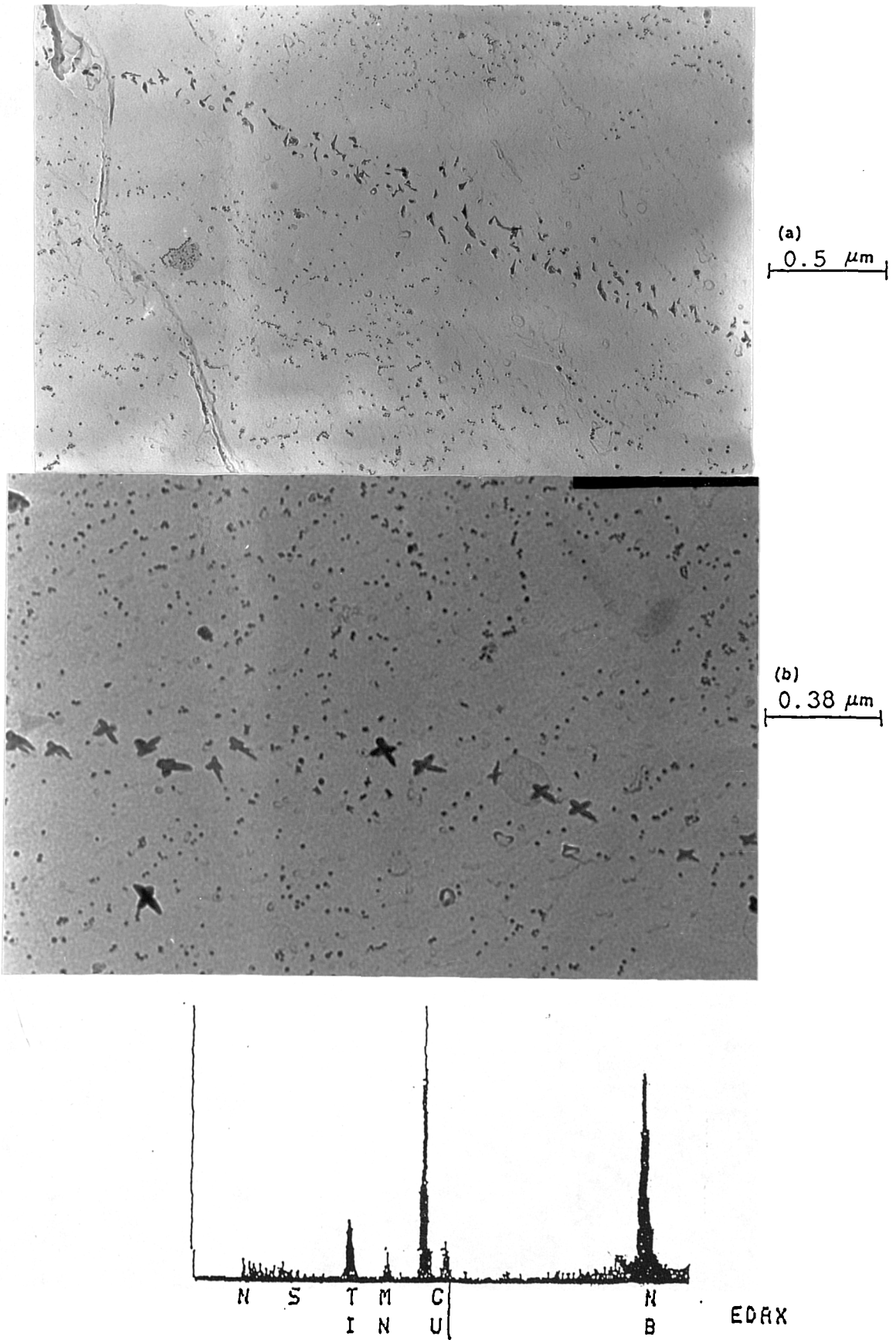
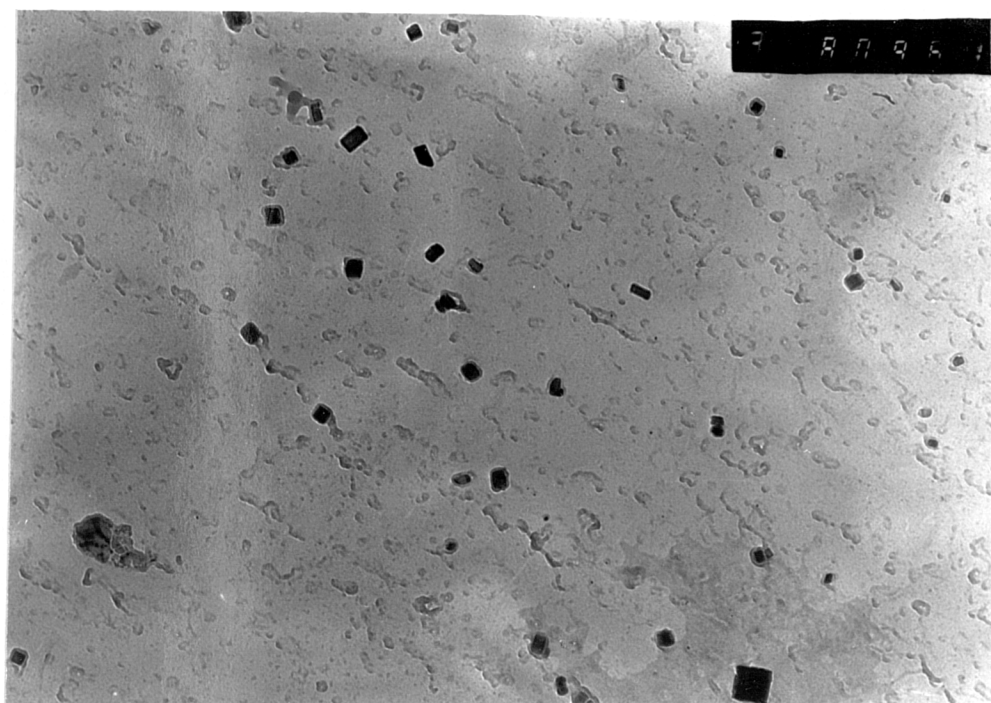


Fig. 8.14 Typical replicas obtained from the Nb/Ti steel in the as cast state, sample tested at 900 °C, showing coarse grain boundary precipitates and fine matrix precipitation with associated X-ray spectrum for the large particles



0.38 μm

RATE: 0CPS TIME: 200LSEC
 00-20KEV: 10EV/CH PRST: 200LSEC
 A: 852302 8:
 FS= 7428 MEM: A FS= 200
 |02 |04 |06 |08 |10

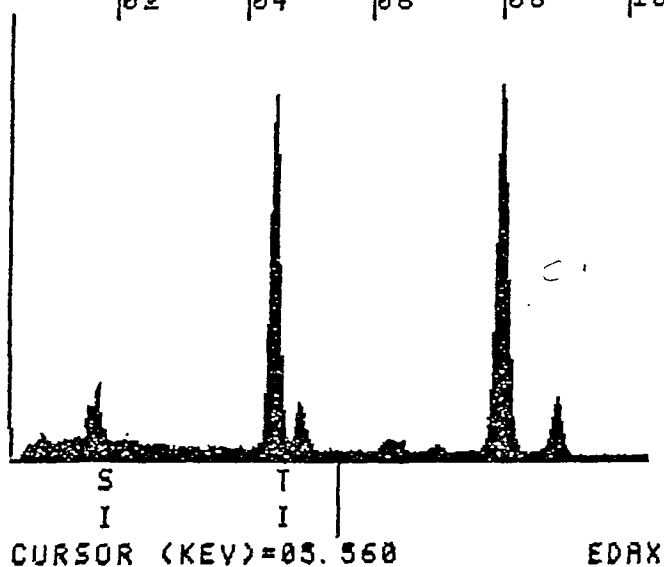
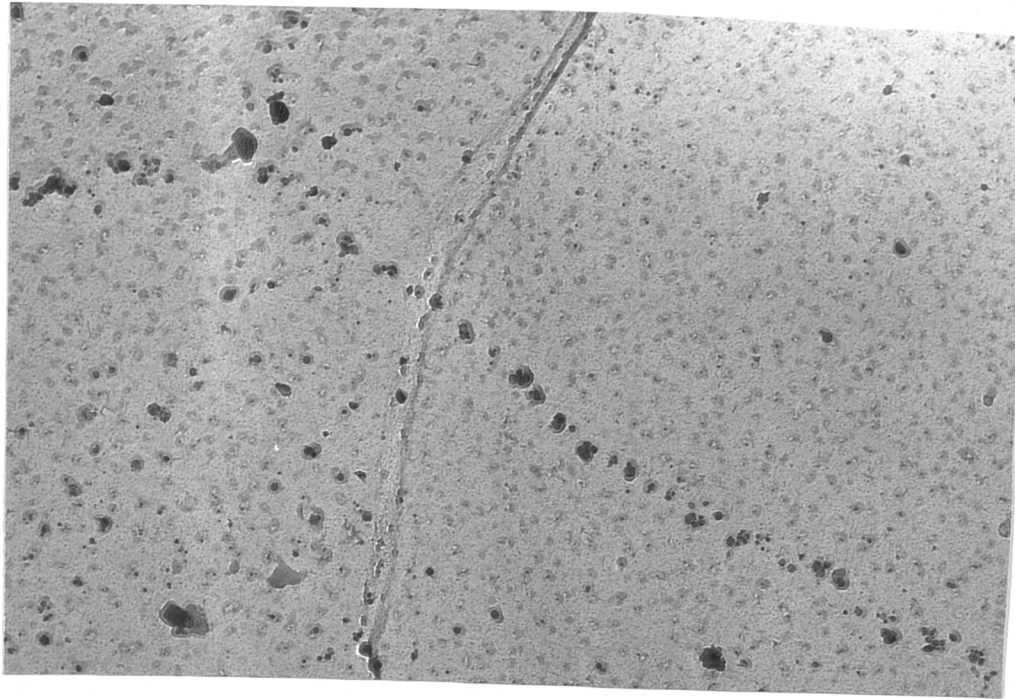
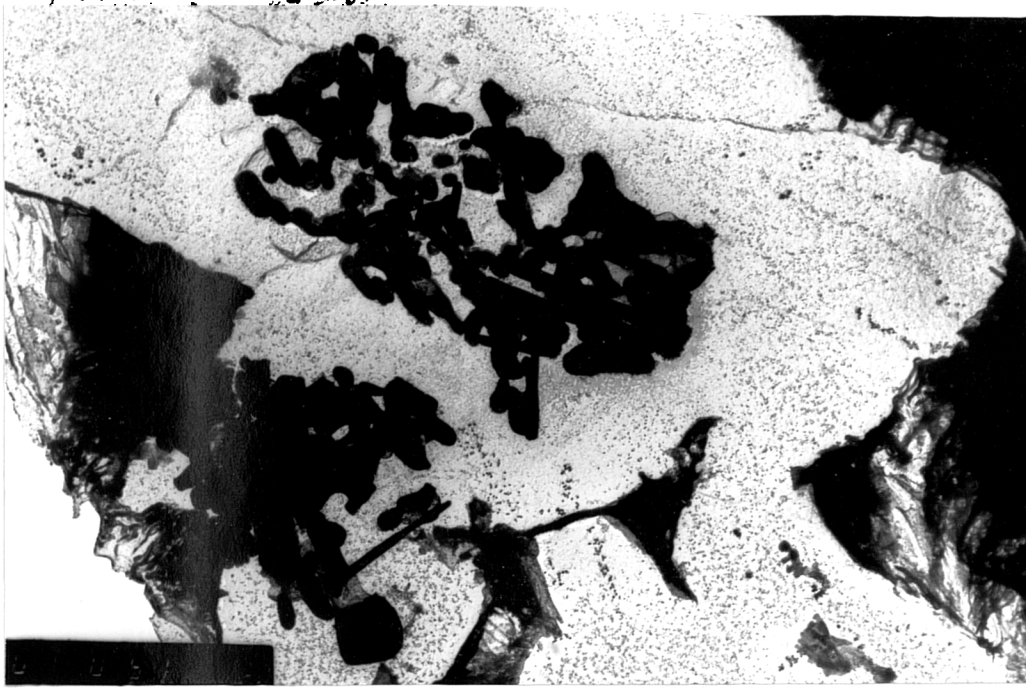


Fig. 8.15 Typical TiN precipitation observed in the Nb/Ti steel in the "reheated hot rolled" condition with associated X-ray spectrum, for sample tested at 850 °C.



0.43 μm

Fig. 8.16 Fine NbCN precipitation observed in the Nb steel in the "as cast" condition at test temperature of 850 °C.



1 μm

RATE: 6CPS TIME: 38LSEC
 00-20KEV: 10EV/CH PRST: 200LSEC
 A: B:
 FS= 700 MEM: A FS= 700
 |00 |02 |04 |06 |08 |10 |12 |14 |16 |18

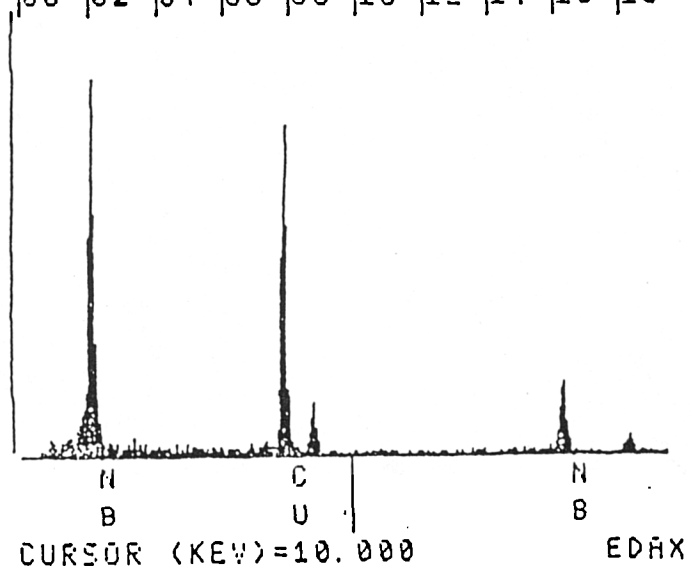


Fig. 8.17 Coarse NbCN eutectic extracted from 'as cast' sample tested at 950°C, with associated X-ray spectrum.

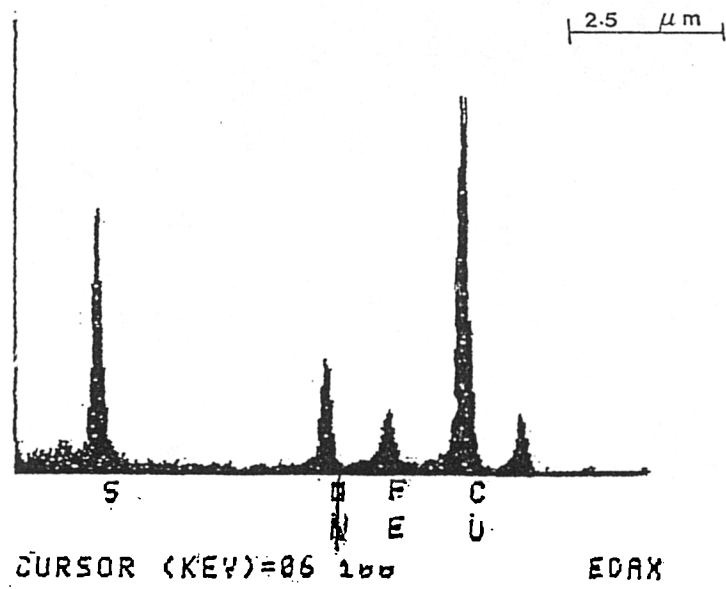
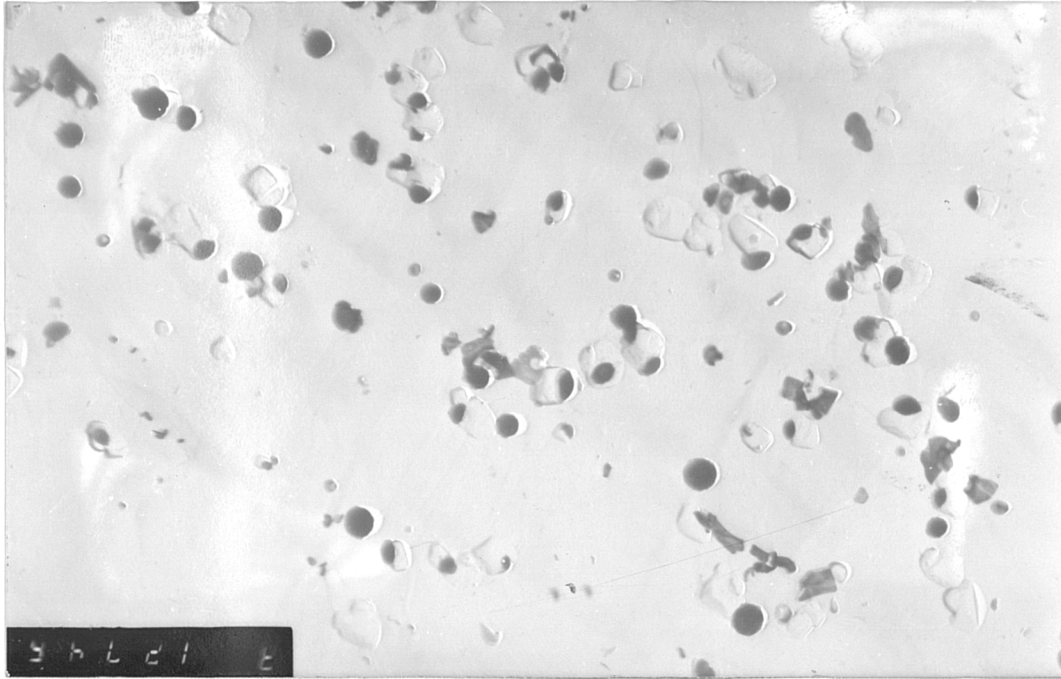


Fig. 8.18 Fine MnS inclusions extracted from "as cast" C-Mn-Nb-Al sample tested at 900 °C, with associated X-ray spectrum.

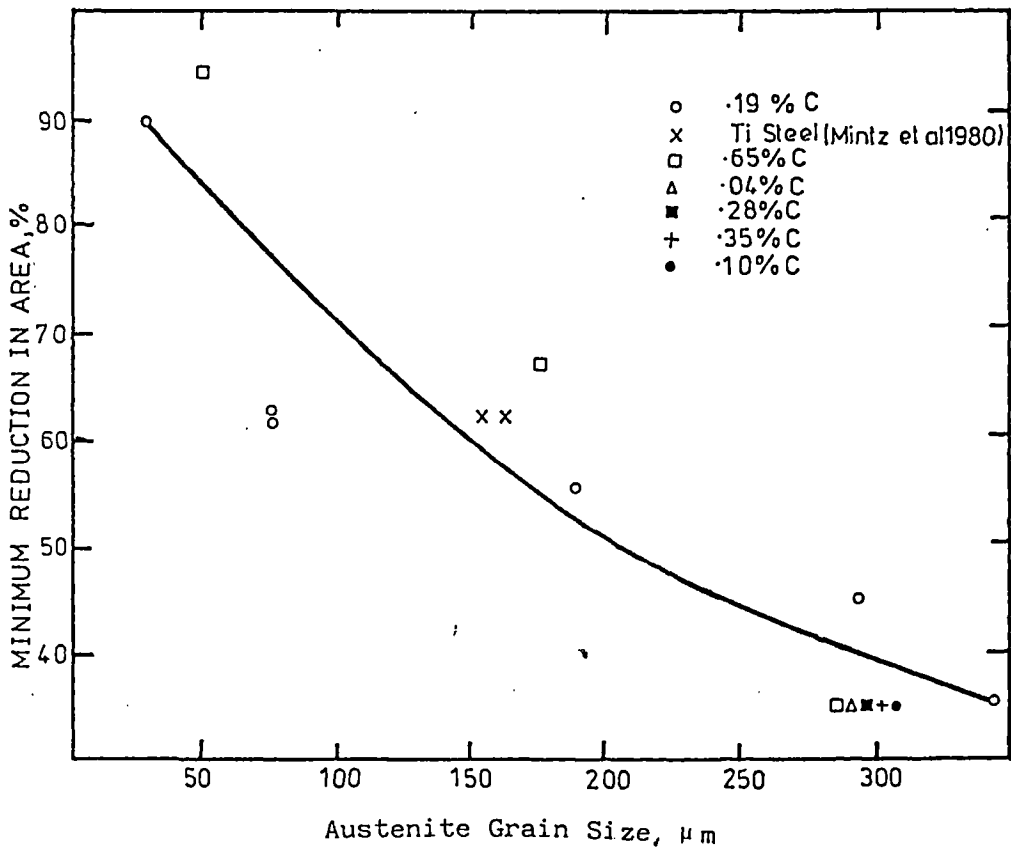


Fig. 8.19 Variation of minimum R of A values with γ grain size following testing in the range 700 to 1000 °C at strain rate of $3 \times 10^{-3} \text{ s}^{-1}$.

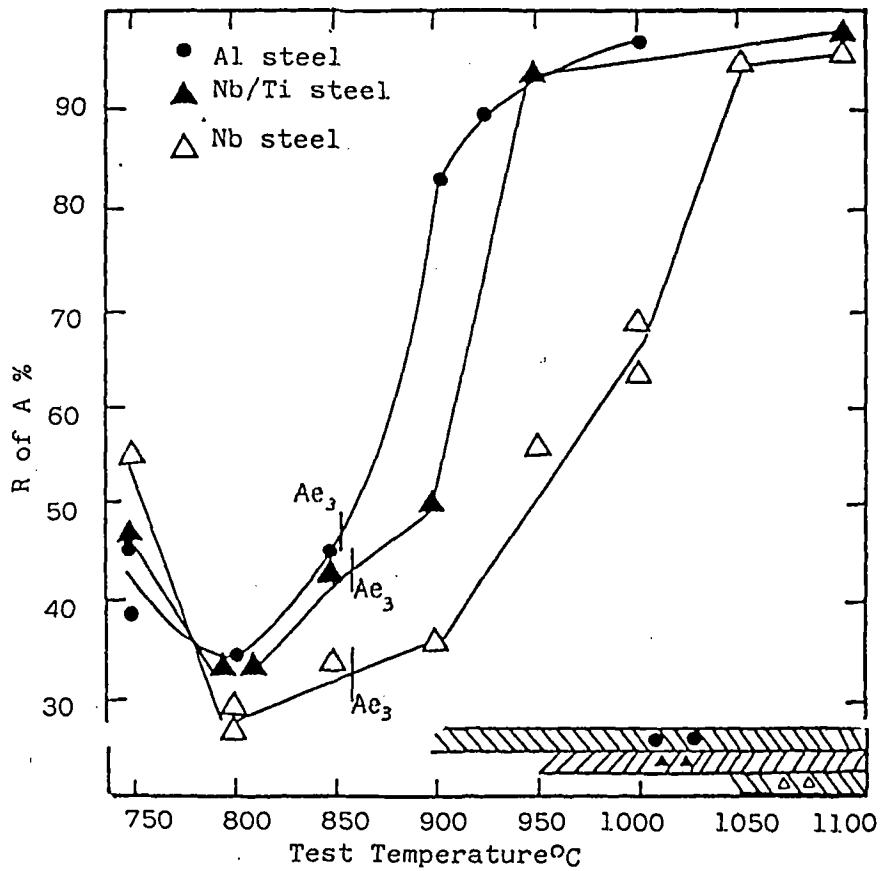


Fig. 8.20 Hot ductility curves for as-cast steels, A, B, and C.

CHAPTER 9

EFFECT OF MANGANESE AND
SULPHUR ON THE HOT DUCTL
ILITY OF MICRO-ALLOYED
STEELS

9.1 INTRODUCTION

The ductility troughs exhibited by micro-alloyed steels during high temperature deformation have been mostly attributed to the nitrides and/or carbides precipitated at the austenite grain boundaries. They are believed to inhibit boundary mobility, so that intergranular fracture occurs. Apart from these small particles, inclusions are always present in steels and their role is less well understood.

It is well known that S is soluble in the molten steel phase, but its solubility in the solid phase is very low. It precipitates in the form of metal sulphides during solidification and the precipitation patterns are influenced by its strong segregation tendency (Kiessling, 1978). To prevent FeS formation, which could lead to the hot shortness in the temperature range 900 - 1150 °C (Kiessling, 1968), a theoretical Mn:S ratio of 1.7 is required, although in practice much higher ratios are commonly used.

Also S itself is detrimental to hot ductility, even when the Mn:S ratio is sufficiently high to prevent FeS formation (Bellot and Gantois, 1978). High S steels have a larger volume fraction of inclusions, which can reduce hot ductility.

Sulphur also has a marked detrimental effect on hot ductility near the solidus temperature (Sopher, 1958) and this is believed to be due to the presence of liquid films in the inter-dendritic regions which do not freeze until a temperature below the solidus is reached. (Brimacombe

and Sorimachi, 1977). The solidification temperature of the sulphide inclusions are related to the Mn content in the steel (Kinoshita and Kuroki, 1972), as can be seen in Fig. 9.1, which shows for example that for Mn levels less than 0.7% in a 0.2% carbon steel, the sulphides could exist in the liquid form at 1480 °C, for the S levels 0.01 - 0.04%.

Many studies have been carried out to understand the role of S in intergranular fracture, for example: Weinberg (1979) and Suzuki et al., (1982), reported after examining some steels with Mn:S ratios below 60, that increasing the S content in the steel, both deepens and widens the ductility trough. Osinkolu et al., (1985) and Heritier et al., (1981), have examined many high-purity iron-base alloys with different S concentrations, but without Mn, they concluded that the ductility troughs observed in the temperature range 850-1100 °C were a product of the interaction between the hardening effect of AlN precipitates and the intergranular segregation of S. Beside that, they have noted that AlN precipitation alone without the availability of S in the metals, does not lead to loss in ductility. Nachtrab and Chou (1986), noted after examining the hot ductility of Al and Nb containing steels, with different S levels (0.001-0.019%) and for Mn:S ratios greater than 69, that the detected segregation of S and Mn does not cause embrittlement.

To date it appears, there is no information available

about the effect of S and Mn on hot ductility of micro-alloyed steels, heated directly to test temperatures, and this has formed the basis of the present chapter.

Although not directly relevant to the continuous casting process, it was hoped that such results would provide further information to aid in understanding the hot ductility of these steels by producing precipitate distributions and grain sizes very different to those produced after high temperature solution treatment.

Also, many hot forming processes do involve direct heating followed by deformation, e.g. the production of pipeline fittings, which commonly use micro-alloyed steels. It was therefore hoped that the hot ductility and strength data obtained from carrying out directly heated hot tensile tests would be of some relevance to such processes.

9.2 EXPERIMENTAL

The compositions of the steels examined are given in Table 9.1, they were supplied as 12 mm hot rolled plates.

Steels A and B, are low S steels (0.002-0.003%) containing Al, with Mn contents of 1.42 and 0.32%, respectively.

Steels C and D, have high S contents (0.03-0.032%) again Al containing steels with Mn levels of 1.41 and 0.31%, respectively.

Steels E and F, are Nb/Al containing steels, with medium S content (0.007%) and Mn concentrations of 1.41 and 0.29%, respectively.

All the steels were normalised at 920 °C for 30 mins., to remove any possible grain shape effect introduced by rolling. After normalising, tensile samples with diameter 5.04 mm and gauge length 25.4 mm were machined longitudinally from each plate. Hot tensile tests were performed using the Instron equipment described in chapter 4. Tests were conducted in a flowing Argon atmosphere, and the samples were also nickel plated as described by Crowther (1986) to prevent decarburization. The samples were heated to test temperatures in the range 600-1100 °C at a constant rate of 15 °C/min., and held 15 mins., prior to testing at the strain rate of $3 \times 10^{-4} \text{ s}^{-1}$. After fracture, the samples were cooled to room temperature at a rate of $\sim 25 \text{ °C/min.}$

Metallographic longitudinal sections were prepared from selected samples, for carbon extraction replicas, and examined using a JEOL 100 KV, TEM, operating at 60 KV. Fracture surfaces were examined using a JEOL T100 SEM, operating at 25 KV.

Ferrite grain sizes were measured in the normalised condition, using the linear intercept method. To establish austenite grain sizes prior to deformation, small samples were heated in a muffle furnace to simulate the thermal cycle of the hot tensile test, and then cooled at a rate to produce ferrite outlinement of the austenite grains.

After obtaining the hot ductility curves for all steels in the normalised condition, the hot ductility behaviour of steels A and C was also investigated in the as received condition, with the same experimental procedures as described above.

9.3 RESULTS

9.3.1 HOT DUCTILITY CURVES

A- NORMALISED CONDITION

The curves of reduction in area against test temperature for the low and high S steels containing Al with different Mn levels are shown in Figs. 9.2-9.3, respectively. As can be seen in Fig. 9.2, heat A (1.42% Mn and 0.002% S), showed excellent reduction in area values over the entire temperature range examined with a minimum ductility of 85% at 900 °C. Heat B (0.32% Mn and 0.003% S) also showed excellent hot ductility, but the lower Mn level resulted in a greater ductility loss, minimum R of A value being 70% at 1000 °C.

Increasing the S level in these steels from 0.0025% to 0.03% (heats C and D), both deepened and widened the ductility troughs, Fig. 9.3. In heat C (1.41% Mn and 0.03% S), ductility started to fall at 700 °C and reached a minimum of 70% at 900 °C, whilst heat D (0.31% Mn and 0.032% S), showed the most severe embrittlement with a minimum R of A value of less than 50% at 1000 °C.

The temperature range over which dynamic recrystallisation occurred for each steel is also shown in Fig. 9.2-9.3, denoted by shaded region and it is noticeable that for the steels with high Mn content (~1.4%), dynamic recrystallisation is observed at test temperatures \geq 900 °C, whereas in the low Mn steels (~0.3%), recrystallisation was first observed at temperatures greater than 1000 °C.

Similar trends have been noted in the Nb containing steels with different Mn levels, Fig. 9.4. Heat E (1.41% Mn and 0.007% S) gave minimum R of A values of 70% in the temperature range 700-1000 °C, whereas heat F (0.29% Mn and 0.007% S) gave a minimum R of A value of 60% at 1000 °C. Again increasing the Mn level in the steel resulted in a decrease in the temperature at which dynamic recrystallisation is first observed, being 1000 °C in the high Mn steel and greater than 1000 °C in the low Mn steel.

B. AS RECEIVED CONDITION

Figs. 9.5-9.6 show the R of A values against test temperature for heats A and C respectively in the as received condition. The hot ductility curves for the normalised condition have been added in the figures to aid comparison. In both heats normalising has been shown to improve hot ductility.

For heat A, the ductility trough in the as received condition is wider and deeper (minimum R of A is 75% compared to 85% on normalising). A similar trend was observed in heat C (minimum R of A is 50% compared to 70% after normalising).

In the low S steel (heat A), dynamic recrystallisation was first noted at a test temperature of 900 °C for both test conditions, whereas in the high S steel (heat C), recrystallisation started at 900 °C for the normalised condition and at 1000 °C for the as received condition.

9.3.2 PEAK STRESSES AND CRITICAL STRAIN FOR DYNAMIC RECRYSTALLISATION

The influence of test temperature on peak stress, σ_p , for all steels examined in the normalised and as received conditions are shown in Fig. 9.7. There is a continuous decrease in σ_p as the temperature is increased. Compositions of the steels have little influence on σ_p above 800 °C when they are austenitic. However, at test temperatures below 800 °C, a recognizable difference in strength between high and low Mn level for the same S content is evident (σ_p being higher in the steels with higher Mn concentrations). On the other hand, a slight increase of peak stress in heats A and C is noticeable in the normalised condition compared with the as received condition at the lower test temperature, probably due to their finer grain sizes.

The stress-total elongation curves for the steels examined in the normalised condition and for heats A and C in the as received condition are shown in Figs. 9.8-9.9 respectively. The occurrence of dynamic recrystallisation has been arrowed in the figures.

According to Rossard (1973), nucleation of dynamic recrystallisation occurs at a critical strain level, ξ_c , which is less than the strain at the peak stress, ξ_p , as measured from the flow curve and is given by:

$$\xi_c = 0.83 \xi_p$$

The critical strain to nucleate dynamic recrystallisation

for the steels examined in normalised and as received conditions, have been calculated using the above equation and are summarized in Table 9.2.

As can be seen in Fig. 9.10, increasing the Mn content (at constant S level) from ~ 0.3 to $\sim 1.4\%$, decreases ξ_c for all the steels examined. Also increasing the S content in the steel (at constant Mn level), can increase ξ_c slightly in the normalised and as received conditions, Fig. 9.11. The effect of test temperature on ξ_c is very well known, (McQueen and Jonas, 1975). ξ_c decreases continually with increasing temperature, Fig. 9.12. It is also evident from Fig. 9.12 that, values are much higher for the as received state compared to the normalised condition, probably reflecting the coarser grain size of the as received state (see next sub-section).

9.3.3 MICROSCOPY

A. GRAIN SIZE MEASUREMENTS

The variation in austenite grain size with reheating temperature for the normalised condition for the Al and Nb containing steels, are shown in Figs. 9.13-9.14, respectively. The ferrite grain sizes for these steels have also been included in the figures to aid comparison.

For all steels examined, the austenite grain size remained approximately constant in the temperature range $900-1000^\circ\text{C}$, but increased rapidly as the temper-

ature increased above 1000 °C, Figs. 9.13-9.14. At the same S level, increasing the Mn content refines the grain size, Figs. 9.13 and 9.14. This behaviour was observed in the Al steels with high and low S levels (Fig. 9.13) and to a less marked extent in the Nb containing steels (Fig. 9.14). Mn probably influences the austenite grain size because it lowers the transformation temperature (Figs. 9.2-9.4), giving a finer ferrite start grain size.

Increasing the S level in the Al containing steels at constant Mn content also refines the austenite grain size (Figs. 9.13-9.14). This probably occurs because the austenite grain size may be dependent on two factors:

1. The initial ferrite grain size, which showed the same trends, as those shown by the austenite grain size, (Figs. 9.13-9.14).
2. The effectiveness of micro-alloying precipitates in pinning the austenite grains at higher temperatures. In this case it would be expected that the higher S steels with their higher solubility product of Al.N would have finer austenite grain size than the lower S steels.

Normalising the steels has been shown as would be expected to refine the austenite grain sizes as can be seen in Fig. 9.15 for heats A and C.

It should be noted that the Nb steels have shown

the finest γ grain size of the steels examined (Figs. 9.13-9.14). This is expected since Nb steels have NbCN precipitation at the austenite grain boundaries as well as AlN precipitation.

B. FRACTURE EXAMINATIONS

Scanning electron microscope examinations revealed three distinct fracture modes. Low temperature ductile rupture (LTDR), high temperature ductile rupture (HTDR) and intergranular failure (IG). The first two fracture modes were identical to those previously observed in chapter 5 for micro-alloyed steels and by Crowther and Mintz (1986 a) for plain C-Mn steels.

The IG failure mode was observed in steels which failed with R of A values less than 60%, Fig. 9.16, and they are similar to those observed by Crowther et al., (1987), with no micro-voids on the grain facets.

C. REPLICAS EXAMINATIONS

Carbon replicas taken from regions close to the point of fracture have been extracted from samples tested at 1000 °C for all the steels examined. At this temperature, most of the steels have shown their minimum ductility. Examination of these replicas under the TEM, revealed AlN precipitates for all steels containing Al in the normalised and as received conditions (heats A, B, C, and D). The precipitates were mostly at the austenite grain boundaries, with similar precipitation patterns in

both test conditions, Figs. 9.17-9.19. However, precipitation in the as received state was slightly finer than in the normalised condition.

Nb containing steels (heat E and F), showed AlN and NbCN precipitates at the austenite grain boundaries, and extensive NbCN precipitation in the matrix was frequently observed, Fig. 9.20.

Examining for sulphide inclusions under the TEM was difficult, since they tend to segregate and their were large areas over which none can be seen. However, it was possible to confirm other workers results (e.g. Bellot and Gantois, 1978), in that the higher S steels (heat C and D containing Al, heats E and F containing Nb) had higher volume fraction of MnS inclusions than the lower S steels (heats A and B, containing Al), Figs. 9.21-9.22.

9.4 DISCUSSION

9.4.1 EXPLANATION FOR THE SHAPE OF THE HOT DUCTILITY CURVES

As can be seen in Figs 9.2-9.6, ductility started to fall at temperatures close to the A_{e3} temperature (the A_{e3} points, indicated in Figs. 9.2-9.6, have been calculated using Andrews' formula, 1965). Therefore, it can be concluded, that the ductility troughs occur when the steels are fully austenitic.

Previous work (Crowther et al., 1987) has shown that intergranular failure in the austenite for steels heated directly to test temperatures could occur due to precipitation at the γ grain boundaries, enhancing grain boundary sliding or due to grain coarsening with increasing temperature. In the present work, γ grain sizes are approximately constant (Figs. 9.13-9.15) at temperatures giving the minimum value of ductility (900 and/or 1000 °C) as can be seen in Figs 9.2-9.3. Also the shape of the ductility curves, can be explained by the action of grain refining precipitates at the austenite grain boundaries. Once precipitation is well established at the boundary, sliding is possible, and the particles are able to prevent dynamic recrystallisation, resulting in intergranular failure.

It should be noted however that even though dynamic recrystallisation may have occurred, very different R of A values can be obtained with increasing temperature.

For example, in heat C (Fig. 9.3), dynamic recrystallisation has started at 900 °C with 70% R of A, but full restoration of ductility (100%), does not occur until the temperature reaches 1100 °C. This behaviour could be explained in the present study by the decrease in the critical strain, ϵ_c , (necessary to nucleate dynamic recrystallisation) with increasing temperature, Fig. 9.12, in accord with McQueen and Jonas (1975). This decrease in ϵ_c might be expected to improve ductility, since dynamic recrystallisation starts at earlier stage of deformation with increasing test temperature, which could lead to an increase in the volume fraction of recrystallised grains.

Previous work (Mintz et al., 1983) has shown an increase in precipitate size with test temperature. Thus, they concluded that once the precipitates reach a critical size (Gladman and Pickering, 1967), pinning of grain boundaries is no longer effective. Grain coarsening can then commence, and ductility recovers. Thus, it might be expected that the temperature for the onset of dynamic recrystallisation and the temperature for coarsening of particles above a critical value would be closely associated with each other. Although this relationship is not followed closely in the present work, when boundaries are loosely pinned (e.g. heat C in Fig. 9.3) and ductility is generally good, it does however seem to be the case when ductility is poor (R of A $\leq 60\%$), i.e. boundaries likely to be heavily pinned (e.g. heat D in Fig. 9.3).

9.4.2 EFFECT OF Mn AND S ON HOT DUCTILITY

Decreasing the Mn content from $\sim 1.4\%$ to $\sim 0.3\%$ at similar S contents in the steels examined, has resulted in wider and deeper ductility troughs as can be seen in Fig. 9.2-9.4. This is not surprising, since increasing the Mn concentration in the steels, has been shown to refine the grain size (Figs. 9.13-9.14) which would result in a reduction in the critical strain, ξ_c , necessary to nucleate dynamic recrystallisation, Fig. 9.10.

The beneficial effect of grain size refinement on hot ductility of metals is in accord with many previous studies, as has been mentioned in section 3.7. However, this role is only valid as long as similarity in precipitates volume fraction and size exist. For example, heats A and B have the same low S content and hence volume fraction of sulphides and also the same volume fraction of grain refining precipitates and the finer grain steel A (Fig. 9.13) therefore gives the better hot ductility, Fig. 9.2. Similar trends were noted in the other group of steels examined, the high S steels (heats C and D) and the medium S steels (heats E and F), i.e. other things being equal the finer grained steels (higher Mn) gave the better hot ductility.

On the other hand, the steels with high S levels when compared to the lower S steels at the same Mn content, show an increased volume fraction of sulphides and also volume fraction of grain refining precipitates, both of which lead to finer grain sizes Fig. 9.13, yet

results in worse hot ductility. This has been shown for heats A and C (S increasing from 0.002 to 0.03%, respectively at constant Mn level, 1.4%) and for heats B and D with 0.3% Mn and different S levels.

This is in accord with the effect of precipitation in retarding dynamic recrystallisation, ξ_c increases as can be seen in Figs. 9.11-9.12 (in Fig. 9.12 heats A and C are comparable). Also ξ_c increases with increasing volume fraction of precipitate and as their size decreases (Weiss and Jonas, 1979). The influence of temperature on ξ_c would be expected to be temperature dependent, since at high temperatures, precipitates size will be increased and volume fraction decreased.

9.4.3 EFFECT OF NORMALISING ON HOT DUCTILITY

The variation of hot ductility with deformation temperatures for the Al containing steels, A and C in the normalised and as received conditions are shown in Figs. 9.5-9.6, respectively. For both steels ductility after normalising has been improved. Since the precipitation in the as received condition was only slightly smaller than in the normalised condition, it would be expected that the improvement in hot ductility is mostly due to the grain size refinement produced by normalising, Fig. 9.15. This has been shown to reduce the ξ_c for dynamic recrystallisation markedly, Fig. 9.12, with the result of better hot ductility.

9.5 CONCLUSIONS

1. Refining the austenite grain size improves hot ductility as long as similarity in precipitate volume fraction and size exist. Better ductility under this condition has been achieved in the present study by increasing the Mn content (from ~ 0.3 to $\sim 1.4\%$) or by normalising.
2. Increasing the S level in the steel also refined the grain size but this was accompanied by more effective pinning of γ grain boundaries possibly by sulphides, although increased micro-alloying precipitates may be important as the higher S steels also had higher $[Al] \cdot [N]$ solubility products. The more effective pinning of the boundaries dominated the hot ductility process leading to inferior hot ductility.

Code	Steel	C	Si	Mn	P	S	Al	Nb	N
A	C-Mn-Al	.11	.32	1.42	.011	.002	.038	---	.0036
B	C-Mn-Al	.11	.32	.32	.01	.003	.038	---	.0036
C	C-Mn-Al	.094	.29	1.42	.011	.03	.034	---	.005
D	C-Mn-Al	.095	.28	.31	.01	.032	.032	---	.0049
E	C-Mn-Al-Nb	.098	.3	1.41	.009	.007	.04	.031	.0042
F	C-Mn-Al-Nb	.099	.31	.29	.009	.007	.038	.031	.0041

Table 9.1 Compositions of the steels examined (Wt.%).

steels examined in normalised condition	test temperature, °C			
	1100	1050	1000	900
A	9.75	--	12.86	13.5
B	12.03	12.87	--	--
C	9.54	--	12.45	15.15
D	11.62	13.5	--	--
E	11.2	--	14.5	--
F	12.86	--	--	--
steels examined in as received condition				
A	12.45	--	16.6	18.7
C	13.7	--	18.26	--

Table 9.2 Critical strain (ϵ_c in %) for dynamic recrystallisation calculated from Figs. 9.8-9.9 after Rossard (1973) equation.

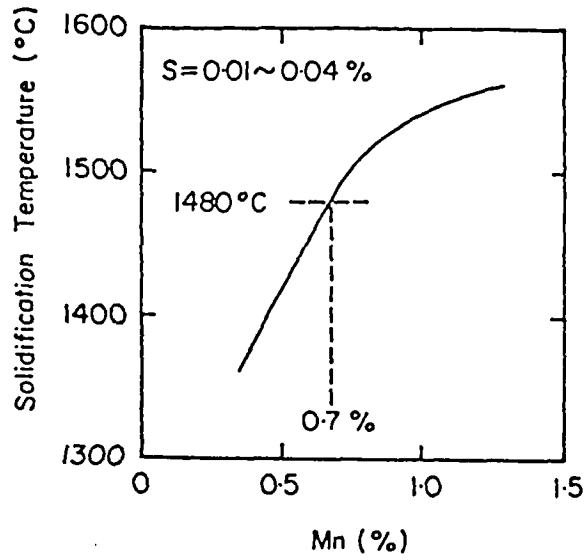


Fig. 9.1 Effect of Mn content in the steel on the solidification temperature of sulphide inclusions, (After Kinoshita and Kuroki, 1972).

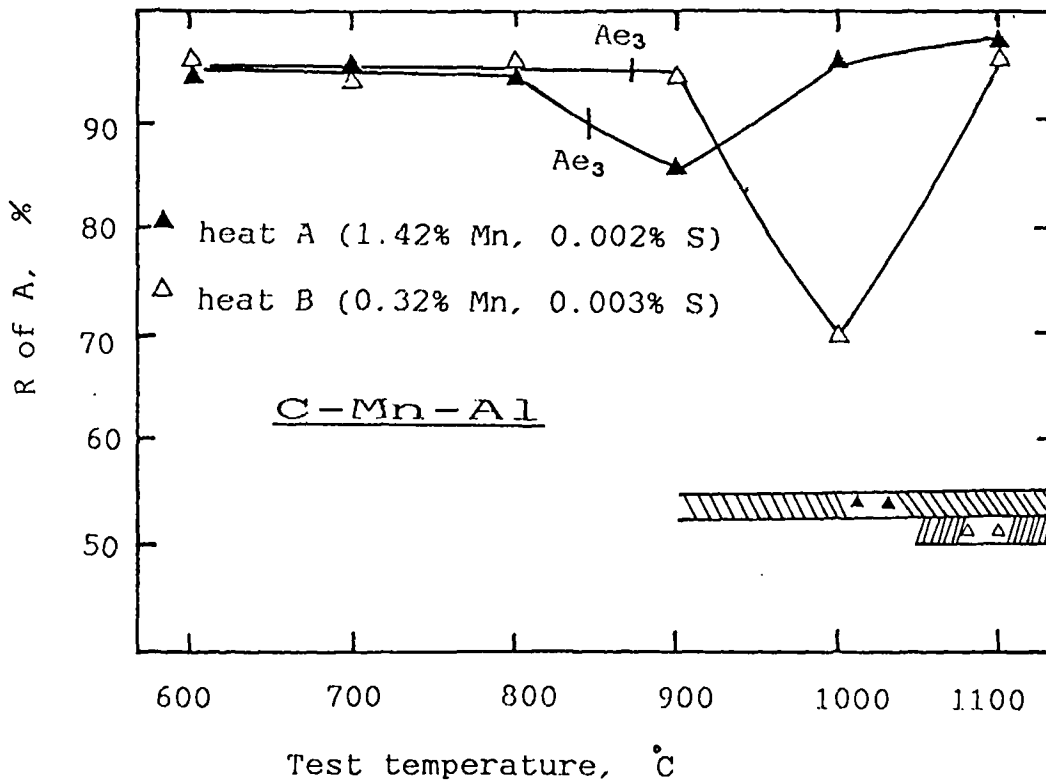


Fig. 9.2 Hot ductility curves for the low S steels, containing Al.

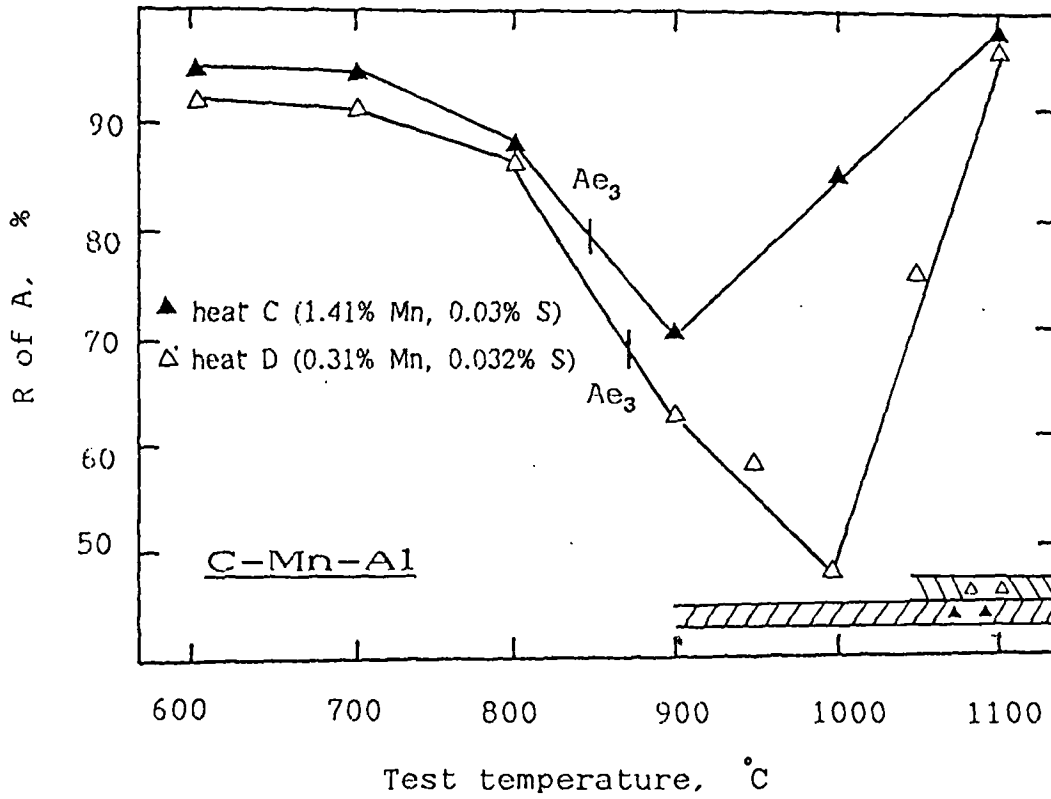


Fig. 9.3 Hot ductility curves for the high S steels, containing Al.

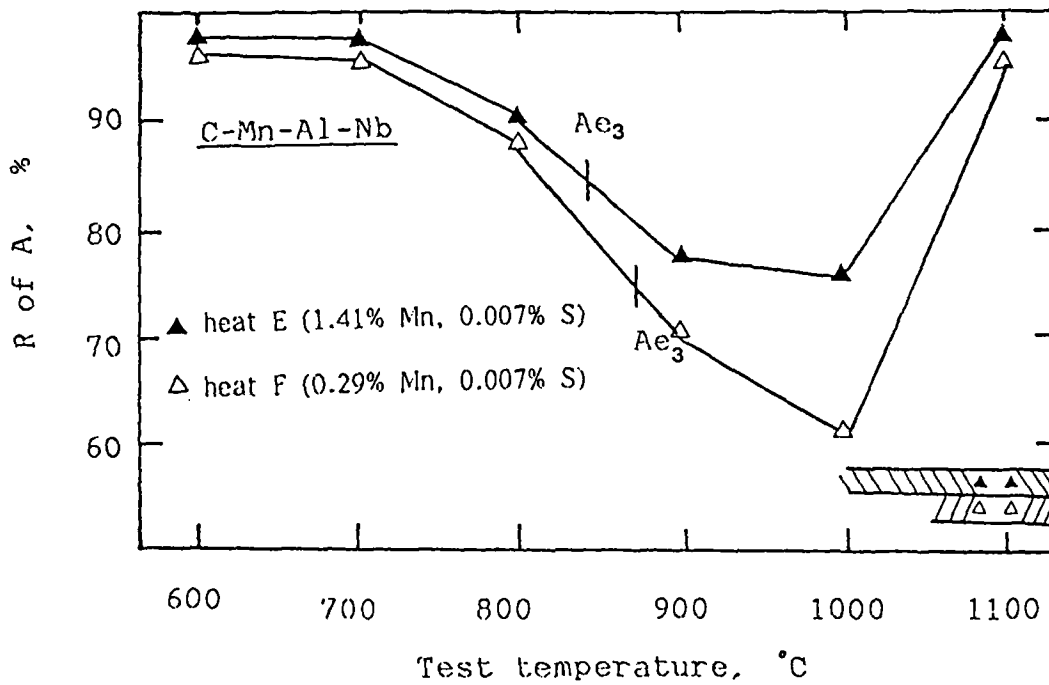


Fig. 9.4 Hot ductility curves for the Nb containing steels.

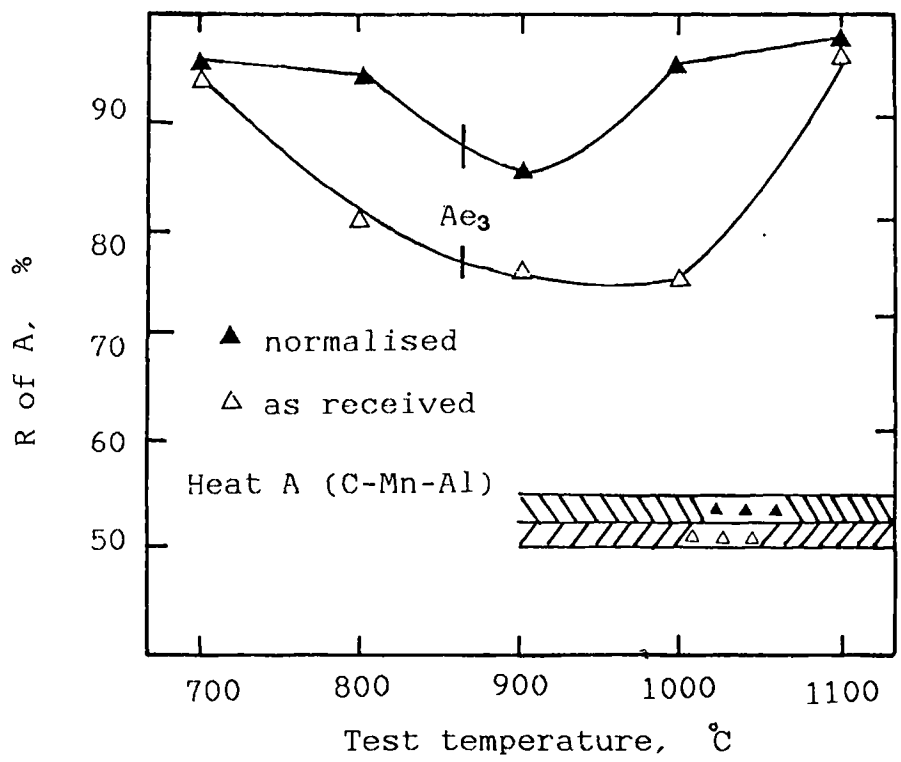


Fig. 9.5 Hot ductility curves for the Al containing steel with low S content in normalised and as received conditions.

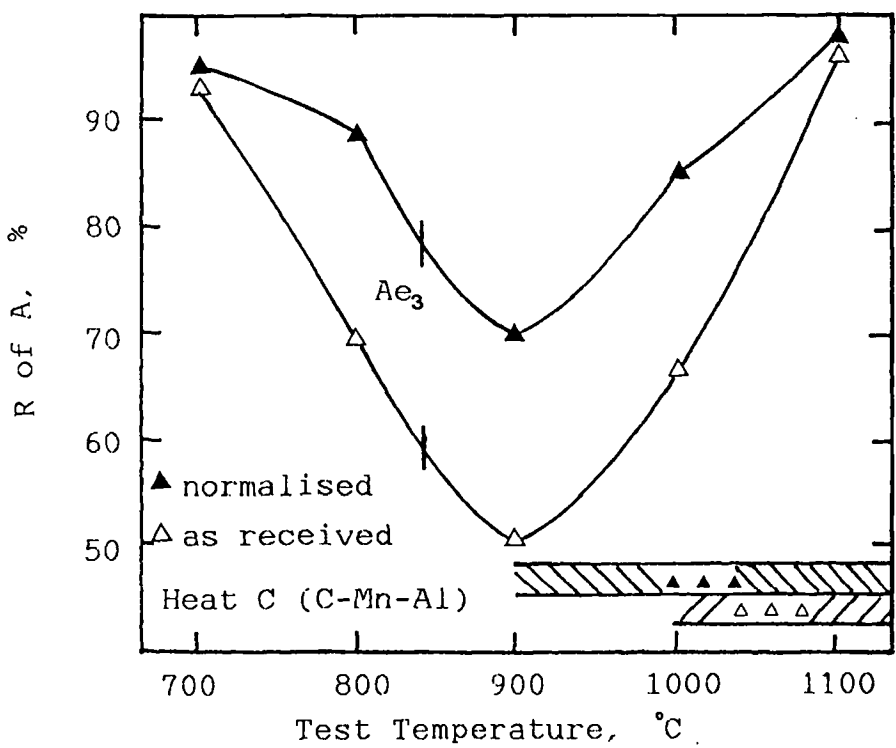


Fig. 9.6 Hot ductility curves for the Al containing steel with high S content in normalised and as received conditions.

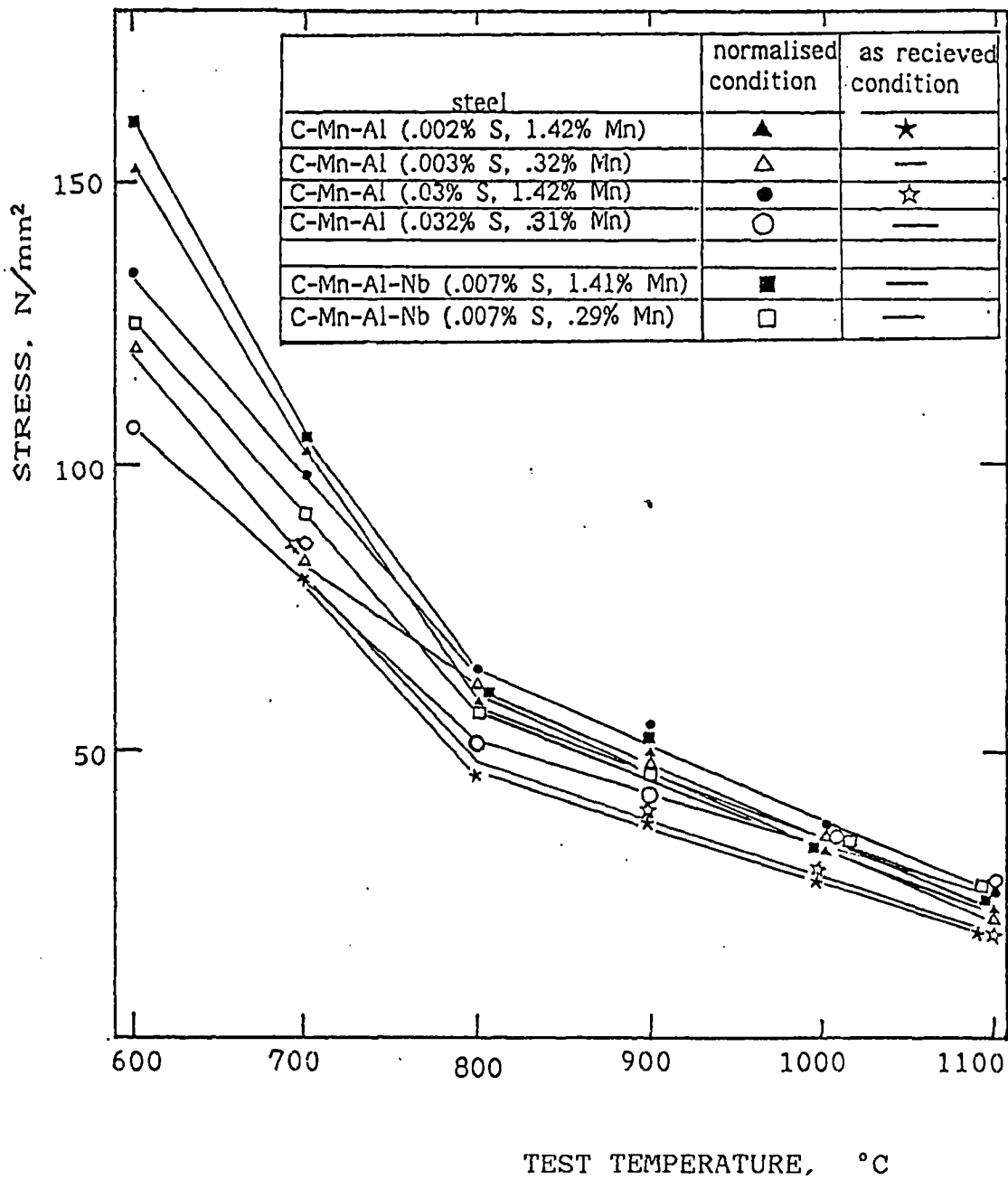


Fig. 9.7 Variation of peak stress, with test temperature for the steels examined in normalised and as received conditions.

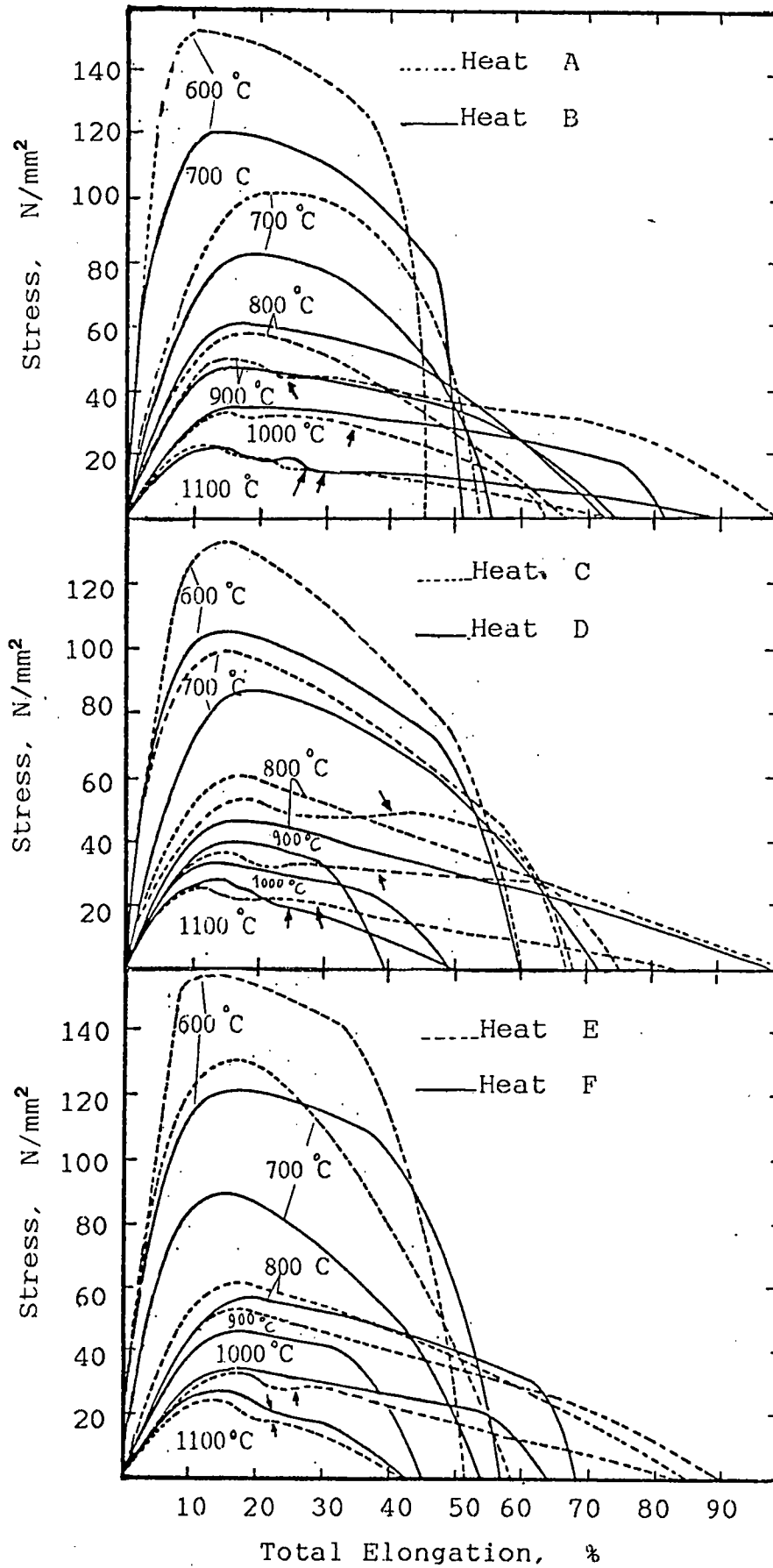


Fig. 9.8 Stress-total elongation curves for the steels examined in normalised condition.

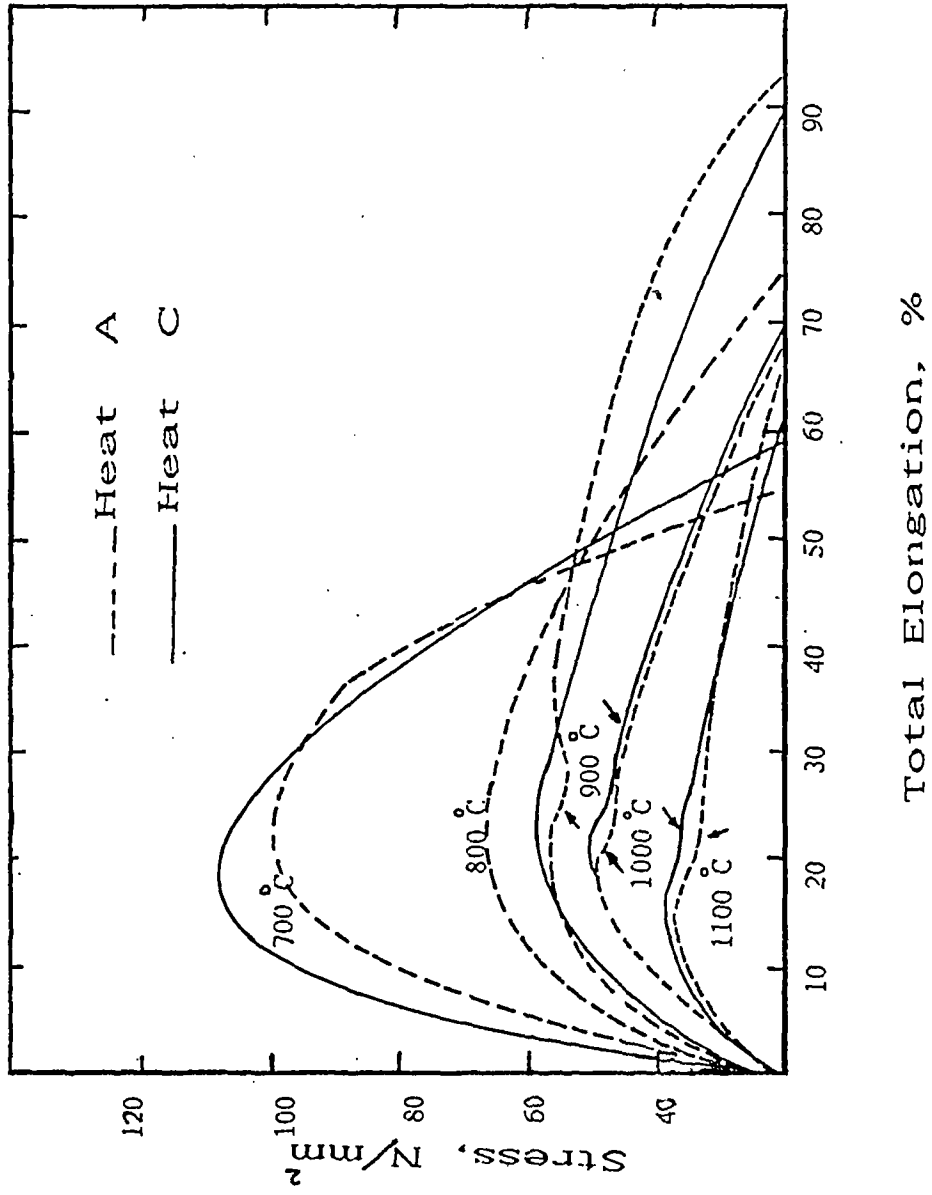


Fig. 9.9 Stress-total elongation curves for the steels examined in the as received condition.

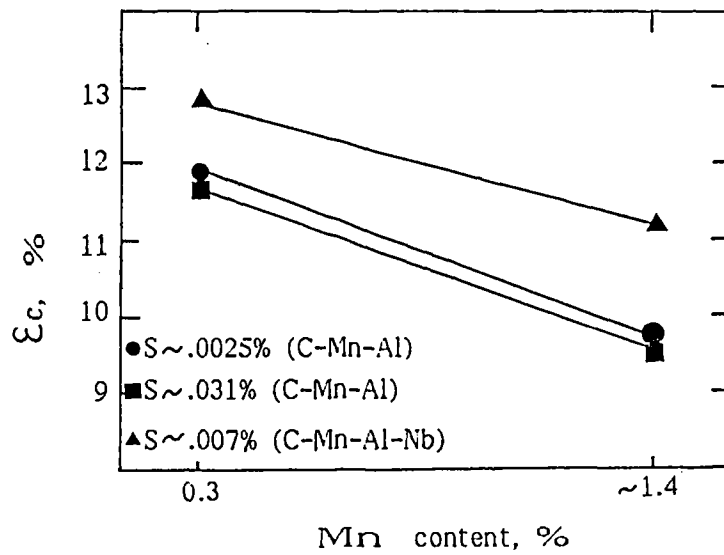


Fig. 9.10 Effect of the Mn content on the critical strain necessary to nucleate dynamic recrystallisation for the steels examined at 1100 °C in the normalised condition.

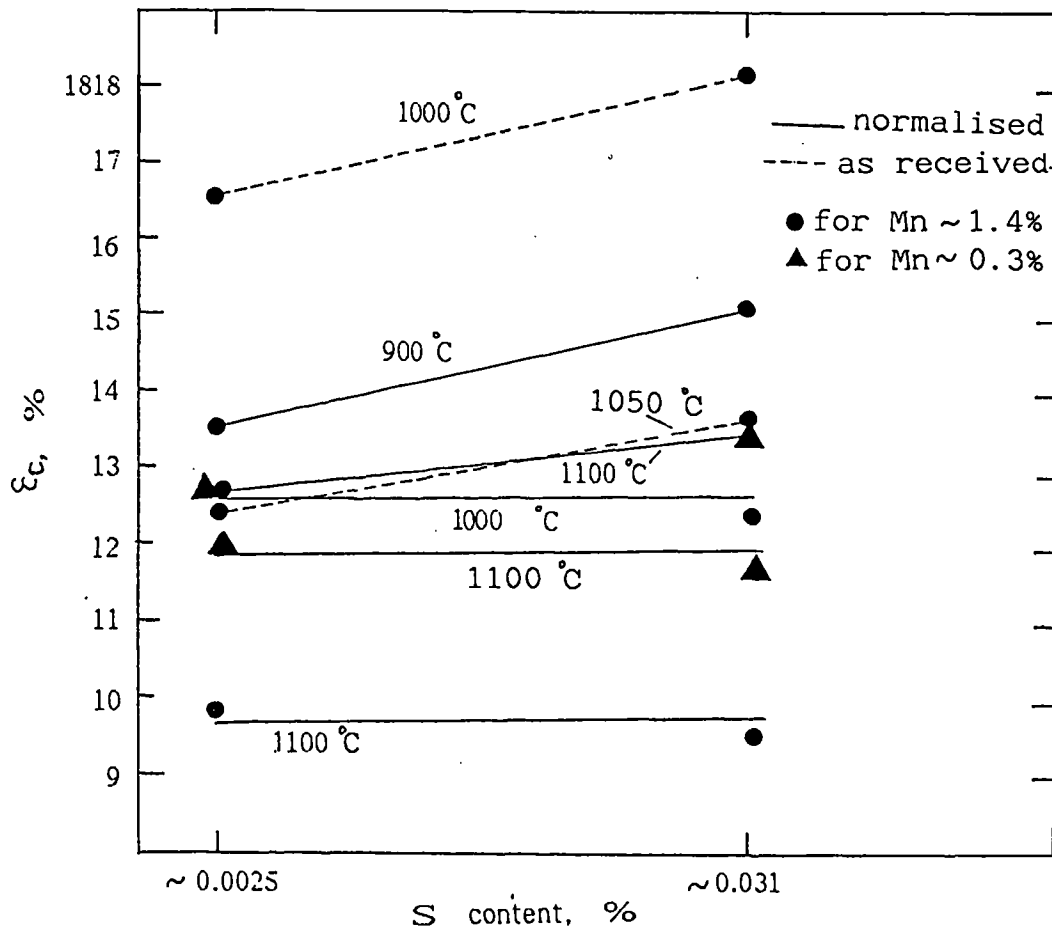


Fig. 9.11 Effect of S content on the critical strain necessary to nucleate dynamic recrystallisation for the Al containing steels examined in different conditions.

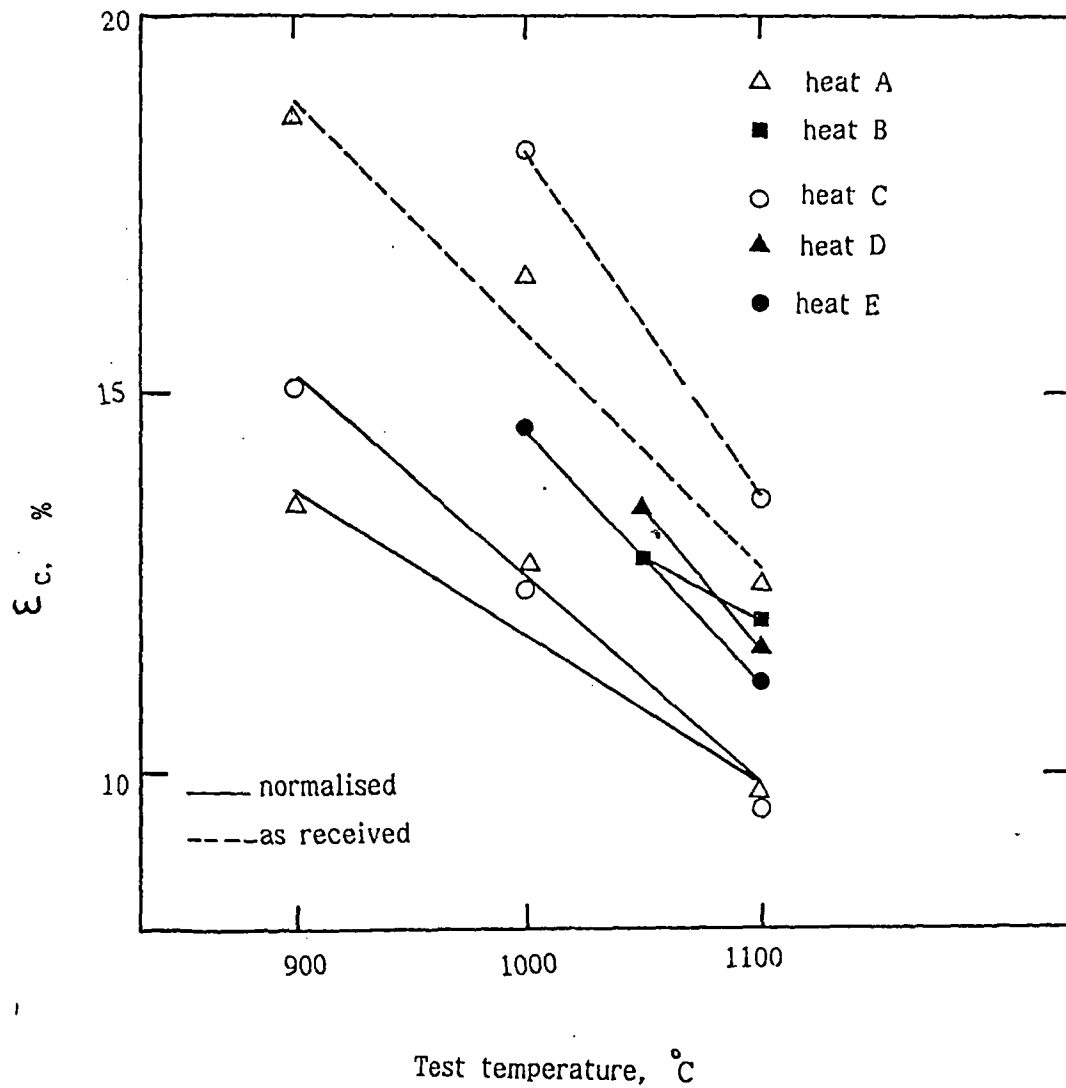
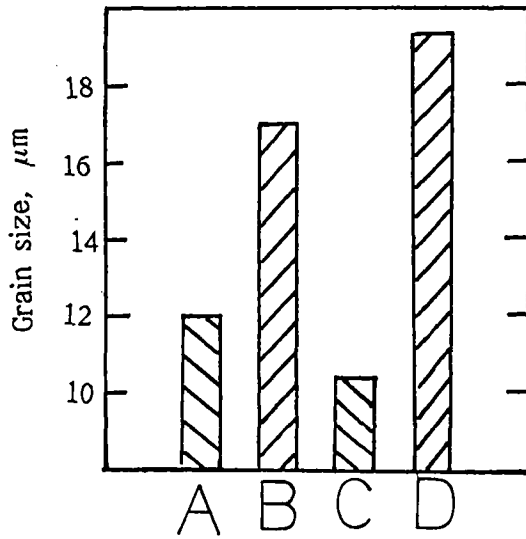


Fig. 9.12 Effect of test temperature on ϵ_c for the steels examined in normalised and as-received conditions.

a. Ferrite grain sizes



b. Austenite grain sizes

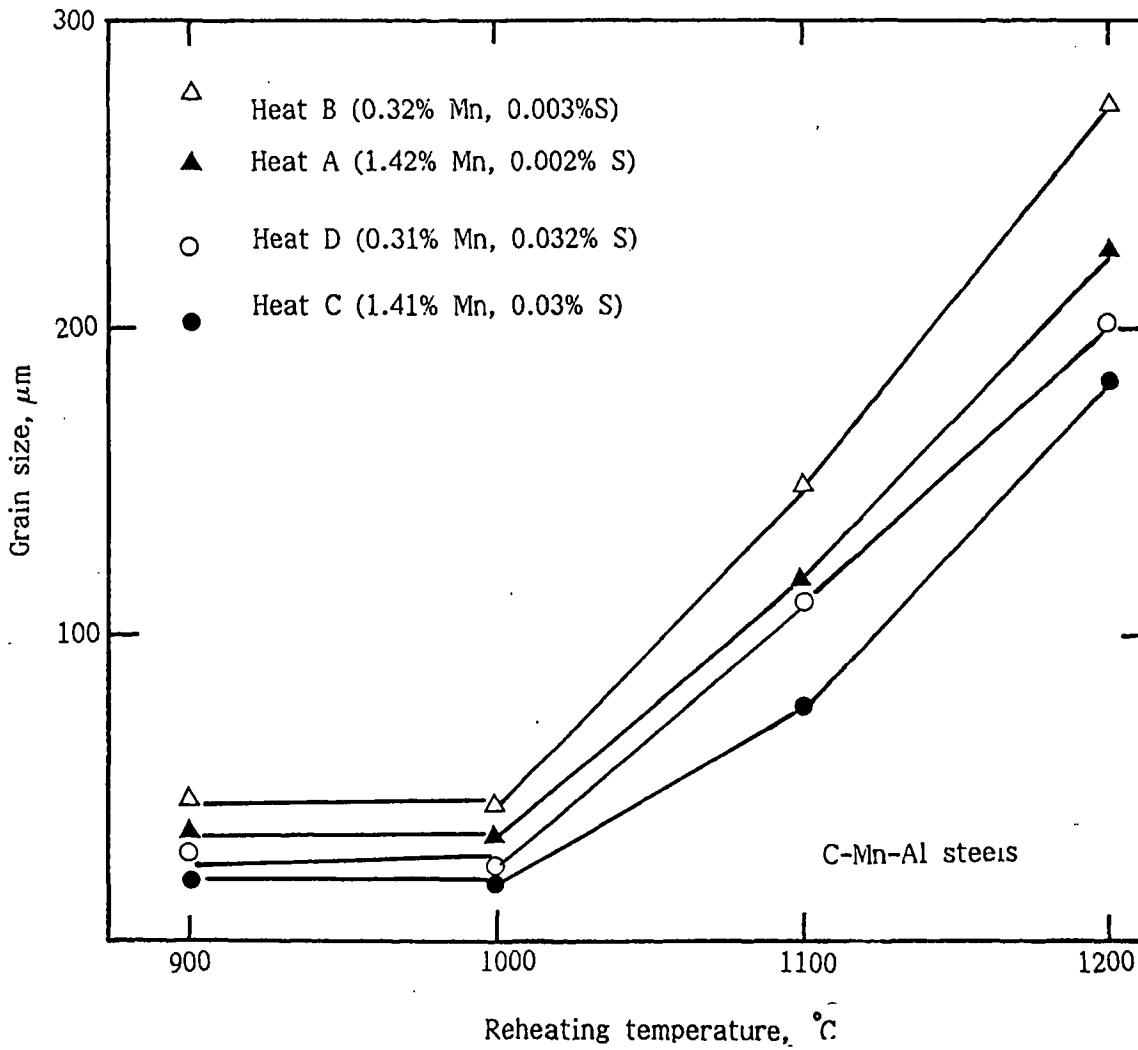
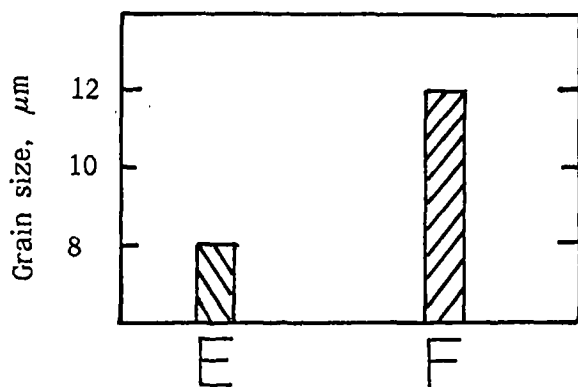


Fig. 9.13 Grain size measurements for the C-Mn-Al steels examined in the normalised condition.

a. Ferrite grain sizes



b. Austenite grain sizes

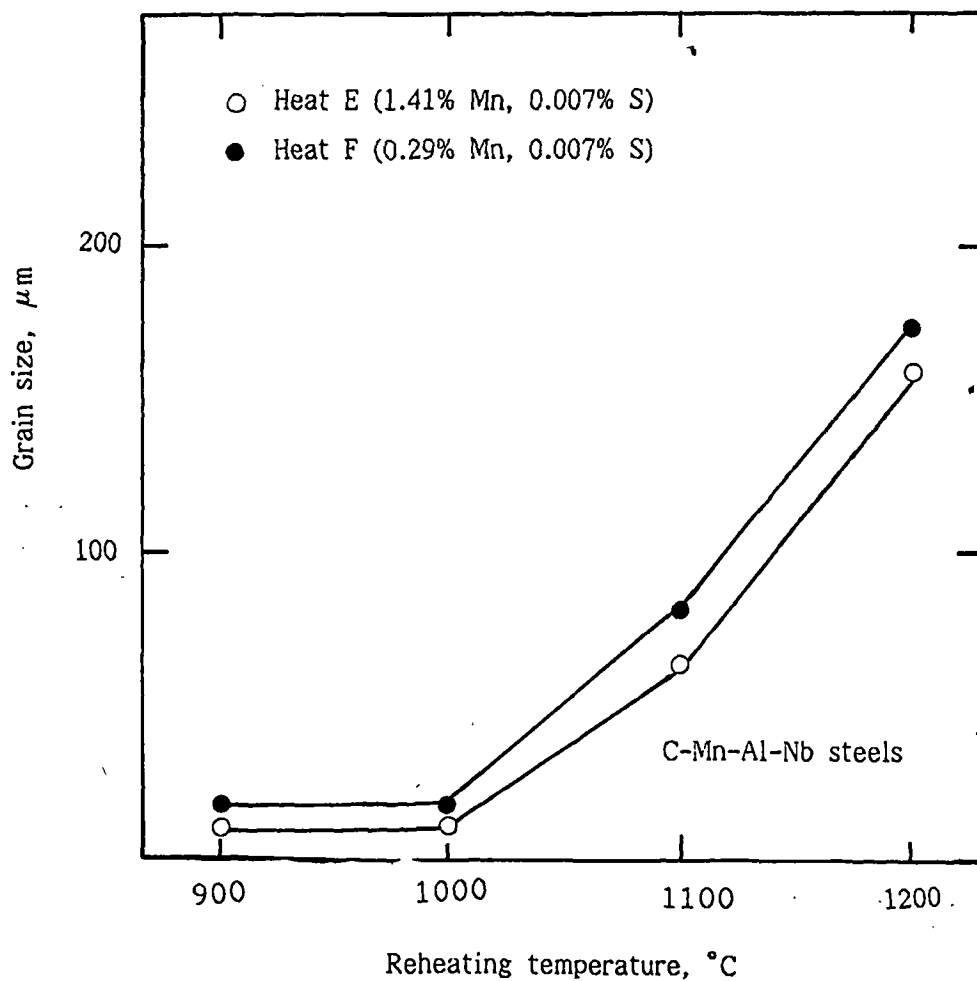


Fig. 9.14 Grain size measurements for the Nb containing steels in the normalised condition.

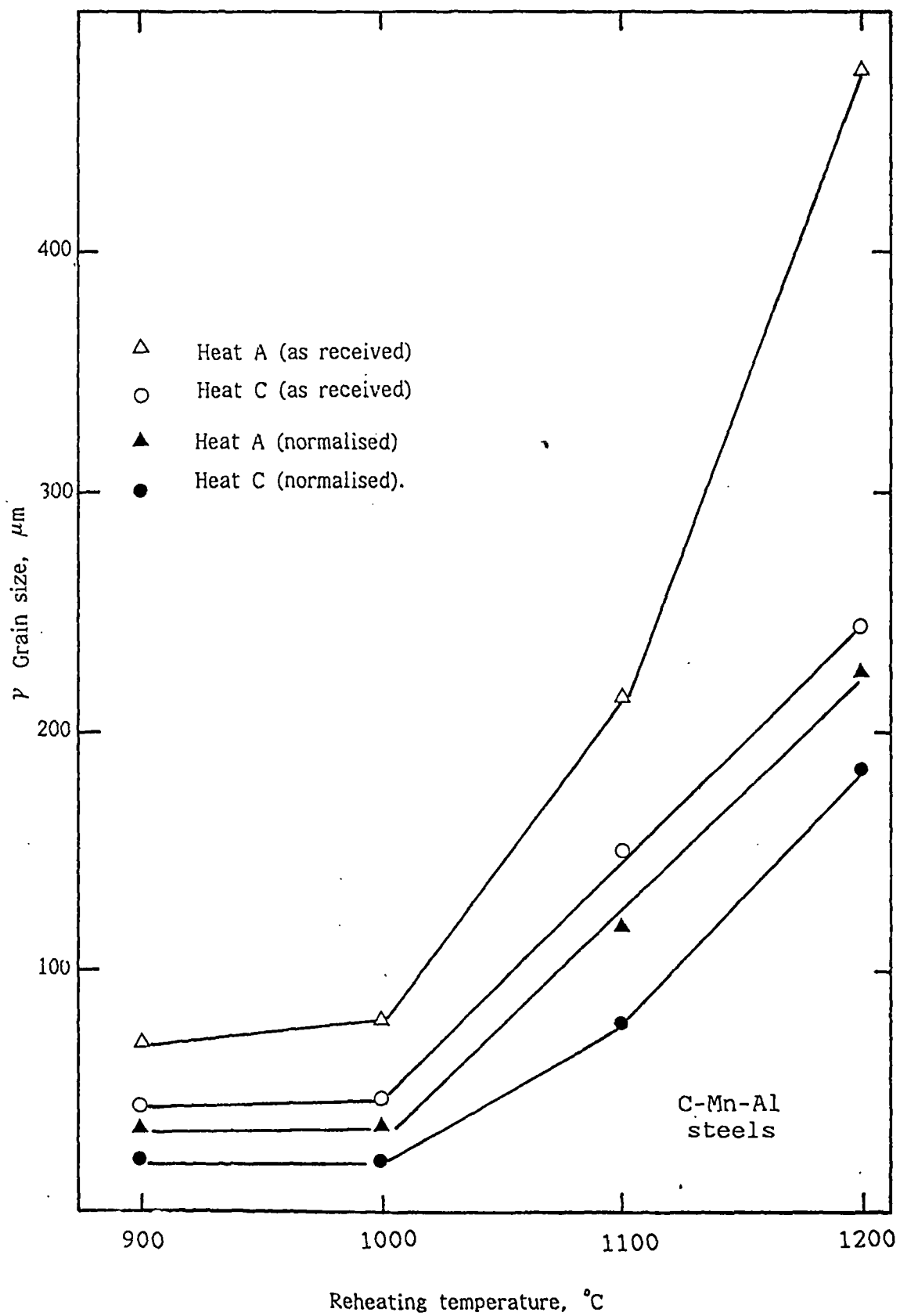
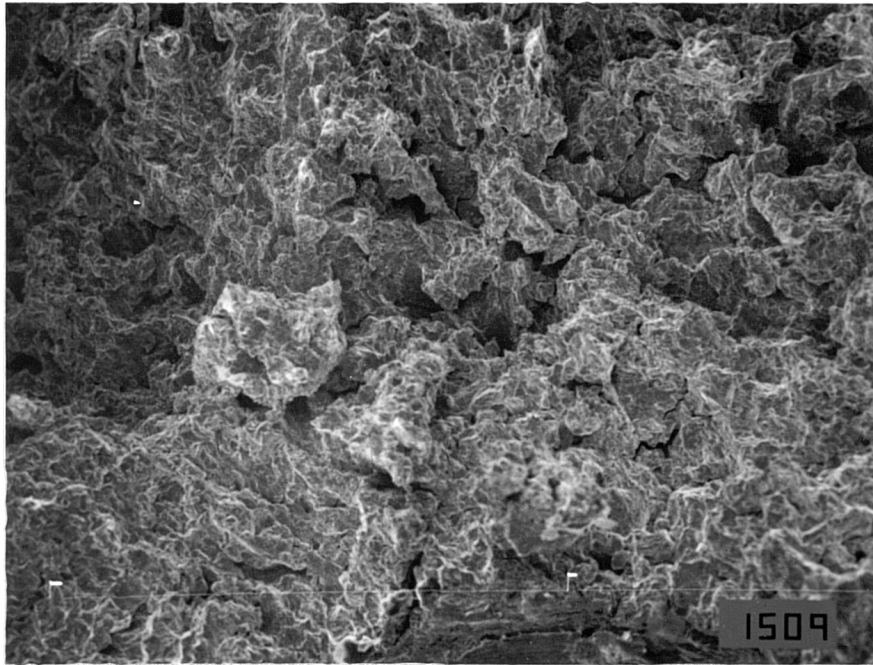
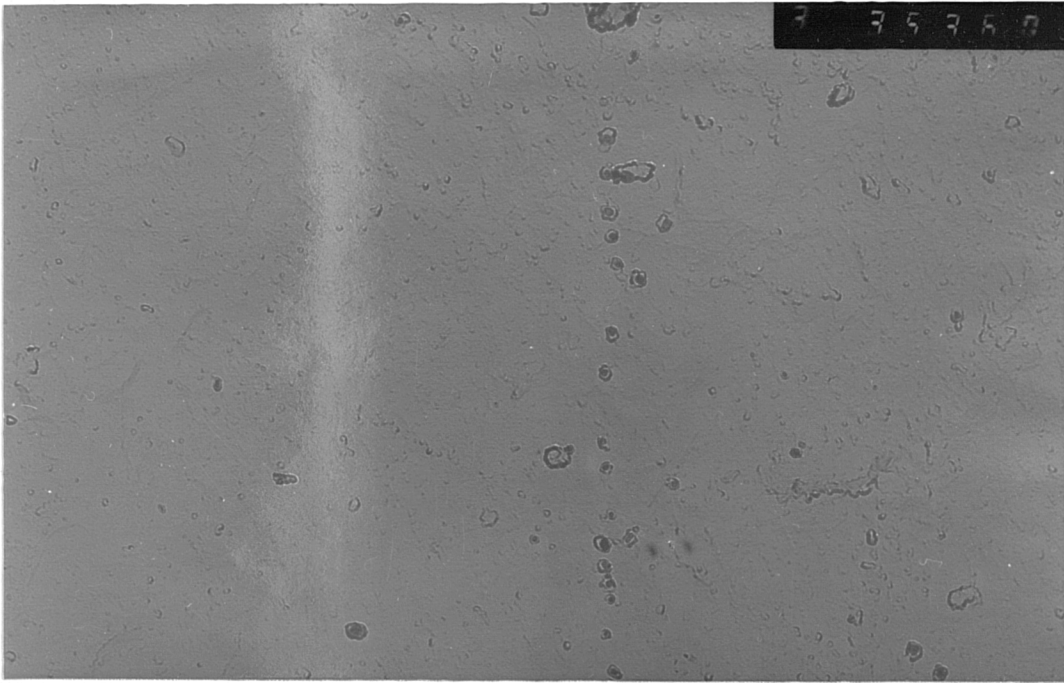


Fig 9.15 Variation of γ grain size with temperature for Al containing steels with high Mn content (1.4%) in normalised and as received condition.



267 μm

Fig. 9.16 Fracture surface of C-Mn-Al steel (heat D) tested at 1000 °C, showing typical intergranular failure.



(a). heat A

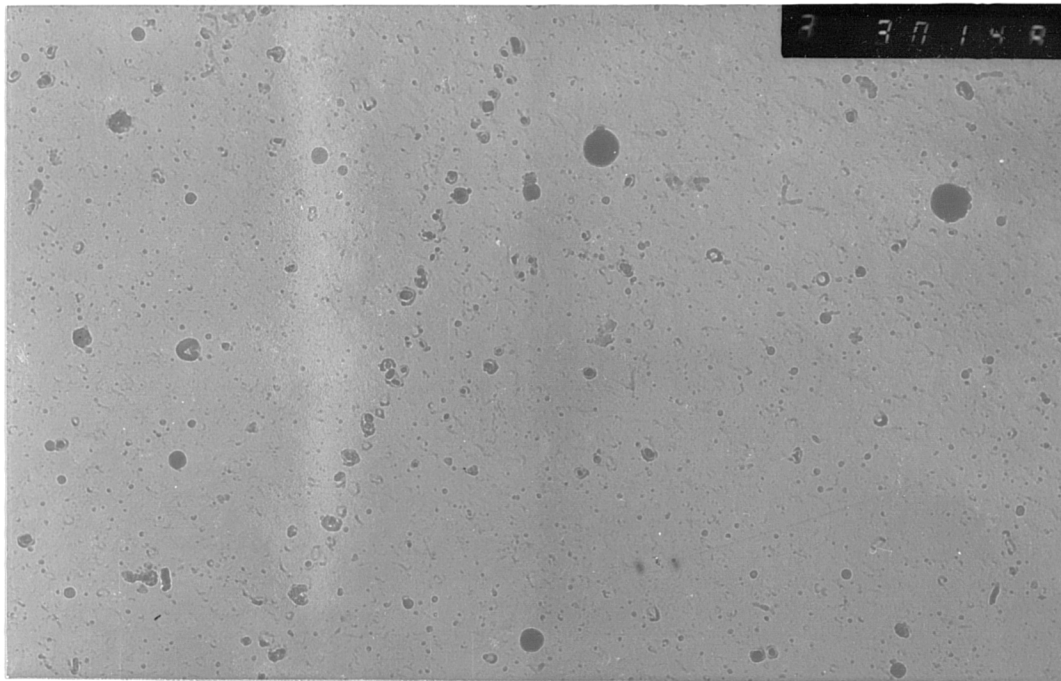
0.85 μm



(b). heat B

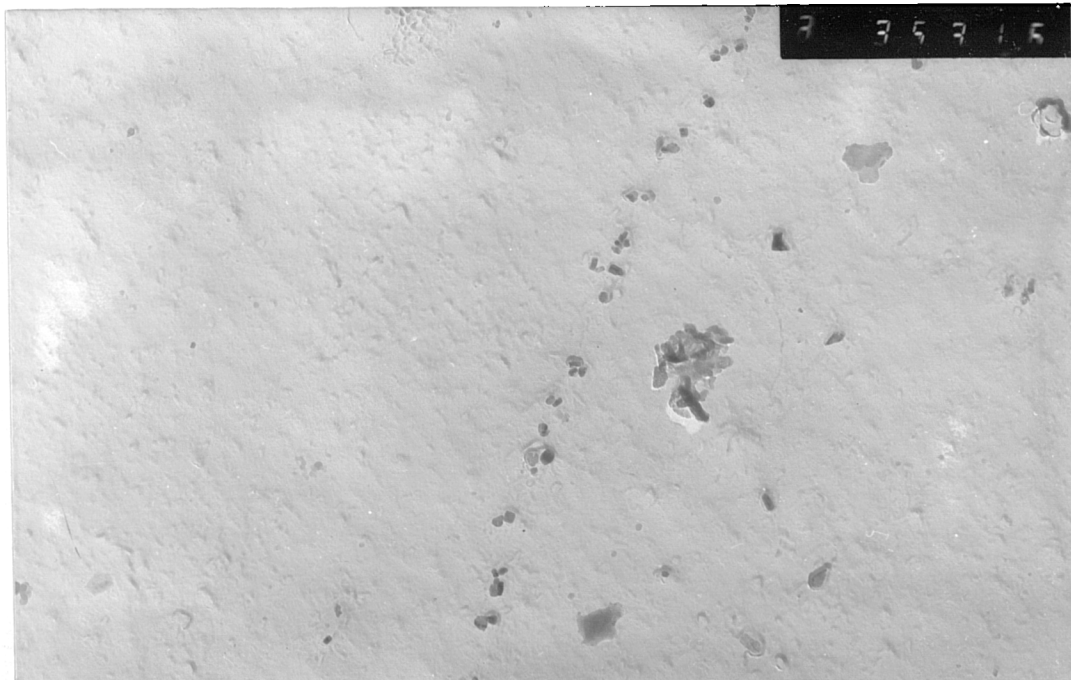
0.85 μm

Fig. 9.17 Examples of AlN precipitation observed in the Al containing steels (heats A and B) with low S contents (.002-.003%S) at test temperature of 1000 °C, in normalised condition.



(a). heat C

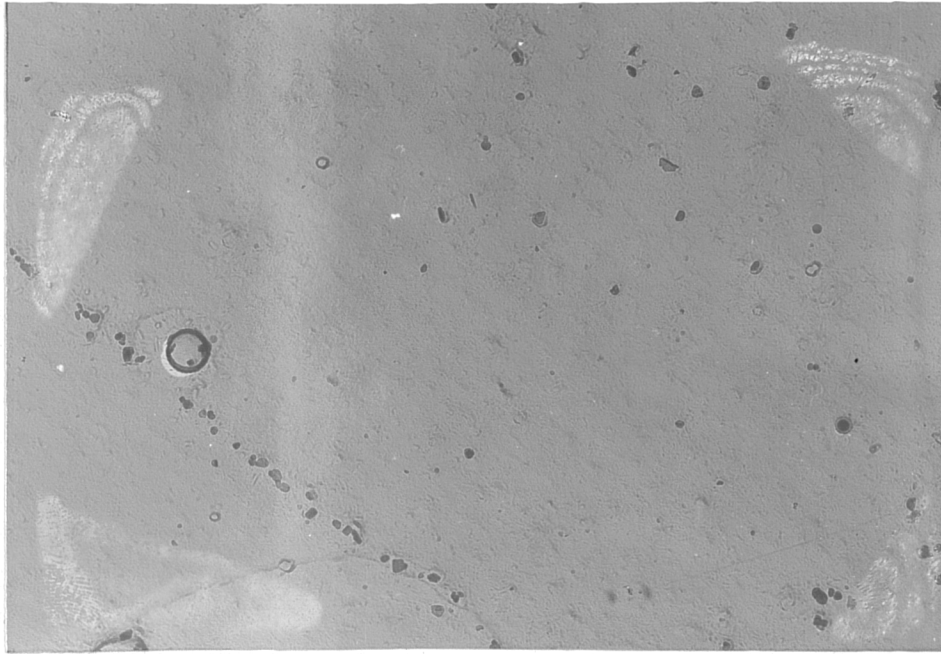
0.85 μm



(b). heat D

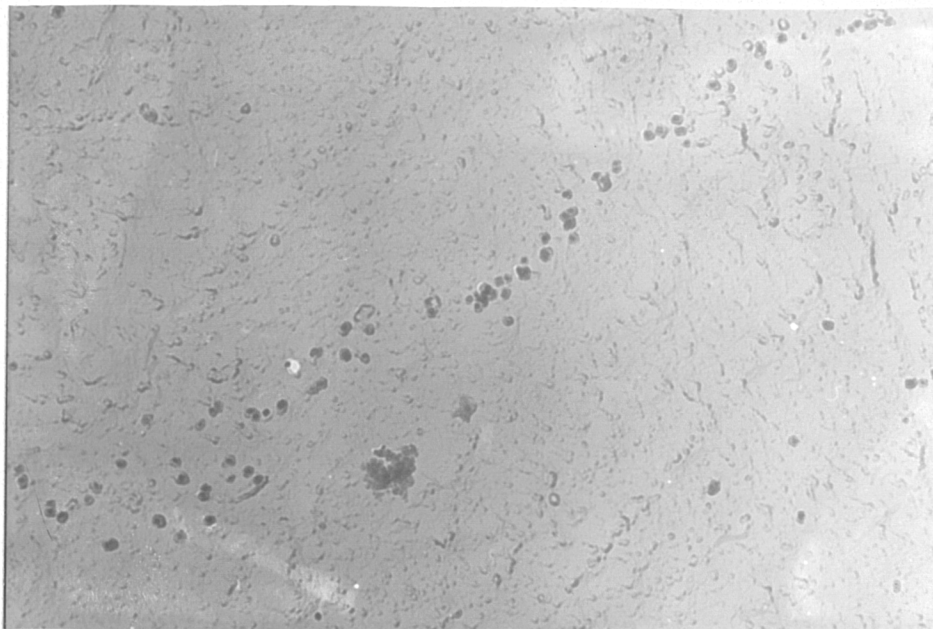
0.85 μm

Fig. 9.18 Example of AlN precipitation observed in the Al containing steels (heats C and D) with high S contents (.03-.032% S) at test temperature of 1000 °C, in normalised condition.



(a). heat A

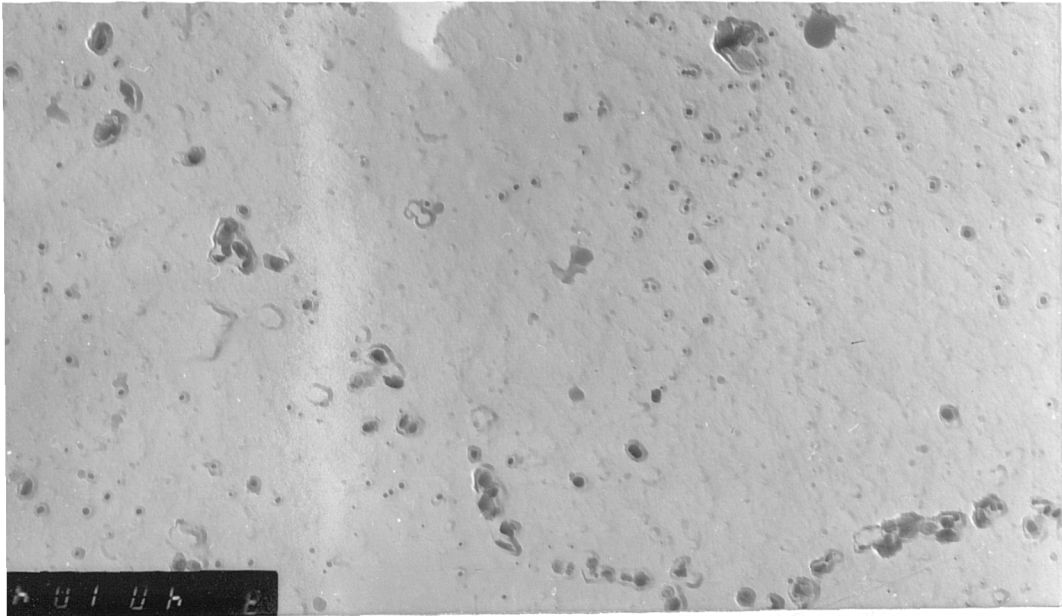
0.85 μm



(b). heat C

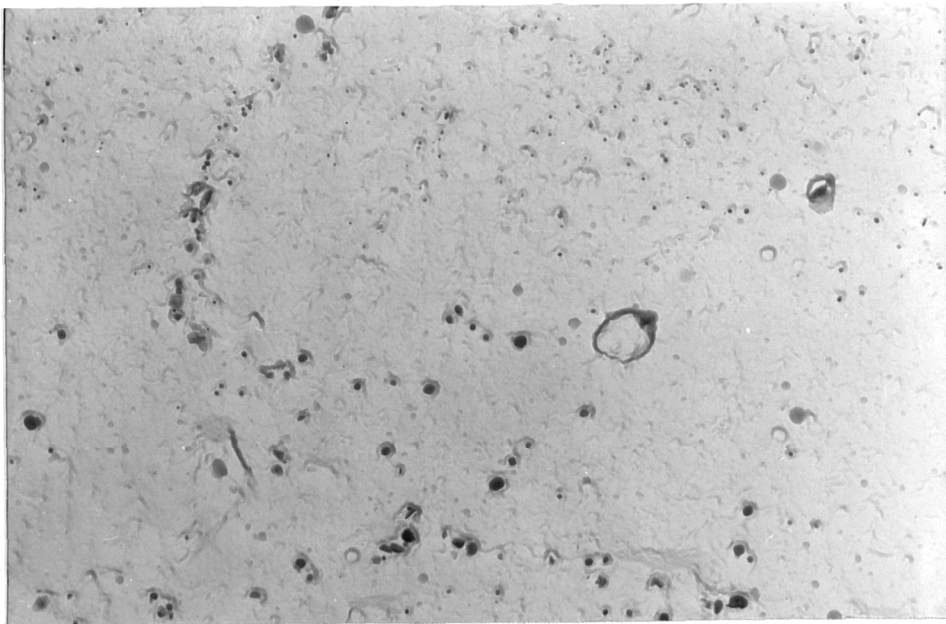
0.85 μm

Fig. 9.19 Examples of AlN precipitation observed in Al containing steels with high Mn contents (1.4%) at 1000°C in as received condition.



(a). heat E

0.75 μm



(b). heat F

0.75 μm

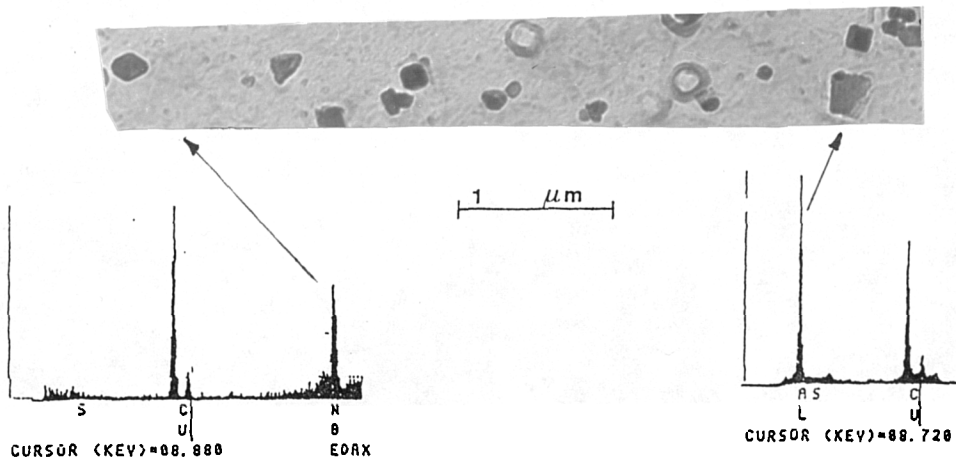
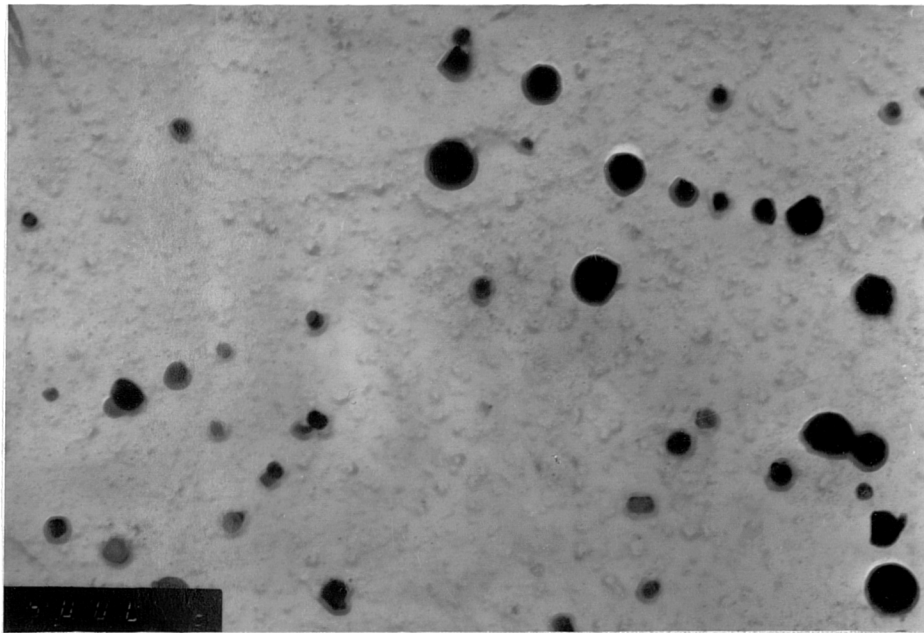
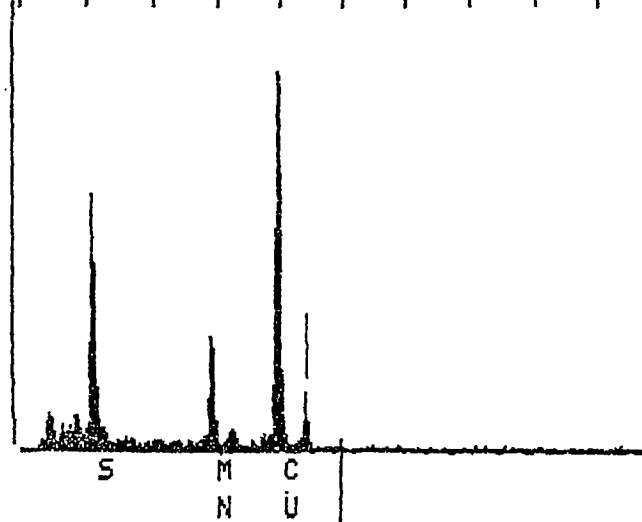


Fig. 9.20 Examples of AlN and NbCN precipitation observed in the Nb/Al steels (heats E and F) at test temperature of $1000\text{ }^\circ\text{C}$, in the normalised condition, with associated X-ray spectrum.



2.5 μm

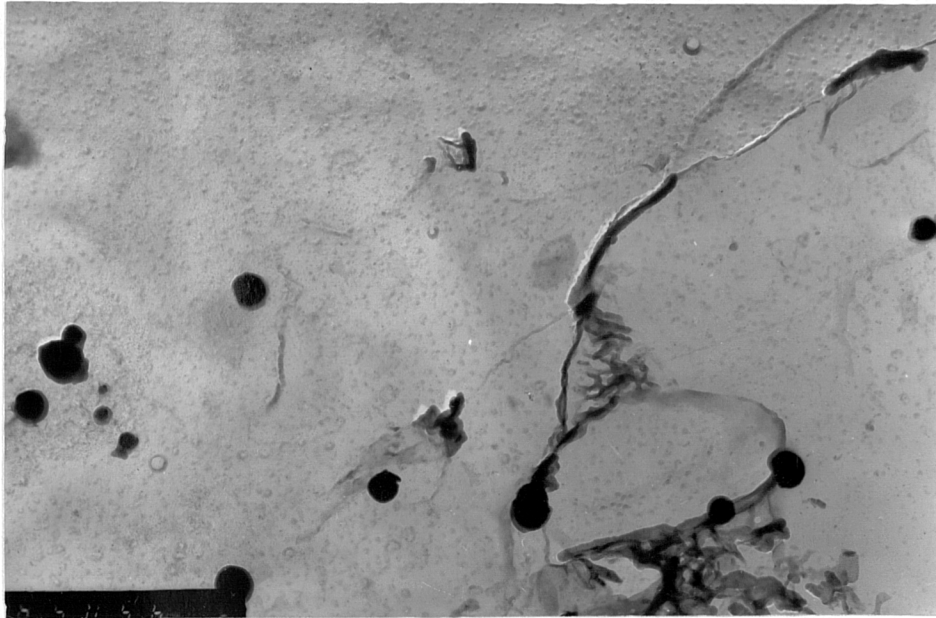
RATE: 333CPS TIME: 127LSEC
 00-20KEY: 10EV/CH PRST: 200LSEC
 A: B:
 FS= 314 MEM: A FS= 200
 |00 |02 |04 |06 |08 |10 |12 |14 |16 |18



CURSOR (KEY)=10.000.

EDAX

Fig. 9.21 Example of MnS inclusions observed in the high S steel (heat D) in the normalised condition, at test temperature of 1000 °C.

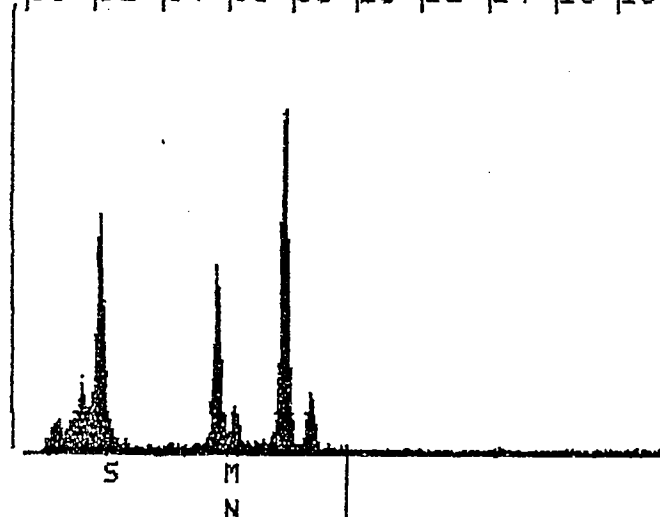


2.5 μ m

```

RATE:          7CPS TIME:      60LSEC
00-20KEV:10EV/CH PRST:      200LSEC
A:             B:LIST-AUTO BKG
FS=      829   MEM: A      FS=   1789
|00 |02 |04 |06 |08 |10 |12 |14 |16 |18

```



CURSOR (KEV)=09.840 EDAX

Fig. 9.22 Example of MnS inclusions observed in the low S steel (heat A) in the normalised condition, at test temperature of 1000 °C.

CHAPTER 10

THE INFLUENCE OF TEST
DIRECTION ON THE HOT
DUCTILITY OF AUSTENITE

10.1 INTRODUCTION

The fact that rolled steel products exhibit a marked anisotropy of tensile ductility and notch toughness at room temperature has been known for a long time, (Bernard et al., 1975 ; Speich and Spitzig, 1982). This has been attributed to the presence of inclusions and segregation in the steel.

Spitzig and Sober (1981) have reported that the loss of ductility in the short transverse direction is to be largely determined by S content and the type, shape, and distribution of sulphides and other non metallic inclusions in the steel.

Inclusions do not only act as region of weakness but depending on their shape relative to the test direction, can act as stress concentrators in the same way as a notch or a crack. The strain concentration associated with elongated inclusions are normally regarded as being proportional to the ratio of the axis normal and parallel to the stress axes, (Morrison, 1975). Hence when a plate is tested in the rolling direction, the strain concentration is very low but increases on testing in the transverse, and is most marked in the short transverse direction.

Some recent work by Crowther and Mintz (1986d) has also shown that similar behaviour occurs when hot rolled plates of C-Mn-Al and C-Mn-Al-Nb steels containing elongated MnS inclusions are tensile tested in the temperature range 600 to 1100 °C in both longitudinal and transverse direction at low strain rate ($3 \times 10^{-4} \text{ S}^{-1}$). Transv-

erse hot ductility was slightly lower than that from longitudinal samples ($\sim 10\%$ R of A lower). Modification of the sulphides using calcium, removed this directionality as well as giving a marked improvement in hot ductility. Because the steels used in the exercise had low S level (0.01%) and the sulphides were fine and few in number, the directional differences were small and it was difficult to identify the role of inclusions in the intergranular fracture process. The present exercise is an extension of this work to a high S free machining steel containing a high volume fraction of coarse elongated MnS inclusions. The plate thickness has also been chosen to enable samples from the short transverse direction to be taken. It was hoped that these changes would exaggerate the directional effects, making interpretation easier.

10.2 EXPERIMENTAL

The steel selected for this work is a free machining steel (EN 7A), with a high S content (0.154% Wt.), which has been used by Mayes and Baker (1986) in a similar exercise to investigate the anisotropy of fatigue crack growth. The composition of the steel is given in Table 10.1. The major advantage of this steel was that it contained a large volume fraction of elongated inclusions, which would exaggerate any anisotropy in hot ductility behaviour. As its composition did not contain any micro-alloying additions, the influence of fine micro-alloyed precipitation could also be ignored. The steel has been forged from a 110 mm square billet to give a 65 mm thick slab. This had resulted in a relatively large aspect ratio of the MnS inclusions in the major direction of rolling (6 to 1). Lateral spread was significantly less, the average aspect ratio being 1.2 to 1, with many of the inclusions having aspect ratios of 2 to 1 (Fig. 10.1).

Polished sections of this steel from longitudinal and transverse planes are shown in Fig. 10.2. Longitudinal, transverse and short transverse to the rolling direction tensile samples with diameter 5.04 mm and gauge length 25.4 mm were machined from the plate. The samples were tested using the Instron equipment described in chapter 4. They were heated directly to test temperatures in the range 700-1100 °C at constant rate of 15 °C/min., held for 15 mins. prior to testing and strained to failure using a strain rates of 3.3×10^{-4} and $1.3 \times 10^{-2} \text{ s}^{-1}$.

Although this thermal cycle is not directly

relevant to the continuous casting process, it was hoped that such results would provide further information to aid in understanding the effect of inclusion shape on the hot ductility of steels. Also, many hot forming processes do involve direct heating followed by deformation, e.g. the production of pipeline fittings. In addition, transverse properties are particularly important in thick walled tubes, like pressure vessels, which are subjected to high internal pressures.

After fracture the samples were cooled to room temperature at a rate of $\sim 25^\circ\text{C}/\text{min}$. Fractographic examination on fracture surfaces was carried out on a JEOL T100 Scanning Electron Microscope, operating at 25 KV.

To estimate the A_{e_3} temperature, small samples were heated in the temperature range $800\text{-}900^\circ\text{C}$ at 20°C intervals for 15 mins., quenched in ice brine and then examined under the Optical Microscope. The A_{e_3} temperature was taken as the temperature at which ferrite was first observed.

To establish the austenite grain size prior to deformation, small samples were heated in a muffle furnace to simulate the thermal cycle of the tensile test, and then cooled at a rate to produce outlining by ferrite of the austenite grains. γ grain size was measured using the linear intercept method. A 5% nital etchant was used to reveal the γ grain boundaries.

10.3 RESULTS

10.3.1 HOT DUCTILITY CURVES

The hot ductility curves for samples taken from the longitudinal, transverse and short transverse directions for low and high strain rates (3.3×10^{-4} and 1.3×10^{-2} S^{-1}) are shown in Figs. 10.3 and 10.4 respectively. The ductility can now be seen to be very sensitive to test direction, temperature and strain rate.

At the lower strain rate, Fig. 10.3, all the directions showed a marked ductility trough over the temperature range 700-1100 °C, the ductility improving markedly as test direction changed from through-thickness to transverse through to longitudinal. The samples tested at the higher strain rate (Fig. 10.4), generally showed better hot ductility than those tested at the lower strain rate. The depth of the trough varied with plate orientation and strain rate, whereas the width and position seemed to remain constant. At the highest testing temperature of 1100 °C, ductility was very high except for the through-thickness sample tested at the lower strain rate. Decreasing the temperature below 1100 °C caused the ductility to fall for both strain rates. Ductility reached a minimum at 1000 °C and started to recover on lowering the test temperature further to 900-800 °C. Recovery at the higher strain rate was however short-lived before being interrupted by a sudden large increase in strength and rapid fall in ductility.

10.3.2 HOT STRENGTH

A comparison of the peak stresses (Fig. 10.5) between the three directions at the same test temperature and strain rate give occasionally small differences, but there are no consistent trends, suggesting test direction has no effect on the strength at elevated temperatures. Peak stresses at a strain rate of $1.3 \times 10^{-2} \text{ S}^{-1}$ were approximately twice the value of the peak stresses at $3.3 \times 10^{-4} \text{ S}^{-1}$.

Plots of $\ln \sigma_p$ against $1/T$ are shown in Fig. 10.6, where T is the absolute temperature and σ_p is the average peak stress in the three testing directions for high and low strain rate. These plots show a linear relationship between $\ln \sigma_p$ and $1/T$ at constant strain rate in the γ phase, in agreement with the equation 3.6 described in Chapter 3.

$$\dot{\epsilon} = A_1 \sigma^n e^{-Q/RT}$$

The activation energy for deformation, Q , is obtained by plotting $\ln \dot{\epsilon}$ against $1/T$ at constant σ_p . Q is determined from the gradient of the resulting straight lines, and these curves are shown in Fig. 10.7.

The activation energy is 273 KJ/mol., which is in a reasonable agreement with Crowther and Mintz (1986). The stress exponent, n , is determined from the gradients of the plots of $\ln \dot{\epsilon}$ versus $\ln \sigma_p$ at constant temperature, and are shown in Fig. 10.8. The n value is 4.77. Again this value is in good agreement with previous work. (Crowther et al., 1987). The Q and n values are compared with the results of other workers in Table 10.2

10.3.3 STRESS-ELONGATION CURVES

The engineering stress-total elongation curves for the three test directions at both strain rates are shown in Figs. 10.9-and 10.10. It is clear that increasing the temperature and decreasing the strain rate decreases the stress. It was sometimes possible to detect the occurrence of dynamic recrystallisation from the form of the stress-elongation curves. The fall in the rate of strain hardening leading to the peak in stress followed by work softening and fluctuations (Jonas et al., 1968), is evident of dynamic recrystallisation. This has been observed at test temperatures ≥ 1000 °C for the higher strain rate and at temperatures ≥ 900 °C for the lower strain rate, as can be seen in Figs. 10.9-10.10.

The good hot ductility at a test temperature of 1100 °C for all directions and strain rates (except the short transverse tested at the lower strain rate) suggests that good ductility involves dynamic recrystallisation. However, as in previous work (Crowther et al., 1987), dynamic recrystallisation occurred at a lower temperature than 1100 °C, in many cases at the minimum ductility temperature showing that this in itself is not sufficient to guarantee good ductility. For good ductility, grain boundary migration rates have to be sufficiently high to prevent crack linkage. This means that higher temperatures or higher strain rates are needed to ensure good hot ductility.

10.3.4 GRAIN SIZE MEASUREMENTS

The variation in γ grain size with reheating temperature for the steel examined is shown in Fig. 10.11. The steel showed a continual increase in γ grain size with temperature from 35 μm at 900 °C to 70 μm at 1000 °C. This behaviour contrasts with the previous work on micro-alloyed steels, where grain size remained essentially constant in this temperature range, (Crowther et al., 1987). Also shown in Fig. 10.11, are the results for a previously examined low S, plain C-Mn steel. The change in austenite grain size with temperature is much more marked for this steel, suggesting that the high volume fraction of MnS inclusions in the high S steel is restricting grain growth.

10.3.5 FRACTURE EXAMINATIONS

SEM examination showed that for all the failures in which the R of A was less than 60%, the failure mode was predominantly intergranular, Fig. 10.12. For samples showing intergranular fracture, the fracture surfaces had both flat regions indicating that grain boundary sliding was an important failure mode, and also regions of ductile voiding. The importance of grain boundary sliding was also confirmed by the large number of wedge type cracks present on polished sections close to fracture, Fig. 10.13. Inclusions were sited at the γ grain boundaries, Fig. 10.14 and the intergranular nature of the fracture process is clearly shown in Fig. 10.15. The elongated MnS inclusions were found to be present at

the fracture surface for all test directions but were particularly evident in through-thickness samples, Fig. 10.16. In the case of the through-thickness samples fracture was observed to start at the surface and work inwards, Fig. 10.17.

10.4 DISCUSSION

10.4.1 EXPLANATION FOR THE SHAPE OF THE DUCTILITY TROUGH

The ductility troughs for the examined steel, are interesting in that they occur entirely in the austenite, Figs. 10.3 and 10.4. Previous work has shown that the low ductility intergranular failures can occur either by grain boundary sliding in the austenite or on transformation, when cooling from the austenite produces a thin film of the softer ferrite phase around the austenite grains allowing strain concentration and voiding to occur at inclusions, (see chapter 5).

In the case of intergranular failure in the austenite, it is noticeable in micro-alloyed steels heated directly to the test temperature, that the low temperature side to the ductility trough corresponds to the change from a ferritic to a fully austenitic structure, as can be seen in chapter 9 and by Crowther and Mintz (1986 α). The first attainment of a fully austenitic structure corresponds to the minimum ductility because precipitation is then well established at the boundaries and considerable grain boundary sliding is now possible. The R of A values then remain low with further increase in temperature until the temperature is sufficiently high to make dynamic recrystallisation effective in restoring hot ductility, (Crowther and Mintz, 1986 α).

The ductility troughs for the high S steel in the present study are however very different in that the

major part of the trough only starts to form once the A_{e_3} temperature has been exceeded. This unique behaviour is believed to be due to the significant coarsening of the austenite grains which occurs with increase in grain size in the temperature range from the A_{e_3} temperature to 1000°C , Fig. 10.11. The austenite grain size at 900°C was $35\ \mu\text{m}$ and this increases to $70\ \mu\text{m}$ at 1000°C , the minimum ductility temperature. Previous work has shown that coarsening the austenite grain size would be expected to reduce hot ductility (Crowther and Mintz, 1986b). Micro-alloyed steels do not show this marked further fall on hot ductility on raising the temperature above the A_{e_3} as grain size changes are generally small due to the action of the grain refining precipitates. As with the micro-alloyed steels, ductility only improves at higher temperatures when dynamic recrystallisation is well established.

10.4.2 INFLUENCE OF ELONGATED INCLUSIONS ON HOT DUCTILITY

As has been amply demonstrated in the high S steel, the influence of test direction on the hot ductility of flat rolled or forged plate steel with elongated inclusion is very similar to its influence on ductility at room temperature. Longitudinal test samples have better ductility than transversely tested samples, which are in turn superior to samples tested in the short-transverse direction, Figs. 10.3-10.4. Micro-alloyed steels in accord with their finer and much lower volume fraction of elongated MnS inclusions, only showed small

differences in ductility between the longitudinal and transverse direction, as has been shown by Crowther and Mintz (1986^d). However, although the anisotropy of hot ductility behaviour is identical to that shown at room temperature, the mode of failure is different being intergranular, rather than matrix ductile failure due to micro-void coalescence at inclusions. Previous work (Crowther et al., 1987), on intergranular failure of steels at temperatures in the range 700-1000 °C indicates that intergranular failure is favoured by:

1. grain boundary sliding
2. void formation at the boundaries
3. prevention or retardation of dynamic recrystallisation
4. pinning of austenite boundaries to the extent that they are slowed down sufficiently for cracks formed by (1) and (2) to link up.

The present work has clearly shown that the MnS inclusions are mainly situated at the austenite grain boundaries and are therefore in a position to influence intergranular failure. Grain boundary sliding as evidenced by the 'w' wedge type cracks has also been shown to be a major mode of intergranular failure and cavitation round the inclusions is clearly evident.

Work on micro-alloyed steels (Crowther et al., 1987), has generally suggested that when second phase particles influence hot ductility and encourage intergranular failure they are fine. In the case of NbCN and AlN particles,

sizes less than 50 nm are required to prevent or slow down dynamic recrystallisation sufficiently to enable cracks formed by grain boundary sliding to link up to give intergranular failure, (Crowther et al., 1987). Coarser particles give rise to good hot ductility. However, MnS inclusions even in steels with low S levels ($> 0.02\%$ S) are generally much bigger, often an order of magnitude bigger than the AlN or NbCN particles and therefore might not be expected to influence the hot ductility. However, there is other evidence in the literature to indicate that the "coarser" sulphides do influence intergranular failure. Crowther and Mintz (1986c) and Coleman and Wilcox (1985) have both shown that the fractured faces of C-Mn-Nb-Al and C-Mn steels that have failed intergranularly often show ductile dimples which contain MnS inclusions. Hannerz (1985), has also shown that raising the S level in continuously cast steels increases the tendency for transverse cracking, a problem which is associated with intergranular failure.

MnS inclusions may therefore be influencing hot ductility in a different way to micro-alloyed precipitates and this has led to the suggestion (Coleman and Wilcox, 1985) that in the case of the micro-alloyed steels, MnS inclusions could have an important influence in developing cavitation at the boundaries once the fine grain refining precipitates have restricted grain boundary movement sufficiently to enable cavitation to occur. However in the present instance there are no fine micro-alloying precip-

itates to pin the boundaries. Nevertheless in the high S steel examined, the large volume fraction of MnS inclusions is restricting grain boundary movement as can be seen in Fig.10.11. Furthermore, examination of the stress-elongation curves in relation to the hot ductility curves suggests that dynamic recrystallisation is not fully effective in restoring hot ductility until temperatures in excess of 1000 °C, Figs. 10.3-10.4 . Thus in the trough although the boundaries are not actually pinned they are probably very much restricted in movement, particularly at the lower strain rate.

Inclusions at the boundaries may first weaken the boundary by marked voiding particularly if they are situated at triple points and these cracks may then extend by grain boundary sliding. Baker (1974), has suggested that inclusions in steel are only weakly bonded to the matrix and the mechanism of normal ductile fracture at room temperature is almost invariably micro-void formation due to decohesion of the inclusion-matrix interface followed by void coalescence. Similar behaviour probably occurs at elevated temperatures but because the sulphides are at the boundaries the easy decohesion of the inclusion-boundary interface will probably encourage grain boundary sliding.

The shape of the inclusions then becomes important in relation to the direction of testing as it influences the strain concentration at the boundary. This strain concentration is greatest in the through-thickness direction and

least in the longitudinal. Void formation at the boundaries and grain boundary sliding would consequently be greatest in the short transverse and least in longitudinal direction. Also once cracks have been formed it will be very much easier to propagate them along the weak inclusion-boundary interface when the major plane of the inclusion is perpendicular to the tensile stress, i.e. in the through-thickness direction. This probably accounts for the ease of crack propagation from the surface inwards in the case of through-thickness samples.

10.4.3 INFLUENCE OF DYNAMIC RECRYSTALLISATION ON HOT DUCTILITY

As in previous work (Crowther et al., 1987), the present results show that although dynamic recrystallisation is essential for good ductility it is not sufficient in itself to produce good ductility. The minimum in ductility troughs occurred at a temperature when dynamic recrystallisation was taking place ($\geq 1000^{\circ}\text{C}$), Figs. 10.3-10.4. Crowther et al., (1987), have shown that grain boundaries have to be moving sufficiently fast to prevent crack linkage from occurring and that depending on strain rate, temperatures in excess of that needed to produce dynamic recrystallisation are required to isolate grain boundary cracks and give good ductility.

It is interesting to note that at the lower strain rate

the temperature for dynamic recrystallisation increases as the direction changes from the length or transverse to the short transverse direction (900 °C compared to 1000 °C). This probably arises because the R of A values are so low in the short transverse direction at the 'lower' temperatures that the critical strain for dynamic recrystallisation is never achieved before fracture.

At the higher strain rate the temperature for dynamic recrystallisation increased to 1000 °C for all directions of testing. The critical strain for dynamic recrystallisation was however noticeably higher at this strain rate (5% higher) and this may again account for the higher temperature required for dynamic recrystallisation. Ouchi and Matsumoto (1982), have also noted that the critical strain for nucleation of dynamic recrystallisation increases with increase in strain rate.

10.4.4 INFLUENCE OF STRAIN RATE ON THE HOT DUCTILITY

Previous work by Suzuki et al., (1984b) and Yasumoto et al., (1985) on the effect of sulphides on hot ductility after high temperature solution treatment have shown that increasing the strain rate decreases not increases hot ductility in the temperature range 900 to 1200 °C. In their examinations the steels chosen and heat-treatments applied have resulted in very fine FeMnS and/or FeMnO inclusions which precipitate out at the boundaries and on occasions within the matrix. In the case of Yasumoto et

al's work (1985), finely dispersed sulphides were found within the grains (30 nm in size) and coarser sulphides (100 nm) at the austenite grain boundaries as well as precipitate free zones. All of these would be expected to cause strain localisation at the γ boundaries encouraging intergranular failure. This explanation is identical to that given for the influence of NbCN precipitates in reducing the hot ductility of micro-alloyed steels when cooled to test temperatures in the range 700 to 1100 °C after solution treatment (Mintz and Arrowsmith, 1979). However in the latter case as in the present instance ductility is improved on increasing the strain rate. To explain this difference in strain rate behaviour, Yasumoto et al., (1985) have suggested that the sulphides are able to coarsen during the long test times at slow strain rates so reducing their embrittling effect. Clearly such behaviour is unlikely to occur with the very coarse pure MnS found in the present investigation. In this case, the improvement in hot ductility with increase in strain rate is in accord with the intergranular failure process being dominated by creep processes. Creep studies (Davies and Evans, 1965) have shown that grain boundary sliding is responsible for nucleation of both cavities and wedge cracks. Raising the strain rate will decrease the E_g/E_t ratio where E_g is the strain due to grain boundary sliding and E_t is the total strain. Furthermore grain boundary migration rates are increased by raising the strain rate making crack linkage more difficult.

Finally, it should be noted from previous work (Crowther and Mintz, 1986d) that for hot rolled structural steels with normal S levels ($\sim 0.01\%$), anisotropy of hot ductility was only observed at low strain rates $3 \times 10^{-4} \text{ S}^{-1}$. At a strain rate of $3 \times 10^{-3} \text{ S}^{-1}$ no difference could be discerned between length and transverse direction. Furthermore modification by calcium treatment removed anisotropy of hot ductility at $3 \times 10^{-4} \text{ S}^{-1}$ and virtually removed the ductility trough.

10.5 CONCLUSIONS

- 1- At strain rates of 3×10^{-4} and $1.3 \times 10^{-2} \text{ S}^{-1}$, the hot ductility of hot worked steels in the temperature range 700 to 1100 °C has been found to be dependent on test direction. Samples tested in the longitudinal direction have the highest R of A values and samples tested in the short transverse the lowest.
- 2- At strain rate of $3 \times 10^{-4} \text{ S}^{-1}$ this anisotropy was very marked in the presence of a high volume fraction of large elongated MnS inclusions (present work), but only just observable in hot rolled steels with normal S levels (0.01%), as has been shown by Crowther and Mintz (1986d).
- 3- Fracture was transgranular dimpled rupture when ductility was good but intergranular when poor. Intergranular failure occurred when the steel was austenitic.
- 4- The deepening of the trough in the steel examined arises probably through the coarsening of the γ grain size with increasing temperature, whilst in the case of micro-alloyed steels, precipitation pinning the γ grain boundaries and an increasing volume fraction at the γ grain boundaries encouraging grain boundary sliding are responsible.
- 5- The elongated MnS inclusions were found to be situated at the γ boundaries, and probably influenced intergranular failure by restraining grain boundary movement allowing

voiding and decohesion at the inclusion/boundary interface, thus encouraging grain boundary sliding.

6- Raising the strain rate to $1.3 \times 10^{-2} \text{ s}^{-1}$ in the temperature range 800-1000 °C improved hot ductility in the longitudinal direction. This is probably due to a reduction in the amount of grain boundary sliding and an increase in the grain boundary migration rate making it difficult for cracks to link up.

C	Mn	Si	S	P	N
0.18	1.25	0.19	0.154	.033	0.007

Table 10.1 Composition of the steel examined (Wt.%).

Reference	Q (KJ/mol.)	n
Present work	273	4.77
Crowther et al., (1987)	290	4.9
Crowther and Mintz (1986)	290	5.2
Sankar et al., (1979)	308	5.2
Sellars and Tegart(1966)	300	4.6

Table 10.2 Comparison of activation energy, Q, and stress exponent, n, of present work with previous studies for C-Mn steels.

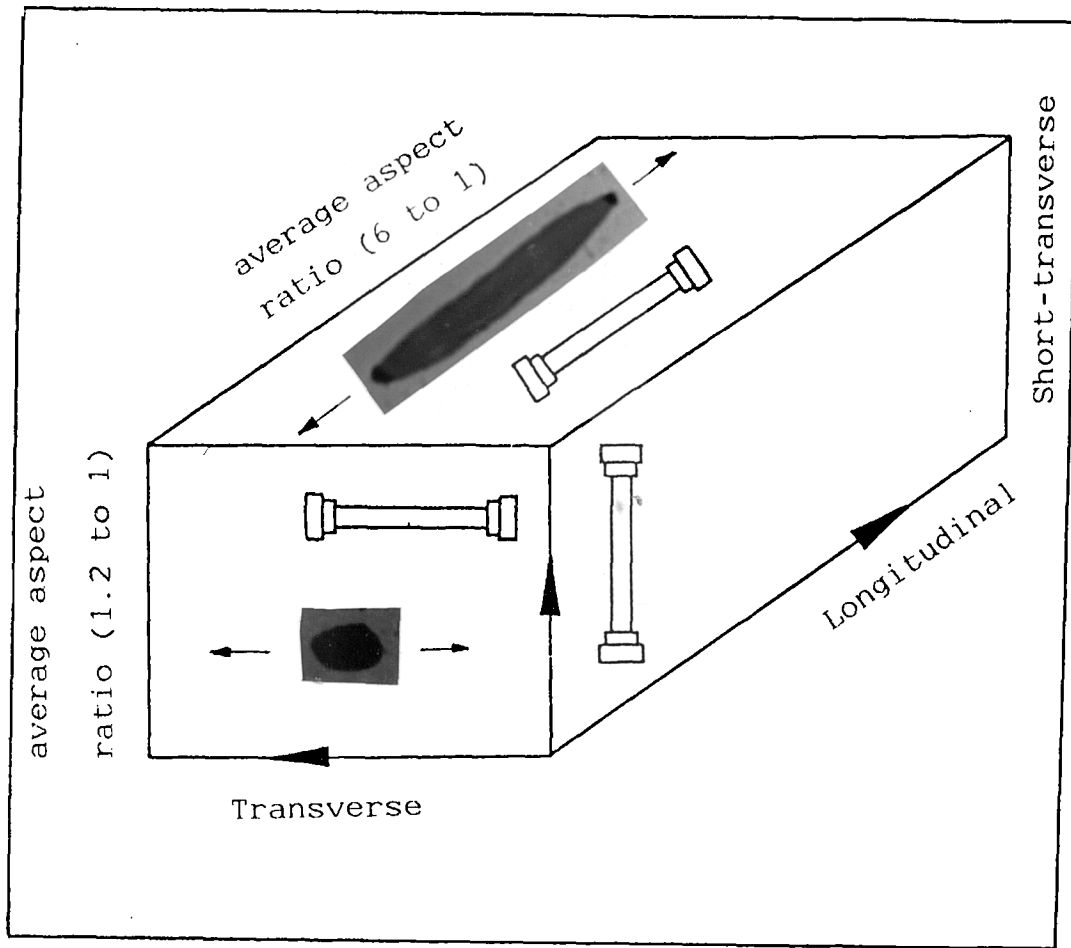
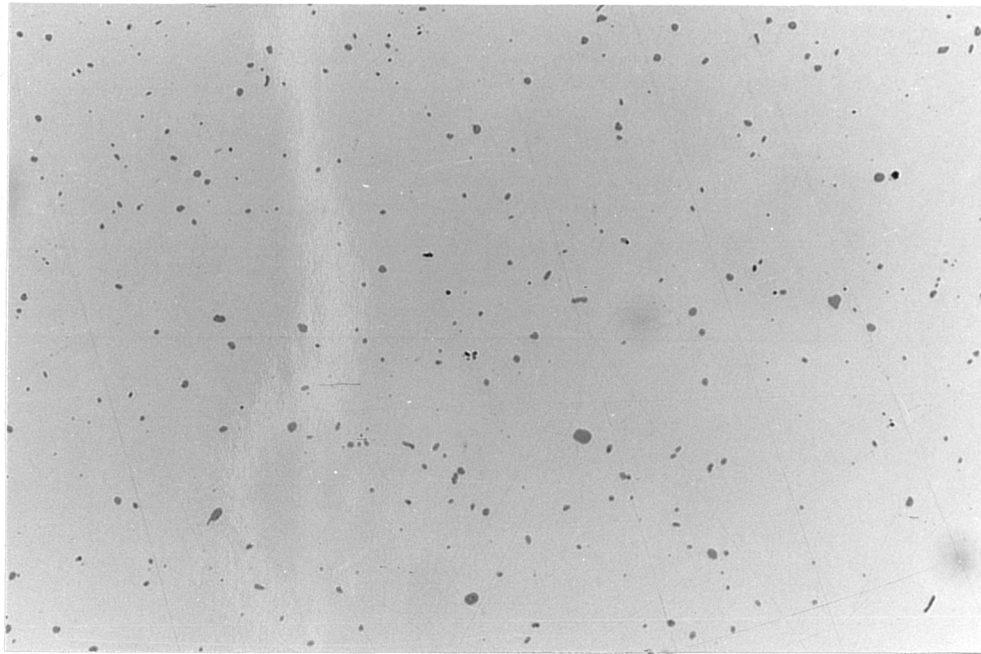
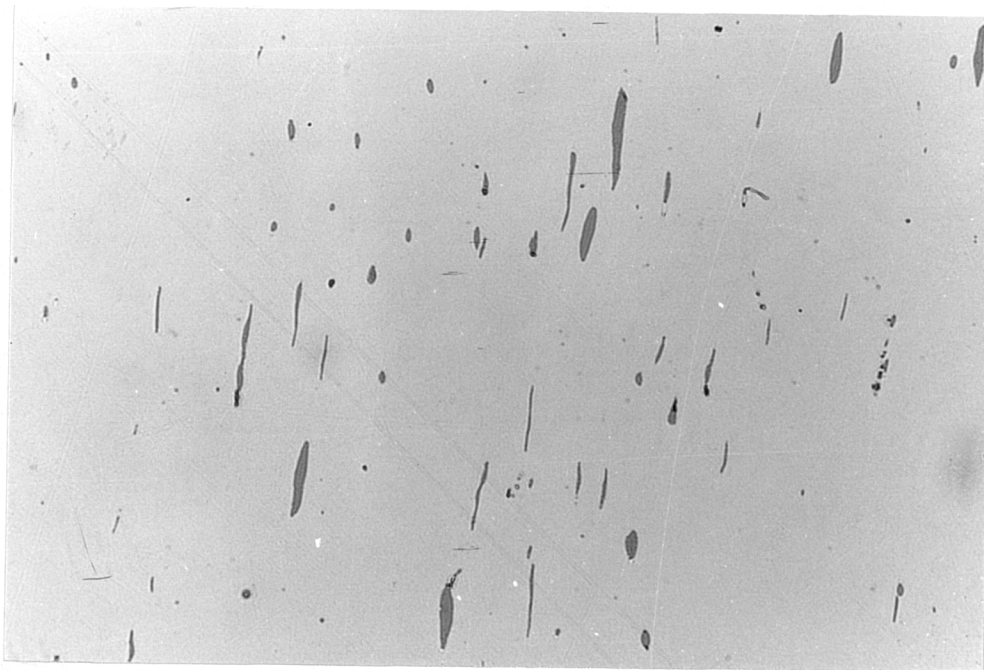


Fig. 10.1 Testing orientation, showing the average aspect ratio of MnS inclusions.



(a)



(b)

Fig. 10.2 Coarse MnS inclusions present in the high S steel.

- (a) transverse plane
- (b) longitudinal plane

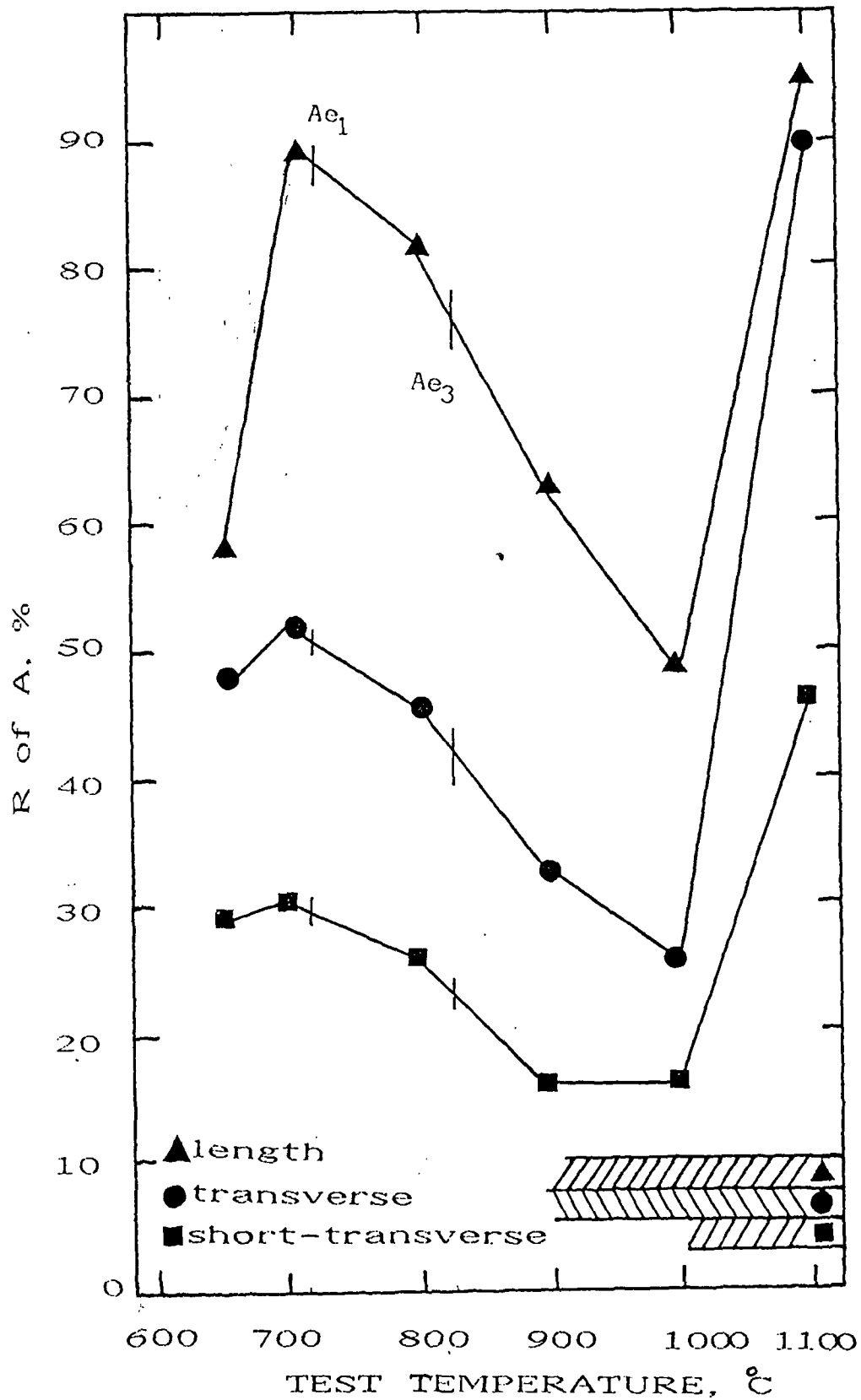


Fig. 10.3 Hot ductility curves for the high S steel examined at strain rate of $3.3 \times 10^{-4} \text{ s}^{-1}$. (Temperature range for dynamic recrystallisation indicated by shaded region).

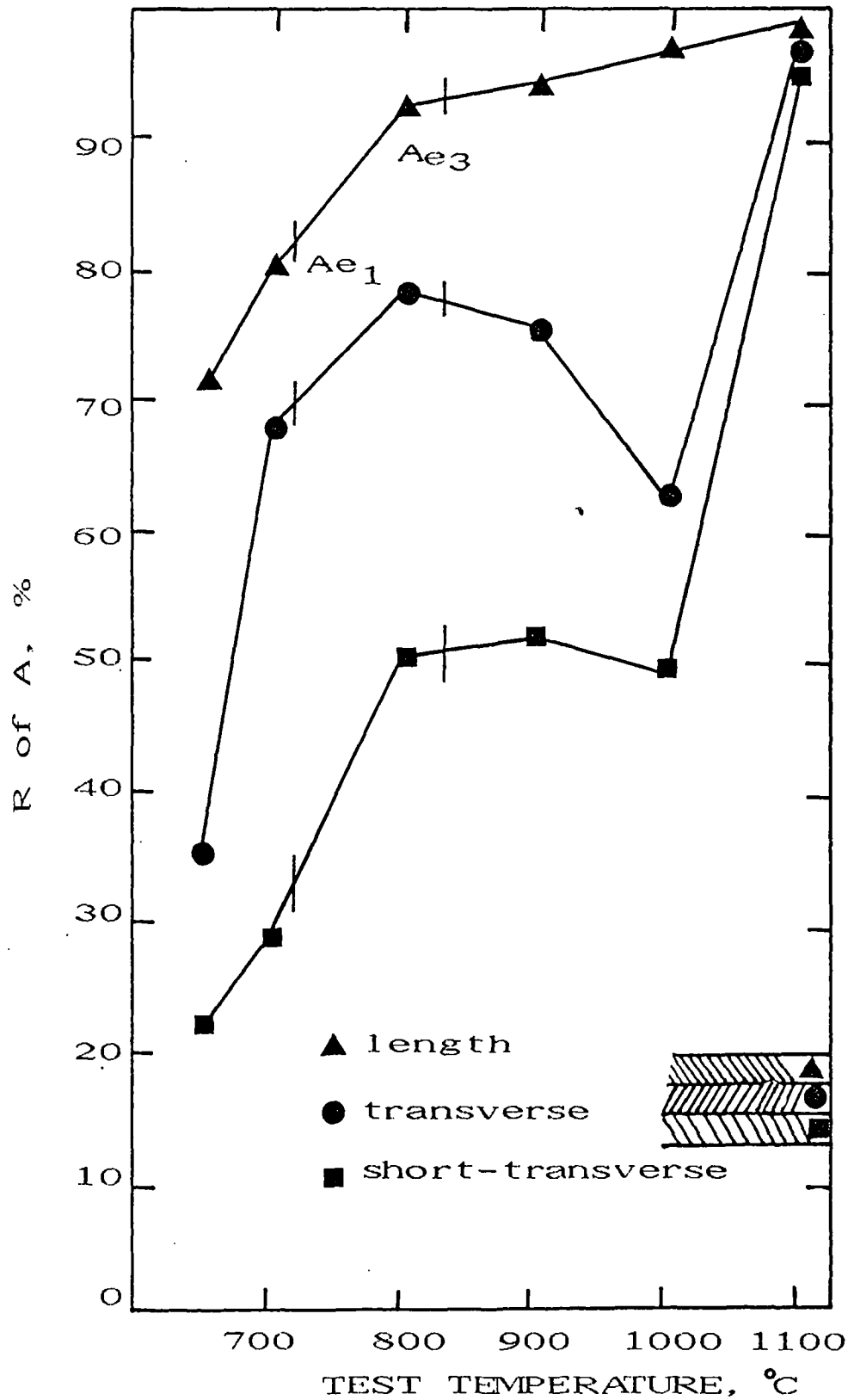


Fig. 10.4 Hot ductility curves for the high S steel examined at strain rate of $1.3 \times 10^{-2} \text{ S}^{-1}$. (Temperature range for dynamic recrystallisation indicated by shaded regions).

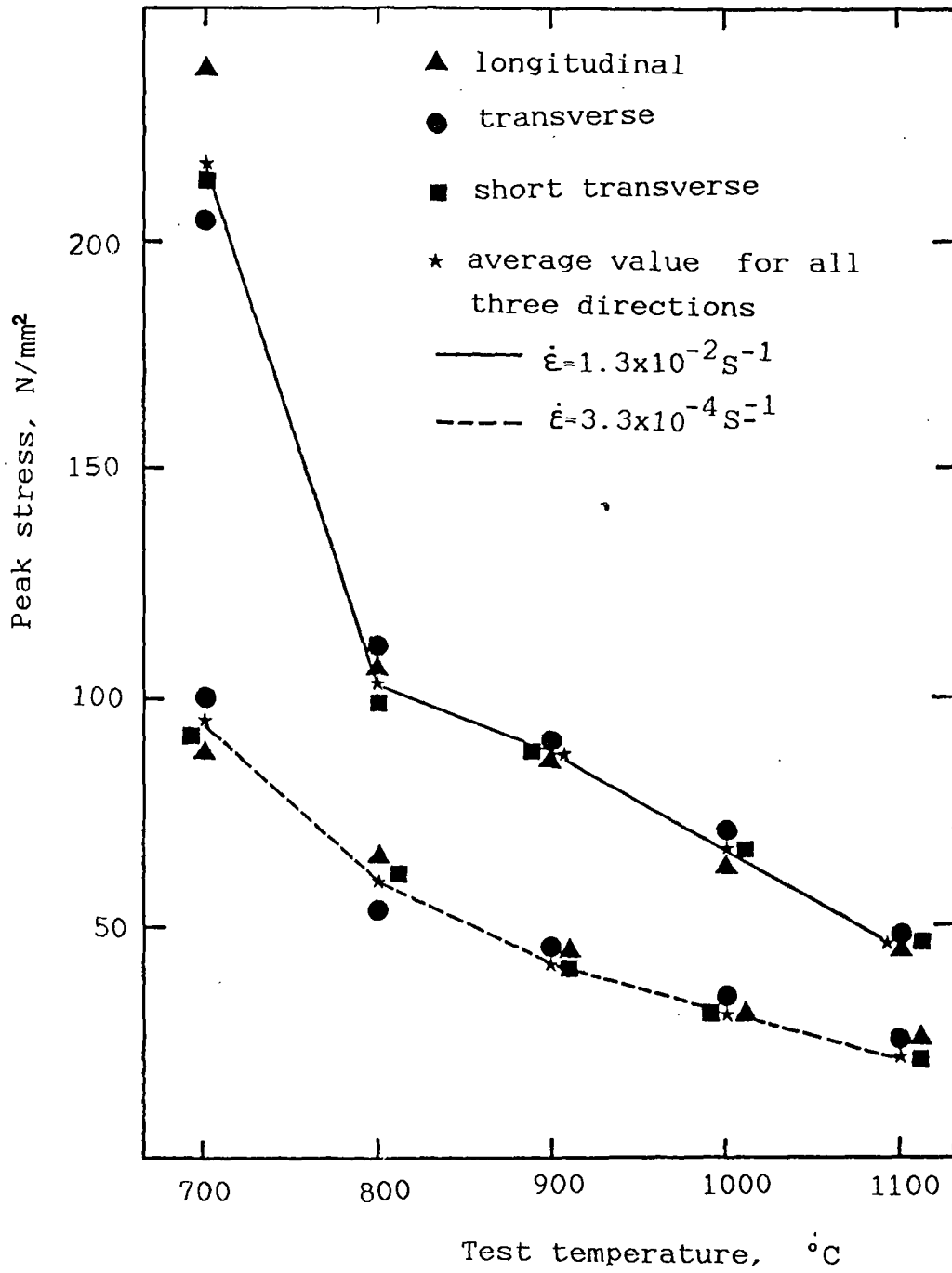


Fig. 10.5 Variation of peak stress with test temperature for the three test directions at low and high strain rate.

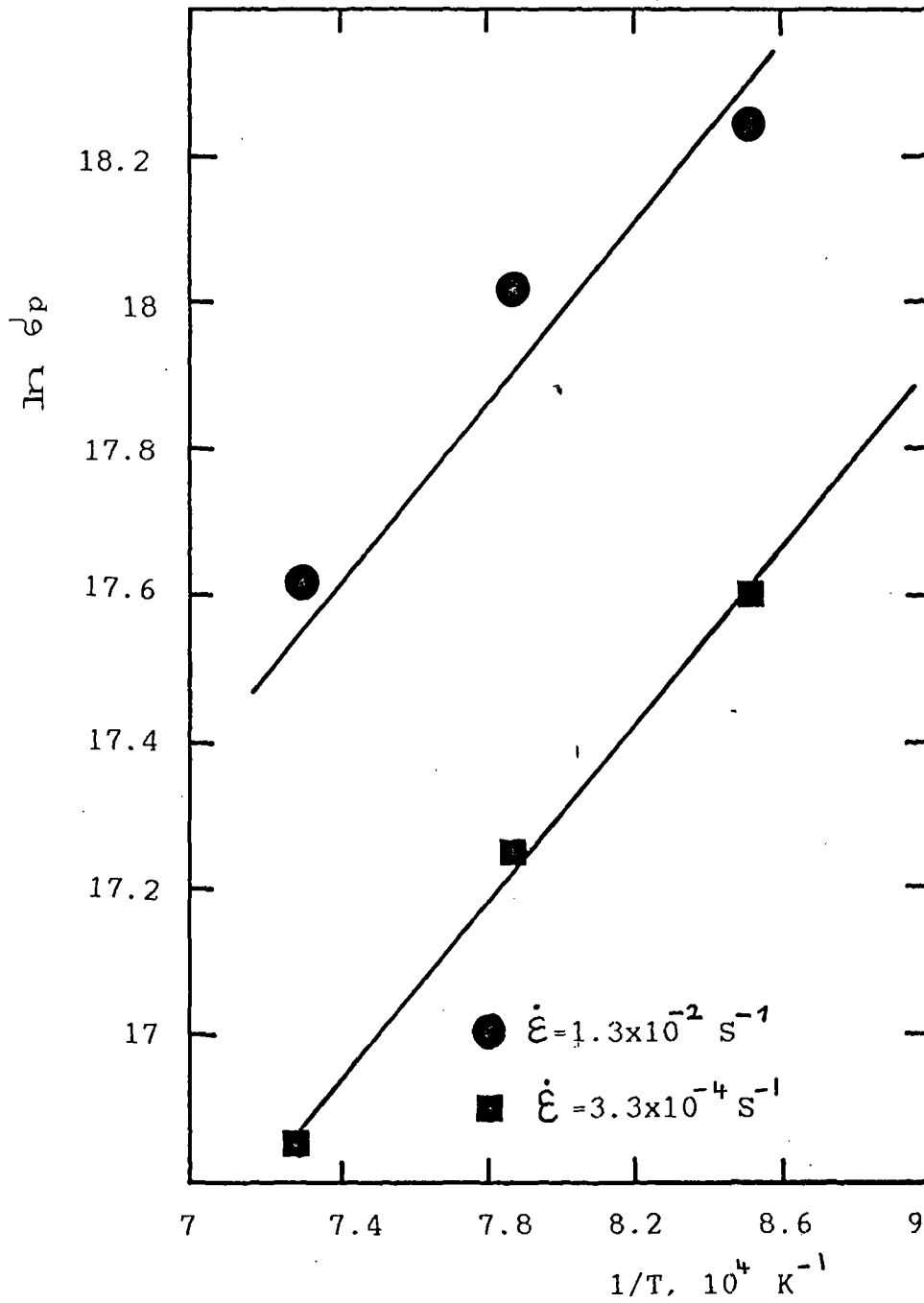


Fig. 10.6 Plots of $\ln \dot{\epsilon}_p$ versus $1/T$

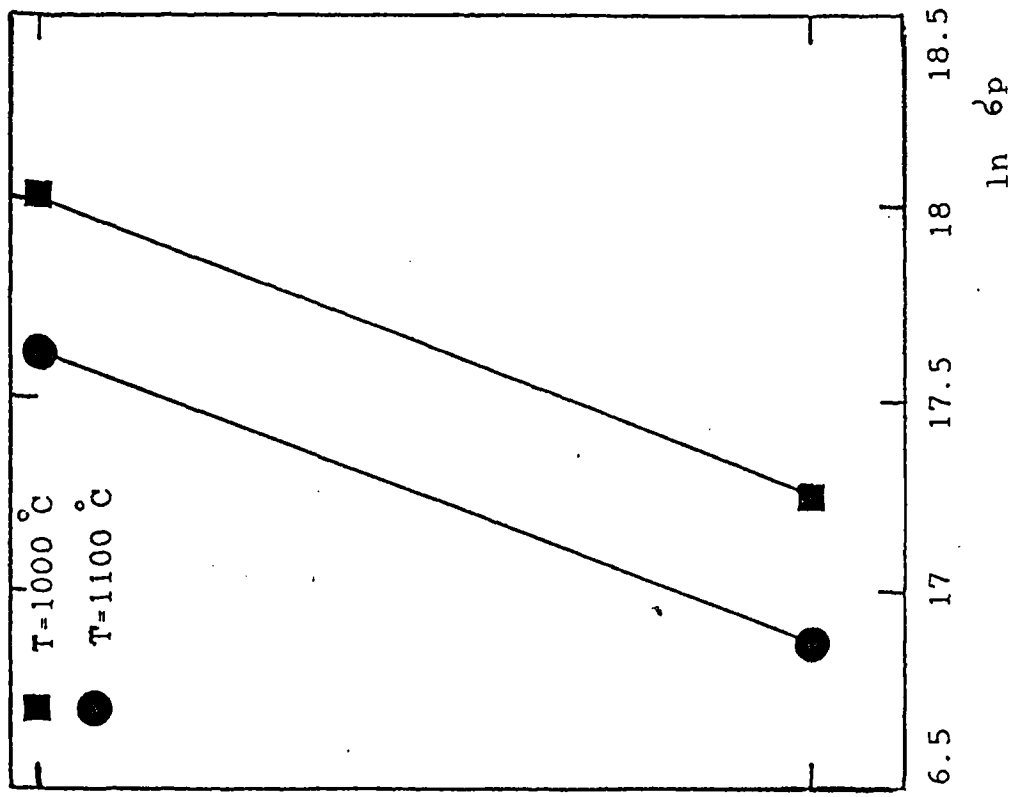


Fig. 10.7 Plot of $\ln \dot{\epsilon}$ against $1/T$ at constant σ_p .

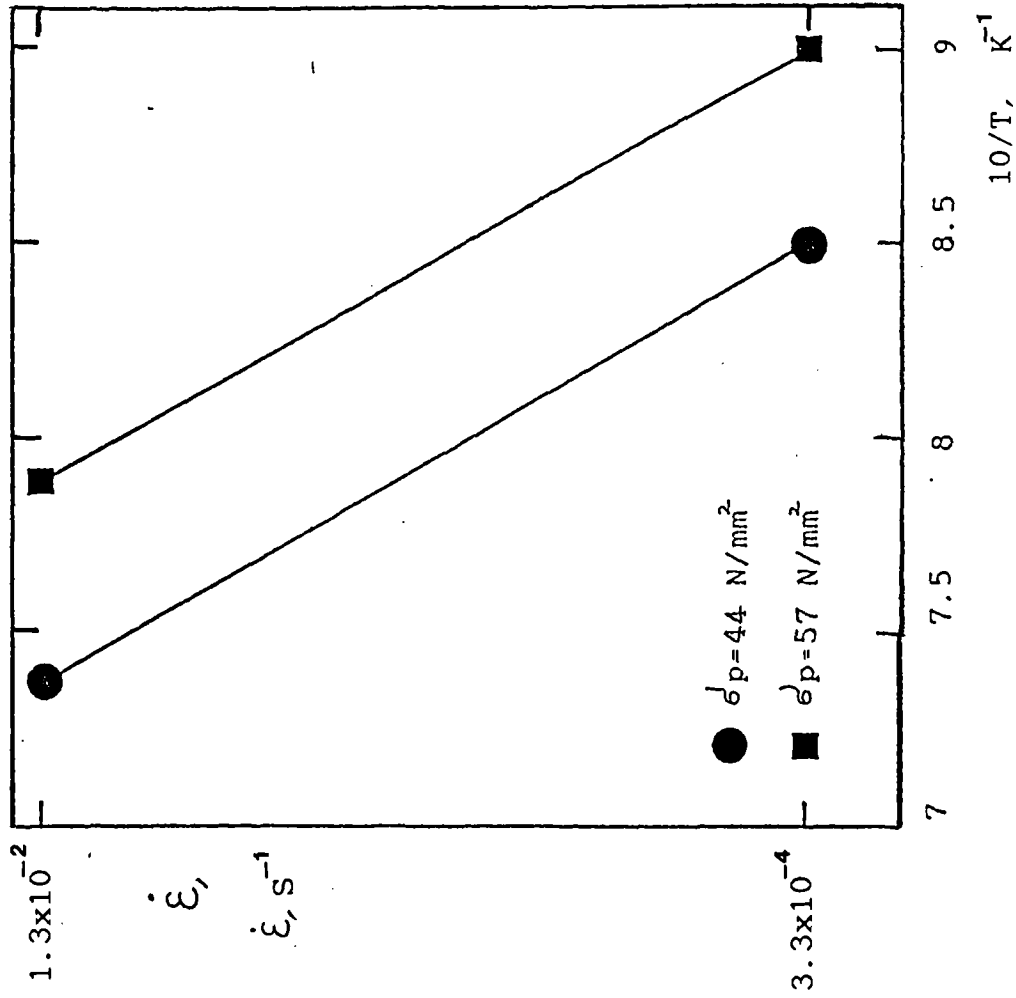


Fig 10.8 Plot of $\ln \dot{\epsilon}$ against $\ln \sigma$ at constant temperature.

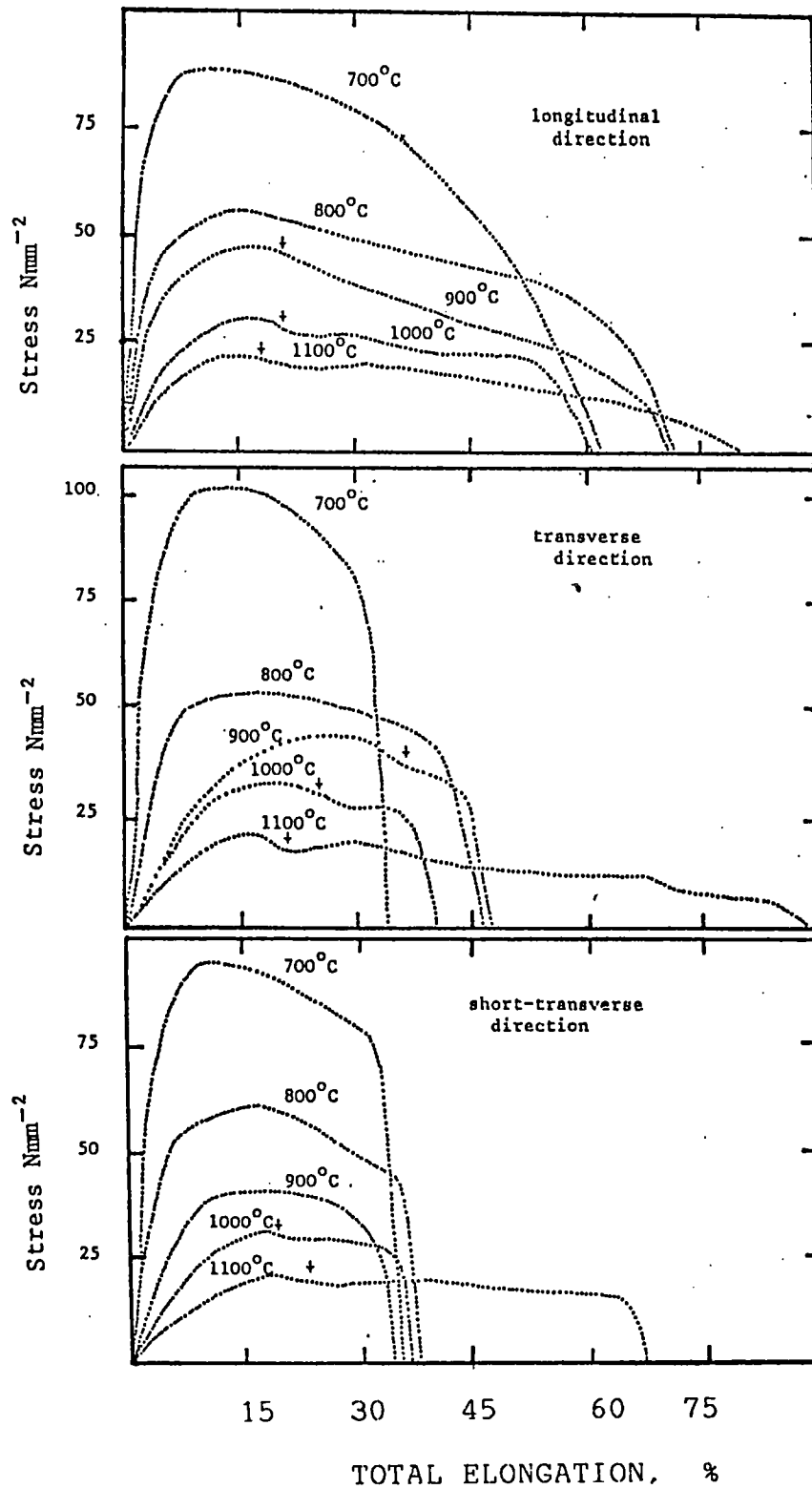


Fig. 10.9 Stress-total elongation curves for the three test directions at strain rate of $3.3 \times 10^{-4} \text{ S}^{-1}$. (Arrows indicate dynamic recrystallisation).

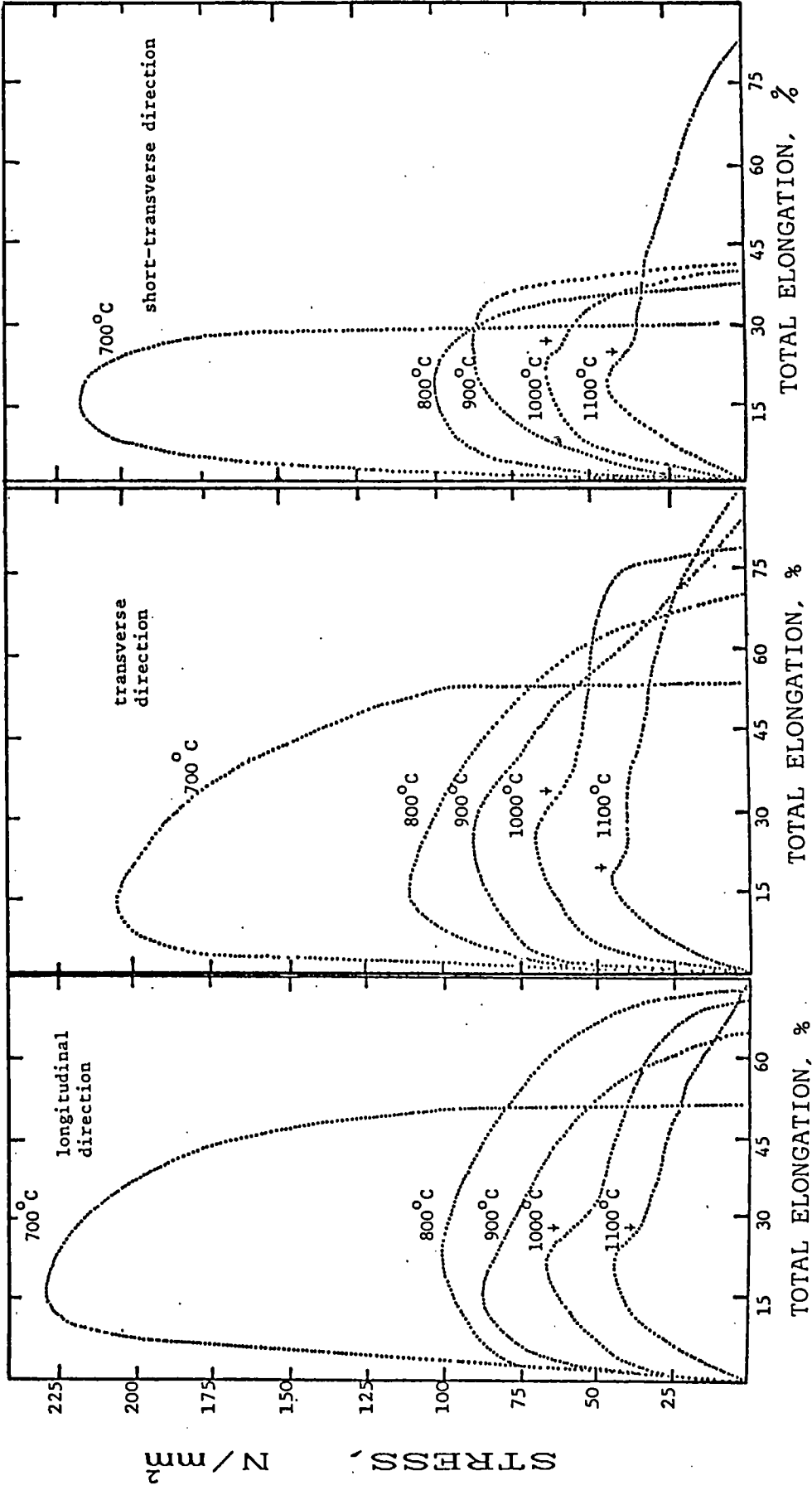


Fig. 10.10 Stress - total elongation curves for the three test directions at strain rate of $1.3 \times 10^{-2} \text{ S}^{-1}$. (Arrows indicate dynamic recrystallisation).

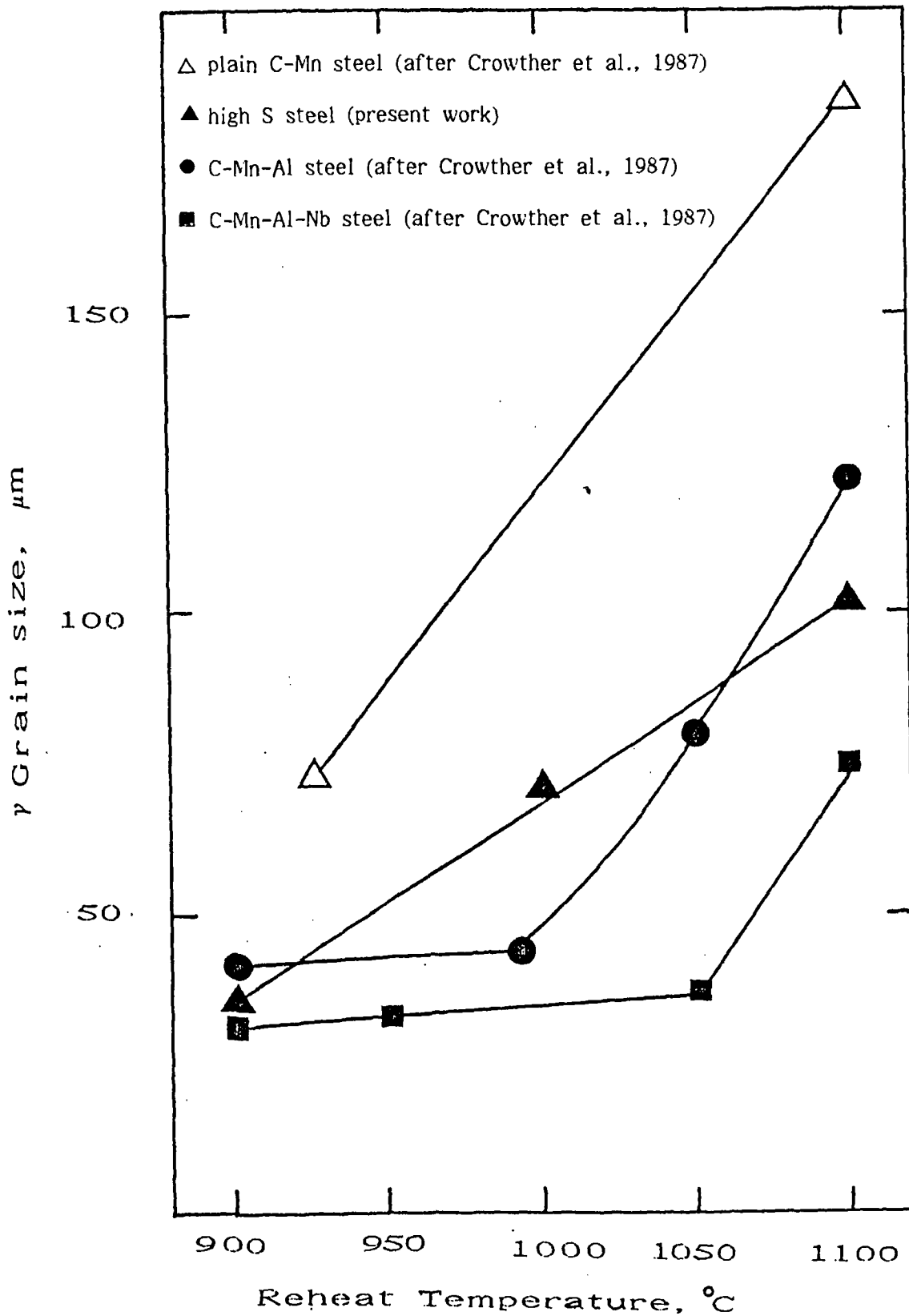


Fig. 10.11 Variation in austenite grain size with reheating temperature for different steels

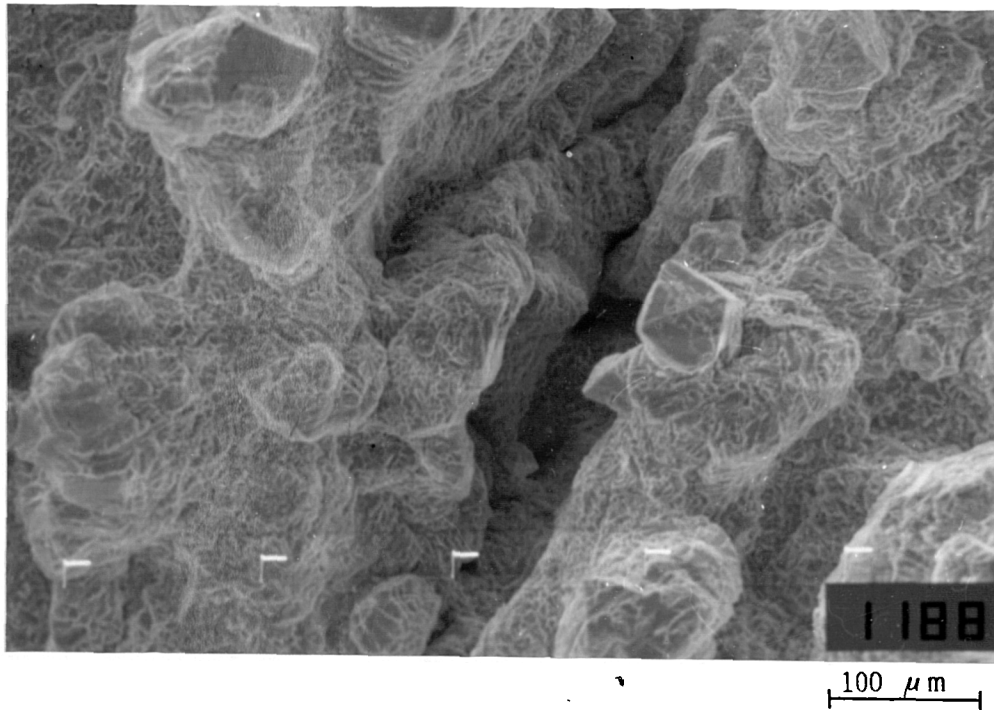
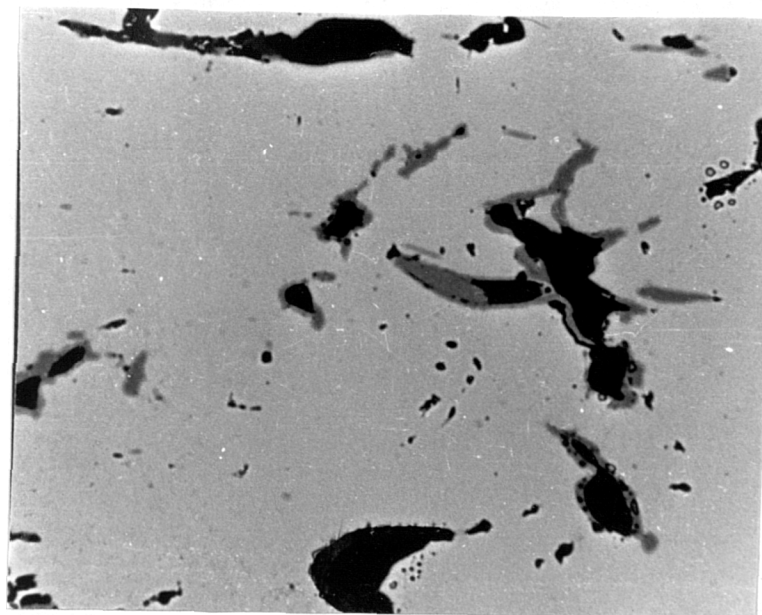


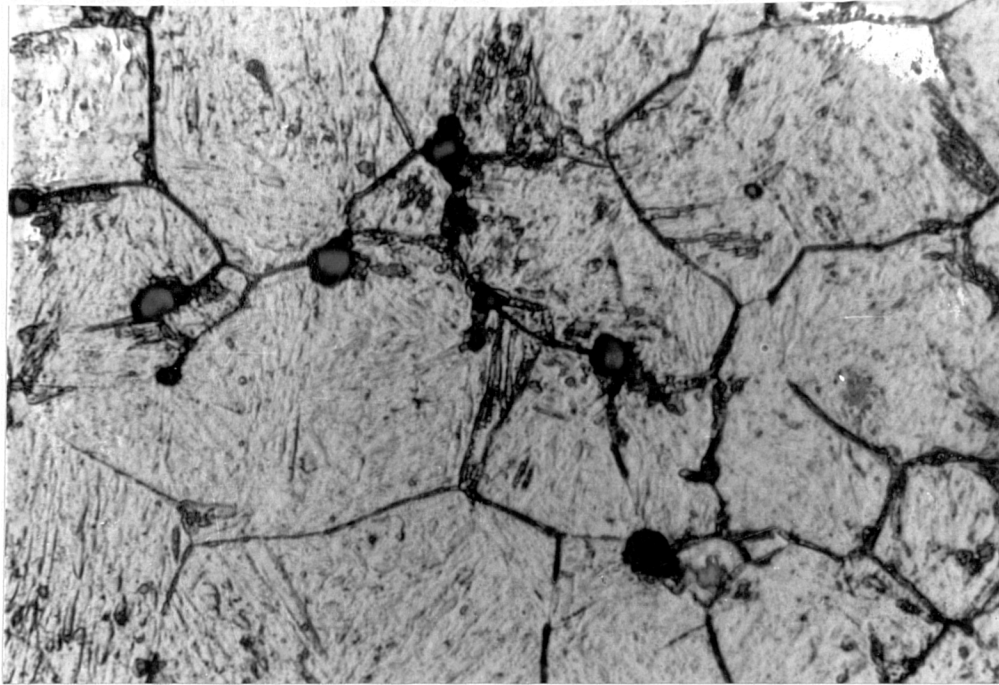
Fig. 10.12 Typical intergranular failure observed in the high S steel in the short transverse direction at strain rate of $3.3 \times 10^{-4} \text{ S}^{-1}$ at 1100°C .



← tensile direction →

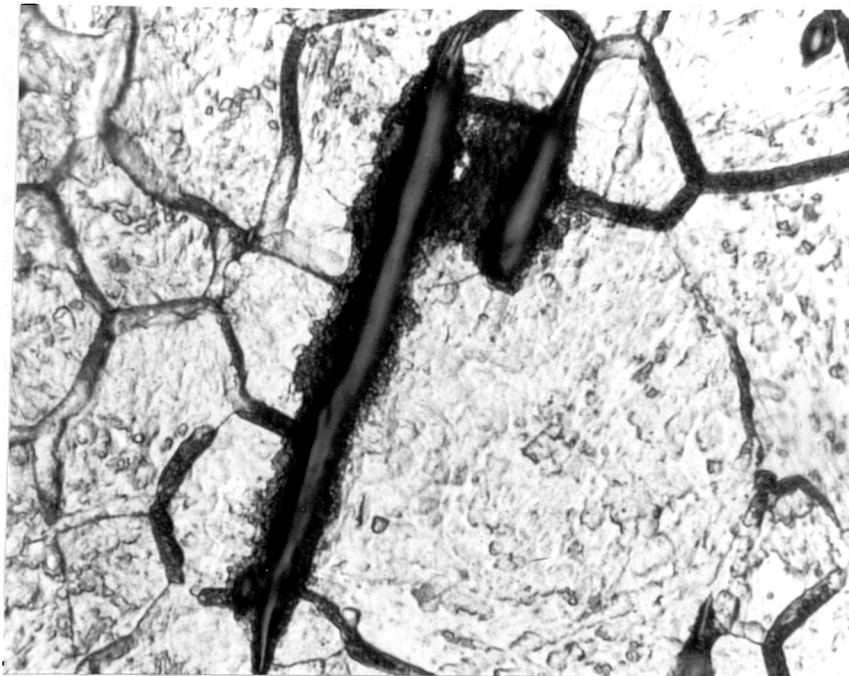
40 μm

Fig. 10.13 Typical wedge type cracks found in polished section close to fracture. Sample tested at 1000°C at a strain rate of $3 \times 10^{-4} \text{ S}^{-1}$ in longitudinal direction.



(a)

40 μm



(b)

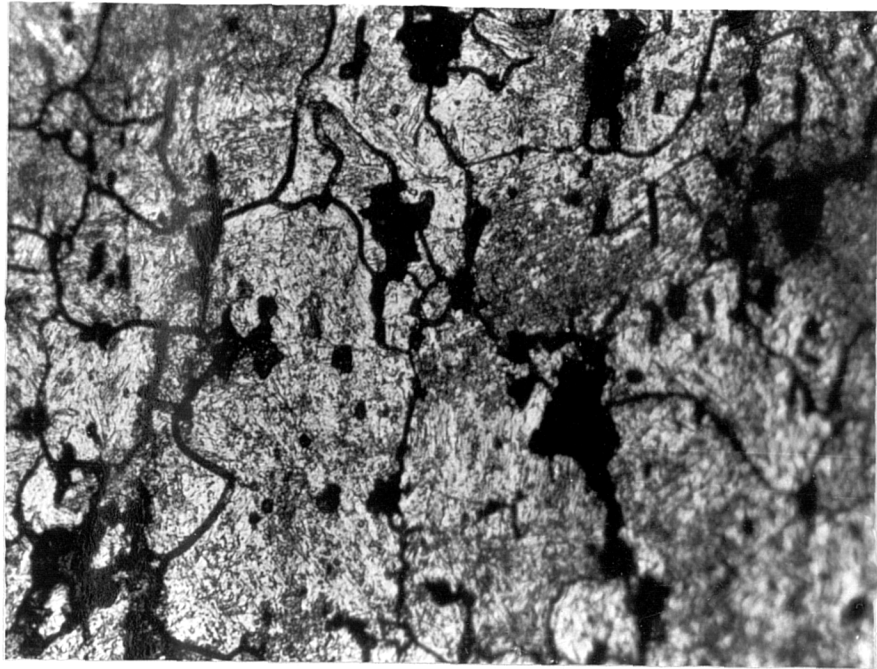
40 μm

Fig. 10.14 MnS inclusions cited at the γ grain boundaries

(a) transverse plane

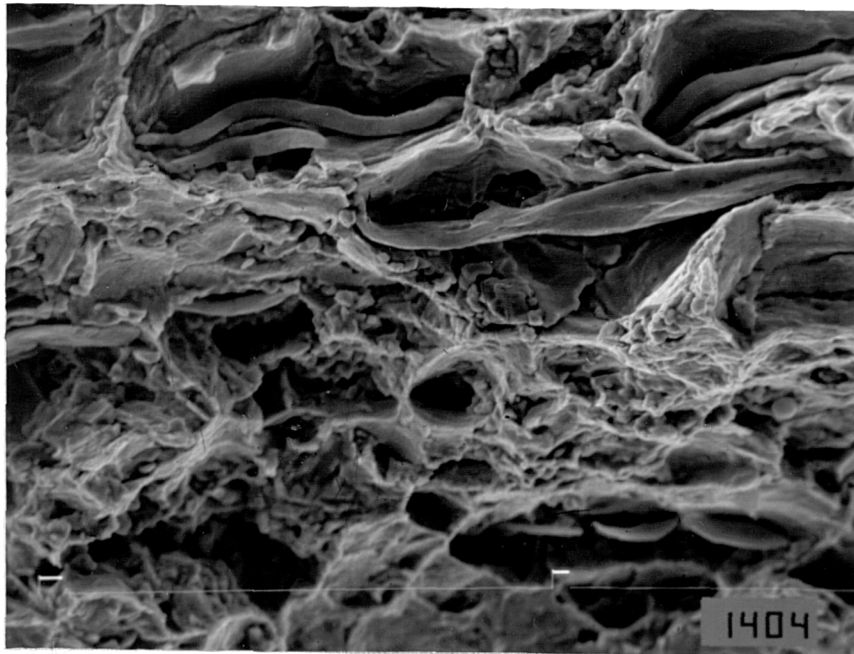
(b) longitudinal plane

Samples heated to 1100°C for 15 mins. and quenched into ice brine



115 μm

Fig. 10.15 Cracks formed along γ grain boundaries in a sample tested at 1000°C and strain rate of $3.3 \times 10^{-4} \text{s}^{-1}$ in transverse direction. (Sample quenched immediately after failure into ice brine).



1404
27 μm

Fig 10.16 MnS inclusions present on the fracture surface of a short transverse sample tested at 900°C at a strain rate of $3.3 \times 10^{-4} \text{s}^{-1}$.



3.3 mm

Fig. 10.17 Sample tested at 1000 °C in the short transverse direction at strain rate of $3.3 \times 10^{-4} \text{ S}^{-1}$, showing cracks at the outer surface.

CHAPTER 11

SUMMARY AND RECOMMENDATIONS

11.1 INTRODUCTION

The hot ductility behaviour of micro-alloyed and plain C-Mn steels has been examined at elevated temperatures (700-1000 °C) and intermediate strain rates (10^{-4} — 10^{-3} S⁻¹). The tests have in general been chosen to simulate the conditions experienced during the straightening operation in the continuous casting process in which transverse cracks propagate, so as to provide a more fundamental background into understanding the problem. It is intended in this chapter to summarize the results obtained in these studies and to give a coherent picture of the hot ductility behaviour of the steels examined.

From the conclusions reached in the present study and previous studies, recommendations will be suggested to aid in the reduction of transverse cracking, and suggestions will be made for future work.

11.2 SUMMARY

For steels solution treated at 1330 °C, cooled to test temperatures in the range 700-1000 °C, and tested at a strain rate of $\sim 3 \times 10^{-3} \text{ s}^{-1}$, the following conclusions can be made:

1. Raising the carbon level from 0.06% to 0.15% in a C-Mn-Al steel was found to move the ductility trough to lower temperatures and the movements were similar to those expected from the changes in the A_{e_3} and A_{r_3} temperatures. It is therefore concluded that the fall in ductility is due to strain concentration in the thin films of deformation induced ferrite, producing voiding round inclusions which gradually link up to give intergranular failure.

Introducing Nb into the steel widened the trough. Raising the C level in the C-Mn-Al-Nb steel from 0.014% to 0.16% did not influence the position of the trough but the depth increased with C level. Quite a marked deterioration in hot ductility occurred on raising the C level from 0.014% to 0.1% but a further increase to 0.16% produced only a small change. The widening of the trough was due to NbCN precipitation and quite good agreement was obtained between the degree of NbCN precipitated, as calculated from the solubility data and the Reduction of Area values. At the lower temperature side of the ductility trough both precipitation and deformation induced ferrite were present.

2. For C-Mn-Al and C-Mn-Al-Nb steels with solubility product $[Al] \cdot [N]$ less than 2.7×10^{-4} , aluminium does not influence hot ductility, because no AlN precipitation forms under the conditions of cooling and strain rate used in the test. This behaviour can therefore be regarded as the same as that for plain C-Mn steels. However, for a C-Mn-Al with a solubility product $[Al] \cdot [N]$ of 2.7×10^{-4} , static precipitation of AlN took place at the austenite grain boundaries after long holding times (4 hours) at test temperature, leading to intergranular failure with reduced hot ductility.

3. It has been found that NbCN particles, can precipitate statically (before the test) and dynamically (during the test), and both types are effective in delaying the onset of dynamic recrystallisation long enough for intergranular failure to occur. However, the dynamically precipitated NbCN were finer than the equivalent statically precipitated particles, and it can be concluded that dynamic precipitation is most effective in reducing hot ductility.

4. Vanadium was found to deteriorate hot ductility but not to such an extent as Nb, and the statically precipitated VCN were more effective in reducing hot ductility than dynamically precipitated particles.

5. In contrast to Nb and V, titanium was found to be beneficial to hot ductility due to the grain refinement produced by the stable TiN compound. However, solution

treatment at 1330 °C is not in this case high enough to redissolve the TiN particles so caution must be exercised in assuming similar behaviour might apply under conditions of continuous casting.

6. MnS inclusions have been found to deteriorate hot ductility possibly in two different ways. If the test temperatures are above the A_{e3} , inclusions can act in a similar way to a fine precipitation (delaying the onset of dynamic recrystallisation) and also acting as weak interfaces encouraging grain boundary sliding.

For test temperatures below the A_{e3} , (ferrite starts to form), again inclusions reduce hot ductility as they are the most suitable sites for micro-voids to occur.

7. Calcium treatment of steels improves their hot ductility because it reduces the amount of S able to redissolve and precipitate in a fine form at the new austenite grain boundaries produced on solution treating. The fewer sulphides present at the boundaries will allow an earlier onset of dynamic recrystallisation and will offer less sites for micro-voiding.

In the case of the hot ductility behaviour of "as cast" steels, ductility was generally poor due to the very coarse grain size. Although, the R of A value for the minimum ductility did not vary significantly for steels with different micro-alloying additions, the extent of the ductility trough depended on the degree of precipitation increasing in the order C-Mn-Al, C-Mn-Al-Nb-Ti and C-Mn-Al-Nb.

For steels heated directly to test temperatures in the range 700-1100 °C, again inclusions deteriorated the hot ductility by delaying the onset of dynamic recrystallisation and encouraging grain boundary sliding. Not only the volume fraction of precipitated inclusions at the austenite grain boundary was important in controlling hot ductility, but the shape of these inclusions, relative to the testing direction, played an important role. As with ductility at room temperature, hot ductility was lowest in the short transverse direction and greatest in the longitudinal direction.

On the other hand, austenite grain size refinement has been shown to improve ductility as long as similarity in precipitate volume fraction and size exist. Better hot ductility under these conditions have been achieved in the present study by increasing the Mn content or by normalising.

11.3 INTERGRANULAR FRACTURE

Previous work and the present study have shown, two temperature ranges of reduced hot ductility, for steels solution treated (~ 1330 °C) and cooled to test temperatures in the range 700-1000 °C. The first one exists in the two-phase austenite/ferrite region and is due to the concentration of strain in primary ferrite films at γ grain boundaries. The most deleterious form of ferrite with regards to hot ductility are the thin films formed along the γ grain boundaries by deformation as described in chapter 5 and by Crowther and Mintz (1986a). However, grain boundary ferrite produced under more equilibrium condition is still capable of producing a significant ductility trough (Crowther, 1986).

In such two phase structures, as deformation proceeds, strain is concentrated in the ferrite films, and micro-voids nucleate at second phase particles, mainly MnS, within the ferrite films. These micro-voids grow and coalesce as deformation proceeds, resulting in intergranular failure. Ductility begins to recover as the test temperature is lowered below the transformation temperature, and the ferrite films begin to thicken, hence reducing strain concentration. Wray (1981) reported that strength difference between austenite and ferrite decreases with decreasing temperature, which may be an additional factor responsible for the recovery of ductility.

The temperature range over which the ductility trough extends depends on composition, grain size and cooling rate from the solution temperature. For constant cooling rate and grain size, increasing carbon content lowers the transformation temperature, and hence lowers the temperature at which the ductility begins to fall as has been shown in chapter 5 for Al containing steels with different carbon contents in the range 0.056 to 0.15%.

The second ductility trough which has been observed occurs in the single phase austenite region. Fractures in this temperature range, with low ductility values ($\leq 60\%$) are again intergranular being along the austenite grain boundaries, and fracture surfaces exhibit precipitates of sulphides, nitrides and/or carbonitrides. In this case the kinetics of dissolution, nucleation and growth of precipitates are central to our understanding of the hot ductility in this temperature range.

Two types of grain boundary fracture were identified in this region, intergranular decohesion (ID), which showed relatively flat facets and intergranular micro-void coalescence (IMC), which showed micro-voids on the grain facets.

It appears from the majority of cases examined in the previous chapters, good hot ductility is associated with dynamic recrystallisation in the austenite region.

However, dynamic recrystallisation does not always guarantee good hot ductility especially at lower strain rates, (see chapter 10). It has been suggested, (Crowther et al., 1987), that grain boundary migration rates have to be sufficiently fast to prevent crack linkage from occurring and this depends on strain rate. Usually, grain boundary migration rates decrease on lowering the strain rate, making crack linkage more easier (Davies and Evans, 1965). In addition, at lower strain rates ($\leq 10^{-4} \text{ S}^{-1}$), recrystallisation is periodic in nature and it is possible that intergranular cracks may develop between each recrystallisation cycle, (Crowther et al., 1987).

11.4 RECOMMENDATIONS

1. It has been shown in chapter 5 that increasing the the carbon level from 0.014 to 0.1% in C-Mn-Al-Nb steels reduced the hot ductility by increasing the amount of NbCN precipitation. Very low carbon levels in these steels would be expected to reduce transverse cracking.

Crowther and Mintz (1986b) and the present work has also shown that refining the grain size, improves hot ductility and hence a refinement in grain size prior to slab straightening might be expected to reduce transverse cracking. Again this could probably be achieved by lowering the C level to below 0.1%, since Maehara et al., (1985) have shown that the maximum grain size produced after solidification is for the carbon level between 0.1 and 0.15%.

The composition ranges below 0.1% and above 0.15% would limit the time spent during solidification and in the single phase austenite region of the phase diagram, thus reducing the γ grain size.

2. It was found in chapter 6 that adding calcium to the steel improves its hot ductility by reducing the amount of sulphur redissolved at 1330 °C to very low levels. This results in less precipitation at the γ boundaries during cooling to test temperature, and this might lead to less cracks in the continuously cast slabs. However, the influence of calcium additions on the hot ductility of steels has so far been

examined only after solution treatment (chapter 6) and for samples heated directly to test temperature, (Crowther and Mintz, 1986d). In both these cases a large improvement in hot ductility occurs. Of more relevance to the continuous casting process is the hot ductility after casting in-situ. This is an area in which further work is required, particularly as Ca additions to the melt should lower the amount of S precipitated at the boundaries during solidification and cooling to the straightening temperature.

3. The results of chapter 7 show that, dynamic precipitation of NbCN is more effective in reducing hot ductility than static precipitation at the same test temperature. Thus a reduction in cooling rate following solidification might reduce the supersaturation of Nb at the slab straightening temperature, and hence reduce the quantity of dynamically precipitated NbCN formed during straightening.
4. Adding Ti to a Nb containing steel has been shown to improve hot ductility in the "as cast" state. It is presently not clear whether this improvement is due to the lower S level of the Ti containing steel or whether it is due to the relatively coarse NbTi(CN) particles formed at the austenite grain boundaries during cooling from the melt. Further work is required to isolate the individual effect of Ti and S on hot ductility in the "as cast" state. Also, one of the major advantages of adding Ti is

to produce a fine grain size in hot rolled plate. Although this fine grain size was not achieved in the "as cast" state. It may be possible by suitable cooling during solidification to produce TiN particles which are sufficiently fine to refine the "as cast" grain size.

5. Differences in hot ductility behaviour between "as-cast" and "reheated hot rolled" conditions for Al and Nb containing steels are small, justifying the use of the hot tensile test to simulate the continuous casting process by reheating to 1330 °C and cooling to test temperatures. However, big differences are apparent between the "as cast" and "reheated hot rolled" for the Nb/Ti steel because the solution temperature of 1330 °C does not dissolve the TiN or NbTi(CN) particles. Thus, as-cast samples may have to be used to assess the hot ductility behaviour of such steels.
6. As recommended by Crowther (1986), the recovery of hot ductility by increasing the test temperature is often due to the onset of dynamic recrystallisation. To date, it appears that very little work has been done on the volume fraction of recrystallised material required to bring about this recovery in hot ductility. Measurement of these recrystallised volume fractions would be most easily made on fractured samples of an austenitic stainless steel, which had been quenched rapidly after fracture.

APPENDICES

APPENDIX 1

CARBON EXTRACTION REPLICA PREPARATION AND EXAMINATION (Crowther, 1986)

Samples for replication were first ground flat, and the area to be examined was defined by the application of a non-conducting lacquer. The sample was then electropolished for three minutes using an electropolishing solution consisting of 200 parts ethanol, 100 parts 2-butoxyethanol and 52.5 parts perchloric acid. The electropolishing solution was cooled to 0 °C, and electropolishing carried out at 11 V, using a stainless steel cathode. After electropolishing, the sample was etched for approximately 30 seconds using 2% nital solution, and then a carbon film was evaporated onto the prepared surface at a pressure of 10^{-4} torr. The carbon film was then scribed into 3 mm squares, and the replicas removed by immersion in a 5% nital solution. The replicas were then washed in distilled water, and finally collected on 4 mm diameter copper grids.

Replicas were examined using a JEOL 100B TEM operating at 60 KV. The microscope was equipped with EDAX X-ray system, capable of identifying elements with atomic number greater than 11. The system was therefore, not capable of distinguishing between carbide and nitride precipitates. The smallest spot size available was 50 nm in diameter, and this determined the minimum distance between precipitates which could be analysed separately. precipitate sizes were measured directly from the negatives. To calculate a mean precipitate diameter, assuming spherical precipitates, at least 200 measurements were taken

from 3 separate replicas taken from same sample. The procedure adopted to calculate the mean precipitate diameter, D_m , for a precipitate distribution was that used by Weiss and Jonas (1980). It is assumed that precipitates of diameter d_i are extracted from a layer of matrix d_i thick, as illustrated in Fig. A1. N_{si} , the number of precipitates per unit area of diameter d_i , is measured directly from the negative. However, it is N_{vi} , the number of precipitates per unit volume of diameter d_i which is required to calculate D_m . As shown in Fig. A1, N_{si} and N_{vi} are related by:

$$N_{vi} = N_{si}/d_i \quad \dots\dots\dots (A1)$$

D_m is then calculated using the formula:

$$D_m = \left[\frac{\sum_i N_{vi} d_i^3}{\sum_i N_{vi}} \right]^{1/3} \quad \dots\dots\dots (A2)$$

To gain at least a semi-quantitative estimate of the particle distribution at the austenite grain boundaries, the number of particles in a measured length of grain boundary was counted and the interparticle spacing, was calculated. For any particular steel, these measurements were based on approximately 200 particle counts taken from different grain boundary regions, and from different replicas. Such measurements, although not providing absolute measurements of grain boundary precipitate distributions, are adequate for making comparisons between different steels.

APPENDIX 2 (Publications)

Some of the results presented in this thesis have been published or accepted for publication.

The results of chapter 7 have been published in Metallurgical Transactions, volume 18A, November 1987, page 1929.

The results of chapter 8 have been published in the International Conference CANMET on Physical Simulation of Welding, Hot Forming and Continuous Casting, May 2-4/1988, Ottawa, Ontario, (Canada).

The results of chapter 10 have been accepted for publication in "Materials Science and Technology".
(see next page).

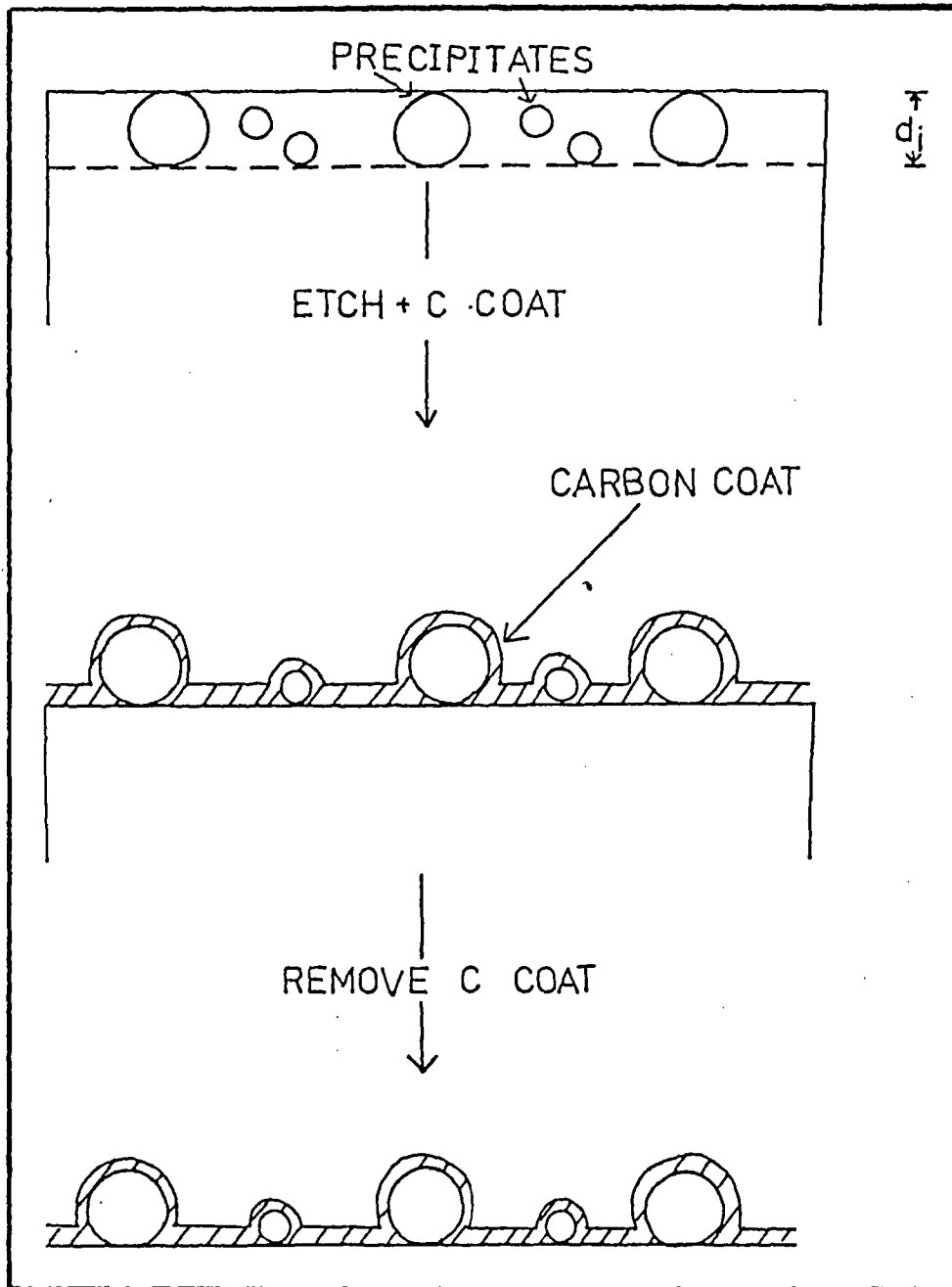


Fig. A1 Extraction of precipitates using single stage carbon replicas.

MATERIALS SCIENCE AND TECHNOLOGY

A PUBLICATION OF THE INSTITUTE OF METALS

Consulting Editor
Professor D.R.F. West
Imperial College of Science
and Technology, London

The Institute of Metals
1 Carlton House Terrace
London SW1Y 5DB
Telephone 01-839 4071
Telex 8814813 Fax (01) 839 2289

10 February 1988

GCS/AJM/MST/776

Dr B Mintz
The City University
Department of Mechanical Engineering
Northampton Square
LONDON
EC1V 0HB

Dear Dr Mintz

THE INFLUENCE OF TEST DIRECTION ON THE HOT DUCTILITY OF AUSTENITE

Many thanks for sending in the revised version of your paper and also for your helpful letter giving details of the revisions. I confirm acceptance of the paper and it will now be passed to the Production Department. In due course you will receive proofs for checking.

With regard to Fig. 1, we have the original version with the glossy prints and this has been substituted for the Xeroxed copy which was with the revised figures.

Yours sincerely

Mary Chin

Gerald C Smith
EDITORIAL CONSULTANT

REFERENCES

- Akben, M.G. Weiss, I., and Jonas, J.J. (1981). Acta. Met., 29, 111
- Andrews, K.W. (1965) JISI, 203, 721.
- Ashby, M.F., Gandhi, C., and Taplin, M.R. (1979). Acta Met., 27, 669.
- Baker, T.J. (1974), Conf. on inclusions and their effects on steel properties. Paper No.11, Leeds, British Steel Corporation.
- Banks, T.M. and Gladman, T. (1979). Met. Technol., 6, 512.
- Bellot, J. and Gantois, M. (1978). Trans. ISIJ, 18, 536.
- Bernard, G., Grumbach, M. and Moliexe, F. (1975). Met. Technol., 5, 512.
- Bernard, G., Birat, J.P., Conseil, B. and Humbert, J.C. (1978). Rev. Met., 75, 467.
- Birat, J.P., Larrecq, M., Le Bon, A., Jeanneau, M., Poupon M. and Senaneuch, D. (1981) Steelmaking Procs., 64, 53.
- Blum, E.E., Grin, A.V. and Gol'dshteyn, M.I. (1966). Fiz. metal. metalloved, 21, 474.
- Brimacombe, J.K. and Sorimachi, K. (1977). Metall. Trans., 8B, 489.
- Bywater, K.A. and Gladman, T. (1976). Met. Technol., 3, 358.
- Carlsson, C.G. (1964). Jernkont, Ann., 184, 152.
- Chen, Z., Loretto, M.H., and Cochrane, R.C. (1987). Mater. Sci. Technol., 3, 836.
- Cochrane, R.C. (1982), unpublished work.
- Coleman, T.H. and Wilcox, J.R. (1985). Mat. Sci. and Technol., 1, 80.
- Cotterill, P. and Mould, P.R. (1976). In "Recrystallisation and Grain Growth in Metals", Surrey University Press.

- Crowther, D.N. (1986) PhD Thesis, The City University.
- Crowther, D.N. and Mintz, B. (1985), unpublished work.
- Crowther, D.N. and Mintz, B. (1986a). Mater. Sci. and Technol., 2, 671.
- Crowther, D.N. and Mintz, B. (1986b). Mater. Sci. and Technol., 2, 951.
- Crowther, D.N. and Mintz, B. (1986c). Mater. Sci. and Technol., 5, 1099.
- Crowther, D.N. and Mintz, B. (1986d). Proc.Int.Con. "On the effects and control of Inclusions and Residuals in steels", Toronto, Canada, 1986, 3, 83.
- Crowther, D.N., Mohamed, Z. and Mintz, B. (1987). Trans. ISIJ, 27, 366.
- Davies, P.W. and Evans, R.W. (1965). Acta Metall., 13, 353
- Dieter, G.E., (1984). In "Mechanical Metallurgy", edi., McGRAWHILL, Tokyo, Japan.
- Dyson, B.F. and McLean, P., (1972). Met. Sci. Journal, 6, 220.
- Ericson, L. (1977). Scand. J. Met., 6, 116.
- Evans, H.E. (1969). Met. Sci. J., 3, 33.
- Evans, H.E. (1984). In "Creep Fracture", Pergamon Press.
- Evans, R.W. and Jones, F.L., (1976). Met. Technol., 3, 494.
- Evans, R.W. and Jones, F.L., (1978). Met. Technol., 5, 1.
- Farkas, S., Shaw, J.W., and Gricol, J.D., (1971). Open Hearth Proc., 54, 68.
- Fleck, R.G., Cocks, G.J., and Taplin, D.M.R., (1970). Metall. Trans., 1A, 3415.
- Fuchs, I.A., (1975). ESTEL, 3, 127.
- Fujii, H., Ohashi, T., Hiromoto, K. and Oda, M. (1975). Testsu To Hogane, 61, 5556.

- Funnell, G.D., (1980). In "Hot Working and Forming Processes", Met. Soc. Book No. 264, 104.
- Funnell, G.D. and Davies, R.D., (1978). Met. Technol., 5, 150.
- Garofalo, F. (1968). In "Ductility", American Society for Metals, Metals Park, Ohio, 87.
- Garofalo, F., (1963). Trans. AIME, 227, 351.
- Gielen, P.M., (1981). Metallurgie, 21, 73.
- Gittins, A., (1977). Int. Met. Rev., 22, 212.
- Gladman, T. and Pickering, F.B. (1967). JISI, 205, 653.
- Glover, G. and Sellars, C.M., (1973). Metall. Trans., 4, 765.
- Hannerz, N.E., (1985). Trans. ISIJ, 25, 149.
- Hannerz, N.E., Lindborg, U. and Lehtinen, B., (1968). JISI, 206, 68.
- Harding, R.A., Sawle, R. and Sellars, C.M., (1977). Met. Technol., 4, 142.
- Hater, M., Klages, R., Redent, B. and Taffner, K., (1973). Open Hearth Proc., 56, 202.
- Heidenreich, R.D. and Shockly, W., (1948). Report on strength of solids, Phys. Soc., London.
- Heritier, P., Fourdex, A., and Kobylanski, (1981). Scripta Met., 15, 753.
- Hilty, D.C. and Farrell, J.W. (1974). In "Inclusions and their effects on steel properties", Conf. paper No.4, University of Leeds.
- Hirsh, P.B., (1958), (1958), Internal Stresses and Fatigue in Metals ed. G.M. Rassweiler and G.L. Grube, Elsevier, Amsterdam, 1958, 139.
- Honeycombe, R.W.K., (1981). In "Steels, Microstructure and Properties" edi., Edward Arnold, London.
- Irvine, K.J. and Pickering, F.B., (1957). Iron and Steel, June 1957, pp. 219-223.

- Irvine, K.J., Pickering, F.B. and Gladman, T., (1967). JISI, 205, 161.
- Jonas, J.J., Sellars, C.M. and Tegart, W.J. McG., (1968). In "Deformation under Hot Working Conditions", Special Report No. 108, London ISI, 21.
- Jonas, J.J. and Weiss, I., (1979). Met. Sci. Journ., 13, 238.
- Kawasaki, M., Marukawa, K., Watanabe, T., and Nakajima, K. (1987). In "HSLA Steels '85; Beijing, China, Chinese Society of Metals
- Kiessling, R. (1978). JISI, 208, 699.
- Kiessling, R., (1968). "Non Metallic Inclusions in Steel" Part II, The Iron and Steel Institute.
- Kinoshita, T. and Kuroki, S., (1972), Imono, 44, 1080.
- Kozasu, I., Ouchi, C., Sampei, T., and Okita, T., (1977). In "Microalloying '75", New York, United Carbide Corp., 120.
- Kutumba Rao, V., Taplin, D.M.R., Rama Rao, P., (1975), Metall. Trans., 6A, 77.
- Lankford, W.T., (1972), Metall., Trans., 3, 1331.
- Le Bon, A., Rofes-Vernis, J., and Rossard, C., (1975). Met. Sci., 9, 36.
- Leslie, W.C. (1954). Trans. ASM, 46, 1470.
- Lucke, K., and Stuwe, H.B., (1963). In "Recovery and Recrystallisation of Metals" New York, ed. L. Himmel.
- Luton, M.J., and Sellars, C.M., (1969). Acta. Met., 17, 1033.
- Maehara, Y., and Ohmori, Y., (1984). Met. Sci. and Eng., 62, 109.
- Maehara, Y., Yasumoto, K., Sugitani, Y., and Gunji, K., (1985), Trans. ISIJ, 25, 1045.
- Mayes, I.C., and Baker, T.J., (1986). Mater. Sci. Techn. 2, 133.

- McQueen, H.J., and Bergerson, S., (1972). *Met. Sci. J.* 6, 25.
- McQueen, H.J., and Jonas, J.J., (1975). In "Treatise on Materials Science and Technology", New York Academic Press, vol. 6, 393.
- McQueen, H.J., Wong, W.A., and Jonas, J.J. (1967). *Can. J. Phys.*, 45, 1225.
- Mercer, R.E., and McPherson, N.A., (1979). *Ironmaking and steelmaking*, 7, 167
- Meyer, L., Strassburger, C., and Schneider, C., (1987). In "HSLA Steels'85; Beijing, China, Chinese Society of Metals.
- Michel, J.P., and Jonas, J.J., (1981). *Acta Metall.*, 29, 513.
- Mintz, B., (1979), Unpublished technical note, Scottish Laboratories, British Steel Corporation.
- Mintz, B., (1988), Private Communication.
- Mintz, B., and Arrowsmith, J.M., (1979). *Met. Technol.*, 6, 24.
- Mintz, B., and Arrowsmith, J.M., (1980). In "Hot Working and Forming Processes", *Met. Soc. Book No. 264*, 99.
- Mintz, B., Ang, S.H., and Crowther, D.N., (1983). In "Deformation of multi-phase particle containing materials", *RIS Ø Int. Conf.*, Danmark.
- Mintz, B., Stewart, J.M., and Crowther, D.N., (1987). *Trans. ISIJ*, 27, 961.
- Mintz, B., Wilcox, J.R., and Arrowsmith, J.M., (1980). In "Recrystallisation and Grain Growth of Multi-phase and Particle Containing Materials", *Ris Ø National Laboratory*, Denmark.
- Mintz, B., Wilcox, J.R., and Crowther, D.N., (1986). *Mat. Sci. and Technol.*, 2, 589.
- Moore, P.G., (1968). In "Deformation under hot working conditions", *Special Report No. 108*, London ISI, 68.

- Mori, H., (1974). Tetsu To Hagane, 60, 784.
- Morrison, W.B., (1975). Met. Technol., 2, 33.
- Nachtrab, W.T., and Chou, Y.T., (1986). Metall. Trans., 17A, 1995.
- Norstrom, L.A., (1977). Scan. J. Met., 6, 269.
- Norstrom, L.A., and Johansson, B., (1982). Scand. J. Met., 11, 139.
- Nozaki, T., Matsuno, J., Murata, K., Ooi, H., and Kodama, M., (1978). Trans. ISIJ, 18, 330
- Offerman, C., Dacker, C.A., and Enstrom, C., (1981). Scand. J. Met., 10, 115.
- Ohmori, Y., and Maehara, Y., (1984). Trans. J. Inst. Met., 25, 160.
- Osinkolu, G.A., Tacikowski, M., and Kobylanski, A., (1985). Mat. Sci. and Technol., 1, 520.
- Ouchi, C., and Matusumoto, K., (1982). Trans. ISIJ, 22, 181.
- Ouchi, C., and Okita, T., (1982). Trans. ISIJ, 22, 543.
- Pircher, H., and Klapdar, W., (1977). In "Microalloying '75'", new York, United Carbide Corp., 232.
- Reynolds, J.H., and Gladman, T., (1980). In "Hot working and Forming Processes", Metals Soc. Book No. 246, 171.
- Robbins, J.L., Shepard, O.G., and Sherby, O.D., (1967). Trans. ASM, 60, 205.
- Roberts, W., Boden, H., and Ahblom, B., (1979). Met. Sci., 13, 195.
- Roberts, W., Liddefelt, H., and Sandberg, A., (1980). In "Hot Working and Forming Processes", Metals Soc. Book No. 264, 38.
- Rogberg, B., (1983). Scand. J. Met., 12, 175.
- Rossard, C., (1973). In "Proceedings of 3rd ICSMA".
- Ruibal, E., Urcola, E.E., and Fuentes, M., (1984). Met. Technol., 11, 189.

- Sakai, T., and Ohashi, M., (1981). *Tetsu-to-Hagane*, 67, 2000.
- Sankar, J., Hawkins, D.N., and McQueen, H.J., (1979). *Met. Technol.*, 6, 325.
- Schmidt, L., and Josefsson, A., (1974). *Scand. J. Met.*, 3, 193.
- Sekine, H., and Maruyama, T., (1976). *Trans. ISIJ*, 16, 427.
- Sellars, C.M., (1980). In "Hot Working and Forming Processes", *Metals Soc. Book No. 264*, 3.
- Sellars, C.M., and Tegart, W.J. McG., (1966). *Mem. Sci. Rev. Met.*, 63, 731
- Sellars, C.M., and Tegart, W.J. McG., (1972). *Int. Met. Rev.*, 17, 1.
- Smallman, R.E., (1985). *Modern Physical Metallurgy*, Butterworths & Co.
- Sopher, R.P., (1958). *Welding Journal*, 37, 481
- Speich, G.R., and Spitzig, W.A., (1982). *Metall. Trans.*, 13A, 2239.
- Spitzig and Sober, R.J., (1981). *Metall. Trans.*, 12A, 281.
- Stuart, H. (1987). In "HSLA Steels'85; Beijing, China, Chinese Society of Metals.
- Subramanian, S.V., Shima, S., Ocampo, G., Castillo, T., Embury, J.D., and Purdy, G.R. (1987). In 'HSLA Steels'85; Beijing, China, Chinese Society of Metals.
- Suzuki, H.G., et al., (1981). *Tetsu-to-Hagane*, 56, 1.
- Suzuki, H.G., et al., (1980). In "100th ISIJ Meeting, October 1980.
- Suzuki, H.G., Nishimura, S., Imamura, J., and Nakamura, Y., (1984a) . *Trans. ISIJ* 24, 169.
- Suzuki, H.G., Nishimura, S., and Nakamura, Y., (1984b). *Trans. ISIJ*, 24, 54.

- Suzuki, H.G., Nishimura, S., and Yamaguchi, S., (1982). Trans. ISIJ, 22, 84.
- Swann, P.R., and Nutting, J., (1961). J. Inst. Metals, 90, 133.
- Tanaka et al., (1981). "Formation Mechanism of Surface Cracks along the Oscillation Mark," 101st ISIJ Meeting, April 1981.
- Taplin, D.M.R. and Whittakers, V.N. (1963). J. Ins. Met., 92, 426.
- Tegart, W.J. McG., (1977). In "Ductility", Metals Pak, Ohio, 133.
- Tegart, W.J. McG., and Gittins, A. (1977). In "The Hot Deformation of Austenite", Met. Soc. AIME, New York 1.
- Thomas, B.G., Brimacombe, J.K., and Samarasekera (1986). ISS Trans., 7, 7.
- Tomono, H., (1977). In; CONAST Slab Seminar, Zurich.
- Turkdogan, E.T., Ignatawics, I., and Pearson, J. (1955). JISI, 180, 349.
- Vodopivec, F., (1973). JISI, 211, 664.
- Vodopivec, F., (1978). Met. Technol., 5, 118.
- Watanabe, H., Smith, Y.E., and Pewke, R.D. (1977). In "The Hot Deformation of Austenite", Met. Soc. AIME, New York, 140.
- Weinberg, F., (1979). Metall. Trans., 10B, 219.
- Weiss, I., and Jonas, J.J., (1979). Metall. Trans., 10A, 831.
- Weiss, I., and Jonas, J.J., (1980). Metall. Trans., 11A, 403.
- White, F.E., and Rossard, C., (1968). In "Deformation under Hot working conditions", Special Report No. 108, London, ISI, 14.
- Wilber, G.A., Batra, R., Savage, W.F., and Childs, W.J., (1975). Metall. Trans., 6A, 1727..

Wilcox, J.R., (1982). PhD Thesis, University of Cambridge. Cambridge.

Wilcox, J.R., and Honeycombe, R.W.K., (1984). Met. Technol., 11, 217.

Wilcox, J.R., and Honeycombe, R.W.K., (1980). In "Hot Working and Forming Processes", Metals Soc. Book No. 264, 108.

Woodhead, J.H., and Keown, S.R., (1987). In "HSLA Steels'85; Beijing, China, Chinese Society of Metals.

Wray, P.J., (1975). Metall. Trans., 6A, 1379.

Wray, P.J., (1981). Met. Technol., 8, 466.

Wright, J.A., and Quarrell, A.G., (1962). JISI, 200, 299.

Yamaguchi, S., Kobayashi, H., Matsumiya, T., and Hayami, H., (1979). Met. Technol., 5, 170.

Yamanaka, K., Terasaki, H., Ohtani, H., Oda, M., Yoshihara, M., (1980). Trans. ISIJ, 20, 810.

Yasumoto, K., Maehara, Y., Ura, S., and Ohmori, Y., (1985). Mat. Sci. and Technol., 1, 111.